The Quantification of Achilles Tendon Neovascularity

Thesis submitted to Cardiff University for the degree of

Doctor of Philosophy

Xin Yang

Cardiff University

Ph.D. Thesis

2011

ProQuest LLC
789 East Eisenhower Parkway
P.O. Box 1346
Ann Arbor, MI 48106-1346

Abstract

The exact role of neovascularization found in painful Achilles tendons is unknown. The amount of the neovascularization is thought to be related to the clinical severity. To investigate the quantification of neovascularization and its correlation with the clinical severity in the symptomatic Achilles tendon, a novel 3D power Doppler ultrasound scanning system I firstly developed to prospectively examine ten patients with twelve symptomatic Achilles tendons, as well as twenty asymptomatic Achilles tendons as a control group. The novel 3D evaluation system consisted of a scanning rig, a pixel analysis programme, and a 3D reconstruction software. By scanning the entire length of the Achilles tendon, the continuous slices of the transverse image of the tendon were acquired. The pixel analysis programmed then selected a representated frame with maximum vascular lumen from each slice over a normally scanning distance of 6 cm. All the frames were fed into the 3D reconstruction software for visualization and volume calculation. The volume of the neovascularity (VON) was then outputted. The mean volume of neovascularity (VON) in the whole Achilles tendon was calculated during the phase of the cardiac cycle displaying maximum and minimum vascularity. The mean VONs in the control group were found to be 0.41 mm^3 (maximum) and 0.02 mm^3 (minimum), respectively. The mean VONs in patients with painful Achilles tendon were 380 mm^3 (maximum) and 70.3 mm^3 (minimum), respectively. The initial results showed that the novel 3D power Doppler ultrasound system could be used to measure the mean VON in controls and in patients with symptomatic Achilles tendinopathy. The results also demonstrated a significantly greater VON in the maximum phase compared to the minimum phase as well as in the patient group compared with that in the control group. The system was therefore capable of defining the degree of vascularity in the Achilles tendon. Furthermore, to investigate the correlation between the VON and clinical severity, forty

tendons from 30 patients with chronic painful Achilles tendons were examined. VON was evaluated for each tendon. Visual analog scale pain (VAS) and the Victorian Institute of Sport Assessment-Achilles questionnaire (VISA-A) were used to assess the subjective severity of the Achilles tendinopathy. Of the 40 symptomatic tendons, neovascularization was registered in 97.5% (n = 39). The VON ranged from 0 mm^3 to 618 mm^3 with a mean VON of 111 mm^3. The Spearman correlation coefficients between the VAS and the VON, VSIA-A and VON were 0.326 (p = 0.04, power = 0.75, effect size = 0.39), -0.246 (p = 0.127, power = 0.89, effect size = 0.46), respectively. As conclusion, the VAS showed a positive correlation with VON, while no correlation was found between VISA-A score and VON. The VON can be used to interpret the level of the pain in Achilles tendinopathy.

Acknowledgement

It is a pleasure to thank the many people who made this thesis possible.

It is difficult to overstate my gratitude to my Ph.D. supervisor, Prof. Len D.M. Nokes. With his enthusiasm, his inspiration, and his great efforts to supervise clearly and simply, he helped to make sports medicine fun for me. Throughout my Ph.D. period, he provided encouragement, sound advice, good teaching, good company, great demonstration and lots of good ideas. I would have been lost without him.

I would like to thank the many people who have taught me ultrasound and clinical experiments: Dr. Neil Pugh, Dr. Declan Coleman. For their kind assistance with demonstrating machine, explaining theory and practice, correcting writings, organizing patients, helping with various applications, and so on, I wish to thank in addition Reith, Kate, Paul, and Gill.

I wish to thank Prof. Peter N. Wells and Prof. John P. Woodcock, for reading and correcting my articles, and for all the emotional support and caring they provided.

Lastly, and most importantly, I wish to thank my parents, Lin Yang and Fengyan He. They bore me, raised me, supported me, taught me, and loved me. To them I dedicate this thesis.

Table of Contents

List of figures

List of tables

1. Introduction

Achilles tendon pathology is one of the more common conditions encountered by the foot and ankle surgeon. While it most frequently affects the athletic population, it can also lead to significant morbidity in the older and sedentary patient (Nicol et al. 2006; Tan and Chan 2008; Daftary and Adler 2009; Krahe and Berlet 2009). It has been recommended that the clinical syndrome, characterized by a combination of pain, localized tenderness, impaired performance and swelling, is labeled "Achilles tendinopathy" (Paavola et al. 2000).

The diagnosis of Achilles tendinopathy is mainly based on a careful history and detailed clinical examination (Longo et al. 2009). The natural history of symptomatic chronic Achilles tendinopathy and its relationship to future pain or tendon pathology is unknown (Ohberg and Alfredson 2002; Maganaris et al. 2008; Tan and Chan 2008). An increasing degree of degeneration with limited or no inflammation was present. The cause of pain in chronic Achilles tendinopathy is thought to be related to the presence of neovascularization (Richards et al. 2005; van Snellenberg et al. 2007). However, there are always some arguments about the correlation between the severity of symptoms and the neovascularization score. Some studies believed that the presence of neovascularization in the Achilles tendon was shown to correlate with pain in patients with chronic midportion Achilles tendinosis (Ohberg and Alfredson 2002; Alfredson et al. 2003; Ohberg and Alfredson 2003; Alfredson and Ohberg 2005; Lind et al. 2006; Sengkerij et al. 2009). Though other evidence demonstrated that a negative correlation existed between the presence of intratendonous neovascularization and functional tests (Peers et al. 2003; Zanetti et al. 2003; Miquel et al. 2009).

Diagnosis of Achilles tendon disorders is often done by imaging (Schepsis et al. 2002; Harris and Peduto 2006). Magnetic resonance imaging (MRI) is often employed to reliably indicate the potential for measuring tendon structural changes after an injury, disease, and altered loading(Shin et al. 2008). Some reports (Romaneehsen and Kreitner 2005; Gardin et al. 2006) interpreted the severity of pain and functional impairment was correlated to increased mean intratendinous signal in the painful tendon in all MR sequences. High resolution ultrasonography has been likely to be introduced in the observation of the Achilles tendinopathy in the last decade, providing high levels of accuracy and reproducibility in the hands of experienced examiners (Reiter et al. 2004). Additional advantages in the use of ultrasound is that it is readily available, noninvasive, and low cost (Astrom et al. 1996).

Recently power Doppler ultrasound (PDU) has been often applied in the evaluation of potential tendinopathy (Weinberg et al. 1998; Ohberg L 2001; Richards et al. 2001; Premkumar et al. 2002; Richards et al. 2009), especially in correlating the PDU findings with the clinical severity of the symptom (Breidahl et al. 1998; Reiter et al. 2004; Sengkerij et al. 2009). The preferential use of PDU is because it shows more tendon microvascularity than colour Doppler ultrasound (CDU) in tendinopathy (Richards et al. 2005). Most of the previous work concluded there was a non-linear relationship between Achilles tendonopathy and the amount of microvascularity, but not between PDU and duration of symptoms (Fenwick et al. 2002; Richards et al. 2005; Richards et al. 2008). In other words, the symptomatic Achilles tendin can exist with or without detectable neovascularization. There might be neovascularization in all Achilles tendinopathy; however, a report indicated that a flow slower than 4-6 mm/sec is not detectable on Doppler ultrasonography (Peers et al. 2003).

The clinical applications of vascular 3D ultrasound (3D US) imaging has been developed in the last decades and the assessment of flow in the kidney, placenta, prostate and carotid artery (Fenster and Downey 1996; Nelson and Pretorius 1998). The benefit of 3D US is that

it is able to localize and visualize a functional abnormality relative to the underlying anatomy. In addition, a study (Katamay et al. 2009) presented a new method for measurement of the volumetric blood flow in absolute units in the ophthalmic artery by using an ordinary 3 - 12 MHz linear ultrasound transducer.

A previous study in corpses showed that the quantitative assessment of intravascular volume and the vascular patterns of the human Achilles tendon may play an important role in the pathogenesis of Achilles tendon rupture (Stein et al. 2000).

A special 3D PDU analysis system was therefore devised to observe the vascular conditions in the symptomatic Achilles tendon, in order to acquire the overall neovascularization flow pattern. In addition, by knowing the quantification of neovascularity, the thesis also aims to correlate the neovascularization to the clinical severity in Achilles tendinopathy.
The presence of neovascularization in Achilles tendon is associated with the tendinopathy, the VON correlates with the clinical severity.

2. Achilles Tendon Anatomy

A tendon is a tough bundle of fibrous connective tissue that usually connects muscle to bone and is capable of withstanding tension (Franchi et al. 2007). Tendons are similar to ligaments and fascia as they are all made of collagen. The difference is that ligaments join one bone to another bone, while fascia connects muscles to other muscles. Tendons and muscles work together and can only exert a pulling force (Jozsa et al. 1980).

2.1 Tendon Structure

2.1.1 Macrostructure

Tendons are anatomic structures interposed between muscles and bones transmitting the force created in the muscle to bone. Basically, each muscle has two tendons, proximal and distal. The point of union with a muscle is called a myotendinous junction (MTJ), and the point of union with a bone an osteotendinous junction (OTJ) as shown in Fig. 2.1. The attachment of the proximal tendon of a muscle to bone is called a muscle origin, and that of the distal tendon an insertion (Kannus 2000).

Healthy tendons are brilliant white in colour and fibro-elastic in texture, varying considerably in shape and in the way they are attached to bone ranging from wide and flat tendons to cylindrical, fanshaped, and ribbon-shaped tendons. The shape and properties of tendons are significantly related to the behaviour of the entire muscle-tendon complex (Kannus 2000; Magnusson et al. 2003; Franchi et al. 2007).

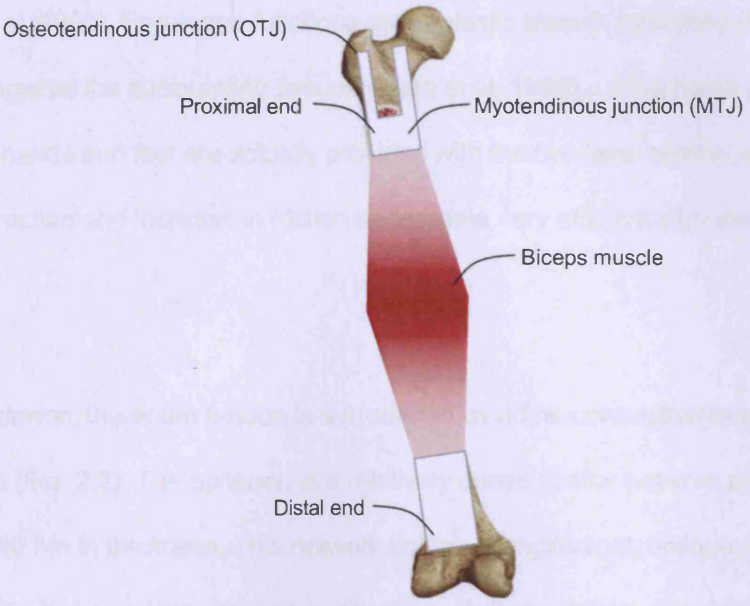

Fig. 2.1 Tendons are anatomic structures interposed between muscles and bones transmitting the force created in the muscle to bone

There are five surrounding structures of the tendon: (1) the fibrous sheaths or retinacula, are the canals through which the tendons glide during their course; (2) the reflection pulleys, are the anatomic reinforcements of the fibrous sheaths located in places where there are curves along the course of the tendon; (3) the synovial sheaths, are access tunnels for tendons at bone surfaces or other anatomic structures that might cause friction; (4) the peritendinous sheets or paratenons, are alternative structures to reduce friction in some tendons without a true synovial sheath; (5) the tendon bursae, are the fifth extratendinous structure playing an important role in the reduction of friction (Kannus 2000).

2.1.2 Microstructure

The appreciable movement of a tendon may cause friction against the surrounding tissues, then the tendon is often surrounded by a connective tissue called paratenons (Franchi et al. 2007). The main components of the paratenons are type I and type III collagen fibrils and elastic fibrils (Kvist et al. 1985), also the paratenon is lined on its inner surface by synovial

cells (Jozsa et al. 1990). Paratenon functions as an elastic sleeve, permitting free movement of the tendon against the surrounding tissues (Hess et al. 1989). Only some parts of a few tendons in the hands and feet are actually provided with the two-layer tendon sheaths, where a change of direction and increase in friction necessitate very efficient lubrication (Kannus 2000).

Under the paratenon, the entire tendon is surrounded by a fine connective tissue sheath called epitenon (Fig. 2.2). The epitenon is a relatively dense fibrillar network of collagen with strands of 8 – 10 nm in thickness. This network contains longitudinal, oblique, as well as transversal fibrils. It shows little variation in density or fibril orientation. Occasionally, the fibrils of epitenon are fused with the superficially located tendon fibrils (Jozsa et al. 1991).

On the outer surface, the epitenon is contiguous with paratenon and on its inner surface with the endotenon, which is a thin reticular network of connective tissue inside the tendon that has a well developed crisscross pattern of collagen fibrils (Rowe 1985). The endotenon invests each tendon fibre and binds individual fibres, primary, secondary, and tertiary fibre bundles, together (Jozsa et al. 1991).

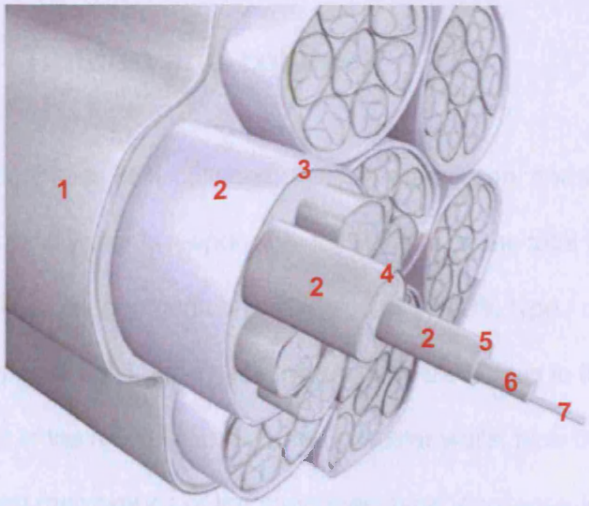

Fig. 2.2 Microstructure of the tendon

(http://patientsites.com/media/img/21/ankle_anatomy_tendons01.jpg)

A bunch of collagen fibres forms a primary bundle or subfascicle (15-400μm in diameter), and a group of primary bundles forms secondary fibre bundles or fascicles whose diameter range from 150 to 1000μm in human tendons. A group of secondary fibre bundles forms a tertiary bundle (diameter from 1000 to 3000μm in human tendons), which makes up the tendon surrounded by epitenon (Silver et al. 1992; Kannus 2000).

Inside each fibre bundle, collagen fibrils are arranged in parallel fibre bundles running longitudinally but also transversally and horizontally, with longitudinal fibrils also crossing each other, forming spirals and plaits (Chansky and Iannotti 1991; Jozsa et al. 1991).

It is concluded that tendon is composed of collagen fibre bundles each of them resulting from the aggregation of single collagen fibrils, namely tens of millions of collagen fibrils, each hundreds of microns long (Canty and Kadler 2002). The collagen fibril is the basic unit of a tendon, and the collagen fibre is the smallest tendon unit visible using light microscopy and is aligned from end to end in a tendon. A fibre also represents the smallest collagenous structure that can be tested mechanically, although a larger fibre bundle makes the testing more reliable (O'Brien 1997).

2.1.3 Tendon and collagen

Tendon contains 86% collagen, 1–5% proteoglycan, and 2% elastin as measured by dry weights, and water is responsible for 60–80% of the total wet weight of the tendon (Lin et al. 2004). The collagen portion is made up of 97-98% type I collagen, with small amounts of other types of collagen. These include type II collagen in the cartilaginous zones, type III collagen in the reticulin fibres of the vascular walls, type IX collagen, type IV collagen in the basement membranes of the capillaries, type V collagen in the vascular walls, and type X collagen in the mineralized fibrocartilage near the interface with the bone (Fukuta et al. 1998).

The mechanical stability of the tendinous collagen is the most important factor for the mechanical strength of a tendon. The function of elastic fibres is not entirely clear, but they may contribute to the recovery of the wavy configuration of the collagen fibres after tendinous stretch (Butler et al. 1978).

2.1.4 Tendon cells

The tendon cells, called tenoblasts and tenocytes, comprise about 90% to 95% of the cellular elements of the tendon. The other 5% to 10% includes the chondrocytes found at the pressure and insertion sites, the synovial cells of the tendon sheath on the tendon surface, and the vascular cells, such as capillary endothelial cells and smooth muscle cells of the arterioles in the endotenon and epitenon (Kannus 2000). In pathological conditions, many other types of cells can be observed in the tendon tissue, such as inflammatory cells, macrophages, and myofibroblasts.

2.1.5 Junctions

The myotendinous junction (MTJ, Fig. 2.1) is a highly specialized anatomic region in the muscle-tendon unit. In this region, the tension generated by muscle fibres is transmitted from intracellular contractile proteins to extracellular connective tissue proteins (collagen fibrils) of the tendon (Trotter and Baca 1987).

Morphological studies show that at the MTJ, the collagen fibrils insert into deep recesses that are formed between the fingerlike processes (endings) of the muscle cells (Fig. 2.3) (Trotter et al. 1983). This type of folding of the basal membrane of the muscle cell endings markedly increases the contact area between the muscle fibres and tendon collagen fibres, by 10- to 20-fold (Tidball 1991). This in turn can significantly reduce the force applied per surface unit of the MTJ during muscle contraction.

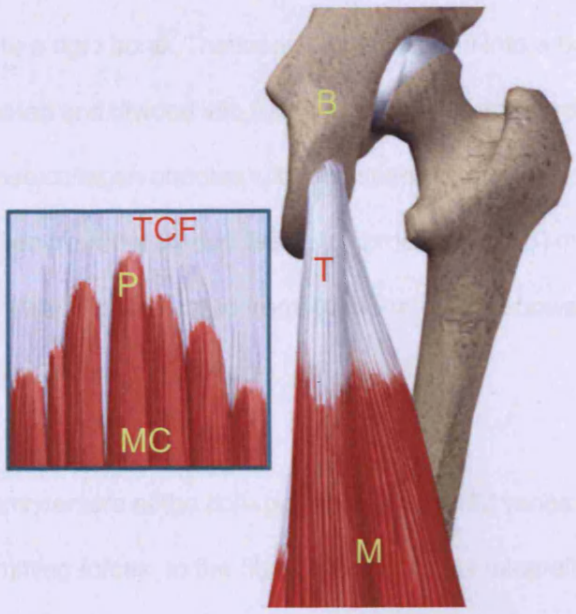

B – Bone
T – Tendon
TCF – Tendinous collagen fibrils
P – Muscle cell processus
M – Muscle
MC – Muscle cell

Fig. 2.3 The collagen fibrils insert into deep recesses that formed between the fingerlike processes of the muscle cells at myotendinous junction

(http://www.medicalmultimediagroup.com/)

It is very likely that the various glycoproteins and glycosaminoglycans found at the MTJ have a joint function in helping to transmit the forces between the muscle-cell membrane and tendinous collagen fibrils. The high concentration of these polysaccharides in the myotendinous interface possibly increase the adhesive forces between the two structures (the glue effect) and therefore may be important in improving the elastic buffer capacity of the MTJ against loading. Chondroitin and dermatan sulfates especially may possess this adhesive function (Trotter et al. 1983).

Despite the membrane folding specific macromolecular composition, the MTJ is the weakest point in the muscle-tendon unit, making it susceptible to strain injuries (Nikolaou et al. 1987). Thus, this area is clinically very important and of special interest in tendon pathology.

The osteotendinous junction (OTJ) is a specialized region in the muscle-tendon unit where the tendon inserts into a bone (Fig. 2.1). In the OTJ, the viscoelastic tendon transmits the

force to a rigid bone. The insertion of a tendon into a bone was first comprehensively presented and divided into four light-microscopic zones (Becker 1971): (1) tendon, consisting of dense collagen bundles with interspersed, elongated tenoblasts; (2) fibrocartilage, the transition from the tendon tissue to fibrocartilage; (3) mineralized fibrocartilage, where the fibrocartilage is separated from; (4) bone, which shows no special features that would separate it from normal bone.

The architecture of the collagen fibre of the OTJ varies considerably with the directions of the transmitting forces. In the fibrocartilage and its mineralized counterpart, the fibres crisscross around the chondrocytes (Becker 1978). The real functional behavior of the OTJ under various loading conditions in vivo is not clear.

2.1.6 Blood supply of tendons

As a general rule, tendons have a vascular supply that is considerably less than that of the more metabolically active muscles with which they are associated. This is why fresh tendons are white and muscles are red. Nevertheless, contrary to the view of early anatomists, tendons are still vascularized, and the presence of vessels is important for the normal functioning of tendon cells and the ability of tendons to repair (Benjamin et al. 2008). The blood flow within the tendon itself and in the muscle belly of gastrocnemius remains at a lower level for an extended period of time after tenotomy and this may inhibit repair. It is also commonly argued that reduced tendon blood supply can lead to tendon degeneration, particularly in association with certain tendons that have avascular or poorly vascularized regions, for example the Achilles tendon, tibialis posterior and supraspinatus (Rees et al. 2006).

The tendons receive their blood supply from three sites: (1) from vessels coming from the muscle, (2) from vessels coming from the bone and periosteum surrounding the OTJ, and (3)

especially from the vessels that surround the tendon (paratenon, mesotenon, and synovial sheath) (Fig. 2.4) (Carr and Norris 1989).

The major blood supply to the tendon is provided through vessels surrounding the tendon and that the tendon cannot receive the entire circulation required from its proximal or distal attachments (Archambault et al. 1995). In the Achilles tendon, for example, a zone of relative avascularity has been demonstrated at between 2 and 6cm proximal to the tendon insertion. At the MTJ, the connective blood vessels of the muscle continue between the fascicule of the tendon and are of the same size as its vessels elsewhere.

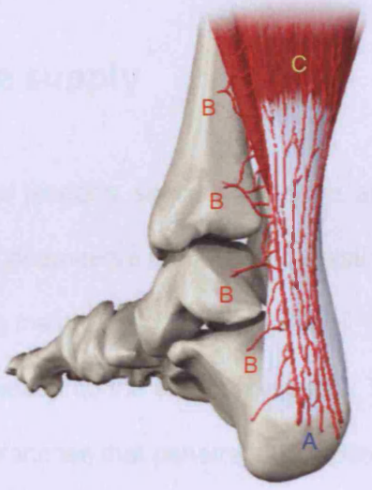

A – Osteotendinous junction (OTJ)
B – Mesotenon
C – Myotendinous junction (MTJ)

Fig. 2.4 Tendon receives blood supply from three sites
(http://images.conquestchronicles.com/images/admin/foot_achilles_tendon_anatomy01a.jpg)

Other small vessels enter by the paratenon, branching several times in the long axis of the tendon, and where there is a synovial sheath, a plexus traverses the mesotenon or vinculum (Elliott 1965). It has been stated that the OTJ is not an important site of entry (Edwards 1946).

There is evidence that blood flow in the peritendinous tissues is increased as a result of enhanced physical activity, and tissues adjacent to tendons, including tendon sheaths and tendon-associated adipose tissue, have a richer blood supply than then tendons themselves.

The vessels run longitudinally in the tendon itself, parallel to the fascicles and within the endotenon. Numerous vessels enter tendons at their MTJ and some vascular injection studies suggested that this is also the case at entheses. Furthermore, there is clear histological evidence of little vascular continuity between bone and tendon (Benjamin et al. 2007).

The venous network of tendons is composed of venules and veins that usually, in pairs, follow the arteries and their branches. Outside the tendon belly, the venous blood is collected into the venous network of the peritendinous tissues (Laszlo G. Jozsa 1997).

2.1.7 Nerve supply

The innervation of tendons, sensory by nature, as deriving from neighbouring muscular, peritendinous, or deep nerve trunks and consisting of a longitudinal plexus with the various terminations lying mainly near the MTJ (Stilwell 1957). Those from the MTJ cross the junction and continue into the endotenon septa. Those from the paratenon form rich plexuses, send branches that penetrate the epitenon, and anastomose with the branches of muscular origin (Ippolito et al. 1980). Where the tendon has a synovial sheath, the nerves go through the mesotenon, branch out into the visceral sheet of the synovial sheath, and then penetrate into the tendon. Many of the nerve fibres do not go inside the tendon but terminate in the sensory nerve endings on the surface of the tendon.

The nerves inside a tendon, which are very few in number, follow the vascular channels that run along the long axis of the tendon, anastomose with each other via obliquely and transversely oriented nerve fibres, and finally terminate in the sensory nerve endings.

It has been suggested that the nerve fibres regulate blood flow within the tendon (Ackermann et al. 2001). Further, free nerve fibres containing substance P and calcitonin gene-related

peptide (CGRP) might be involved in collecting sensory information (including pain) and relaying this to the central nervous system (Ackermann et al. 2001).

The sensory innervations of tendons is of particular interest in relation to tendinopathies and the repair of ruptured tendons (Benjamin et al. 2008). There is now considerable evidence that nerves can grow into damaged or ruptured tendons in association with blood vessels and that the site where this happens correlates with the region of tendon pain (Alfredson and Lorentzon 2007). The neurovascular invasion of damaged tendon tissue has led to an interest in the use of sclerosing agents for treating painful tendons (Hoksrud et al. 2006; Alfredson and Lorentzon 2007) and to the development of training programmes that can reduce tendon neovascularization.

2.2 Tendon Function and Mechanical Behavior

2.2.1 Function

Tendons have been traditionally considered to simply be a mechanism by which muscles connect to bone, functioning simply to transmit forces, thus making joint and limb movement possible (Kannus 2000; Magnusson et al. 2008). It is also well known that tendons are not inextensible, but that they exhibit important elastic and time-dependant characteristics that may influence the function of the overall muscle–tendon complex (Magnusson et al. 2008). In other words, tendons transmit loads with minimal energy loss and deformation. The greater the force generated by muscle is, the greater the stress transmitted through the tendon (Buchanan and Marsh 2002).

Muscle-tendon interactions have been explored during skeletal loading and describe the relation of sarcomere shortening at the expense of tendon lengthening (Lieber et al. 1992).

However, over the past two decades, many studies focused on the elastic properties of tendons and their ability to function as springs (Lieber et al. 1992), which allows tendons to passively modulate forces during locomotion, providing additional stability with no active work (Kannus 2000).

Tendon rotation, if present, plays an important role in tendon mechanics and function. The Achilles tendon, for example, twists as it descends. Rotation begins above the region where the soleus tends to join, and the degree of rotation is greater if there is minimal fusion (O'Brien 1992). In addition to transmit the force developed by a muscle, a tendon possesses certain secondary functions. For instance, the tendon eliminates the need for unnecessary length of muscle between origin and insertion, enabling the muscle belly to be at a convenient distance from the joint over which it acts while concentrating its pull (Elliott 1965). Furthermore, tendons also satisfy both kinematic and damping requirements (TM Best 1994).

2.2.2 Mechanical properties

The mechanical properties of the tendon are dependent on the collagen fibre diameter and orientation. The collagen fibrils are parallel to each other and closely packed, but show a wave-like appearance due to planar undulations, or crimps, on a scale of several micrometers (Hulmes 2002). In tendons, the collagen I fibres have some flexibility due to the absence of hydroxyproline and proline residues at specific locations in the amino acid sequence, which allows the formation of other conformations such as bends or internal loops in the triple helix and results in the development of crimps (Silver et al. 2003). The crimps in the collagen fibrils allow the tendons to have some flexibility as well as a low compressive stiffness. In addition, because the tendon is a multi-stranded structure made up of many partially independent fibrils and fascicles, it does not behave as a single rod, and this property also contributes to its flexibility (Ker 2002).

One study (Butler et al. 1978) demonstrated a force-elongation curve (Fig. 2.5) which is a valuable tool for studying the mechanical properties of tendon.

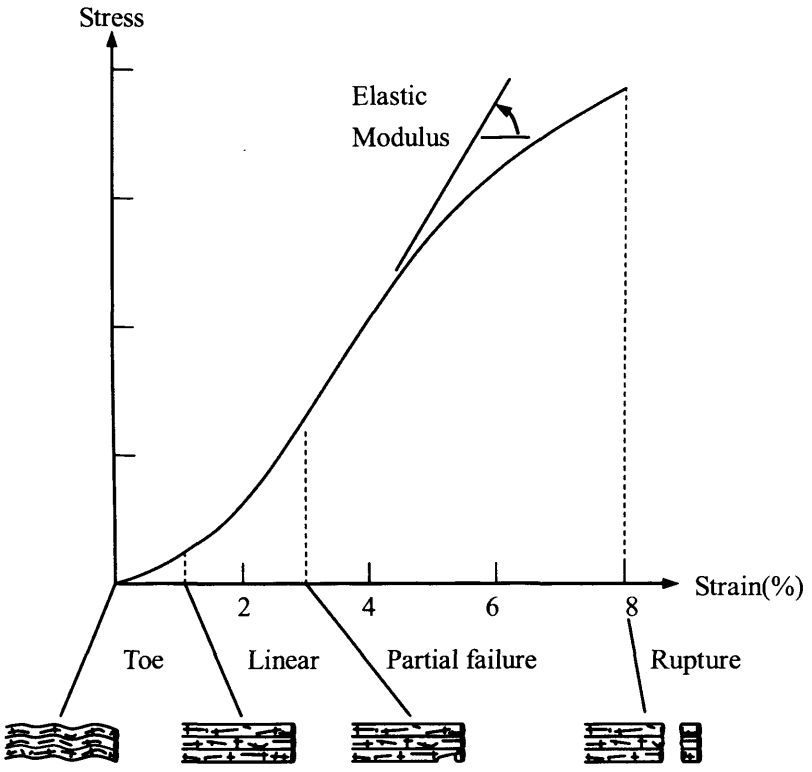

Fig. 2.5 Mechanical properties of tendon

(Butler et al. 1978)

2.3 The Anatomy of the Achilles Tendon

2.3.1 Introduction

The Achilles tendon is one of the longest and strongest tendons in the human body. It is the conjoined tendon of the gastrocnemius and the soleus muscles.

The Achilles tendon has the ability to adapt to mechanical loading with tensile loads up to ten times body weight during running, jumping, hopping, and skipping (Soma and Mandelbaum

1994). The Achilles tendon is subjected to stress when running up and down hill, particularly if there are associated biomechanical malalignments.

The Achilles tendon is one of the most frequently ruptured tendons in the human body. The rupture is thought to be associated with overuse and micro-injuries due to forces affecting the tendon during unsuitable physical activity (Hansen et al. 2003). But the physical activity is not the only cause of the Achilles tendon tendinopathy. The mechanism of tendinopathy is unclear.

2.3.2 Anatomy

The Achilles tendon is a confluence of the gastrocnemius and soleus muscles. The gastrocnemius muscle is composed of a medial and lateral head. The medial head arises from behind the medial supracondylar ridge and adductor tubercle on the posterior surface of the femur. The lateral head arises from the lateral surface of the lateral condyle of the femur, proximal and posterior to the lateral epicondyle. Each of these heads has additional attachments from the posterior capsule of the knee joint and from the oblique popliteal ligament (Cummins E.J. 1946). The soleus muscle lies deep to the gastrocnemius muscle, arising from the posterior surface of the upper tibia along the soleal line, the posterior aspect of the proximal third of the fibula, and from the inter-muscular septum (Schepsis et al. 2002).

The medial and lateral heads of the gastrocnemius muscle gradually coalesce and incorporate into a broad, robust tendon in the posterior aspect of the lower leg. This tendon gradually narrows and becomes more rounded as it extends distally. The soleus muscle forms a broad tendon about midway down the leg, in a position deep to the tendon of the gastrocnemius. This tendon glides freely deep to the gastrocnemius muscle in its more proximal extent, thereby allowing independent movement of the two muscles (Schepsis et al. 2002).

The tendinous components of these two muscles are variable. The gastrocnemius component is the longer potion, contributing 11 to 26 cm. the soleus, in contrast, is shorter, containing a tendinous component from 3 to 11 cm in length. The width of the tendon at its point of insertion into the calcaneus varies from 1.2 to 2.5 cm (Cummins E.J. 1946).

Approximately 5 to 6 cm proximal to the calcaneal insertion, the independent tendons of the gastrocnemius and soleus fuse to become one tendon. At about 12 to 15 cm proximal to the insertion of the tendon (Fig. 2.6), at about the level the soleus muscle begins to contribute fibres to the Achilles tendon is where rotation of the tendon begins. This rotation becomes more marked in the terminal 5 to 6 cm of the tendon. The tendon spirals approximately 90° with the medial fibres rotating posteriorly and the posterior fibres rotating laterally (Schepsis et al. 2002).

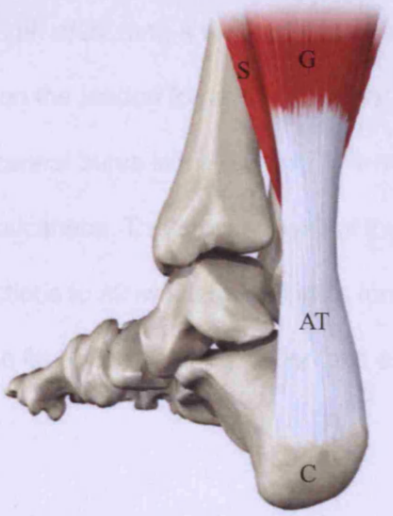

G – Gastrocnemius
S – Soleus
AT – Achilles tendon
C – Calcaneus

Fig. 2.6 Achilles tendon

(http://images.conquestchronicles.com/images/admin/foot_achilles_tendon_anatomy01a.jpg)

Some individuals exhibit a double spiral where the lateral head runs from the dorsal side, then comes ventral, and finally turns to the dorsal aspect. Rotation begins above the region where the soleus tends to join the gastrocnemius component, and the degree of rotation is

greater if there is minimal fusion. Twisting produces an area of stress within the tendon, which is most marked 2 cm to 5 cm above its calcaneal insertion. This is an area of poor vascularity, and is a common site of tendinopathy and rupture (Laszlo G. Jozsa 1997).

The insertion becomes broad distally and has a wide deltoid type of attachment, which varies from 1.2 cm to 2.5 cm (Schepsis et al. 2002). The deep surface of the inferior portion of the tendon above its attachment to the calcaneus has an area of fibrocartilage between the tendon and the upper part of calcaneus (Barfred 1971).

Deep and just proximal to the insertion is the retrocalcaneal bursa, which lies between the tuberosity on the posterior surface of the calcaneus and the Achilles tendon (Fig. 2.7). The bursa that is present at birth is a thick-walled, wedge-shaped sac. It has a horseshoe shape on cross-section; the arms extend distally on the medial and lateral edges of the tendon, with an average length of 22 mm, a width of 4 mm, and a depth of 8 mm. The area of fibro-cartilage on the tendon forms the posterior wall (Schepsis et al. 2002). The anterior wall of the retrocalcaneal bursa is the 0.5-mm to 1-mm thick cartilaginous layer on the posterior aspect of the calcaneus. The proximal wall of the synovial-lined sac consists of folds, or villus synovial projections to allow alterations in its form, that are produced by varying degrees of pressure on the fat above it during flexion and extension of the ankle (Snow et al. 1995).

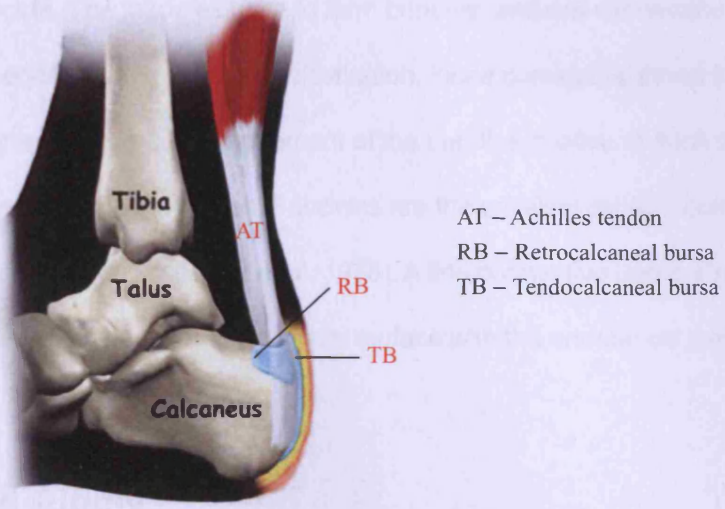

Fig. 2.7 Retrocalcaneal bursa and tendocalcaneal bursa

(http://www.eorthopod.com/sites/default/files/images/foot_achilles_tendon_treatment01.jpg)

The Achilles tendon is not encased in a true synovial sheath but is encased in a paratenon made up of a single layer of cells. This paratenon anteriorly consists of fatty, mesenteric-like areolar tissue. This tissue is richly vascularized and is responsible for a significant portion of the blood supply to the tendon (Carr and Norris 1989). This supply comes through a series of transverse vincula, which function as passageways for blood vessels to reach the tendon. In addition to these mesotenal vessels, the blood supply to the tendon comes from two other sources: the musculotendinous junction and the osseous insertion. Angiographic studies have shown that the area of most tenuous blood supply is 2 to 6 cm proximal to the insertion in the calcaneus (Clain and Baxter 1992). Additionally, the number of intratendinous vessels and the relative area occupied by these vessels is lowest 4 cm from the calcaneal insertion (Saltzman and Tearse 1998).

The Achilles tendon consists of typical parallel bundles of type I collagen (tropocollagen). The average size of the collagen fibres of the Achilles tendon is 60 μm. Collagen fibrils in the Achilles tendon vary from 30 nm to 130 nm in diameter, although most are between 50 nm and 90 nm in diameter. Collagen forms microfibrils, fibrils, and fibres. A group of fibres

constitutes a fascicle. The fascicles unite to form bundles, and are surrounded by the endotenon. The endotenon is a mesh of elastin-rich, loose connective tissue that holds the bundles together and allows some movement of the bundles relative to each other. It carries blood vessels, lymphatics, and nerves. Fascicles are the smallest collagenous structure that can be tested biomechanically (Butler et al. 1978). A fine connective tissue sheath, the epitenon, is continuous throughout on its inner surface with the endotenon and surrounds the whole tendon.

2.3.3 Blood supply

The Achilles tendon has long been known to be poorly vascularized, and the tendon was once considered to be avascular because of its pale colour and lack of visible blood vessels (Peacock 1959). The Achilles tendon is supplied by the peroneal artery laterally and the posterior tibial artery medially. Three vascular territories were identified: proximal section, midportion, and distal section (Fig. 2.8). The distal section of the tendon, comprising the insertion and up to the distal 4 cm of the tendon was found to be supplied by the posterior tibial artery (Chen et al. 2009). The midportion of the tendon, which is 4~7 cm from the insertion, was supplied by the peroneal artery. The proximal section of the tendon, 7 cm from the insertion up to the myotendinous junction, was also supplied by the posterior tibial artery.

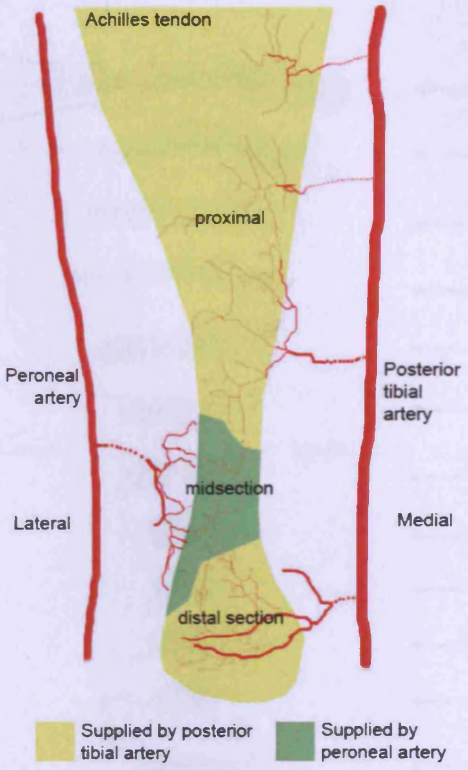

Fig. 2.8 The arterial anatomy of the Achilles tendon

(Chen et al. 2009)

Two areas of anastomosis were identified among the three territories. The proximal area of anastomosis was found between the proximal section and the midportion, whereas the distal area of anastomosis was found between the midportion and the distal section (Fig. 2.8). Both areas were found to be comparatively hypo-vascular on dissection and angiography, with fewer and smaller caliber vessels seen (Chen et al. 2009).

The Achilles tendon is mainly supplied by arteries from its anterior and deep surface, with branches either looping around or passing transverse through the tendon to gain access to its posterior superficial surface. The arteries on the anterior surface of the Achilles tendon were found to be larger and more numerous than the smaller posterior arteries, which contributed less to the tendon blood supply in all regions except for the tendon insertion (Fig. 2.9).

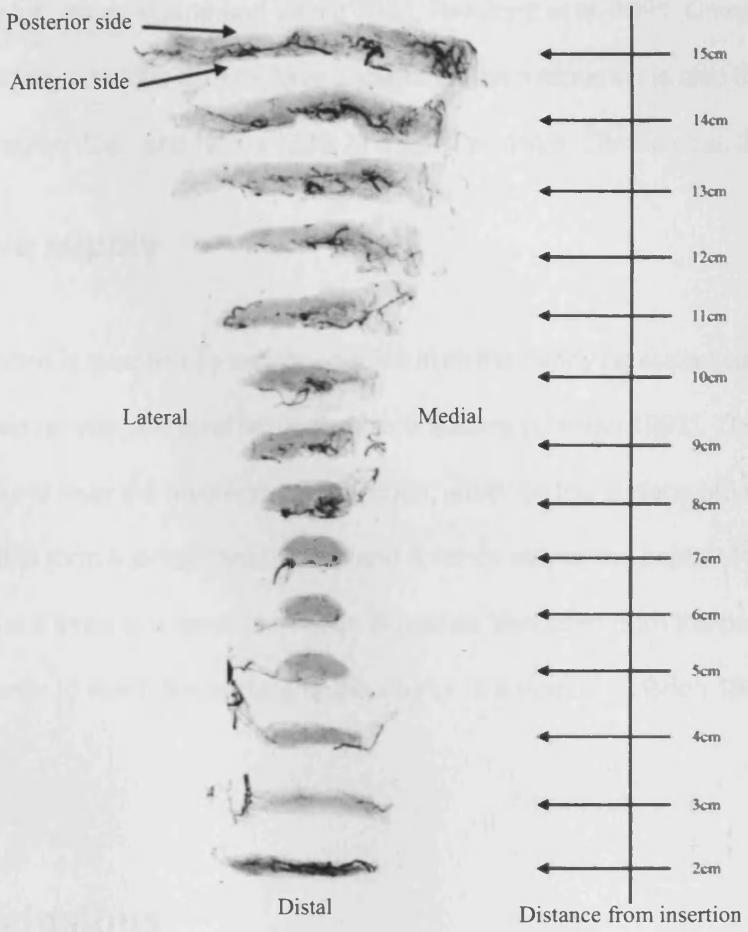

Fig. 2.9 Radiograph of the Achilles tendon cross section

(Chen et al. 2009)

The arteries of the Achilles tendon and its paratenon were orientated in three directions: longitudinal, transverse, deep. In most cases, the large arterial branches ran on the surface of the tendon transversely, in a direction perpendicular to the direction of tendon fibres. These large transverse vessels distributed numerous branches that ran longitudinally along the inter-fibrillar striations. The longitudinal vessels were also seen to run deep into the tendon between the tendon fibres. The Achilles tendon fibres spiral from medial to lateral, with the arteries running within the inter-fibrillar striation also seen to spiral in a medial to lateral direction (Chen et al. 2009).

Because it has the poorest blood supply, the midportion of the Achilles tendon is the most

common region for rupture (Laine and Vainio 1955; Reinherz et al. 1991; Campbell and Lawton 1993). Many previous studies have shown that the midportion is also the most hypo-vascular region (Carr and Norris 1989; Ahmed et al. 1998; Zantop et al. 2003).

2.3.4 Nerve supply

The Achilles tendon is supplied by sensory nerves from the overlying superficial nerves or from nearby deep nerves, the tibial nerve, and its branches (O'Brien 1992). The afferent receptors are found near the myotendinous junction, either on the surface or in the tendon. The nerves tend to form a longitudinal plexus and enter by way of the septa of the endotenon or the mesotenon if there is a synovial sheath. Branches also pass from the paratenon by way of the epitenon to reach the surface or the interior of a tendon (O'Brien 1992; Laszlo G. Jozsa 1997).

2.4 Conclusions

This chapter describes that tendons are anatomic structures interposed between muscles and bones transmitting the force created in the muscle to bone. They have less vascular supply indicated by their white colour. The Achilles tendon is subject to some of the highest loads in the body, and is the thickest and strongest tendon in the body. The tensile loads can be up to 10 times body weight during running, jumping, hopping and skipping. The Achilles tendon is considered to be poorly vascularized and is supplied by posterior tibial artery and peroneal arteries. The next chapter will focus on the injuries to the Achilles tendon.

3. Achilles Tendon Disorders

Achilles tendon disorders are common among athletes and the general public. The number and the incidence of tendon injuries, in general, have increased substantially during the last few decades. It has been reported that 30% to 50% of tendon injuries are related to sports (Jarvinen et al. 2005). Achilles tendon injuries have been divided into overuse injuries and spontaneous ruptures (Schepsis et al. 2002).

3.1 Overuse Injuries

3.1.1 Aetiology

Tendinopathy primarily affects active people, the more active they are, the greater chance of developing some tendon pathology and pain. Currently, very little is understood about the cause of tendinopathy. Experimental and clinical research is attempting to clarify aspects of the aetiology of pain and pathology but the relationship between them is unclear (Jarvinen et al. 2005).

The source of pain in tendinopathy is obscure. Although biochemical substances as a cause have been proposed (Ljung et al. 1999). Vascular and neural mechanisms have also been investigated (Ohberg L 2001); however, it is clear that research is still yet to resolve this clinically essential question (Zanetti et al. 2003). An unknown pain pathway compromises the understanding of the aetiology of symptoms, as both the stimulus for pain and its perpetuation are unknown. It is then certain that the treatment for tendon pain must also be unclear (Arnoczky 2007).

Understanding the relationship and interaction between factors and the pain in tendinopathy examined *in vitro* or in animal models is one of the key challenges in tendon research. Some factors, such as tendon load and vascular changes, are implicated in the aetiology of both pathology and pain and, as such, there must be a priority to investigate these factors (Arnoczky 2007). However, both tendon load and vascularity may be factors that are responsible for, and affected by, a cascade of smaller changes.

A study investigating 891 tendon ruptures demonstrated that although virtually all tendons were pathological prior to rupture, only 34% were painful (Kannus and Jozsa 1991). This study showed that tendon pathology is not always painful. In some further studies, examinations using imaging to study the tendon pathology in athletes have illustrated that pathology not only preceded symptoms in both the Achilles and patellar tendons, but abnormal tendons could remain pain free for years despite continued athletic activity (Khan et al. 1997; Cook et al. 2001; Fredberg and Bolvig 2002). This demonstrated that the aetiology of tendon pathology may be very different to tendon pain.

Although tendon pathology is considered primarily to occur in the tendon, most problematic tendon injuries occur at the OTJ (enthesis, Fig. 3.1). The Achilles tendon is clearly predisposed to develop midportion tendon pathology and more often enthesis pathology, but tendinopathies in athletes primarily occurs at the OTJ, or at sites of functional entheses (Benjamin and McGonagle 2001).

While most tendon disease in athletes occurs at the enthesis, the Achilles tendon suffers midportion tendon pathology more often than OTJ. This is due to the fact that the Achilles tendon is considered to be an energy storage tendon (Komi and Bosco 1978) and breakdown is not only influenced by its capacity to store energy, but also by the dimensions

of the tendon. Therefore, long tendons, like Achilles, appear more at risk of midportion tendinopathy and fatigue rupture than shorter, broader tendons (Ker 2002).

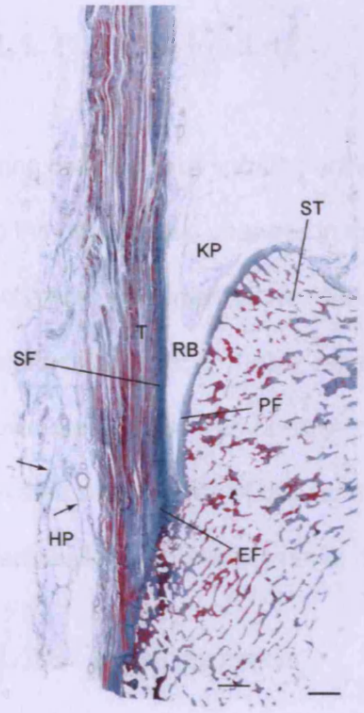

The enthesis organ of the adult Achilles tendon. The enthesis itself is characterised by an enthesis fibrocartilage (EF) which is most prominent in the superior part of the attachment. In addition, there is a sesamoid fibrocartilage (SF) in the deep surface of the tendon, immediately adjacent to the enthesis, and a corresponding periosteal fibrocartilage (PF) on the opposing surface of the superior tuberosity (ST) of the calcaneus. The tendon (T) and bone are separated by the retrocalcaneal bursa (RB) into which protrudes the tip of Kager's fat pad (KP). Note that the heel fat pad (HP) extends upwards from the sole of the foot to the posterior part of the Achilles tendon. Arrows, fibrous septa of the fat pad. Masson's trichrome. Scale bar: 2 mm

Fig. 3.1 The enthesis organ of the adult Achilles tendon

(Benjamin and McGonagle 2001)

The basic aetiology of the Achilles tendinopathy is known to be multi-factorial as discussed below:

3.1.1.1 Load

Overloading is often hypothesized to be the reason for the onset of pain and pathology. Traditionally, pathology is reported to be caused by repeated strain that is less than the force necessary to rupture (Arnoczky 2007). The strain is reported to disrupt collagen cross-links and fibrils and may damage blood vessels, resulting in impaired metabolic and oxygen delivery (Kannus and Natri 1997). Collagen tearing caused by tensile load has long been considered to be the primary event in tendinopathy. A study (Ker 2002) suggested that

tendon repair occurred after tendon load, and that collagen showed continued remodeling when collagen cross-links were investigated in human rotator cuff tendon, indicating regular, and continued matrix replacement.

3.1.1.2 Cyclic loading

During daily living or sporting activities the tendon tissue is subjected to repetitive loading and the consecutive changes in mechanical environment can significantly affect the mechanical properties of the tissue. While cyclic loading is known to be beneficial to tendon health (Hannafin et al. 1995), repetitive tissue strain has also been implicated in the aetiology of overuse injuries of tendons (Archambault et al. 1995). In tendon cells the cyclic strain activates a wide array of cellular machinery, including DNA synthesis, mitosis and cell differentiation (Almekinders et al. 1993).

3.1.1.3 Impingement

Tendon reaction to impingement may result in cartilaginous and bony pathology in tendons (Forslund and Aspenberg 2002), and this can cause tendinopathy. The shape of the calcaneus appears to affect the morphology of the Achilles tendon insertion and may be the result of anatomical impingement (Rufai et al. 1995).

3.1.1.4 Thermal

The storage and release of elastic energy in tendons discharges intratendinous heat. The resultant increase in tendon temperature after exercise may induce cell death (Wilson and Goodship 1994). Cell loss affects the tendons ability to respond to stress and remodel the matrix.

3.1.1.5 Hypoxia

Without defining the exact mechanism, hypoxia has been hypothesized as a cause of tendinopathy (Kannus and Natri 1997). Theoretically, cell disablement or death should be the main effect of hypoxia, with a consequent decrease or abolition of the capacity of the tendon to produce tendon matrix components and repair. The presence of hypoxia in tendon pathology is supported by the presence of increased lactate levels in Achilles tendinopathy compared with normal tendons (Alfredson et al. 2002). Increased lactate level suggests some anaerobic metabolism, which is used by tendon cells with a limited supply of oxygen.

3.1.1.6 Vascularity

It is believed that hypoxia is a powerful stimulant to angiogenesis. Alternatively, impaired vascularity may lead to hypoxia. Increased vascularity is the cornerstone of tendinopathy and has been demonstrated histopathologically (Kraushaar and Nirschl 1999), with imaging on Doppler ultrasound (Ohberg L 2001; Terslev et al. 2001), and with laser flowmetry (Astrom and Westlin 1994). In degenerative tendon disorders histopathologic findings and experimental findings revealed increased vascularity and increased blood flow (Kannus and Jozsa 1991). Neoangiogenesis controlled by a variety of mitogenic, chemotactic, or inhibitory peptides and lipid factors may be involved in beneficial but also in detrimental effects to tendon tissue (Ferrara 1999). One of the most important angiogenic factors is the vascular endothelial cell growth factor (VEGF). In degenerative tendons, neovascularization was accompanied by high VEGF levels (Pufe et al. 2001), this suggests that neovascularization may be a reaction to a hypoxic state. However, some pathologic tendons do not demonstrate increased vascularity on imaging (Peers et al. 2003; Zanetti et al. 2003), but few studies have examined both histopathology and vascularity demonstrated on imaging. It is unknown why some tendons react by notably increasing vascularity and why others do not.

3.1.1.7 Neural

The body of a tendon is poorly innervated. The MTJ and OTJ and the peritendon are well innervated. Nerve fibres in the tendon are associated with the vascular, lymphatic, and connective tissue channels, some of these nerve fibres have been reported to have direct contact with tendon collagen (Andres et al. 1985). Although sparse in sections, the nerve supply of the tendon may have important roles in the onset of pathology, pain production, and tendon repair.

3.1.1.8 Pharmacology

There are medications that are known to directly and adversely affect tendon tissue. These substances can induce tendon damage and can affect symptoms negatively or positively (Arnoczky 2007).

3.1.1.9 Blood group

Blood group has been reported to be associated with tendon rupture (Jozsa et al. 1989). The ABO antigens of blood groups are found in other tissues including tendons, and may affect tendon tissue.

3.1.1.10 Gender

Female gender is reported to increase the risk of tendinopathy due to strength, body composition, and biomechanical differences in women compared with men. Despite these reports, women are much less likely than men to present for either conservative or surgical treatment for tendon injury. This suggests that women suffer less tendinopathy than men (Kannus and Natri 1997).

3.1.1.11 Disease

Collagen disease such as Ehlers-Danlos syndrome, Marfan syndrome and Menkes kinky hair syndrome can directly affect tendons. Several other systemic and genetic diseases predispose the tendon to symptoms. Systemic lupus erythematosus and rheumatoid arthritis can be associated with tendon rupture, and glycogen storage disease has also been associated with Achilles tendinopathy (Arnoczky 2007).

3.1.1.12 Age

Aging has been associated with an increase in prevalence of tendinopathy, to a point where the thirtieth birthday has been described as a risk factor for tendinopathy. Exactly what constitutes old age for a tendon is not defined; however, the incidence of ruptures increases in middle age. This suggests that old age for tendon pathology may in fact be earlier than middle age, as pathology precedes rupture (Arnoczky 2007).

3.1.2 Epidemiology

Achilles tendon overuse injuries are associated commonly with strenuous physical activities, such as running and jumping (Laszlo G. Jozsa 1997; Paavola et al. 2002). The occurrence of Achilles tendinopathy is highest among individuals who participate in middle and long-distance running, orienteering, track and field, tennis, badminton, volleyball, and soccer (Kvist 1994). Studies reported an annual incidence of Achilles disorders to be between 7% and 9% in top-level runners (Lysholm and Wiklander 1987).

It has been extensively reported that the most common clinical diagnosis of Achilles disorders is tendinopathy (55% ~ 65%), followed by insertional problems (retrocalcaneal bursitis and insertional tendinopathy; 20% ~ 25%) (Kvist 1994). In a study of the epidemiology of Achilles tendon disorders in a large group (698 patients) of competitive and

recreational athletes who had Achilles tendon problems, 66% had Achilles tendinopathy and 23% had Achilles tendon insertional problems. In 8% of the patients, the injury was located at the MTJ, and 3% of the patients had 3 complete tendon rupture. 98% of the patients were men. Running was the main sports activity in patients who presented with an Achilles tendon disorder (53%); persons who were runners represented 27% of all patients who were studied in the sports medicine clinic where the research was performed (Kvist 1994).

Chronic Achilles tendon disorders are more common in older athletes than in young athletes (Kannus et al. 1989). In a report of 470 patients who had Achilles tendinopathy and insertional complaints, only 25% of subjects were young athletes and 10% were younger than 14 years (Kvist 1994). Patients who had unilateral Achilles tendinopathy seem to have a high risk of sustaining Achilles tendinopathy in the uninvolved leg as well, almost half of the patients who had the Achilles tendinopathy (41%) developed symptoms of this in the contralateral leg during the 8-year follow-up period (Paavola et al. 2000).

3.1.3 Paratendinopathy

The Achilles tendon is surrounded throughout its length by thin gliding membrances, the paratenon. The paratenon functions as an elastic sleeve, although probably not as effectively as a true tendon sheath, and permits free movement of the tendon within the surrounding tissues (Kannus and Jozsa 1991). Under the paratenon, the entire Achilles tendon is surrounded by a fine, smooth, connective tissue sheath, the epitenon. On its outer surface, the epitenon is in contact with the paratenon. The inner surface of the epitenon is continuous with the endotenon, which binds the collagen fibres and fibre bundles together and provides the neural, vascular, and lymphatic supply to the tendon (Laszlo G. Jozsa 1997).

The paratenon is richly vascularized and provides the blood supply to the Achilles tendon itself. The neural supply to the Achilles tendon and the surrounding paratenon is provided by

nerves from the attaching muscles and by small fascicule from cutaneous nerves, in particular the sural nerve (Stilwell 1957). In patients who have an Achilles tendon overuse injury, the sensory nerve endings follow the paratendinous neovascularization and may be a cause of Achilles tendon pain (Alfredson et al. 2003).

In the acute phase of Achilles paratendinopathy, inflammatory cell reaction, circulatory impairment, and oedema formation occur (Paavola et al. 2002). Crepitus, due to movement of the Achilles tendon within a paratenon that is filled with fibrin exudates, may be present. If the physiologic healing process fails or is delayed, the fibrin may organize and form adhesions that prohibit the normal gliding between the tendon, paratenon, and crural fascia (Kvist 1994).

In chronic Achilles paratendinopathy, the paratenon tissue becomes thickened as a result of fibrinous exudates; prominent and widespread proliferation of fibroblasts; formation of new connective tissue; and adhesions between tendon, paratenon, and crural fascia (Kvist et al. 1985).

Ultrasonography is a reliable diagnostic method for Achilles paratendinopathy if adhesions can be seen around an Achilles tendon. However, US may fail to detect adhesions and produce false negative results in patients who have few adhesions (Laine et al. 1987). In acute Achilles paratendinopathy, Ultrasonography reveals fluid surrounding the tendon, whereas paratendinous adhesions can be seen as a thickening of the hypoechoic paratenon with poorly-defined borders in the chronic form of the disorder (yellow arrows in Fig. 3.2).

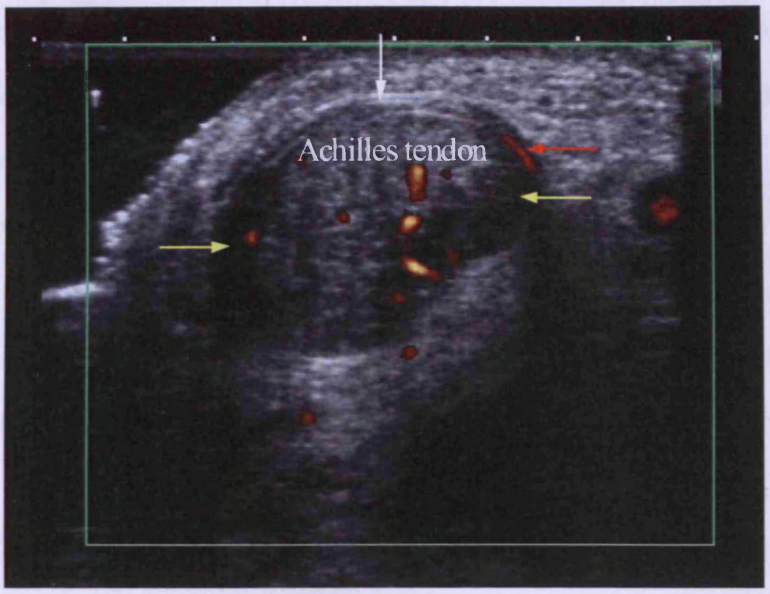

Fig. 3.2 PDU image of chronic paratendinopathy

MRI has been used extensively to visualize tendon pathology (Pope 1992). However, in patients who have pure chronic Achilles paratendinopathy (without tendinopathy of the main body of the Achilles tendon), MRI infrequently reveals any pathologic changes around the tendon (Paavola and Jarvinen 2005).

3.1.4 Midportion tendinopathy

Chronic tendinopathy of the main body of the Achilles tendon is a condition associated with a combination of tendon pain, swelling, and impaired performance ability. Chronic tendinopathy has been described as a condition with symptoms that last longer than 6 weeks (Maffulli and Kader 2002). Excessive loading of the Achilles tendon during athletic activities and work is regarded as the main pathologic stimulus that leads to tendinopathy (Vora et al. 2005). This is possibly as a result of an imbalance between muscle power and tendon elasticity.

Mild Achilles tendinopathy presents as pain in a region 2 to 6 cm proximal to the tendon insertion usually after exercise, namely midportion tendinopathy. As the condition progresses,

pain may occur during exercise, and, in severe cases, the pain interferes with activities of daily living (Vora et al. 2005). Changes in training pattern, poor technique, previous lower extremity injuries, footwear and environmental factors such as training on hard, slippery or slanting surfaces are extrinsic factors which may also predispose the athlete to Achilles tendinopathy (Kvist 1994). Several studies have confirmed the occurrence of sensory neuropeptides in both animal and human tendons, and Substance P (SP) has been found in Achilles tendinopathy (Khan et al. 2000), which is thought to be the cause of pain.

In the acute phase, the tendon is diffusely swollen and oedematous, and on palpation the tenderness is usually greatest in the midportion. Crepitation can also be found in paratendinopathy. In chronic cases, an exercise-induced pain is still the cardinal symptom, but crepitation and oedema diminish. Eventually the tendon becomes thick, firm, and nodular (Maffulli et al. 2003).

Most of the studies agree that the ultrasonography diagnosis correlates quite well with clinical findings (Zanetti et al. 2003; de Vos et al. 2007a; Richards et al. 2008). Conventional ultrasound was used as a primary imaging method to investigate the neovascularization both in transverse and longitudinal planes (Fig. 3.3). Thickening of the midportion Achilles tendon and Doppler signals are detected easily with this method.

(a) Transverse PDU image

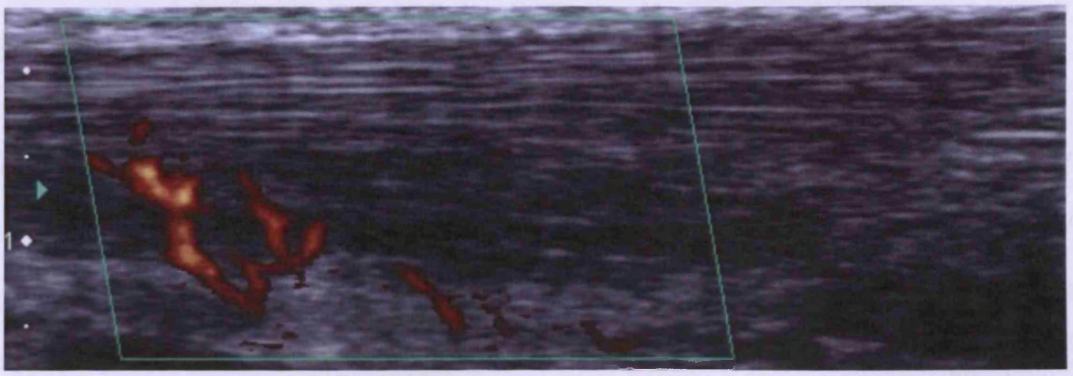

(b) Longitudinal PDU image

Fig. 3.3 PDU images of midportion tendinopathy

One report concluded that in normal Achilles tendons, blood flow was not detectable on CDU, but colour Doppler often reveals blood flow in pathological tendons (Ohberg L 2001). This blood flow was linked to greater pain scores, poorer function and long standing symptoms of the Achilles tendon (Peers et al. 2003), compared with control participants who had no visible flow. However, the long-term clinical importance of blood vessels in a pathological tendon is not clear, especially as more refined examinations also demonstrated vascularization in non-tendinopathic Achilles tendon (Boesen et al. 2006b; van Snellenberg et al. 2007). One study detected arteries in all normal tendons with Doppler after contrast injection (Koenig et al. 2007).

MRI is also a helpful diagnostic way to provide extensive information on the internal morphology of tendons and its surrounding structures, and is useful in evaluating various stages of chronic degeneration and in differentiating between peritendinitis and tendinosis. Areas with increased signal intensity seen on MRI correspond to areas of altered collagen fibre structure and increased inter-fibrillar ground substance. Signal intensity on MRI has also been associated with clinical outcome (Gardin et al. 2006).

3.1.5 Retrocalcaneal bursitis

The retrocalcaneal bursa is a significant structure that is horseshoe-shaped and measured 4 mm in width and 8 mm in depth (Schepsis et al. 2002). It is a distinct entity hallmarked by pain that is anterior to the Achilles tendon and just superior to its insertion. The retrocalcaneal bursa, which lies between the anterior aspect of the tendon and posterior aspect of the calcaneus, becomes inflamed, hypertrophied, and adherent to the underlying tendon. This may be associated with a prominence of the posterosuperior angle of the calcaneus (Schepsis et al. 2002).

Compression of the bursa between the calcaneus and the Achilles tendon occurs every time the ankle is dorsiflexed, and in runners the repetitions are countless, particularly with uphill running where ankle dorsiflexion is increased. Thus, it is not surprising that long-distance runners who use uphill running as a training method frequently develop this clinical entity.

3.1.6 Insertional tendinopathy

The incidence of Achilles insertional tendinopathy is not well established. It was reported as the most common form of Achilles tendinopathy in athletes who presented to an outpatient clinic (Laszlo G. Jozsa 1997). Conversely, 5% to 20% of the Achilles tendinopathies were of the insertional variety (Krishna Sayana and Maffulli 2005). Insertional tendinopathy often is diagnosed in older, less athletic, overweight individuals, and in older athletes.

The insertion of the Achilles tendon, the posterior aspect of the calcaneus, the retrocalcaneal bursa, and the pretendinous bursa constitute the posterior aspect of the heel. The enthesis, the bursa, and the bursal walls form a complex insertional region that protects the Achilles tendon and the posterior aspect of the heel (Krishna Sayana and Maffulli 2005).

Achilles insertional tendinopathy is characterized by early morning stiffness, pain that is localized at the insertion of the Achilles tendon that worsens after exercise, climbing stairs, running on hard surfaces, or heel running. The pain may become constant. There may also be a history of recent increase in training, and poor warm-up or stretching habits. Examination reveals tenderness at the Achilles tendon insertion, thickening or nodularity of the insertion, and limited dorsiflexion of the ankle (Krishna Sayana and Maffulli 2005).

3.1.7 Conservative treatment

Little reliable experimental or clinical scientific work has been performed on the pathophysiology, aetiology, natural course, and management of Achilles tendon overuse injuries (Paavola et al. 2002). Without scientific backing and a firm understanding of the nature of tendon injuries and other tendon disorders, it is difficult to prescribe a proper management regimen for Achilles tendon problems. Conservative and surgical regimens vary considerably among countries, clinics, and physicians. Most management regimens are based only on what seemed to work empirically, without much scientific support (Paavola et al. 2002).

3.1.7.1 Paratendinopathy

Various forms of conservative management are used. Initial nonoperative management aims to identify and correct the above described predisposing factors of the chronic Achilles tendon problems (Paavola and Jarvinen 2005). Although the use of nonsteroidal anti-inflammatory drugs (NSAIDs) did not affect the outcome of Achilles tendinopathy positively in a randomized clinical trial, they often are used for early management of pain from Achilles paratendinopathy (Sandmeier and Renstrom 1997). Surgical management is recommended to those patients who do not respond adequately to 3 to 6 months of conservative management (Kvist 1994). In most studies, surgery for Achilles tendon overuse injury gave satisfactory results in 75% to 100% of patients; however, most of these reports

were retrospective and only in a few were the results based on objective evaluations. The few studies reported of the endoscopic-assisted surgical release of adhesions around the Achilles tendon showed promising preliminary results (Morag et al. 2003), and that the endoscopic technique may reduce early postoperative morbidity. No studies have compared different operative methods in the treatment of Achilles paratendinopathy (Paavola and Jarvinen 2005).

3.1.7.2 Midportion tendinopathy

Traditionally, nonsteroidal anti-inflammatory drugs again have been used in the early phase of midportion tendinopathy, and are prescribed occasionally for chronic Achilles tendinopathy (Vora et al. 2005). One study recently reported that, patients who had Achilles tendinopathy were managed with ultrasound-guided injection of a sclerosing agent (polidocanol) to decrease the neovascularization that was detected in chronic midportion Achilles tendinosis (Ohberg and Alfredson 2002). Ultrasound and colour Doppler studies have demonstrated the presence of neovascularization outside and inside the ventral tendon in areas of tendinopathy (Breidahl et al. 1998; Richards et al. 2001; Peers et al. 2003; Boesen et al. 2006a; de Vos et al. 2007a). Reports (Ohberg L 2001; Ohberg and Alfredson 2003) hypothesized that the neovascularization and the nerve fibres that are associated with neovessels mediate the pain that is associated with Achilles tendinopathy. Hence, by ablation of these neovessels, the underlying pathophysiologic condition is remedied with improvement in symptoms including less discomfort (Ohberg and Alfredson 2002). Physical therapy has been used extensively. Specific therapy protocols have focused on concentric strengthening, eccentric strengthening, stretching based protocols, and other management regimens with accompanying modalities. Of all of the modalities, heavy-load eccentric calf muscle training program was the only one tested in a scientific manner, with great efficacy in multiple studies (Alfredson 2003). These studies found that eccentric training is superior to concentric training in decreasing pain in chronic Achilles tendinopathy, with 81% to 89% of

patients report resolution of symptoms. The mechanism by which improvement occurs may be due to an alteration of the tendon's inherent tensile properties or by lengthening of the muscle-tendon unit with stretch.

3.1.7.3 Insertional tendinopathy

Conservative management produces an 85% to 95% success rate with treatment by rest, ice, modification of training, heel lift, and orthoses (Krishna Sayana and Maffulli 2005). In athletes, nonweight-bearing activities can help to maintain fitness until symptoms improve. Immobilization of the ankle in a below-knee wight-bearing cast or a walker boot can be counterproductive, although it was suggested as a treatment by some investigators (Krishna Sayana and Maffulli 2005). Tendon loading stimulates collagen fibre repair and remodeling. Therefore, complete rest of an injured tendon is not advisable. In addition, sclerosing therapy in insertional tendinopathy showed promising results in a pilot study (Ohberg and Alfredson 2003). Polidocanol was injected into local neovessels that were localized by ultrasound and colour Doppler. Eight of eleven patients experienced good pain relief, and seven of them had no neovascularization at a mean follow-up of 8 months.

3.2 Acute Rupture

3.2.1 Aetiology

Achilles tendon ruptures are relatively common. Although the Achilles tendon is the thickest and strongest tendon in the human body, it remains susceptible to injury. During the last two decades, the incidence of spontaneous ruptures has been rising (C. Niek van Dijk 2008), probably because of the increasing keep-fit culture. Approximately 75% of Achilles tendon ruptures occur during sports activities.

There is little agreement on the aetiology of spontaneous Achilles tendon ruptures. Inflammatory and autoimmune conditions, generically inherited collagen abnormalities, infectious diseases, and neurological conditions have been implicated in the aetiology of a spontaneous rupture (Movin et al. 2005). The blood flow in the tendon decreases with increasing age, and the Achilles tendon site typically prone to rupture is relatively avascular compared with the rest of the tendon. These site usually is the midportion, some 2 to 6, 4 to 7, or 3 to 5 cm proximal to the calcaneal insertion (Ahmed et al. 1998).

A report compared the histopathology of 397 Achilles tendon ruptures with 220 control tendons, using conventional and polarized light microscopy and scanning and transmission electron microscopy. A healthy structure was not found in any of the spontaneously ruptured tendons. However, only two thirds of the control tendons were structurally healthy. There were characteristic histopathologic patterns found in the spontaneously ruptured tendons. Most (97%) of the pathologic changes were degenerative, with hypoxic (45%), mucoid (19%), tendon-lipomatous (6%), and calcifying tendinopathy (3%), alone or in combination. These changes were also found in 31% of the control tendons (Kannus and Jozsa 1991).

The homeostasis of the extracellular matrix components, such as the fibrillar collagens and proteoglycans, may be affected and predispose to a rupture. Type I collagen accounts for 95% of collagen in normal tendons. This parallel arrangement imparts high tensile strength to the tendon (Movin et al. 2005). Ruptured tendons contain significantly greater proportions of type III collagen and reduced amounts type I collagen, together with significantly higher degrees of degeneration, than non-ruptured tendons. Type III collagen is less resistant to tensile forces and may predispose the tendon to spontaneous rupture (Movin et al. 2005).

Clinically painful tendinopathy is not a common etiological factor for complete Achilles tendon ruptures as most patients have no symptoms before rupture (Magnusson et al. 2002).

However, another study indicated that 5% of the 176 patients who presented with a rupture of the Achilles tendon had previous symptoms (Maffulli 1999). Although clinically painful tendinopathy seemingly is a risk factor, patients who had chronic Achilles tendinopathy in reported nonsurgical and surgical series had a long duration of symptoms without sustaining a rupture (Coutts et al. 2002). Conversely, at the time of Achilles tendon rupture, degeneration and necrosis was present in 47 of 50 and 42 of 50 of the contralateral asymptomatic Achilles tendons, respectively. Spontaneous rupture of the Achilles tendon seems to be preceded by widespread, bilateral damage of the tendon (Coutts et al. 2002). Simultaneous bilateral ruptures without preceding factors are rare, whereas subsequent ruptures on one side after the other have been reported in up to 6% of patients (Aroen et al. 2004).

The role of genetic background of the patient in Achilles tendon rupture is almost unknown. Adverse drug use, for example, local and systemic corticosteroids, fluoroquinolone antibiotics, are a risk factor for tendon ruptures (Fisher 2004). There is evidence of a relationship between ABO blood groups and spontaneous tendon ruptures. A strong association between blood group O and Achilles tendon rupture was identified in a large series of patients has been reported (Jozsa et al. 1989).

3.2.2 Epidemiology

Achilles tendon rupture usually occurs in middle-aged men who work in a white-collar profession and during sports activities (Moller et al. 2001). Another report showed an incidence curve with two peaks (Moller et al. 1996), a larger one in young or middle-aged individuals, and a smaller one in patients in their seventies.

The higher proportion of men suffering Achilles tendon rupture is evident in all studies, with a male to female ratio of between 2:1 and 12:1. This probably reflects the greater prevalence

of men who are involved in sports (Movin et al. 2005). Almost all studies report a dominance of left-sided Achilles tendon ruptures, 57% of 1823 Achilles tendon ruptures were left-sided, probably because of the greater prevalence of right-side-dominant individuals who push off with the left lower limb (Arndt 1976).

3.2.3 Diagnosis

Normally, patients presented with sudden intense pain in the distal portion of the Achilles tendon, and often state that something or somebody might have struck their heel. The immediate pain resolves quickly; but persistent weakness, poor balance, and altered gait are common (Movin et al. 2005). On clinical examination, a positive calf squeeze test and a gap in the Achilles tendon, most often 3 to 6 cm above the insertion on the calcaneus, is consistently found. In a surgical study of 303 patients, the average gap was found to be 4.8 cm proximal to the insertion (Krueger-Franke et al. 1995). The most striking sign is the inability to perform a single heel rise in patients with acute as well as chronic Achilles tendon ruptures.

Because the injury may be missed or misjudged by the patient or the doctor especially when sports participation is not involved, Achilles tendon ruptures are missed in diagnosis in up to 25% of patients (Ballas et al. 1998). Further difficulties in reaching the correct diagnosis may occur in elderly patients or if the patient consults a doctor some days after the injury.

The various clinical tests (and their statistic values) are listed in Table 3.1 (Maffulli 1998) and are sufficient for a diagnosis of acute rupture of the Achilles tendon. A more long-standing rupture may produce ambiguous clinical findings and may need to be confirmed by imaging. Real time high-resolution ultrasonography and MRI provide an adjunct to clinical diagnosis.

Table 3.1 Physical examination tests of tendon ruptures

Physical tests	Descriptions
Palpation	A gap in the Achilles tendon, most often 3 to 6 cm above the insertion in the calcaneus (sensitivity 0.73, specificity 0.89).
Single leg heel rise	The patient is asked to perform a single leg heel rise. If the patient is able to lift his or her heel against gravity, the Achilles tendon is not ruptured.
Calf squeeze test	Also known as the Simmond's or Thompson's test. The patient lies prone with both feet hanging from the examination table. The examiner squeezes the affected calf muscle; if the Achilles tendon is intact, the foot will plantarflex. If the Achilles tendon is ruptured, the foot will remain in the resting position, or only minimal plantarflexion will occur. On the affected side, the calf muscle should be squeezed at the level where the largest range of motion will be reached on the healthy side (sensitivity 0.96, specificity 0.93).
Knee flexion test	The patient lies prone, and is asked to flex both knee to 90°.during this movement, the position of both ankles is observed. An Achilles tendon rupture is diagnosed if the foot of the affected limb falls into neutral or dorsiflexion. If the tendon is intact, the foot will remain slightly plantarflexed (sensitivity 0.88, specificity 0.85).
Sphygmomanometer test	The patient lies prone with both feet extending the examination table. The ankle is passively plantarflexed; a sphygmomanometer cuff is placed halfway up the calf, and inflated to 100mmHg. Subsequently, the examiner dorsiflexes the ankle. No pressure rise will be seen if the tendon is

	ruptured. If the Achilles tendon is intact, however, a pressure rise of 35-60 mmHg is measured (sensitivity 0.78).
Needle test	The patient lies prone with both feet hanging from the examination table. Insert a needle 10 cm proximal to the calcaneal insertion of the Achilles tendon. With passive dorsiflexion of the foot, the hub of the needle will tilt rostrally when the Achilles tendon is intact.

High-frequency ultrasound probes improve resolution therefore the imaging capacity of the degenerative changes, but for a rupture a 5-7.5 MHz probe is sufficient (C. Niek van Dijk 2008). The tendon should be examined in both longitudinal and axial planes. An acute tendon rupture mostly appears as a focal lucency in the tendon, with a small amount of fluid in and surrounding the tendon. The frayed ends of the tendons can be detected, and they separate in dorsiflexion.

Ultrasound can be of additional value in localizing the tendon ends where surgery is planned. This might assist the surgical procedure when small incisions are used in case of where there is a large haematoma. The precise location of the tendon ends at a given position of flexion of the ankle should be noted in relation to the posterior-superior corner of the calcaneus (Deangelis et al. 2009).

3.2.4 Management

The goals of management of Achilles tendon ruptures are to minimize the morbidity of the injury, optimized rapid return to full function, and prevent complications (Movin et al. 2005). Several treatment methods and procedures have been described for the management of Achilles tendon rupture (Fig. 3.4). Despite the developments of the last decades, there is no consensus on the best way to heal Achilles tendon ruptures. The modalities of management

can be divided widely into surgical and nonsurgical treatments (Movin et al. 2005). The surgical treatment methods can be subdivided into open operative repair and percutaneous repair.

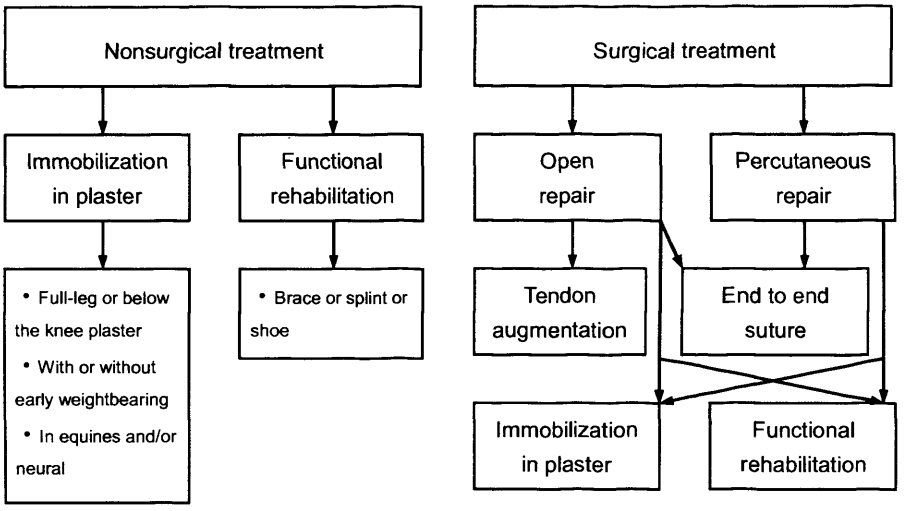

Fig. 3.4 Several treatment methods and procedures for the management of Achilles tendon rupture

3.2.4.1 Nonsurgical treatment

Immobilization in a below-knee plaster cast in a gravity equines position for four weeks is considered to be the most common management protocol. For a further four weeks after that, the limb is placed into a more neutral position (Worth et al. 2007). After a following 1 to 3 weeks of immobilization, braces, splints, or shoes with limitation of dorsiflexion and increased heel height have been used for functional rehabilitation (McComis et al. 1997).

3.2.4.2 Surgical treatment

The preferred method for early diagnosed ruptures has been simple end-to-end suture with Bunnell- or Kessler-type sutures placed 2 to 4 cm from the frayed tendon ends at the rupture site. Because of the reported sural nerve injuries and wound complications, many surgeons prefer a medial incision (Movin et al. 2005). End-to-end suturing can be performed under

local anesthesia, and the tendon can be sutured through a 6- to 8-cm long medial approach with low complications rates. Augmentation is reserved commonly for late-presenting ruptures, neglected cased, or reruptures. The augmentation is the second step of the operation and adds extra strength to the end-to-end suture (Movin et al. 2005). Percutaneous repair uses six stab incisions, three lateral and three medial to the Achilles tendon. A suture is criss-crossed through the tendon and tied on the tendon surface. Arthroscopy has been applied as an adjunct to percutaneous techniques to allow direct visualization of the sural nerve and rupture site (Halasi et al. 2003).

3.3 Shockwave Therapy

Extracorporeal shock wave therapy (ESWT) has emerged as a popular and effective treatment for many orthopedic conditions including plantar fasciitis, Achilles tendinopathy, lateral epicondylitis, calcific tendinitis of the shoulder, tendinosis of the supraspinatus tendon and patella tendinopathy (Rompe et al. 2007). Numerous clinical trials have shown that ESWT is safe, well tolerated, and yields few side effects. Significant complications are rare (Furia 2008). However, the treatment algorithms vary from clinic to clinic and from country to country. There are device-specific and disease-specific protocols. Terminology can be confusing. There are 'high energy' single treatments, 'low energy' multiple treatments, and combinations of both. Some devices use imaging to guide shock wave delivery while others rely on 'clinical focusing'. The treatment parameters such as the total amount of energy delivered, frequency of shock wave delivery, and method of focusing the shock wave have not been standardized. For that reason it is difficult to compare data from different clinical trials (Furia and Rompe 2007).

3.3.1 Principles

Shock waves are acoustic sound waves that propagate rapidly as a pressure disturbance

through a medium. Shock waves are characterized by a high peak pressure (500 bar) with rise times of less than 10 ns, a short life cycle (less than 10 ms), and a broad frequency spectrum (16-20 MHz) (Sems et al. 2006). The rapid rise in pressure is followed by periods of pressure dissipation and of negative pressure before gradually returning to ambient pressure.

Shock waves entering tissue may be absorbed, reflected, or dissipated depending upon the properties of the tissue (Seil et al. 2006). Shock waves have two basic effects on tissue, the direct or primary effect is the result of shock waves propagating through and impacting a direct mechanical effect on targeted tissues. The indirect or secondary effect is the result of cavitation. Shock wave propagation produces cavitation bubbles in targeted tissues. The cavitation bubbles expand and collide, thereby imparting additional energy to the treated tissue (Seil et al. 2006).

3.3.2 Physics

ESWT is traditionally categorized by low (<0.2 mJ/mm^2) and high (>0.2 mJ/mm^2) energy. Low-energy treatment is generally well tolerated, with mild to moderate discomfort and does not require anesthesia. High-energy applications are generally more painful and usually require some local or regional anesthesia (Furia and Rompe 2007). ESWT can be given in single or multiple treatment sessions. Single sessions usually are high energy and performed in either a surgical center or hospital. Multiple treatment sessions are commonly used in low energy treatments. These treatments typically occur in a clinic without the use of anesthesia.

The total amount of energy delivered in one session is simply a concentration of total shock wave energy per unit of area. The calculation of the total energy is the multiplication of the energy per pulse with the number of pulses given in one session. It is postulated that the threshold value of energy density has to be exceeded in order to stimulate a biological

response (Seil et al. 2006).

In our research, a patient was given low-energy ESWT, with the shock wave frequency of 8 Hz. The total number of shocks applied during each treatment session was 2000 impulses. The amount of energy per shock totaled 2.5 bar in all sessions.

3.3.3 Bio-effects

A portion of the energy is absorbed by the tissue, and a portion is reflected, when a shock wave hits a material with altered acoustic impedance (Seil et al. 2006). The ratio of the absorption to reflection varies depending on the specific tissue properties.

One report indicated that the ESWT altered neural activity. It was found that the number of afferent sensory fibres decreased significantly following shock wave applications (Ohtori et al. 2001), which suggested a neuroinhibitory effect of ESWT and helped to explain the clinically observed pain reduction in the treated patients.

In addition, the low-energy ESWT enhances angiogenesis. Another study reported on the effect of ESWT on neovascularization at the OTJ (in rabbits) (Wang et al. 2003). It found that tendons treated with low-energy ESWT had a higher number of neo-vessels and angiogenesis-related markers, including endothelial nitric oxide synthase, vessel endothelial growth factor and proliferating cell nuclear antigens than the untreated controls (Wang et al. 2003).

3.3.4 ESWT and neovascularization in Achilles tendon

In clinical application, ESWT has been shown to be effective in the treatment of Achilles tendinopathy. Despite the success in clinics, the exact mechanism of how ESWT affects Achilles tendinopathies remains unclear. It was speculated that ESWT produces

micro-fracture which in turn causes hematoma formation and subsequent callus formation and eventual fracture healing (Wang et al. 2003).

For tendinopathy, it was postulated that ESWT provokes a painful level of stimulation and relieves the pain due to tendinopathy at the osteotendinous junction by hyper-stimulation analgesia (Maier et al. 2002). Others have hypothesized the theoretical mechanism of ESWT in bone healing including micro-disruption of avascular or minimally vascular tissue to encourage revascularization and the recruitment of appropriate stem cells conclusive to more normal bone tissue healing (Wang et al. 2002b). The results of studies on dog Achilles tendon demonstrated that ESWT enhances neovascularization at the osteotendinous junction (Wang et al. 2002a).

Neovascularization is found to be close to the area of tendinopathy that corresponded to the pain in Achilles tendon. The result of a study (Wang et al. 2003) reported that ESWT induces in-growth of neo-vessels and tissue proliferation associated with the early release of angiogenesis-related factors including VEGF at the osteotendinous junction (in rabbits). The neovascularization may lead to improvement of blood supply and play a role in tissue regeneration at the osteotendinous junction.

In summary, ESWT appears to promote early release of angiogenic factors, and subsequently induce cell proliferation and in-growth of neo-vessels that in turn may stimulate stromal cell growth and differentiation.

3.4 Other Conservative Treatments

There are numerous different types of treatment used in the management of tendon disorders is summarized below. Unfortunately, few have a strong evidence base (Rees et al.

2006).

3.4.1 Non-steroidal anti-inflammatory drugs (NSAIDs)

NSAIDs are used as in the treatment of tendinopathy both in the acute and chronic situations. However, animal studies on the use of NSAIDs in tendon injuries have demonstrated conflicting results, with some studies suggesting increased tendon tensile strength whilst a primate study suggested a reduction in breaking point (Rees et al. 2006).

3.4.2 Cryotherapy

Particularly in sports, the use of cryotherapy in the treatment of acute injury of a tendon is widespread. Cryotherapy is believed to reduce blood flow and tendon metabolic rate and hence reduce swelling and inflammation in an acute injury (Hamilton and Purdam 2004). There is the potential benefit of analgesia, which may help explain the popularity of this treatment.

3.4.3 Manual therapy

There are several manual therapies popular in the treatment of tendon disorders. The two most common are friction massage and soft tissue mobilization.

3.4.4 Eccentric training

Eccentric training or 'loading' regimens have been popularized following successful randomized controlled trials in the treatment of Achilles tendinopathy (Alfredson et al. 1998). Both the initial results and a statistically significant reduction in tendon thickening (from 8.8 mm average to 7.6 mm average) were confirmed in the subsequent long-term follow-up study (Ohberg et al. 2004). Doppler examinations showed that neovascularization also resolved in the responders.

It has been proposed that possible explanations for the positive effects of eccentric training on tendinopathies might be either an effect of stretching, with a "lengthening" of the muscle-tendon unit and consequently less strain during ankle joint motion, or effects of loading within the muscle-tendon unit, with hypertrophy and increased tensile strength in the tendon (Stanish et al. 1986). Thus remodeling of the tendon is induced from eccentric training.

3.4.5 Sclerosant injection

The injection of a sclerosant agent around the neovascularization area in both midportion and insertional Achilles tendinopathy was found to effectively reduce the levels of pain (Ohberg and Alfredson 2002; Ohberg and Alfredson 2003), presumably due to the sclerosant injection being toxic to both the neovascularization and localized sensory nerves.

3.5 Clinical Evaluation

3.5.1 VISA-A questionnaire

Clinically, patients were evaluated using the Victorian Institute of Sport Assessment Achilles (VISA-A) questionnaire (Robinson et al. 2001), which is shown in the following pages. This questionnaire, specifically designed to serve as an index of severity of Achilles tendinopathy, contains eight questions measuring the domains of pain, function in daily living and sporting activity. Scores range from 0 to 100 points, with 100 points representing a perfect score.

VISA-A

A questionnaire based instrument that serves as an index of severity of Achilles tendinopathy

IN THIS QUESTIONNAIRE, THE TERM PAIN REFERS SPECIFICALLY TO PAIN IN THE ACHILLES TENDON REGION

1. For how many minutes do you have stiffness in the Achilles region on first getting up?

100 mins — 0 mins

0 1 2 3 4 5 6 7 8 9 10

Official use Points

2. Once you are warmed up for the day, do you have pain when stretching the Achilles tendon fully over the edge of a step? (keeping the knee straight)

Strong severe pain — No pain

0 1 2 3 4 5 6 7 8 9 10

Official use Points

3. After walking on flat ground for 30 minutes, do you have pain within the next 2 hours? (If unable to walk on flat ground for 30 minutes because of pain, score 0 for this question).

Strong severe pain — No pain

0 1 2 3 4 5 6 7 8 9 10

Official use Points

4. Do you have pain walking downstairs with a normal gait cycle?

Strong severe pain — No pain

0 1 2 3 4 5 6 7 8 9 10

Official use Points

5. Do you have pain during or immediately after doing 10 (single leg) heel raises from a flat surface?

Strong severe pain — No pain

0 1 2 3 4 5 6 7 8 9 10

Official use Points

6. How severe of your pain after 10 single leg hop?

Strong severe Pain/ unable — No pain

0 1 2 3 4 5 6 7 8 9 10

Official use Points ☐

7. Are you currently undertaking sport or other physical activity?

0	☐	Not at all
4	☐	Modified training ± modified competition
7	☐	Full training ± competition but not at same level as when symptoms began
10	☐	Competing at the same or higher level as when symptoms began symptoms began

Official use Points ☐

8. Please complete EITHER A, B or C in this question.

• If you have **no pain while undertaking sport** please complete **Q8a only**.

• If you have **pain while undertaking sport but it does not stop you from completing the activity**, please complete **Q8b only**.

• If you have **pain which stops you from completing sporting activities**, please complete **Q8c only**.

A. If you have no pain while undertaking sport, for how long can you train/practise?

NIL	1-10mins	11-20mins	21-30mins	>30mins
☐	☐	☐	☐	☐
0	7	14	21	30

Official use Points ☐

OR

B. If you have some pain while undertaking sport, but it does not stop you from completing your training/practice for how long can you train/practise?

NIL	1-10mins	11-20mins	21-30mins	>30mins
☐	☐	☐	☐	☐
0	4	10	14	20

Official use Points ☐

OR

C. If you have pain that stops you from completing your training/practice, for how long can you train/practise?

NIL	1-10mins	11-20mins	21-30mins	>30mins
☐	☐	☐	☐	☐
0	2	5	7	10

Official use Points ☐

*Signature:*_____

*Date:*_____

Official use

3.5.2 VAS assessment

A Visual Analogue Scale (VAS) is a measurement instrument that tries to measure a characteristic or attitude that is believed to range across a continuum of values and cannot easily be directly measured. For example, the amount of pain that a patient feels ranges across a continuum from none to an extreme amount of pain. From the patient's perspective this spectrum appears continuous - their pain does not take discrete jumps, as a categorization of none, mild, moderate and severe would suggest. It was to capture this idea of an underlying continuum that the VAS was devised.

Operationally a VAS is usually a horizontal line, 100 mm in length, anchored by word descriptors at each end, as illustrated in Fig. 3.5 below. The patient marks on the line the point that they feel represents their perception of their current state. The VAS score is determined by measuring in millimeters from the left hand end of the line to the point that the patient marks.

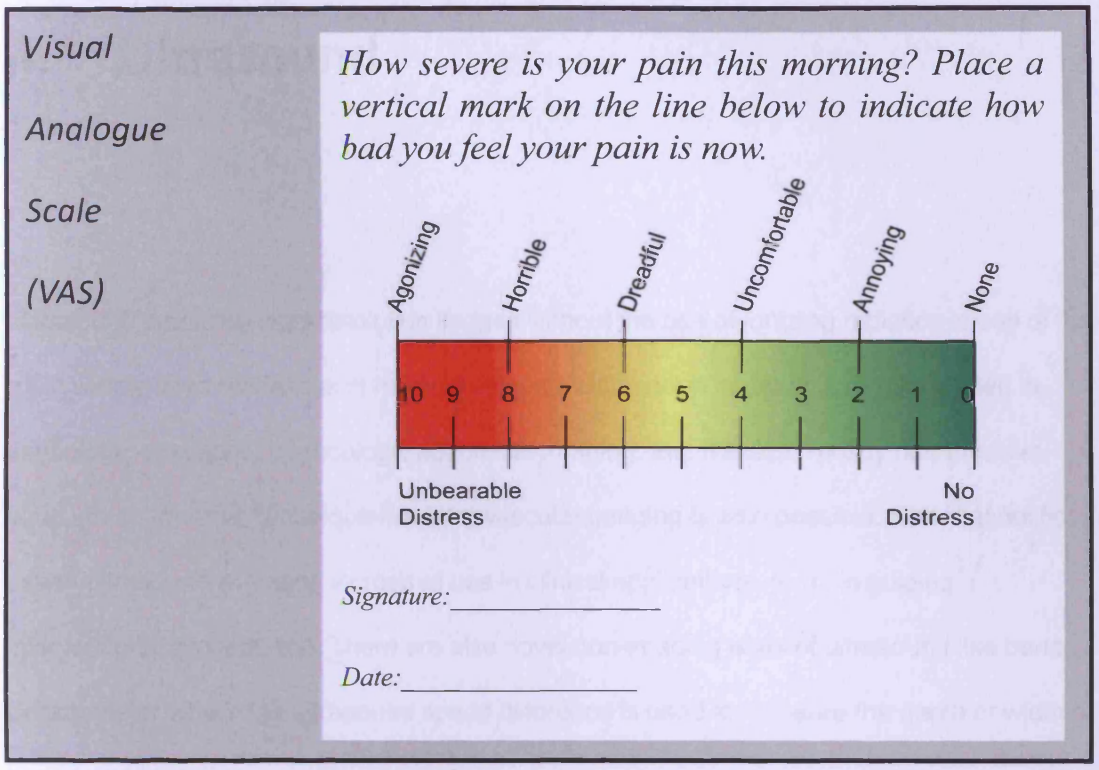

Fig. 3.5 Visual analog scale (VAS) example

3.6 Conclusions

Achilles tendon disorders are common found among athletes and the general public. Two-thirds of Achilles tendon injuries in competitive athletes are paratendinopathy and one-fifth are insertional complaints (bursitis and insertion tendinitis). As described in this chapter, the remaining afflictions consist of pain syndromes of the MTJ and tendinopathy. Achilles tendon injuries have been split into overuse injuries and spontaneous ruptures. Many factors contribute to the development of tendinopathy: extrinsic factors, such as training errors and environmental conditions, as well as intrinsic factors, such as malalignments, age, and gender. ESWT is considered to be an effective and safe treatment for Achilles tendinopathy. In order to obtain the undergoing condition of Achilles tendinopathy, VISA-A and VAS are commonly used to evaluate the clinical severity. The next chapter will focus on the fundamentals of ultrasound which is commonly used in the diagnosis of Achilles tendinopathy.

4. Ultrasound

Ultrasound providing high-resolution images without the use of ionizing radiation is one of the most widely used modalities in medical imaging. Ultrasound imaging is regularly used in cardiology, obstetrics, gynecology, abdominal imaging, etc. It is also mostly non-invasive, although an invasive technique like intra-vascular imaging is also possible. Non-diagnostic use of ultrasound is finding increased use in clinical applications, (e.g., in guiding interventional procedures). There are also novel non-imaging uses of ultrasound like bone densitometer where the ultrasound speed difference is used to measure the depth or width of bones non-invasively.

4.1 Basic Ultrasound Physics

4.1.1 Introduction

Sound waves above a frequency of 20 kHz are termed "ultrasound". Like all sound waves, ultrasound propagates through various media in the form of a pulsating pressure wave. Waves are basically of two types – longitudinal and transverse. Longitudinal waves are those in which particle motion is along the direction of propagation of the wave energy. Sound waves are longitudinal. Transverse waves are perpendicular to the direction of propagation of the wave energy (Hennerici and Neuerburg-Heusler 2006).

4.1.2 Properties of waves

When particle displacement is plotted against distance, the wavelength (λ) of a wave is the distance from crest to crest, or from trough to trough. A wave cycle is a sequence of changes

in the amplitude that recur at regular intervals. The frequency (*f*) of a wave is the number of cycles passing a given point in one unit of time (usually one second). The unit of frequency is the herts (Hz; one cycle per second).

The speed of wave propagation through a medium is known as the acoustic velocity, *c*. This speed depends on the density and compressibility of a medium to be present. In addition, the medium also has to be compressible-that is, it must be able to deform temporarily and then return back to its original shape (Fish 1990).

The speed of ultrasound:

$$c = \sqrt{\frac{K}{\rho}} \quad \text{m/s}$$

Where

ρ = density (kg/m^3)

K = elastic modulus (stiffness) = stress/strain (kgm^{-1}s^{-2})

4.1.3 Reflection

Ultrasound reflections occur when there is an interface between two media with differing levels of resistance to ultrasound. Such interfaces are known as "specular reflectors". Resistance to ultrasound is termed acoustic impedance. Acoustic impedance depends on the speed of ultrasound propagation in tissue and on the density of the tissue concerned. The greater the difference in impedance, the stronger the reflection. Mathematically, acoustic impedance (Z) is given by:

$$Z = \rho c$$

Where

ρ = density (kg/m^3)

c is the speed of ultrasound

Acoustic impedance is thus a measure of the resistance to sound passing through a medium. High density materials are associated with high sound velocities and therefore high acoustic impedances. Similarly, low density media such as gases have low acoustic impedances. It is not important which impedance is larger or smaller for two media forming an interface; the same reflection occurs whether sound is propagating from high impedance tissue to low impedance tissue or vice versa (Shutilov 1988).

4.1.4 Refraction

If a sound beam strikes an interface at an angle other than 90°, the part of the beam that is transmitted further is refracted or bent away from the straight path that would have been expected. This refraction takes place in accordance with Snell's law of optics, which relates the angle of transmission to the relative velocities of sound in the two media. Then bending occurs because the portion of the wavefront in the second medium travels at a different velocity compared with that in the first medium. As may be expected, the amount of deviation from the expected path changes with the angle of incidence and with the velocities in the associated media. If the velocity of sound is the same in both media, then there will be no refraction, even though there may be different acoustic impedances (Fish 1990).

4.1.5 Scattering

Tissue particles that are relatively small in relation to the wavelength (e.g., blood cells), and particles with differing impedance that lie very close to one another, cause scattering or speckling. Reflecting media that lie at an angle to the ultrasound propagation axis can only be recognized due to these scattering phenomena, which are accompanied by an attenuation in the echo intensity (Hennerici and Neuerburg-Heusler 2006).

4.1.6 Attenuation

The stronger the reflections are at the interfaces, the less ultrasound energy is available to reach deeper tissue. If a total reflection occurs at an interface to air, bone, or calcium-containing tissue, then an ultrasound shadow results. Most of the ultrasound energy is converted into kinetic energy within the tissue. The term attenuation characterizes the reduction in the amplitude of an ultrasound wave as it propagates through a medium, due to both scattering and absorption. Attenuation is described by an exponential function. The attenuation coefficient is given by:

$$\alpha = \frac{\Delta I}{I \Delta x} \quad m^{-1}$$

Where ΔI is the loss of intensity from incident intensity I during passage through a thin layer of thickness Δx and where $\Delta I / I$ <<1 (small change of intensity).

The coefficients quantitate the respective fractional loss in amplitude per unit length from absorption, scattering, and both processes together. The special unit used for these coefficients is the neper (Np) per centimeter. The attenuation coefficients at 1 MHz for various tissue types are shown as below (Fish 1990):

Table 4.1 Attenuation of various human tissues at 1 MHz

Tissue	Np/cm
Blood	0.021
Fat	0.069
Brain	0.098
Liver	0.103
Kidney	0.115
Skull bone	2.3
Lung	4.6

4.1.7 The Doppler effect

The flow velocity of corpuscular elements in the blood can be detected with ultrasound by using a principle named after Christian Andreas Doppler (1803-1852). When using this principle to investigate blood flow, it refers correspondingly to a change in frequency called the Doppler shift, f_d (Hz), which is proportional to the flow velocity of blood, V (cm/s), and to the transmission frequency of ultrasound, f_0 (MHz) (Hennerici and Neuerburg-Heusler 2006).

Exact measurement of the Doppler shift requires that the angle θ between the ultrasound beam and the longitudinal axis of the blood vessel is known:

$$f_d = \frac{-2Vf_0 \cos(\theta)}{c}$$

Where

V = scatterer velocity

f_0 = transmitted frequency

c = speed of ultrasound

θ = angle between the bisector of the transmitter and receiver beams and the direction of movement

When blood vessels are examined, the reflection caused by the blood's corpuscular elements, mainly erythrocytes, plays a major role. Since the flow velocity through the different areas of any given cross-section of a blood vessel varies, the Doppler signal itself does not correspond to a single frequency, but contains a broad frequency spectrum (Fish 1990).

4.2 Ultrasound Technology

4.2.1 Introduction

Ultrasound waves are produced by a vibrating crystal using a piezoelectric effect. This effect involves the characteristic that certain materials have of changing their form when subjected to an electric current – or vice versa, of producing an electric current due to changes in their form. These piezoelectric crystals are placed in a specific arrangement within the ultrasound probe.

In order to improve the acoustic coupling (impedance match), a gel is applied between the crystal and the surface of the skin.

4.2.2 A-mode and B-mode ultrasound

4.2.2.1 A-mode

A-mode (Amplitude) displays the amplitude of a sampled voltage signal for a single sound wave as a function of time. This mode is considered 1D and used to measure the distance between two objects by dividing the speed of sound by half of the measured time between the peaks in the A-mode plot, which represents the two objects in question. This mode is no longer used in ultrasound systems (Fish 1990).

4.2.2.2 B-mode

B-mode (Brightness) imaging is the same as A-mode, except that brightness is used to represent the amplitude of the sampled signal. B-mode imaging is performed by sweeping the transmitted sound wave over the plane to produce a 2D image. Typically, multiple sets of pulses are generated to produce sound waves for each scan line, each set of pulses are

intended for a unique focal point along the scan line (Murtaza Ali 2008).

4.2.3 Doppler systems

4.2.2.1 Continuous-wave Doppler ultrasound

Continuous-wave (CW) Doppler equipment uses two piezoelectric elements with overlapping ultrasound fields, which serve as the transmitter and the receiver (Fig. 4.1). The transmitter (T) is connected to an oscillator and transmits ultrasound continuously. The ultrasound reflected and scattered from tissue structures is picked up by the receiver (R) mounted in the same probe. The electrical output from this transducer is amplified and fed to the Doppler demodulator where it is mixed with a signal (the reference signal) from the transmitter oscillator (Fish 1990).

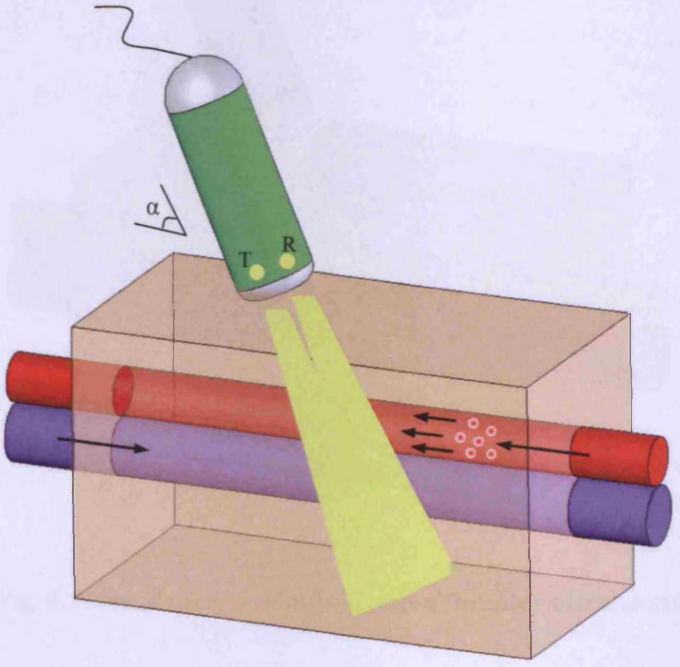

Fig. 4.1 The principle of continuous-wave Doppler ultrasound

Due to the continuous and simultaneous emission and reflection of ultrasound waves, no exact information about depth can be obtained with this equipment (Murtaza Ali 2008).

4.2.2.2 Pulsed-wave Doppler ultrasound

Pulsed-wave (PW) Doppler ultrasound is used to detect blood flow at a specifically defined depth. Using a single piezoelectric element, these systems function alternatingly as the transmitter and receiver (Fig. 4.2). The transducer is driven during transmission by a short burst of voltage from the oscillator when the timing circuits open the gate between the oscillator and the transducer. Ultrasound is backscattered to the receiving transducer, as CW Doppler, amplified and passed to the Doppler demodulator but in this case the output of the demodulator is not monitored continuously but sampled by opening a gate after a delay following the transmitter pulse (Fish 1990).

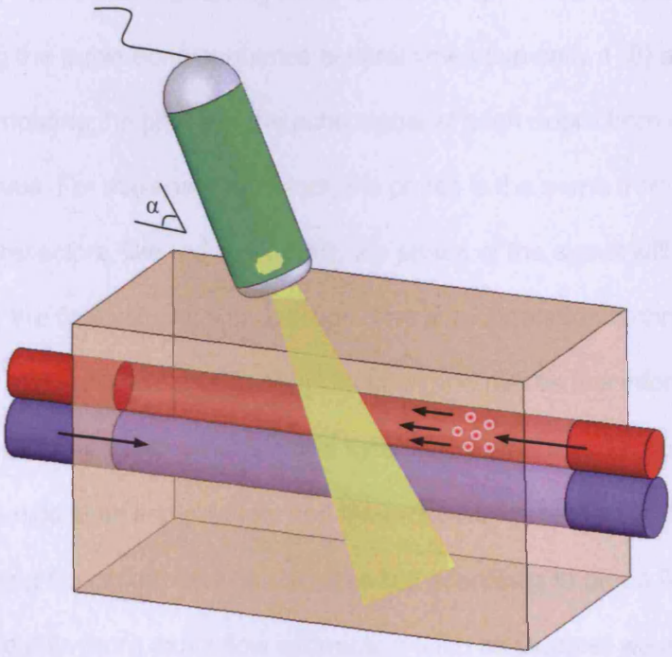

Fig. 4.2 The principle of pulsed-wave Doppler ultrasound

PW Doppler overcomes the range ambiguity inherent in CW Doppler. PW Doppler sends pulses of a certain length to a target at a certain range. The received pulses are dilated (or contracted) due to Doppler, and hence, the delay in the arrival of the pulse also provides velocity information. In CW Doppler, the received frequency is compared to the transmitted frequency but in PW Doppler each received echo is compared to a similar echo from a

previous transmission (Hennerici and Neuerburg-Heusler 2006).

4.2.4 Colour Doppler imaging

Grey-scale B-mode image with superimposed colour indicating blood-flow velocity and direction is termed colour Doppler ultrasound (CDU). Unlike PW Doppler techniques, which acquire Doppler signals at restricted predetermined depths only, CDU acquires Doppler information at multiple locations along each scan line, i.e. at each position of the ultrasound beam during scanning.

A commonly used method for measuring blood-flow velocity in CDU is autocorrelation, which involves repeating the pulse-echo-sequence several times (typically 4–8) along the same scan line, and comparing the phase of the echo signal at each depth from one pulse - echo sequence to the next. For stationary reflectors, the phase is the same from one echo to the next. For moving reflectors, like red blood cells, the phase of the signal will vary from echo to echo according to the flow velocity and direction. The autocorrelation technique estimates the mean velocity and variance at each depth location and places this information in a colour image memory, a process which provides data for a single scan line. The ultrasound beam is then moved to the next scan line position, and the procedure repeated. In the final image, each pixel containing flow information is colour-coded according to blood flow direction and mean velocity. To obtain more exact flow information such as Doppler wave form, maximum velocity, spectral broadening, resistance index etc., CDU must be combined with PW Doppler. Since CDU requires multiple pulse-echo sequences at each scan line, the scanning frame rate is lower than in standard B-mode imaging. To improve time resolution, the colour-coded field may be restricted to only a part of the entire image (Murtaza Ali 2008).

4.2.5 Power Doppler imaging

PDU is an option in CDU instruments, and just as in CDU, the Doppler signal is sampled at

multiple locations along each scan line. The technique differs from conventional CDU in the way the Doppler signals are processed; instead of estimating mean frequency and variance through autocorrelation, the integral of the power spectrum is estimated and colour coded. The colours in the PDU indicate only that blood flow is present; they contain no information on flow velocity (Murtaza Ali 2008).

The colour and brightness of the signals on PDU are related to the number of blood cells producing the Doppler shift. The greater sensitivity of PDU for detecting blood flow in comparison with CDU is due to several factors. Noise can be assigned to a homogeneous background, thus allowing the gain to be increased over the level of CDU. Moreover, in PDU more of the dynamic range of the Doppler signal can be used to increase sensitivity. PDU is also less angle-dependent than CDU, thus allowing better display of curving or tortuous vessels. Finally, relying on the Doppler amplitude means there is no aliasing; this improves the display of vessel wall pathology in areas of turbulent flow. Reports on the clinical value of power Doppler imaging have demonstrated distinct advantages with this technique in assessing the surface structures of atherosclerotic plaque (Griewing et al. 1996).

4.2.6 Transducer/Probe

There are three different types of images obtained by multi-element array transducers, i.e. linear, convex, and phased (Fig. 4.3). The linear array transducer selects the region of investigation by firing a set of elements situated over the region. The beam is moved over the imaging region by firing sets of contiguous elements. Focusing in transmission is achieved by delaying the excitation of the individual elements, so a concave beam shape is emitted.

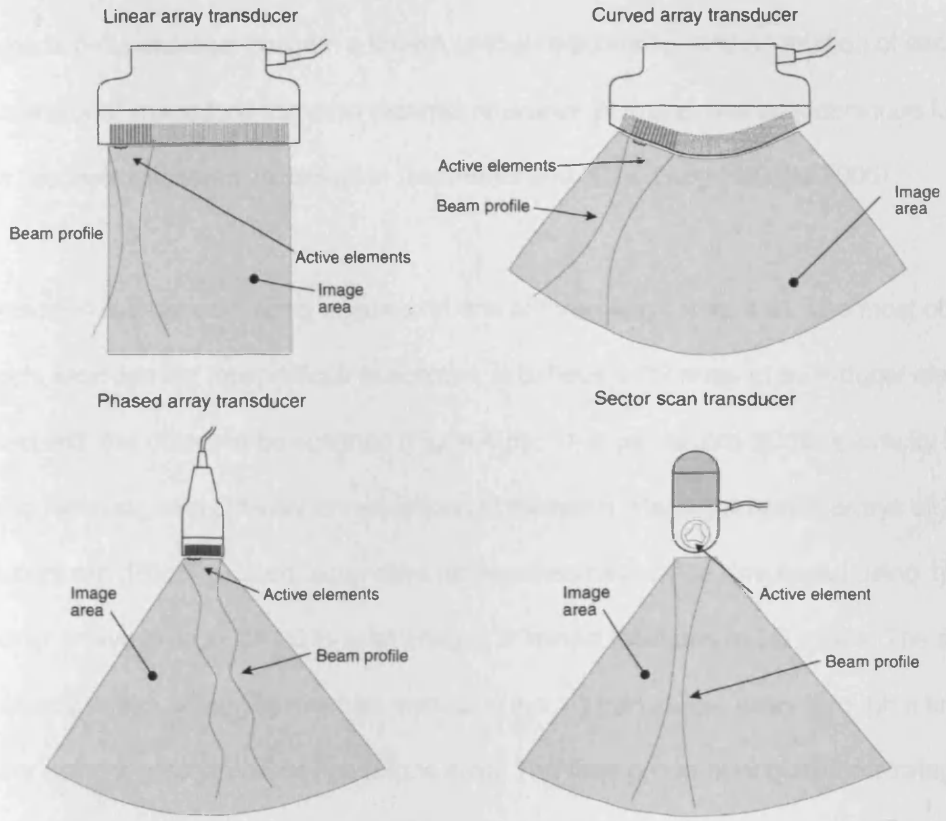

Fig. 4.3 Ultrasound transducers

The linear arrays acquire a rectangular image, and the arrays can be quite large to cover a sufficient ROI. A larger area can be scanned with a smaller array if the elements are placed on a convex surface as shown in Fig. 4.3. A sector scan is then obtained. The method of focusing and beam sweeping during transmission and reception is the same as for the linear array, and a substantial number of elements (often 128 or 256) is employed (Jensen 2007).

4.2.7 3D ultrasound

3D imaging with ultrasound was first described in 1956 for stereoscopic observation of body structure (Howry et al. 1956). This technique has been continuously developed in the last decades. It obtained serial parallel ultrasound images and then created a 3D display by stacking sequential photographic plates of the images. Although rapid developments in ultrasound scanning equipment and in computer hardware and software have occurred, the basic requirements of producing 3D ultrasonographic reconstructions have not changed:

adequate two-dimensional images, a known spatial relationship, and orientation of each two-dimensional image to a common external reference point, as well as techniques for volume reconstruction and visualization (Hennerici and Neuerburg-Heusler 2006).

3D ultrasound is most commonly acquired in one of three ways (Fig. 4.4). The most obvious approach, although the most difficult to achieve, is to have a 2D array of transducer elements in contact with the object to be scanned (Fig. 4.4(b)). This can record 3D data directly by firing and receiving with different combinations of elements. Because dense arrays of 2D transducers are difficult to build, alternative approaches have been developed using 1D transducer arrays to produce 2D B-scan images at known locations in 3D space. The second group of acquisition strategies involves sweeping the 1D transducer array through a known trajectory using a mechanical device (Fig. 4.4(a)). The third group of acquisition strategies involves letting the clinician sweep the 1D transducer array manually across the subject and using some sort of tracking device to measure its trajectory (Fig. 4.4(c)) (Prager et al. 2009).

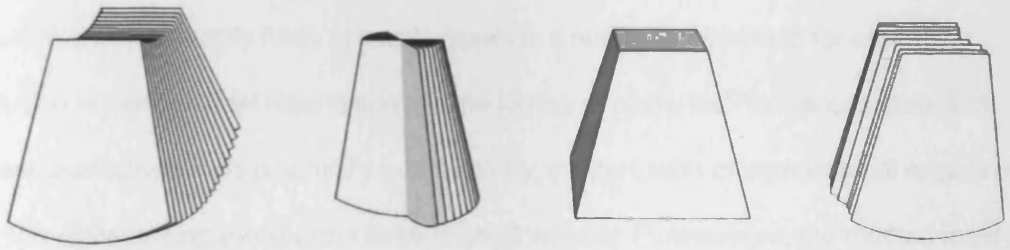

Fig. 4.4 3D ultrasonographic imaging acquisitions

There are some advantages offered by 3D US. Firstly, the 3D US contributes to eliminating operator dependence in the scanning process. 2D ultrasound requires the clinician to sweep the probe back and forth across the subject while mentally visualizing the anatomy from multiple 2D images. 3D, on the other hand, often requires only the acquisition of a single volume. Once this has been acquired it can be visualized using slices at any angle and a variety of measurements may be taken from it (Prager et al. 2009). Secondly, quantitative

estimates in 2D ultrasound are based on heuristic formulae with strong prior assumptions which are prone to error. 3D US provides a more accurate and repeatable way of evaluating anatomic structures and disease entities (Pauletzki et al. 1996).

4.2.8 3D power Doppler

Images of vascular anatomy can be produced using conventional angiography, computed tomography angiography, Doppler ultrasound or magnetic resonance angiography. Angiograms established using these techniques are clinically useful because they allow for the identification of stenoses and aneurysms (Ritchie et al. 1996). Each of these techniques can be applied to investigate the large (greater than 2 or 3 mm diameter) vessels in the head, neck, thorax, abdomen and extremities. Conventional angiography and Doppler ultrasound can also be used to image vessels with diameters on the order of 1 mm or smaller (Ritchie et al. 1996).

Visualizing lower velocity flows in small vessels is a necessary first step for assessing perfusion in parenchymal organs such as the kidney or placenta. The second step is to assess qualitatively, and potentially quantitatively, the perfusion of parenchymal organs by the way of visualizing low-velocity flows in small vessels. Furthermore, the method must also allow for visualization of flow throughout the volume of the organ. Conventional angiography meets these criteria; however, the techniques is invasive and complications are possible during catheterization, and the exposure of pregnant women and others to ionizing radiation should be avoided (Ritchie et al. 1996).

Doppler ultrasound, using transducer frequency from 3 to 12 MHz can resolve small vessels and is able to display low-velocity flows. Some investigators (Ritchie et al. 1996; Porter et al. 2001; Vlaisavljevic et al. 2003) described an ultrasonic angiography system that is able to create 3D images of parenchymal vasculature from 2D power-mode Doppler images. This

system allows for the imaging of low-velocity flows in small vessels.

3D PDU can be applied in all fields of medicine where quantification of vascularization, neovascularization or revascularization is of potential importance in clinical decision making (Schulten-Wijman et al. 2008). Several reports have used 3D PDU to create the visualization of blood flow in the carotid artery, the fetal heart, the breast, the kidney, the placenta, the prostate, the feto-placental vasculature, and the endometrial vasculature (Fenster and Downey 1996; Ritchie et al. 1996; Nelson and Pretorius 1998; Welsh et al. 2001; Mercé et al. 2006).

4.3 Conclusions

This chapter briefly introduced the physics and fundamentals of ultrasonography. Ultrasound imaging is a non-invasive, inexpensive tool used in cardiology, obstetrics, etc. Recently, B-mode ultrasound imaging and Doppler systems have been widely applied in daily diagnosis. 3D Doppler ultrasound can be used in quantifying the vascularization, which is prospectively used to measure the volume of the neovascularity in Achilles tendinopathy from chapter 6. The next chapter will describe the previous studies in the investigation of pain and neovascularization in Achilles tendinopathy, as well as the optimized machine settings we recommended.

5. Achilles Tendinopathy and Ultrasound

Ultrasonography, which is regarded as a readily available, quick, safe, and inexpensive test, has been widely used in the diagnosis of Achilles tendinopathy (Maffulli et al. 1987). The normal Achilles tendon should have an echogenic pattern of parallel fibrillar lines in the longitudinal plane and an echogenic round-to-ovoid shape in the transverse plane. The number of echogenic lines that is visible in the tendon with ultrasound is simply a correlate of the ultrasound probe frequency (Martinoli et al. 1993). Focal hypo-echogenic or diffuse thickening of the Achilles tendon is seen most commonly in association with tendinopathy (Astrom et al. 1996; Ohberg L 2001), the tendon thickness may range from 7 to 16 mm (Fornage 1986).

5.1 Achilles Tendon Neovascularization

5.1.1 Pain and neovascularization

The cause of pain in Achilles tendinopathy is thought to be related to the presence of neovascularization in the tendon as seen on colour and PDU. A research group suggested that all painful tendons demonstrate neovascularization (Ohberg L 2001; Ohberg and Alfredson 2002; Alfredson et al. 2003). When these neo-vessels are sclerosed, in a middle-aged population, the pain has been shown to be remarkably reduced in both a population with mid-tendon and a population with enthesis pain.

5.1.2 Neovascularization and Doppler ultrasound

Much attention has been given in assessing the distribution of neovascularization on colour

and PDU of the Achilles tendon in tendinopathy, and to look for any relationship between tendon morphology and symptoms (Boesen et al. 2006a; de Vos et al. 2007a; Knobloch 2008).

Power Doppler, unlike colour Doppler, is not dependent on the probe being directionally aligned to the flow and therefore will identify all flow independent of velocity, theoretically improving sensitivity over colour Doppler (Rubin et al. 1994). In vitro validation found power Doppler up to 4 times more sensitive than colour Doppler for the detection of micro-vessels with flow detection in tubes as small as 0.3 mm, where flow may sludge and no flow is seen on colour Doppler (Weskott 1997).

With the use of PDU, a retrospective observational study (Richards et al. 2005) suggested a non-linear relationship between the number of vessels seen on power Doppler and Achilles tendon size. They also conclude the following: (1) power Doppler shows more tendon microvascularity than colour Doppler in Achilles tendinopathy; (2) all micro-vessels arise on the ventral side of the Achilles tendon; (3) there is a nonlinear relationship between tendinopathy, Achilles tendon size, and the amount of microvascularity, but not between power Doppler and duration of symptoms; and (4) morphologically abnormal adult Achilles tendons were larger than 5.9 mm, and power Doppler flow was only seen in Achilles tendons above 6.5 mm.

Another study (de Vos et al. 2007a) reported the same results at baseline, with 58 patients with 63 symptomatic tendons. They used the Ohberg score (Ohberg and Alfredson 2002), with 0 for no vessels visible, 1+ for 1 vessel mostly in the anterior part, 2+ for 2 vessels throughout the tendon, 3+ for 3 vessels throughout the tendon, and 4+ for >3 vessels throughout the tendon, with no correlation of the degree of neovascularization (0-4+) and pain on the visual analog scale. After a 12-week treatment with heavy-load eccentric training

with or without an additional night splint, a significant correlation of the level of neovascularization and the visual analog scale score was evident ($r=.43$, $p<.001$).

Another scoring system was used in the evaluation of Achilles tendon neovascularization (Richards et al. 2005). The use of many different scoring systems, none of which have been validated, makes comparing results from different research groups difficult. The lack of validated scoring system means that any changes in score must also be interpreted with caution and is a major weakness in the field of tendinopathy research.

Another research group (de Vos et al. 2007b) performed their study to examine whether the degree of neovascularization detected with power Doppler is correlated with clinical severity before and after conservative treatment. They concluded there was no significant correlation before treatment, yet after treatment, a correlation was found. The role of neovascularization in Achilles tendinopathy is still unclear. The exact origin of the pain in chronic tendinopathies is debatable. A study gave a possible explanation upon the source of pain. It might due to the in-growth of neo-vessels and their accompanying nerves in the tendinopathic part of the tendon (Alfredson 2003).

Eccentric training might decrease the amount of neovascularization. A recent report found (Alfredson and Ohberg 2006) an increase in neovascularization in every patient in the first 3 weeks after treatment with sclerosing injections. After this period, less pain was reported in patients, with a decrease of neovessels; patients with a high neovascularization score reported high pain scores.

One study (Reiter et al. 2004) reported the presence of neovascularization in symptomatic Achilles tendons and this was associated with a low Victorian Institute of Sport Assessment-Achilles (VISA-A) score (Robinson et al. 2001), which is used to assess the

Achilles tendon clinical outcomes. However, another study (Sengkerij et al. 2009) found no correlation between VISA-A score and neovascularization score.

5.1.3 Reliability of power Doppler in the investigation

A recent study (Sengkerij et al. 2009) reported the excellence of the interobserver reliability of determining the neovascularization score using PDU. Neovascularization was present in 70% (23/33) of symptomatic tendons and 29% (5/17) of asymptomatic tendons. The prevalence of neovascularization in symptomatic tendons using PDU was within the range from 47% to 88% reported by several other investigators (Peers et al. 2003; Zanetti et al. 2003; Reiter et al. 2004; de Vos et al. 2007a; Leung and Griffith 2008). On the contrary, some studies (Ohberg L 2001; Ohberg and Alfredson 2002; Lind et al. 2006) demonstrated neovascularization in all symptomatic tendons. Besides examining the prevalence of neovascularization in symptomatic tendons, about 30% of asymptomatic tendons had a degree of neovascularization (Boesen et al. 2006b).

Although analyzing Achilles tendons with PDU is reliable the conflicting results about the presence of neovascularization and correlation between the degree of neovascularization and pain or discomfort do not help to clarify the significance of neovascularization in Achilles tendinopathy. At present, there is insufficient evidence to be able to clearly state the role of neovascularization in chronic tendinopathies. Therefore, this thesis will quantify microcirculatory mapping in the Achilles tendinopathy to detect a potential correlation of patient symptoms with VON.

5.1.4 Summary of the recent studies

Studies regarding the correlation between the neovascularization detected using Doppler ultrasonography and Achilles tendinopathy are summarized in Table 5.1. Some studies (Ohberg L 2001; Ohberg and Alfredson 2002; Alfredson et al. 2003; Zanetti et al. 2003;

Reiter et al. 2004) agree there is a potential or possible correlation between the neovascularization and symptoms, while others (Peers et al. 2003) (Richards et al. 2005; Boesen et al. 2006b; de Vos et al. 2007a; Koenig et al. 2007; van Snellenberg et al. 2007; Sengkerij et al. 2009) disagree.

Table 5.1 Summary of studies investigating the correlation between the Doppler ultrasonography and Achilles tendinopathy

Study	Number of symptomatic tendons examined	Colour or power Doppler used (machine used)	Ultrasound machine settings	Doppler signal found in tendinopathy	Conclusion
(Ohberg L 2001)	28	Colour (ACUSON Sequoia C512)	Frequency: 8-13 MHz. PRF & CG not mentioned	100%	Neovascularization is not seen in pain-free tendons but it might be involved in painful chronic Achilles tendinopathy.
(Ohberg and Alfredson 2002)	10	Colour (ACUSON Sequoia C512)	Frequency: 8-13 MHz. PRF & CG not mentioned	100%	Neovascularization is a potential cause of tendon pain, the probable importance of neovascularization in midportion tendinosis was confirmed.
(Zanetti et al. 2003)	55	Power (Elegra, Siemens)	Frequency: 7.5-9.0 MHz. PRF= 1.25kHz	55%	Neovascularization of Achilles tendons seems to be associated with pain but not with an unfavorable outcome.
(Alfredson et al. 2003)	25	Colour (ACUSON Sequoia C512)	Frequency: 8-13 MHz. PRF & CG not mentioned	100 %	There is a vasculo-neural ingrowth in the structurally changed part of the tendon that possibly can explain the pain suffered from chronic painful Achilles tendinosis tendons.
(Peers et al. 2003)	25	Power (HDI 5000, ATL-Philips)	Frequency: 5-12 MHz. PRF=1kHz, CG=81%	88%	Power Doppler signal does not strictly relate to pain or symptoms but possibly represents an additional risk adding to the clinical information on Achilles

					tendinopathy.
(Reiter et al. 2004)	19	Both (GE LOGIQ 9)	Frequency: 14 MHz CG was optimized to see on flow in the contralateral asymptomatic Achilles tendon.	74%	Neovascularization within the Achilles tendon can be an important condition associated with pain in chronic Achilles tendinopathy.
(Ohberg and Alfredson 2004)	41	Colour (ACUSON Sequoia C512)	Frequency: 8-13 MHz. PRF & CG not mentioned	100%	Action on the area with neovascularization during the eccentric training regimen might possibly be responsible for the good clinical results.
(Richards et al. 2005)	55	Power (ATL HDI 3000 Philips)	Frequency: 5-12 MHz. PRF = 0.8 to 1kHz, CG adjusted to no colour signal was present deep to the cortical bone.	82%	Power Doppler shows more microvascularity than colour Doppler. There was non-linear relationship between tendinopathy, Achilles tendon size and the amount of microvascularity, but not between power Doppler and duration of symptoms.
		Colour (ATL HDI 3000 Philips)		44%	
(Boesen et al. 2006c)	11	Colour (Mountainview, California)	Frequency: 14 MHz. PRF & CG not mentioned	100%	No effect on the intratendinous Doppler signal could be detected, suggesting that the effect is independent of changes in blood flow.
(Koenig et al. 2007)	22	Colour (Mountainview, California)	Frequency: 14 MHz. Optimized for low flow with a gain setting just below the level that produces random noise.	12%	The mere presence of some Doppler signal cannot be regarded as pathological since they found it in asymptomatic individuals.
(van	128	Colour	Frequency &	4%	There was low prevalence of

Snellenberg et al. 2007)		(HDI 5000 SonoCT Philips)	PRF & CG not mentioned		Achilles tendinopathy in the subjects. Neovascularization was rare and was observed regardless of the presence of pain, swelling or tenderness.
(Boesen et al. 2006b)	11	Colour (Mountainview, California)	Frequency: 14 MHz. Gain setting just below the level that produces random noise.	100%	Mere presence of Doppler in the Achilles tendon does not per se indicate disease. Without defined thresholds for the amount of Doppler signal, pathologic and physiologic perfusion cannot be distinguished in all cases.
(de Vos et al. 2007a)	79	Power (Elegra, Siemens)	Frequency: 8-13 MHz. PRF & CG not mentioned	63%	There was no correlation between neovascularization and VISA-A or VAS at baseline, but at follow-up, a higher neovascularization score was significantly correlated with a worse VISA-A and a higher VAS.
(Sengkerij et al. 2009)	50	Power (Elegra, Siemens)	Frequency: 8-13 MHz. PRF=868Hz	70%	An excellent interobserver reliability (ICC 0.85) was found. No correlation was found between VISA-A score and neovascularization score.

5.2 Optimizations in Achilles tendinopathy Studies

5.2.1 The use of power and colour Doppler ultrasound

CDU and PDU have been applied to investigate the role of neovascularization in Achilles tendinopathy. Although CDU and PDU provided equal findings in the detection of blood flow within the Achilles tendons (Reiter et al. 2004), more support was given to power Doppler because it varies from colour Doppler in that the imaging is relatively independent of the angle of incident beam (Zanetti et al. 2003). Another advantage of power Doppler is that it is more sensitive than colour Doppler to detect flow in vessels as small as 0.3 mm in diameter

(Weskott 1997), that is an area of 7.065×104 μm^2. However, from Table 5.1, colour Doppler was applied more often than power Doppler in the evaluation of Achilles tendinopathy.

In certain circumstances power Doppler is preferred over colour Doppler for examination of blood flow (Richards et al. 2005); the former could demonstrate a greater number and extent of vessels. Therefore, power Doppler ultrasound was applied in all the patients in this thesis.

5.2.2 The importance for settings optimization

Some researchers in Table 5.1 (Ohberg L 2001; Ohberg and Alfredson 2002; Alfredson 2003; Ohberg et al. 2004; Boesen et al. 2006b; Boesen et al. 2006c; Lind et al. 2006) reported neovascularization was noted in all symptomatic tendons, whilst another studies (Peers et al. 2003; Koenig et al. 2007; van Snellenberg et al. 2007) showed that in chronic Achilles tendinopathy tendon blood flow measured by power Doppler did not directly correlate to pain or symptom evaluation.

Part of the difference may result from the fact that neovascularization is a dynamic finding that may be most pronounced during acute exacerbation of pain and then disappear at inconstant rates (Zanetti et al. 2003). Another reason that might cause these contradictory conclusions may be due to the difference of performing Doppler ultrasound examination, in terms of the transducer frequency, settings of ultrasound machine (Yang et al. 2010). The PRF values listed in Table 5.1 range from 868 to 1250 Hz. There are no comparative studies between the set value or using a range of values for the PRF. The colour gain (CG) settings are not clearly indicated in most studies. The standard settings are essential to distinguish between physiological (slight) Doppler signals and possible pathological signal (Boesen et al. 2006a). The optimization of machine settings is of importance for reproducing results and allowing comparison among studies. Specifying settings will assist in standardization (Joshua et al. 2006). Therefore, the possible parameters were investigated on ultrasound

machine to achieve the optimization of examination conditions prior to scan any Achilles tendon.

5.2.3 The pulse repetition frequency

The settings of pulse repetition frequency (PRF) are potential factors affecting the Doppler signal which have not been widely discussed in the examinations of Achilles tendons. PRF setting determines the sensitivity of both colour and power Doppler; high-velocity flow is able to be detected by high PRF, and therefore filters that remove low flow to remove noise are applied (so-called linked controls) (Torp-Pedersen and Terslev 2008).

It has been reported that the area of the intratendinous vessels ranges from 6.99×104 μm^2 to 14.97×104 μm^2 (the radius ranges from 149.2 μm to 218.4 μm.) (Carr and Norris 1989), Another study by Wescott reported that the detectable flow velocity for colour Doppler under this range is no less than 0.7 cm/sec (Weskott 1997). They concluded that in order to reasonably investigate the blood flow of 0.7 cm/sec, the PRF should be adjusted to 1 kHz with the measuring angle between the probe and the flow of 45° (Weskott 1997). However, to test these settings, a Toshiba Aplio machine was used with the PRF of 1.1 kHz to ultrasound the radial artery (Fig. 5.1a). At these values, the "flash" artifacts caused by moving soft tissue were very pronounced. This is because the intensity echo signal from moving soft tissue has much higher amplitude than intensity echo signal from flowing blood (Campbell et al. 2004), whereas the study by Wescott looked at blood flow detection in a flow phantom. It is found that at a PRF of 2.1 kHz with the blood flow scale of 1.5 cm/sec, most of the 'flash' artifacts were eliminated (Fig. 5.1b).

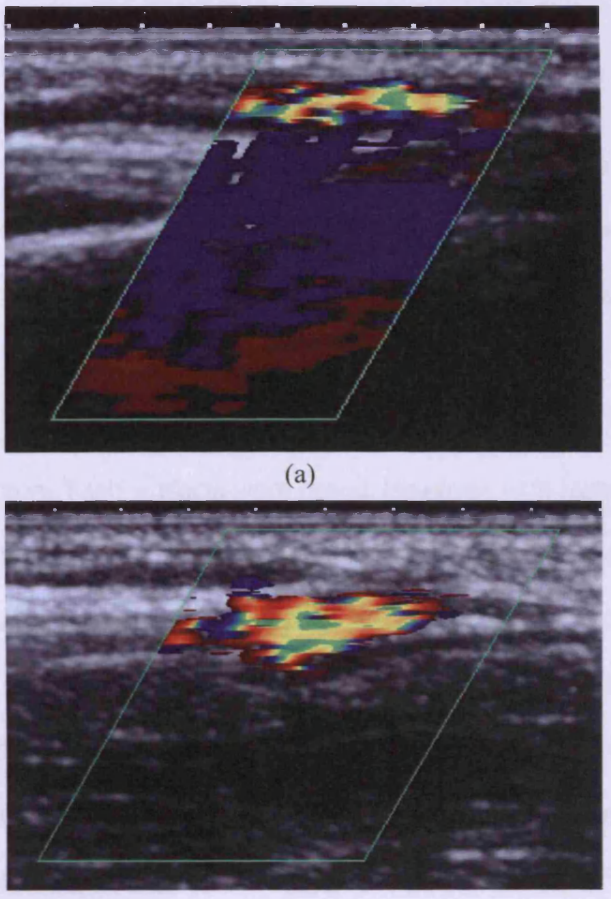

(a)

(b)

Fig. 5.1 Colour Doppler image of radial artery (a) with PRF of 1.1 kHz and scale of 0.7 cm/sec, (b) with PRF of 2.1 kHz and scale of 1.5 cm/sec

During the test, the PRF was found to be synchronically altered with the adjustment of either the sensitivity, depth, or the width of the Doppler box. For example, when increasing the width of the Doppler box, the PRF also automatically goes up while changes on the height of the Doppler box have no variance on PRF. The change of PRF and the hue on the Doppler image may differ between machines and between different manufacturers. Thus it is recommended to find a threshold for the PRF under specific settings of sensitivity, depth, and width of the Doppler box for a particular machine that just eliminates the 'flash' artifacts. Also, to reduce tissue motion the motion artifact eliminator (MAE), on the ultrasound machine, is suggested to set to the highest position.

5.2.4 Machine settings optimization

If it is agreed the neovascularization is essential in evaluation of Achilles tendinopathy, the goal in the ultrasound investigation must be to detect as much flow as possible, thus, the machines settings should be adjusted to allow the machine to achieve its highest sensitivity without noise.

The lower PRF, the more 'flash' artifacts were noted. However, with higher the PRF, the scatterer with low Doppler frequency shift may be ignored. The PRF must therefore be chosen carefully, based on a tradeoff between maximum velocity resolution and the reduction of velocity aliasing and range ambiguity problems. To find out the optimized PRF value, the same ultrasound machine with a 12 MHz linear array probe was used to examine six healthy Achilles tendons. At the same transverse plane, subjects were observed with different sensitivity settings, 0.4(PRF=3.1 kHz), 0.8(PRF=6.1 kHz), 1.1(PRF=7.6 kHz), 1.7(PRF=12.1 kHz), 2.6(PRF=18.9 kHz), 3.4(PRF=16.4 kHz), respectively (Fig. 5.2). All tendons showed 'flash' artifacts with the sensitivity settings below 1.1. Therefore, with a Doppler box of constant width, a PRF was deduced to 7.6 kHz in our examinations, which was suitable to remove "flash" artifact and detect flow.

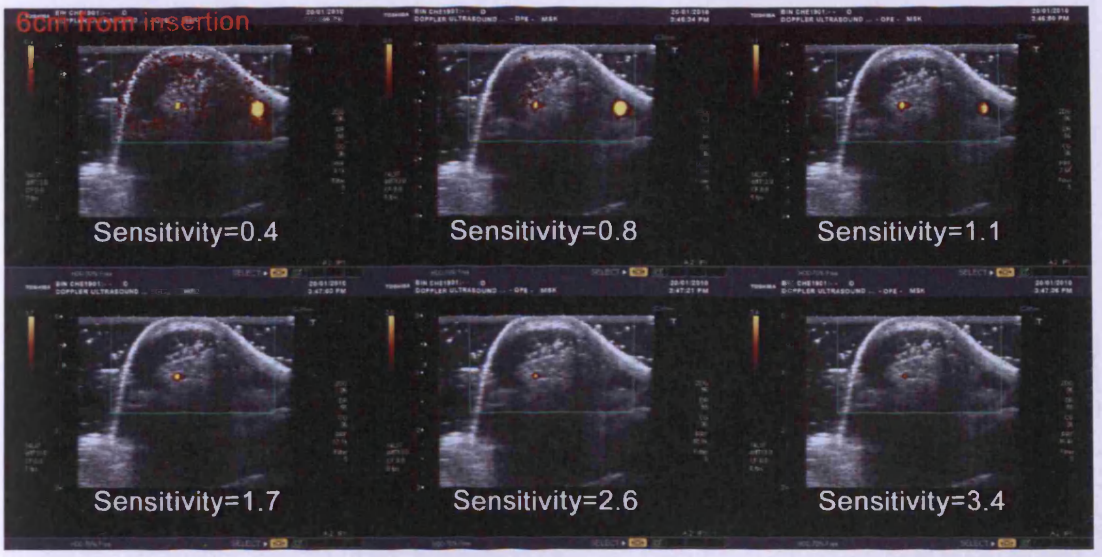

Fig. 5.2 Achilles tendon transverse ultrasonography planes with different sensitivity settings at 6 cm from the calcaneal insertion

When I turned the sensitivity scale knob, the PRF increases up to a certain level, then jumps down, decreases to a similar maximum to previously, as indicated by the PRF difference between the sensitivity of 2.6 and 3.4. What is almost certainly happening is that the machine is re-setting to avoid range ambiguity. That is, if the PRF exceeds a certain value, the echoes returning from the maximum depth will reach the transducer after having sent out the next pulse. The machine will interpret it as being a shallow echo from the second pulse, rather than a deep echo from the first. I am not sure what, then, it is adjusting to allow the scale to increase even if the PRF is lower - it is presumably that there is an allowable window. It may involve coded excitation, or any number of complex processes in the machine.

The second parameter should be optimized is CG. The CG setting determines the sensitivity of the system to flow (Torp-Pedersen and Terslev 2008), weak flow signals are undetected and motion artefacts may be prevented by lowering the CG (Martinoli and Derchi 1997). So the settings on ultrasound machine were adjusted to the threshold to noise.

Obtaining the maximized spatial resolution and have good blood flow is affected by another

important machine setting, Doppler frequency, which is not generally specified in the literature listed in Table 5.1. Higher Doppler frequency gives better spatial resolution i.e. a more detailed image of the blood vessels but at the expense of penetration (Torp-Pedersen and Terslev 2008). Frequency effects are much more important in Doppler than in B-mode grayscale imaging because the echo intensity from the moving scatters are much weaker than echoes used to create grayscale images. So there needs to be a trade-off between having a Doppler frequency low enough to detect the blood flow (penetration) and high enough to maximize spatial resolution. The more superficial the structure scanned, the higher the frequency can be used. Increasing Doppler frequency improves spatial resolution which decreases pixel size. The Doppler frequency was therefore chosen as highest as possible to maximize spatial resolution.

The machine settings under the preset of MSK mode are given in Table 5.2.

Table 5.2 Other parameters under the preset of MSK mode on the ultrasound machine

2DR	80	DR	55
CG	40	PRF	17.3kHz
Filter	5	Probe	14L×7
CF	8.8	DiftT	13.0
FR	12fps	ApliPure	2
2D-Post Process	5	2D-AGC	0
2D-Time Smooth	4	2D-Edge enhance	1
2D-Psel	5	Focal No.	1
2D-Map	2	CDI-Map	6
Data No.	1	M.A.E.	2
CDI-Focal Position	50	Frame Interpolate	2
Cut-off	4	CDI-Time Smooth	4
Spatial Smooth	1	Power DR	20
CDI-Frequency	8.8MHz		

5.2.5 Inclusion criteria

On B-mode gray-scale ultrasonography, it is generally considered that a fibrillar pattern must be present without localized hypoechoic areas or calcifications in the normal tendons (Fornage 1986; Martinoli et al. 2002), while hyperaemia has been regarded to signify abnormality (Ohberg L 2001; Martinoli et al. 2002). The inclusion criteria for normality and abnormality still remain to be defined in longitudinal studies of an age-stratified reference material (Koenig et al. 2007). To our knowledge, two previous studies offered a similar inclusion criteria table during the investigations (de Vos et al. 2007a; Sengkerij et al. 2009). Without the reasonable inclusion criteria, discrepancy in individual studies may not be confidentially explained, therefore, an inclusion and exclusion criteria were developed, as shown in Table 5.3, to define the patients in the study group.

Table 5.3 Inclusion and exclusion criteria

Inclusion Criteria	Exclusion Criteria
Aged 18 to 70 years (de Vos et al. 2007a)	Previous eccentric loading exercise programme just prior to scanning (de Vos et al. 2007a)
Have symptoms in the Achilles tendon more than 6 weeks (el Hawary et al. 1997)	Previous Achilles tendon surgery or rupture on the symptomatic lower limb (Munteanu et al. 2009)
Be able to complete the VISA-A and VAS questionnaire (Robinson et al. 2001)	Previous lower limb trauma which may have caused structural changes in the Achilles tendon (Munteanu et al. 2009)
Score less than 80 on VISA (el Hawary et al. 1997) and VAS not equal to 0 on VAS	Pathology at insertional location (de Vos et al. 2007a), bilateral tendinopathy and bursitis (Knobloch et al. 2008)
Pain and swelling positioned at 2 to 6 cm proximal to the calcaneal insertion(Vora et al. 2005)	Injection of local sclerotic or other anaesthetic effect agents into the Achilles tendon or surrounding area (Ohberg and Alfredson 2002)
B-mode ultrasound detects a local thickening and/or irregular fibre orientation and/or irregular tendon structure with hypoechoic areas (Alfredson et al. 2003; Zanetti et al. 2003)	Other systemic disorders

5.2.6 Physical activity and other factors

Prior physical activity can influence the neovascularization score in the Doppler investigation (de Vos et al. 2007a). Blood flow, oxygen demand and the level of collagen synthesis increase with mechanical loading of the tendon (Boushel et al. 2000), thus the tendon should not be evaluated immediately after activity or eccentric training, which may create a physiological response (Boesen et al. 2006b). Standardization of physical activity before the Doppler scan is necessary. A study (de Vos et al. 2007a) recommended 24 hours' abstinence from heavy-load eccentric training, sporting activity, or physical exertion.

Other factors including the degree of ankle plantar flexion, probe pressure impacted onto the skin during the examinations also needed to be validated and standardized in future studies.

5.3 Conclusions

This chapter focuses on the ultrasonic investigation of Achilles tendinopathy, specially the observation of neovascularization in Achilles tendon. In the experiment, the amount of neovascularization denoted by Doppler signals was found to be associated with the ultrasound machine settings. Optimized machine settings including PRF and CG were recommended, as well as inclusion criteria, physical activity, and other factors. The next chapter will describe a novel 3D Doppler ultrasound system to be used in the measurement of VON.

6. Methods to Quantify Neovascularization

In PDU imaging, the integral of the power spectrum of the local blood flow is estimated and encoded in colour and superimposed over the 2D B-mode image. Power Doppler imaging therefore provides a spatial distribution of flow in relation to the associated anatomic structure, thus depicting the flow field. Currently, power Doppler imaging is therefore used mainly for qualitative analysis of blood flow, especially where blood flow volume is low. In this thesis, a new modality of ultrasound imaging, 3D power Doppler imaging, was applied to depict directly the VON for Achilles tendinopathy.

Figure 6.1 is a block diagram of our experimental system. The 3D power Doppler imaging system, developed in our laboratory, includes a Toshiba Apilo ultrasound machine with a 12-MHz high resolution linear array probe, a specially constructed motor-driven translation assembly controlled by a custom-controller, and a Toshiba laptop workstation. The workstation is capable of image acquisition, reconstruction and display of 3D images in surface rendering and texture mapping modes. The linear array ultrasound probe was mounted on the translation assembly with the transducer axis parallel to the Achilles tendon (patients at prone position). A set of planar 2D power Doppler images, transverse to the Achilles tendon, was acquired while translating the probe along the Achilles tendon at a fixed interval. These 2D images were digitized in a form of video clips in the ultrasound machine. After acquisition, a frame from each video clip was selected based on its maximal Doppler signal using a specially developed computer program. With the representative frames selected, they were reformatted into a 3D volume image to compensate for the intervals and recover the correct geometry using the commercial software. The resulting 3D volume image was viewed on the same workstation using the some software also. The software allowed

rotation of the 3D image and interactive slicing into the volume in any plane in real-time with a computer mouse. A detailed technical description of the 3D power Doppler imaging system will be introduced as below.

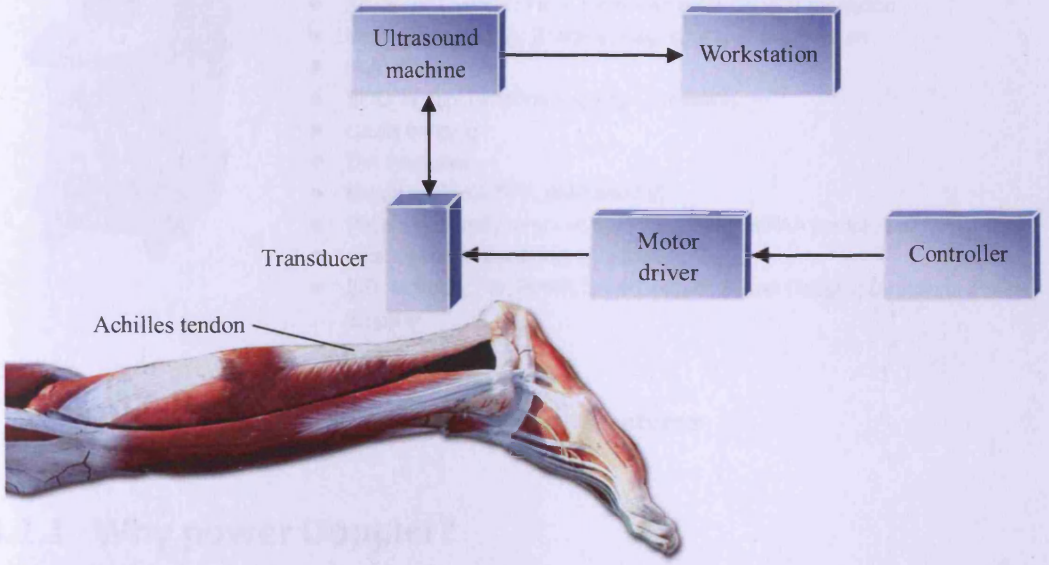

Fig. 6.1 Block diagram of system

6.1 Ultrasound Machine and Probe

For this study, a Toshiba Apilo ultrasound machine (Fig. 6.2) with a 12-MHz high resolution linear array probe was used. The features of the machine are below.

- 3 transducer ports
- 19" color LCD screen
- Panoramic Zoom
- Trapezoidal imaging
- Dual and Quad screen imaging
- Duplex / Triplex
- Advanced Dynamic Flow: Increased color Doppler resolution
- Micro Flow Imaging: Enables imaging of contrast medium
- Hard drive
- STIC: Spatio-Temporal Imaging Correlation
- Cavity Imaging
- DVI interfaces
- Export to JPEG, TIFF, BMP and AVI
- Patient info easily removed from images for HIPAA compliance
- Flexible control panel for repositioning
- 2-D, M-Mode, PW, HPRF, Color Doppler, Power Doppler, Directional Power Doppler

Fig. 6.2 Toshiba Aplio features

6.1.1 Why power Doppler?

The reason why power Doppler was used in the 3D system is the power Doppler imaging has many promising properties for flow field mapping (Guo et al. 1995). It was initially developed for the assessment of low velocity flow. Instead of displaying the mean Doppler frequency shit, the colour map of power Doppler imaging displays the integrated power of the Doppler signal. The background noise is normally white and uniformly distributed and has lower power than the flow signal, therefore the noise will be represented as a homogeneous background colour even when the gain is increased beyond the level at which the random colour noise dominated the conventional colour Doppler image. This increases the sensitivity of flow mapping (Guo et al. 1995).

Because power Doppler imaging maps the power of the Doppler signal, it is in some way velocity-independent when there is no red cell aggregation or when a blood mimic is used. In fact, the Doppler power spectral curve has a wider bandwidth with lower amplitude for high-velocity flow and a narrower bandwidth with higher amplitude for low-velocity flow, making the integral under the curve almost identical.

Power Doppler imaging has been used to detect soft-tissue hyperemia and to depict the Achilles tendon vasculature. In this study, 3D power Doppler imaging has been used to depict the neovascularization of the Achilles tendinopathy. The appearance of the 3D power Doppler image, after they have been rendered in 3D, was found to be similar to subtraction angiograms.

6.1.2 Settings on machine

In the power mode, the B-mode image in the colour overlay window give the information of soft tissue, i.e. Achilles tendon and its surroundings. The power Doppler images itself looks like a subtraction angiogram. The geometry of the neo-vessels was well defined and provided a reference for locating the examination, determining the colour gain, and the region of interest (Fig. 6.3).

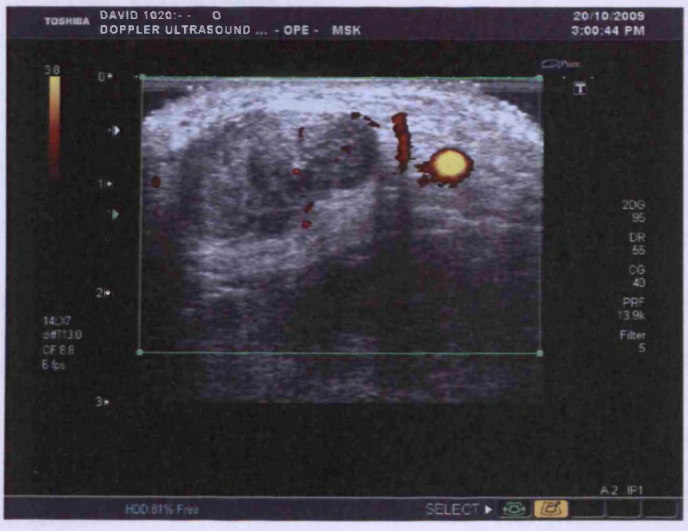

Fig. 6.3 Transverse image of neovascularization in Achilles tendon

The cutoff sensitivity setting in power Doppler mode in the investigation of neovascularization in the Achilles tendinopathy had not been widely discussed. In several 2D power Doppler examinations, a PRF from 600 to 1000Hz was used in order to obtain maximal sensitivity without background noise (Peers et al. 2003; Silvestri et al. 2003; Richards et al. 2005;

Sengkerij et al. 2009); however, the wall filter applied in these studies had not been clearly indicated. One study (Silvestri et al. 2003) reported that they always adjusted the colour gain setting by carrying out a manual elevation of the power Doppler gain knob until the next highest signal above the noise baseline began to appear in the power Doppler box. This setting was achieved with the scan head directly in contact with air which has not been applied in other studies. A 3D power Doppler study to the pulmonary artery however applied the medium wall filter with PRF of 2 kHz (Christiaens et al. 1997).

6.1.3 Investigation of the sensitivity

Because of the discrepancy of the sensitivity settings in different examinations of the Achilles tendinopathy as well as in other 3D power Doppler studies, five healthy volunteers was first investigated to find out the cutoff sensitivity in the power Doppler images. All these volunteers have been marked 100 score in the VISA-A assessment which showed they are all asymptomatic for any Achilles tendon disease.

The protocol for investigating the sensitivity in power Doppler is to observe the signals with six different sensitivities ranged from 0.4 to 3.4 at three different locations between 2 and 8 cm from the insertion (Fig. 6.4). The results show that the micro-vascularity as well as the movement between the ultrasound probe and volunteers were significant with the sensitivities lower than 1.1. In some of them noise was still detected with the settings between 1.1 and 3.4. Therefore, the settings of 3.8 was used in the following 3D power Doppler investigations in order to discriminate the original supply blood vessels and movement noise.


4cm from insertion
Sensitivity=0.4
Sensitivity=0.8
Sensitivity=1.1
Sensitivity=1.7
Sensitivity=2.6
Sensitivity=3.4
6cm from insertion
Sensitivity=0.4
Sensitivity=0.8
Sensitivity=1.1
Sensitivity=1.7
Sensitivity=2.6
Sensitivity=3.4
8cm from insertion
Sensitivity=0.4
Sensitivity=0.7
Sensitivity=1.1
Sensitivity=1.7
Sensitivity=2.6
Sensitivity=3.4

Volunteer 1


2cm from insertion
Sensitivity=0.4
Sensitivity=0.8
Sensitivity=1.1
Sensitivity=1.7
Sensitivity=2.6
Sensitivity=3.4
4cm from insertion
Sensitivity=0.4
Sensitivity=0.8
Sensitivity=1.1
Sensitivity=1.7
Sensitivity=2.6
Sensitivity=3.4
8cm from insertion
Sensitivity=0.4
Sensitivity=0.8
Sensitivity=1.1
Sensitivity=1.7
Sensitivity=2.6
Sensitivity=3.4

Volunteer 2

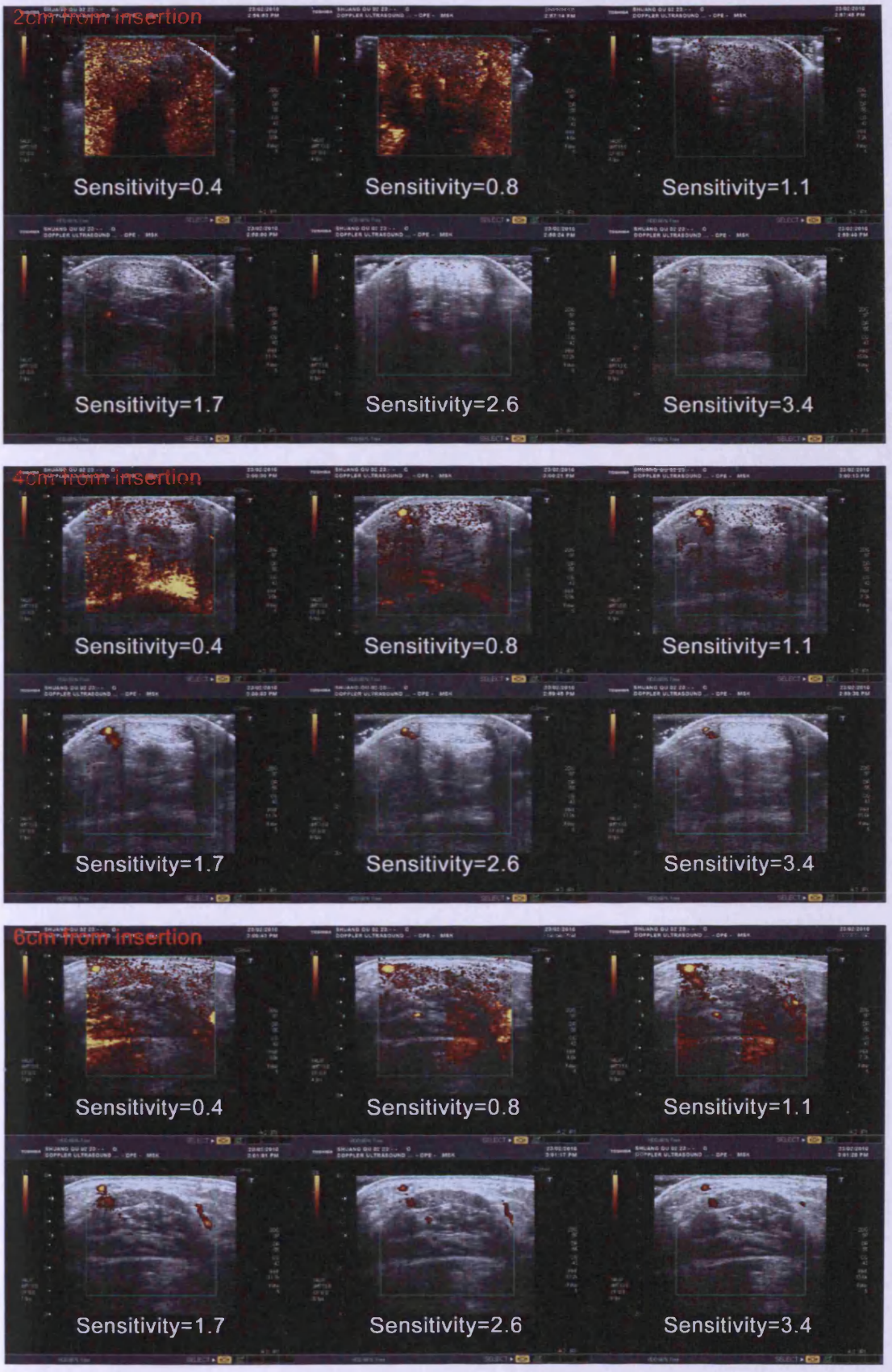
2cm from insertion
Sensitivity=0.4
Sensitivity=0.8
Sensitivity=1.1
Sensitivity=1.7
Sensitivity=2.6
Sensitivity=3.4
4cm from insertion
Sensitivity=0.4
Sensitivity=0.8
Sensitivity=1.1
Sensitivity=1.7
Sensitivity=2.6
Sensitivity=3.4
6cm from insertion
Sensitivity=0.4
Sensitivity=0.8
Sensitivity=1.1
Sensitivity=1.7
Sensitivity=2.6
Sensitivity=3.4

Volunteer 3

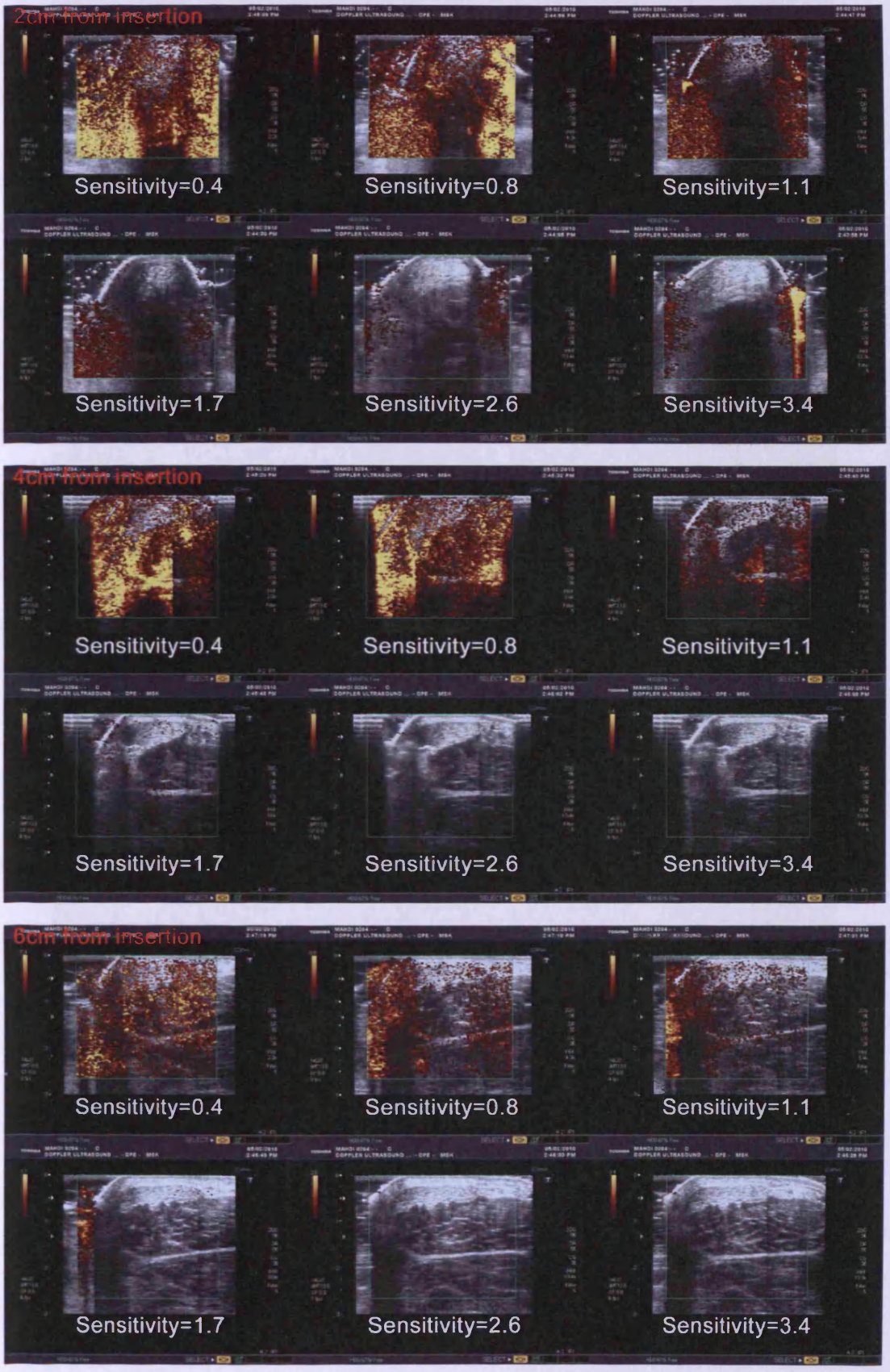
2cm from insertion
Sensitivity=0.4
Sensitivity=0.8
Sensitivity=1.1
Sensitivity=1.7
Sensitivity=2.6
Sensitivity=3.4
4cm from insertion
Sensitivity=0.4
Sensitivity=0.8
Sensitivity=1.1
Sensitivity=1.7
Sensitivity=2.6
Sensitivity=3.4
6cm from insertion
Sensitivity=0.4
Sensitivity=0.8
Sensitivity=1.1
Sensitivity=1.7
Sensitivity=2.6
Sensitivity=3.4

Volunteer 4

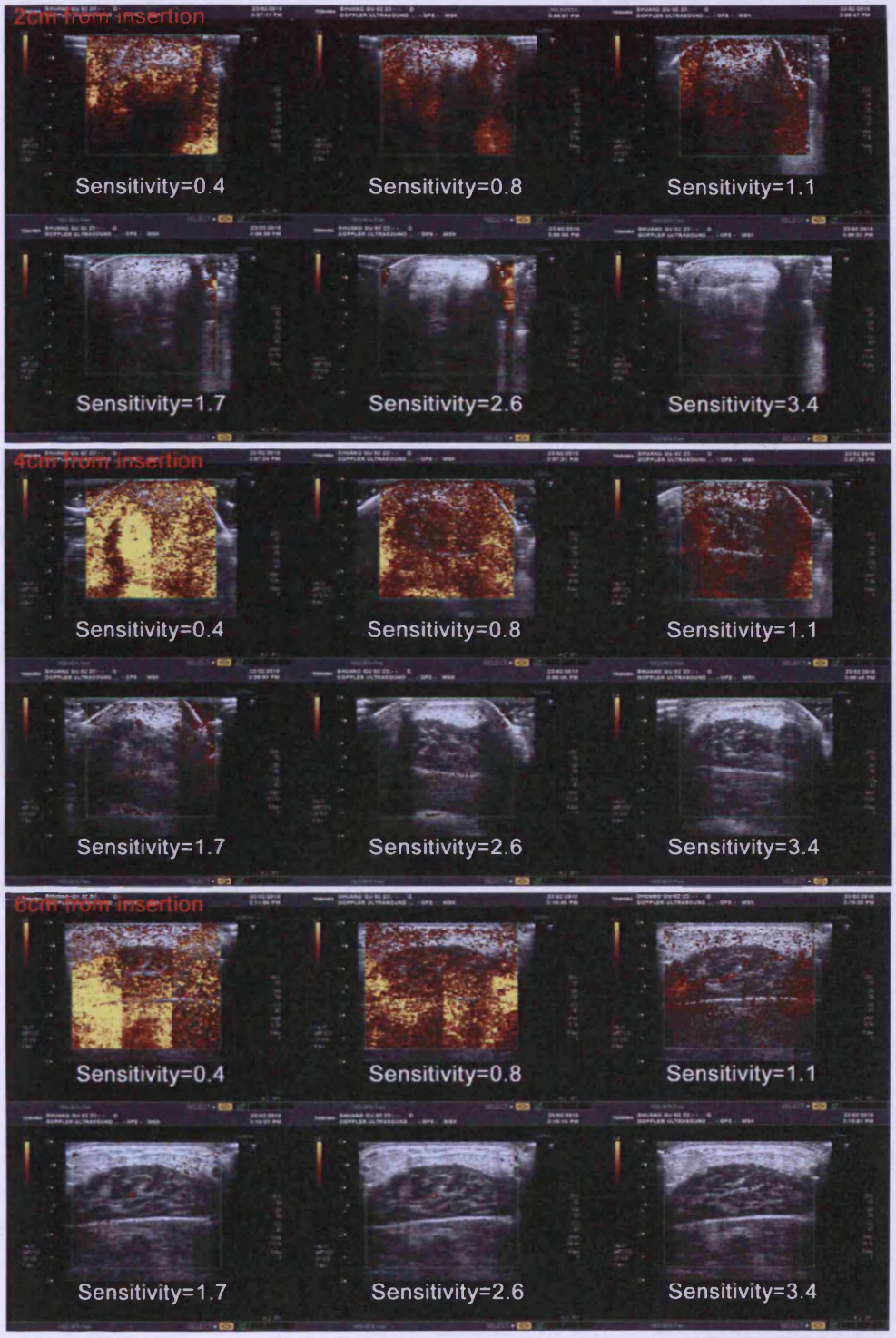

Volunteer 5

Fig. 6.4 Images of healthy Achilles tendon in different sensitivity settings

6.1.4 Patient and probe positions

Ultrasound images were taken in the transverse plane. The patient was scanned while prone

on the ultrasound bench, with the foot stabilized and hanging over the edge of the apparatus described below. The patient was asked to keep as still as possible to minimize motion artefacts. In order to improve the acoustic coupling (impedance match), a gel is applied between the probe and the surface of the skin.

6.2 Computerized Motor-driven Track

To obtain the imaging slices along the Achilles tendon to ultimately form the visualization of 3D power Doppler neovascularization images, I designed and built a specially constructed computerized motor-driven track (Fig. 6.5). The details and structures of the track will be introduced in the following sections. A sequential transverse power Doppler image was obtained with the track that moves the ultrasound probe at a controlled, uniform speed. The stopping interval was designed to achieve 0.5 mm to 2 mm image spacing. Other operating parameters, for example the driving direction and the total step, are able to be adjusted using the computerized controller.

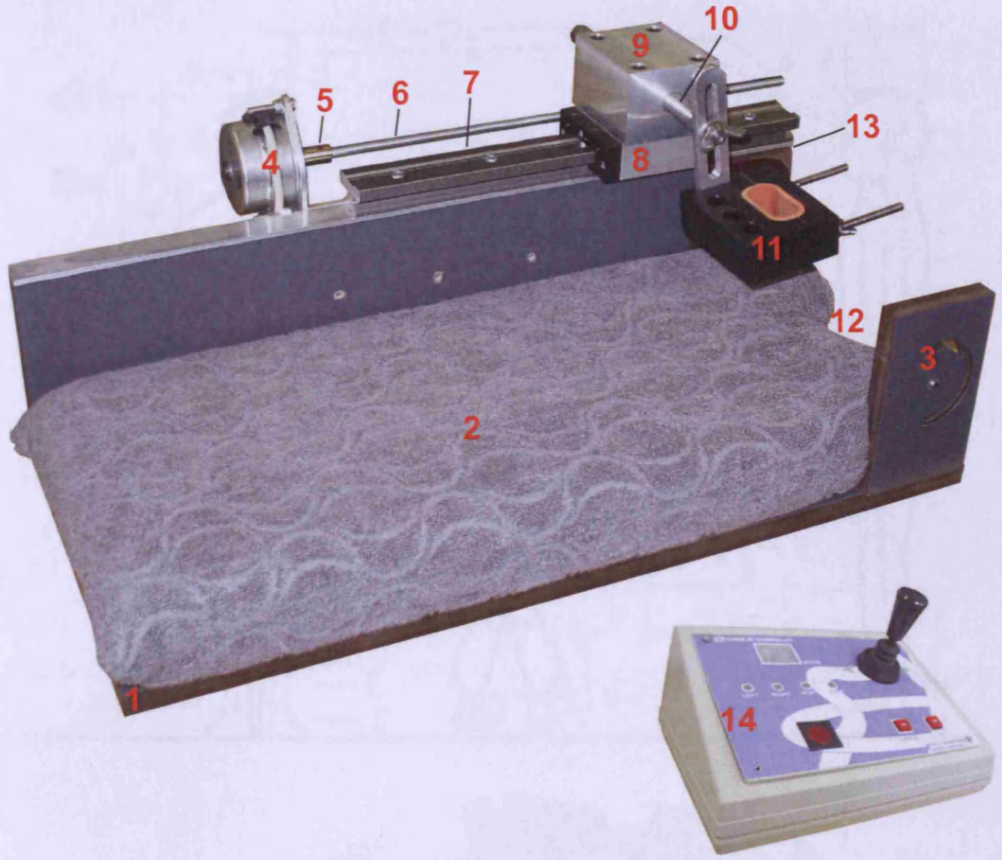

1-base board	2-memory foam pad	3-foot plate stand	4-stepper motor
5-motor shaft	6-driving screw	7-track	8-slider
9-carriage	10-bridge	11-probe clamp	12-foot hole
13-adjustable top	14-computerized controller		

Fig. 6.5 Motor driven track

6.2.1 Anthropometry

Anthropometry plays an important role in industrial design, clothing design, ergonomics and architecture where statistical data about the distribution of body dimensions in the population are used to optimize products. The dimensions of the rig were designed according to the leg data from an anthropometric data for men at the 97.5, 50, and 2.5 percentiles (Fig. 6.6) (Diffrient et al. 1974).

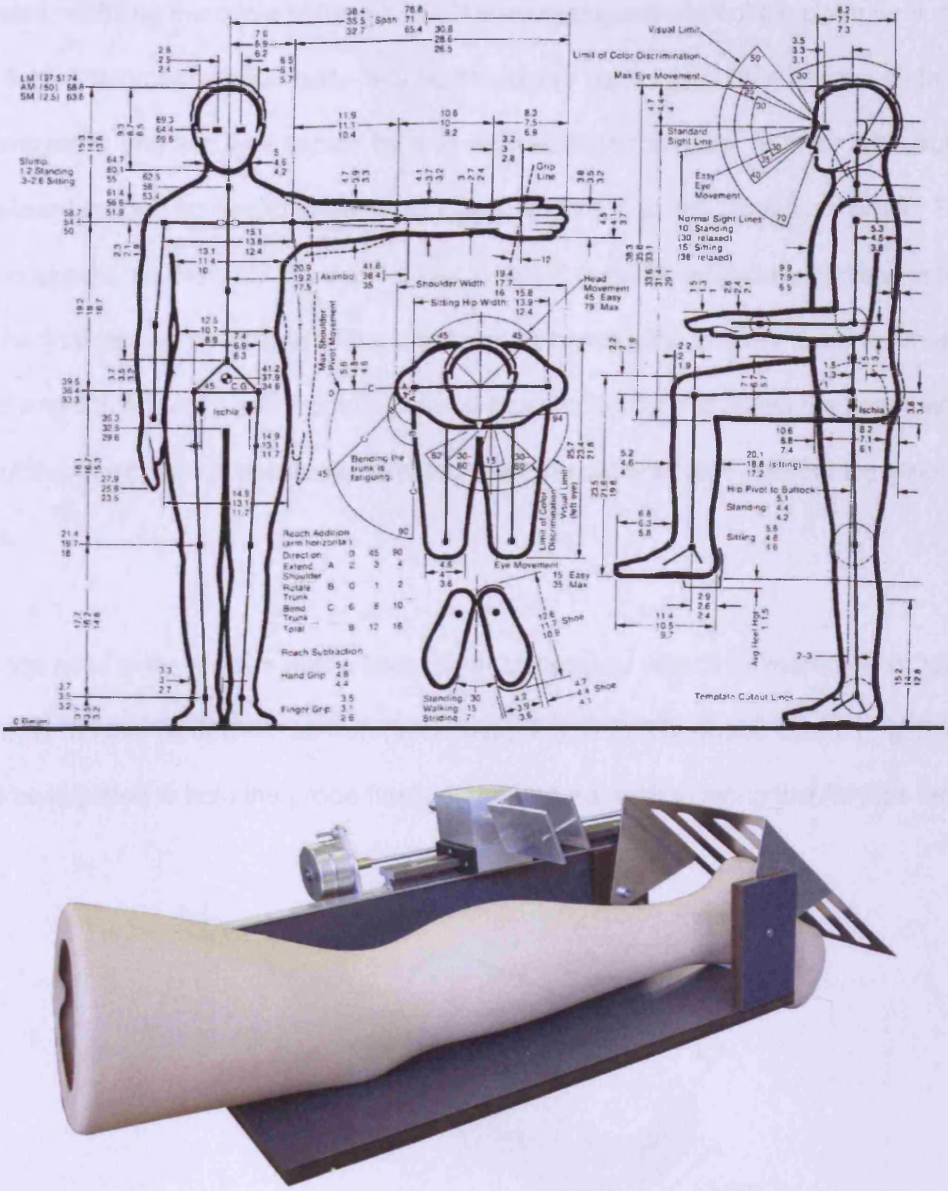

Fig. 6.6 Anthropometry data

6.2.2 Probe clamp

The most difficult part of the rig was the design of a proper ultrasound probe clamp with some reasonable flexibility. The initial idea was a simple U-shaped clamp made by aluminium (Fig 6.6), which was connected to the slider via an aluminium pin. The probe could be positioned into the clamp and squeezed by the arms using a long screw. The problem with this simple U-shaped clamp was that it was less stable and flexible since the

arms were not fitting the curve of the probe. The second generation of the clamp is illustrated in Fig. 6.11. The probe was properly held by the rubber pads fixed at the internal surfaces of the clamp arms, one arm was carried by a lift connected to the slider, another arm could travel along two long screws to release the clamp and position the ultrasound probe. This clamp increased the flexibility but didn't adapt to some patients, especially those with thick legs. The final version overcame all the problems by introducing another entity as shown in Fig. 6.8 and 6.9. An entity with multiple position holes could further adjust the height and swing of the clamp, which eventually adapted to all the patients with different leg sizes and shapes.

The probe used in the studies was a linear array transducer with the dimensions of 125 mm (length) × 55 mm (width) × 25 mm (thickness) (Fig. 6.7). The probe clamp (Fig. 6.8) is able to be adjusted to hold the probe firmly during the translation along the Achilles tendon.

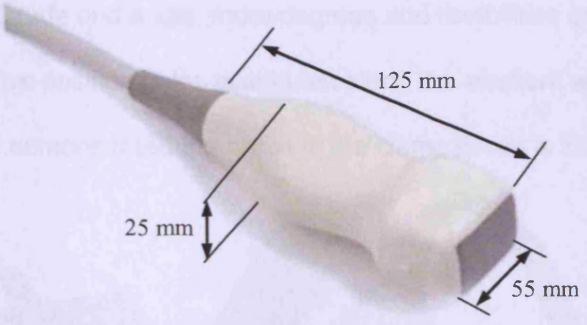

Fig. 6.7 Probe dimensions

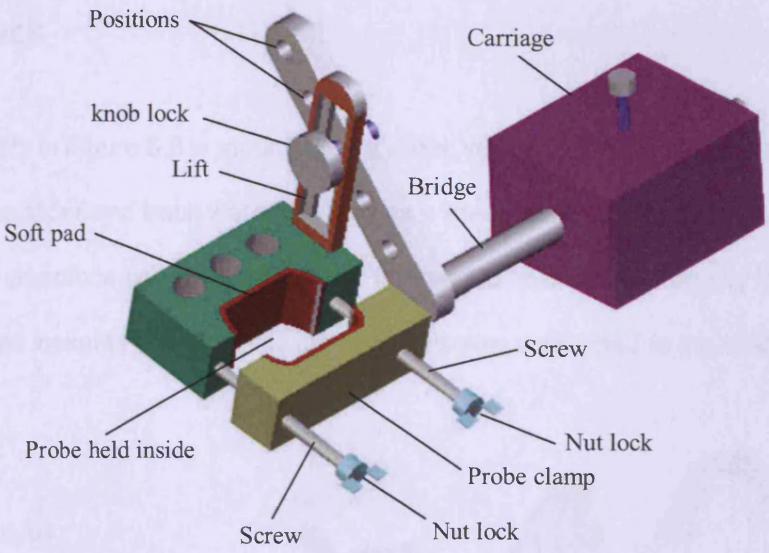

Fig. 6.8 Probe mounting schematic

To clamp the probe, release the nut locks (Fig. 6.8) to separate the probe clamp, stick the ultrasound probe between the soft pads. Rotate the nut lock back to clamp the mid-part of the probe. The probe clamp can be shifted up and down or swung using the lift and knob lock to achieve a proper altitude and angle, more degrees and flexibilities can be achieved by altering the clamp in five position holes distributed along the element whose end is fixed on the bridge. Figure 6.9 demonstrated the probe in the clamp which is locked at the top hole.

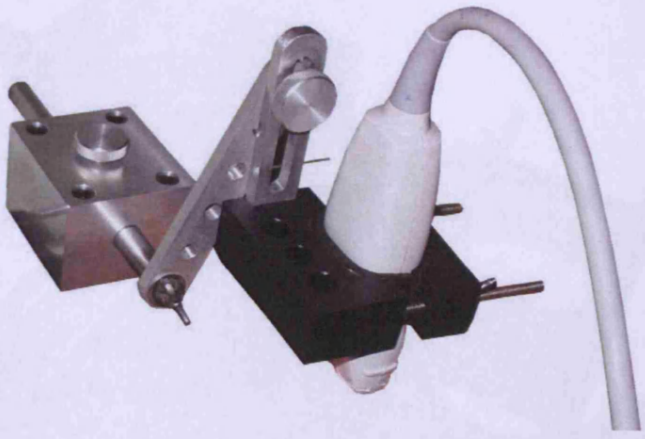

Fig. 6.9 Probe mounting

6.2.3 Track

The entire entity in Figure 6.9 is mounted on a slider, which can freely run on a metal rail (Fig. 6.10). Both the slider and track were provided as a linear guide system product from RS. The slider, whose clearance can be adjusted and trimmed to level the carriage by loosening or tightening three locknuts (Fig. 6.11), is driven on a screw connected to the shaft of a stepper motor.

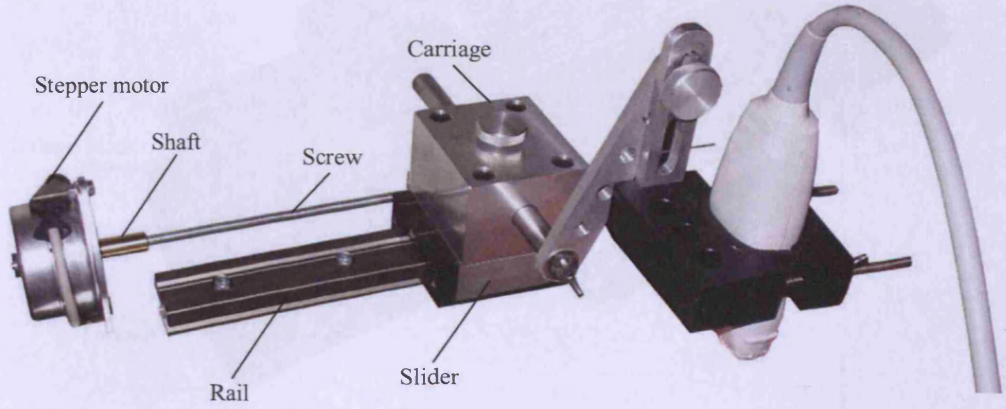

Fig. 6.10 Probe mounting attachment

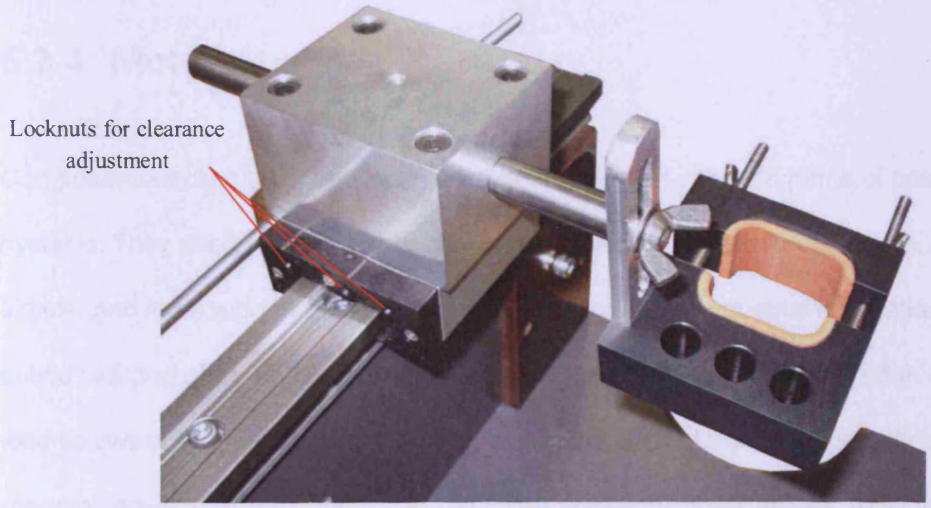

Fig. 6.11 Clearance adjusting locknuts

The rail is 300 mm in length and 31 mm in width which is sufficient for the translation of the

probe (100 mm as maximum). The stepper motor as well as the rail is mounted on an L shape aluminium block whose clearance to the top of the stand can be altered by locknuts (Fig. 6.12). This will further compensate the slope of the limb during scanning.

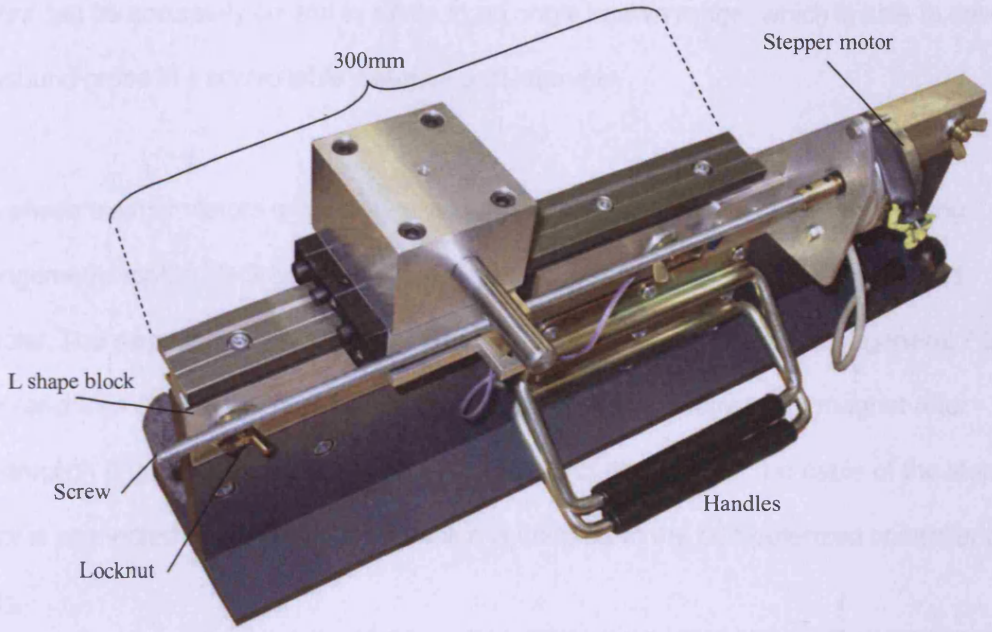

Fig. 6.12 Stepper motor mounting

6.2.4 Motor

Computer-controlled stepper motors are one of the most versatile forms of positioning systems. They are typically digitally controlled as part of an open loop system, and are simpler and more rugged than closed loop servo systems. Industrial applications are in high speed pick and place equipment and multi-axis machine CNC machines often directly driving lead screws or ballscrews. In the field of lasers and optics they are frequently used in precision positioning equipment such as linear actuators, linear stages, rotation stages, goniometers, and mirror mounts. Other uses are in packaging machinery, and positioning of valve pilot stages for fluid control systems.

Stepper motors operate differently from DC brush motors, which rotate when voltage is applied to their terminals. Stepper motors, on the other hand, effectively have multiple "toothed" electromagnets arranged around a central gear-shaped piece of iron. Stepper motors can be accurately control to rotate in an angle known range, which is able to drive the ultrasound probe in a controllable distance and intervals.

Two phase stepper motors are widely used in industries. There are two basic winding arrangements for the electromagnetic coils in a two phase stepper motor: bipolar and unipolar. The stepper motor (RS no. 332-953) used to drive the carriage is a general 7.5° unipolar-driven device with four 12V DC windings (coils) and permanent magnet rotor construction (Fig. 6.13, Appendix A has more details of the motor). The cable of the stepper motor is connected to a circular socket which is coupled to the computerized controller (Fig. 6.14).

Unipolar 7.5 deg stepper motor
12V 5.3W

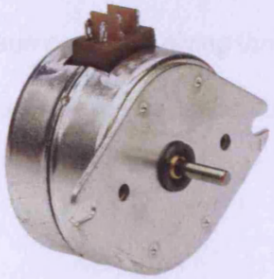

	Size 2	Units
Power consumption of motor only	5.3	W
Maximum working torque	57	mNm
Holding torque	85	mNm
Torque derating	-0.4	%/°C
Maximum pull-in rate	130	steps/s
Resistance per phase at +20°C	47	Ω
Inductance per phase	400	mH
Current per phase	240	mA
Permissible ambient temperature range	-20 to +70	°C
Permissible storage temperature range	-40 to +100	°C
Permissible motor temperature	120	°C
Insulation resistance at 500V (CEE 10)	>2	MΩ
Step angle	7° 30'	
Step angle tolerance, not cumulative	±20'	
Number of steps per revolution	48	
Direction of rotation	reversible	
Rotor inertia	45	gmc²
Mass	300	g
Maximum radial force	10	N
Maximum axle force	1.5	N
Bearings	Slide (sintered bronze)	

Fig. 6.13 Stepper motor and its specifications

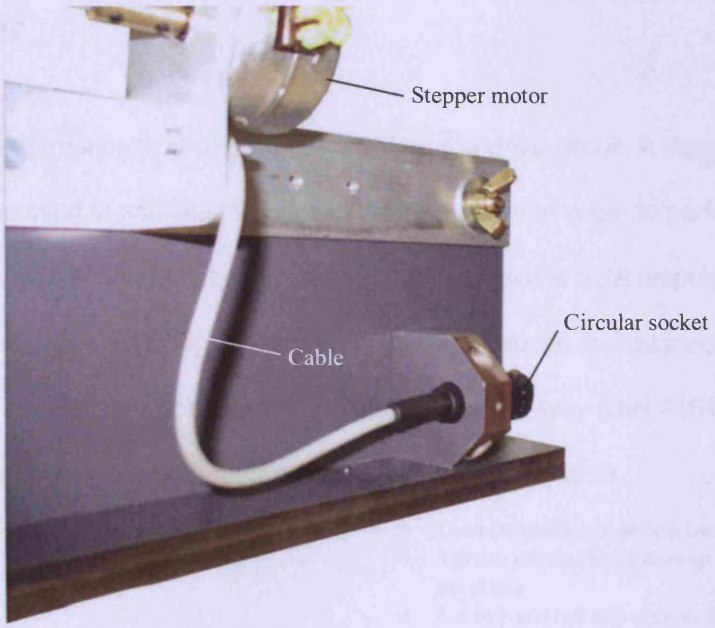

Fig. 6.14 Motor construction

The reason for using a unipolar stepper motor in the track is it has two windings per phase, one for each direction of magnetic field (Fig. 6.15). Since in this arrangement a magnetic pole can be reversed without switching the direction of current, the commutation circuit can be made very simple for each winding. Typically, given a phase, one end of each winding is made common: giving three leads per phase and six leads for a typical two phase motor. Often, these two phase commons are internally joined, so the motor has only five leads.

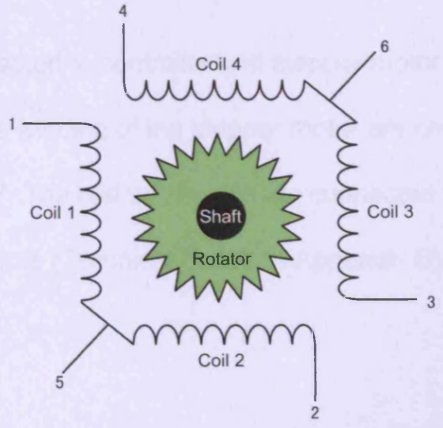

Fig. 6.15 Structure of a unipolar stepper motor

6.2.5 Driver

Stepper motor performance is strongly dependent on the drive circuit. A stepper motor controller must be used to activate the drive in the right order in order to perform accurate controls. The driver used to energize the stepper motor above is a 2A unipolar stepper motor drive board (RS no. 217-3611, Fig. 6.16). The drive board above is designed for stand-alone operation. It is a standard Euroboard size complete with a 32-way (DIN 41612) plug connector for plugging into any Eurocard compatible racking system.

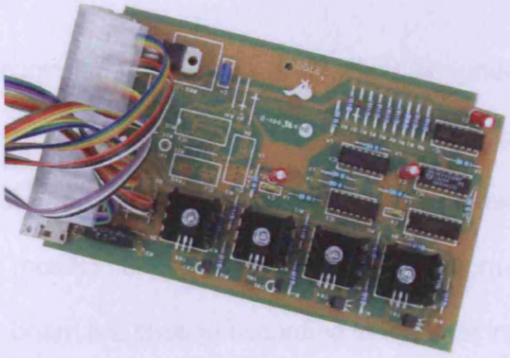

- Compatible with any stepper motors up to 2A
- 4-phase unipolar motor drive up to 2A/ 30Vdc per phase
- Full step and half step drive modes
- Higher resolution, greater performance stability and faster stepping rates)
- External control inputs are C-MOS and open collector TTL logic compatible
- Pre-set control for setting predetermined motor phase excitation pattern
- On-board 12Vdc, 50mA output for external use
- Drive board and the motor can share the same dc. power supply
- Provision for assembly of on-board oscillator (if external clock not available) having clock pulse output, base speed, top speed and stop/run control inputs

Fig. 6.16 Driver board

The plug connector is connected to controller and stepper motor using the connection schematics in Fig. 6.17. The winding of the stepper motor are connected to the K part of the board according to Fig. 6.17. The rest of the pins are connected to the controller for speed, interval, step, direction controls (Technical details in Appendix B).

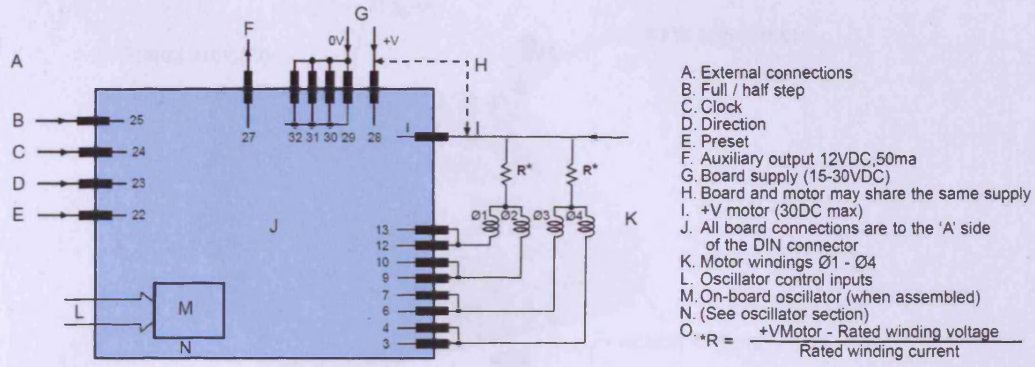

Fig. 6.17 Connection schematic

6.2.6 Controller

The controller (Fig. 6.18) was specially designed for the scanning rig above, which provides man-machine interface for scanning functions settings and communications with the drive board. The core of the controller is a generic microcontroller, AT89S51, which is a widely used model in 8051 series microcontroller from Atmel. The signals used to communicate the drive board are created according to the user inputs through buttons and a joystick. The system block diagram is in Fig. 6.19.

The schematic diagram of the controller is shown in Figure 6.20, as well as the printed circuit board (PCB) in Figure 6.21. Details for each part will be described below.

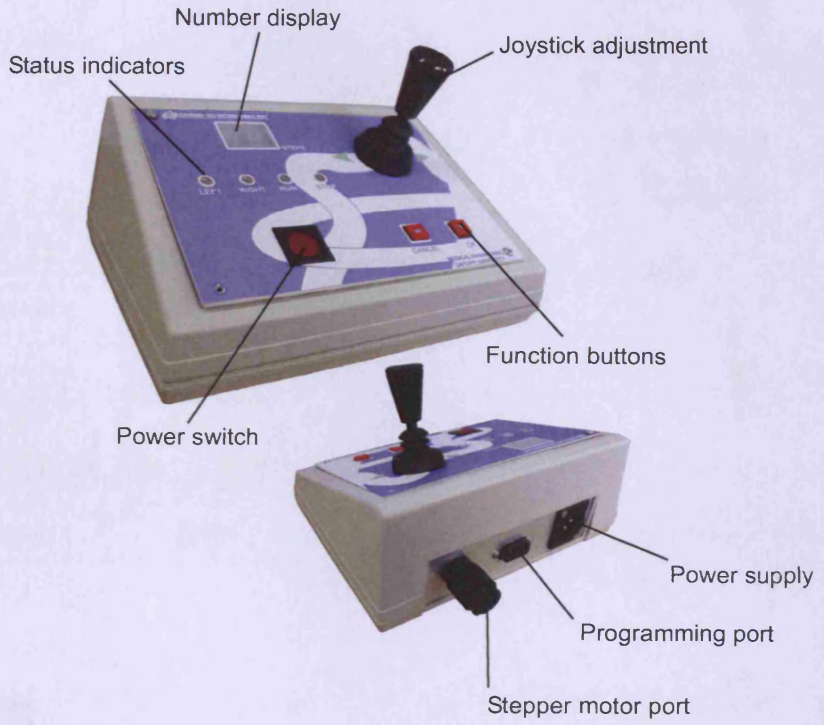

Fig. 6.18 Stepper motor controller

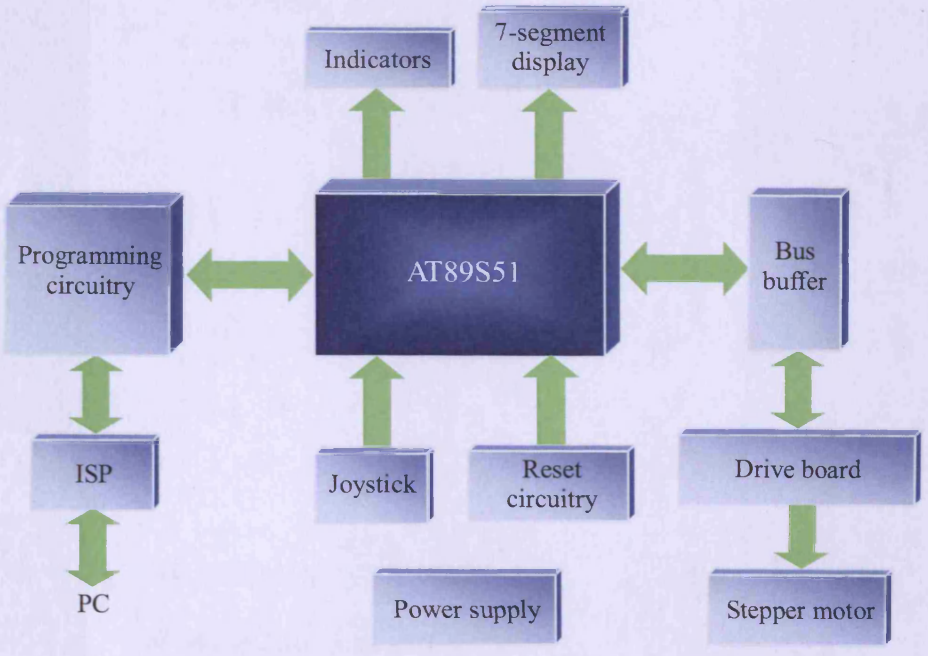

Fig. 6.19 Controller block diagram

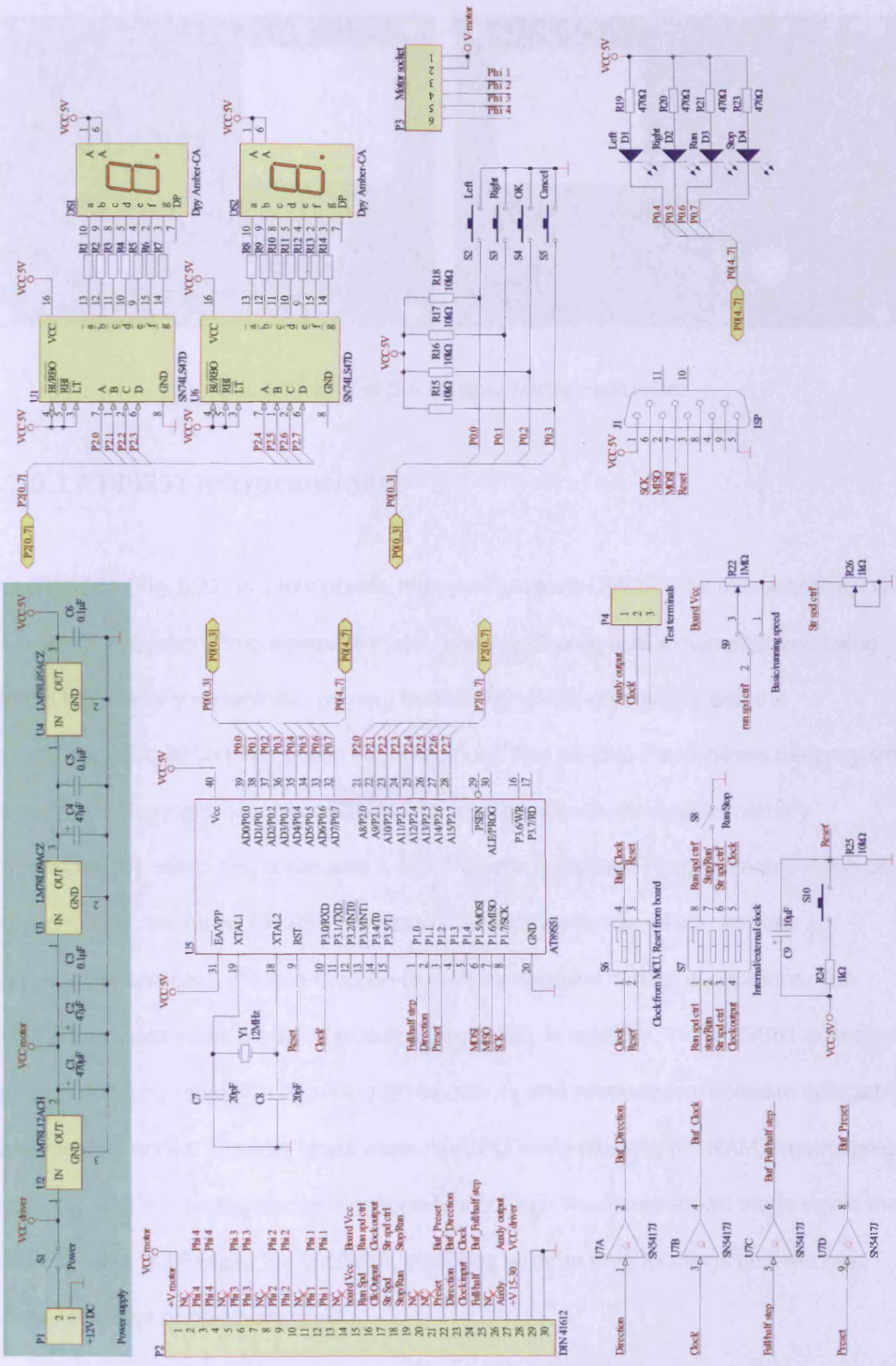

Fig. 6.20 Schematic diagram of the stepper motor controller

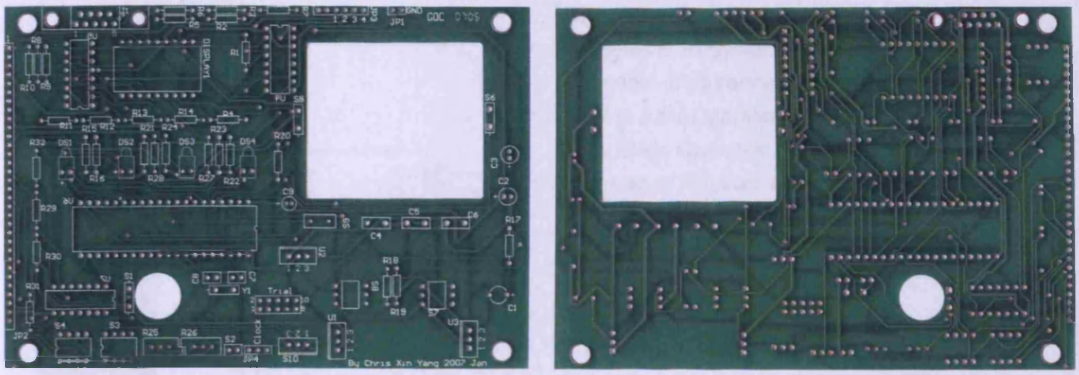

Fig. 6.21 PCB of the stepper motor controller

6.2.6.1 AT89S51 microcontroller

The AT89S51 (Fig. 6.22) is a low-power, high-performance CMOS 8-bit microcontroller with 4K bytes of In-System Programmable Flash memory. The device is manufactured using Atmel's high-density nonvolatile memory technology and is compatible with the industry-standard 80C51 instruction set and pinout. The on-chip Flash allows the program memory to be reprogrammed in-system or by a conventional nonvolatile memory programmer. By combining a versatile 8-bit CPU with In-System Programmable Flash on a monolithic chip, the Atmel AT89S51 is a powerful microcontroller which provides a highly-flexible and cost-effective solution to many embedded control applications. The AT89S51 provides some standard features (Fig. 6.22). In addition, the AT89S51 is designed with static logic for operation down to zero frequency and supports two software selectable power saving modes. The Idle Mode stops the CPU while allowing the RAM, timer/counters, serial port, and interrupt system to continue functioning. The Power-down mode saves the RAM con-tents but freezes the oscillator, disabling all other chip functions until the next external interrupt or hardware reset.

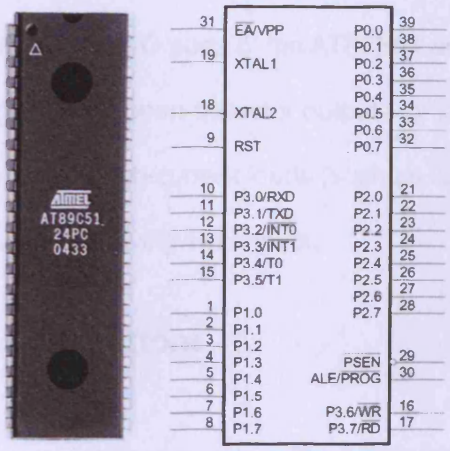

- Compatible with MCS®-51 Products
- 4K Bytes of In-System Programmable (ISP) Flash Memory – Endurance: 10,000 Write/Erase Cycles
- 4.0V to 5.5V Operating Range
- Fully Static Operation: 0 Hz to 33 MHz
- Three-level Program Memory Lock
- 128 x 8-bit Internal RAM
- 32 Programmable I/O Lines
- Two 16-bit Timer/Counters
- Six Interrupt Sources
- Full Duplex UART Serial Channel
- Low-power Idle and Power-down Modes
- Interrupt Recovery from Power-down Mode
- Watchdog Timer
- Dual Data Pointer
- Power-off Flag
- Fast Programming Time • Flexible ISP Programming (Byte and Page Mode) • Green (Pb/Halide-free) Packaging Option

Fig. 6.22 AT89S51 microcontroller and its features

6.2.6.2 Reset circuitry

Reset is an active High input in AT89S51, when RST pin is set to high, the chip goes back to the power on state. The AT89S51 is reset by holding the RST pin high for at least two machine cycles and then returning it low. The capacitor C9 is conducted in a very short period when the power is supplied, the short pulse is enough to reset the microcontroller and start the system. After the reset, the RST pin of AT89S51 stays low until the manual reset switch S10 is pressed.

6.2.6.3 Oscillator

XTAL1 and XTAL2 are the input and output, respectively, of an inverting amplifier that can be configured for use as an on-chip oscillator, as shown in Fig. 6.20. A 12MHz quartz crystal (Y1) is used.

6.2.6.4 Buffers

In order to match the logic levels, SN5417J buffers (U7) are used to couple the signals between the I/O ports of the AT89S51 and the drive board. SN5417J buffers feature high-voltage open-collector outputs for interfacing with high-level circuits (such as MOS) or for driving high-current loads (such as lamps or relays) and also are characterized for use as buffers for driving TTL inputs.

6.2.6.5 Buttons

Two push button switches (S4 & S5) are used to confirm or cancel the setting respectively, a joystick (S1 & S3) is applied to set the steps, direction, and interval.

6.2.6.6 Display

Two digits seven-segment display (DS1 & DS2) and four LEDs (D1 – D4) are used to indicate the system status. Two decoders SN74LS47D (U1 & U6) convert the BCD to seven-segment display indicators. The SN74LS47 are Low Power Schottky Decoder, offering active low, high sink current outputs for driving indicators directly.

6.2.6.7 Programmer

The AT89S51 microcontroller is an in-system programmable device, in order to use the download the codes into the microcontroller, an in-system programmer cable (Fig. 6.23) was also designed and made, which communicates serially with the AT89S51 and reprograms it in the circuit without removal. The software to download the codes into the cable is Atmel Microcontroller ISP Software®. The Atmel Microcontroller ISP Software is the primary means for performing in-system programming (ISP) for the Atmel devices. It provides an intuitive interface for in-system programming that can be run from a personal computer. The Atmel

ISP Software has a comprehensive set of features and allows the user to view, program, and erase data from an Atmel ISP device.

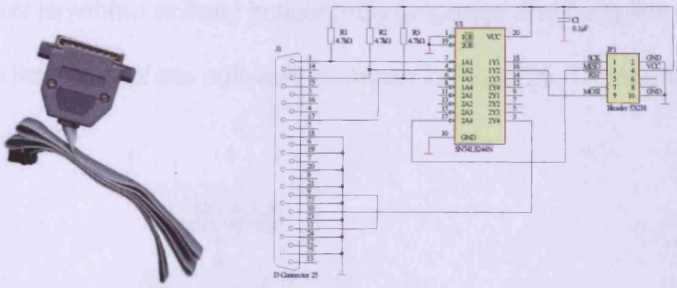

Fig. 6.23 ISP cable and schematic diagram

6.2.6.8 Assembly

The controller box is an ABS plastic 7.013 x 5.015 inch enclosure (dimensions in Appendix C). According to the positions and dimensions of the joystick, push buttons, indicators, seven-segment display, and sockets, the plastic enclosure was constructed in the workshop in School of Engineering, Cardiff University. The controller printed circuit board, drive board, peripheral devices, and necessary connections are assembled into the enclosure as shown in Fig. 6.24.

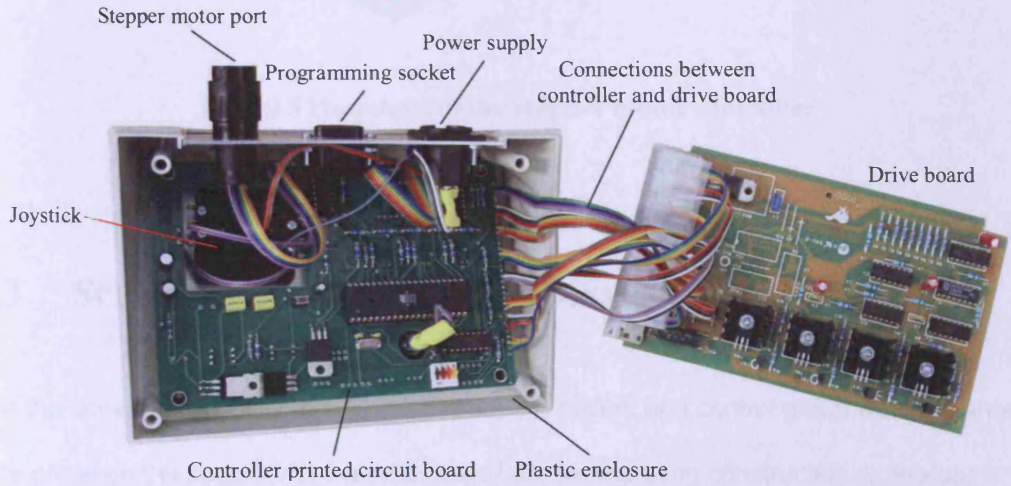

Fig. 6.24 The assembly of the controller

6.2.6.9 Software

The controller driver is written entirely in assembly language and compiles under Keil C51 (from Keil™). The flowchart of the software is shown in Fig. 6.25. There entire codes are attached in Appendix G.

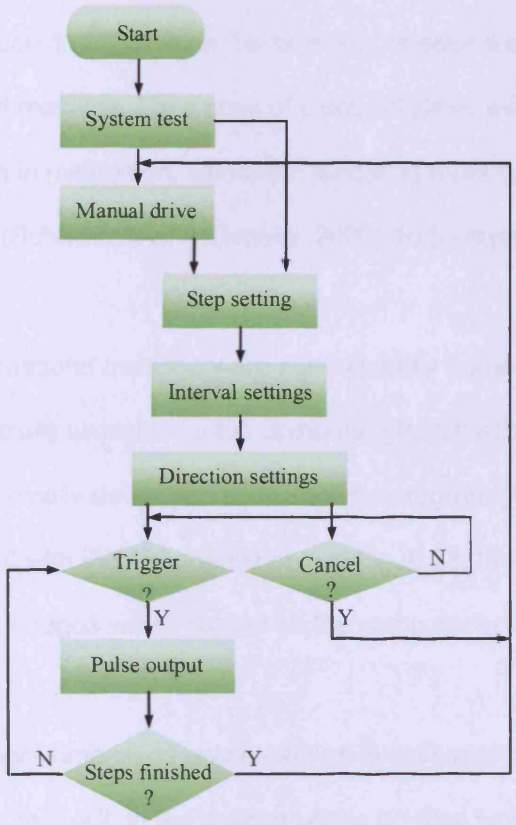

Fig. 6.25 Flowchart of the stepper motor controller

6.3 Scanning and Image Processing

After the conventional PDU examination, both the patient and control group were scanned while prone on the couch with the limb placed on the scanning constructed apparatus, consisting of a motorized track driving the same linear array transducer at a controlled, uniform step along the length of the Achilles tendon (Fig. 6.26).

The patient was asked to keep as still as possible to minimize motion artefacts. Sufficient acoustic coupling gel was spread on the skin to couple the transducer and the subject. The tendon was scanned in the transverse plane in all cases. The transducer was stopped at consecutive positions with an interval of 1 mm, typically over a length of 6 cm from the calcaneal insertion. At each 1 mm position, 38 frames of images were saved as a 2 second AVI file on the ultrasound machine. For a scan of 6 cm, 60 slices were produced, to allow the entire neovascularization in midportion, where the tendon is most susceptible to degeneration and injury (Schweitzer and Karasick 2000), to be registered.

All the AVI files in the ultrasound machine were subsequently burned into a CD-ROM and transferred to a commercially available laptop computer (Toshiba Satellite Pro) with a T2400 1.83 GHz CPU. In the specially developed pixel analysis program (Fig. 6.27, developed in Microsoft Visual Basic 6.0 with the flowchart shown in Fig. 6.28, the entire codes are attached in Appendix D), images were recalled on the computer screen.

At the beginning, the programme could only create an ovoid superimposition on the region of Achilles tendon. This worked well on the images where Achilles tendons are regular, as shown in Fig. 8.2. However, in the majority the Achilles tendons showed non-ovoid transverse slices (Fig. 3.2). To match the borders of the Achilles tendon on the transverse slice, I updated the programme to be able to manually outline a polygon to follow the trend of the borders. By doing this, a region of interest (ROI) was manually marked by the edges of polygon based on the boundary between the Achilles tendon and surrounding tissue.

Then a region of interest (ROI) was manually marked by the edges of polygon based on the boundary between the Achilles tendon and surrounding tissue. This ROI outline ensured that only the Doppler signals within the Achilles tendon were statistically evaluated and that

surrounding signals were excluded. Since the ROIs on each slice contained the entire section through the desired structure, the visualization of the Achilles tendon was obtained after the 3D reconstruction.

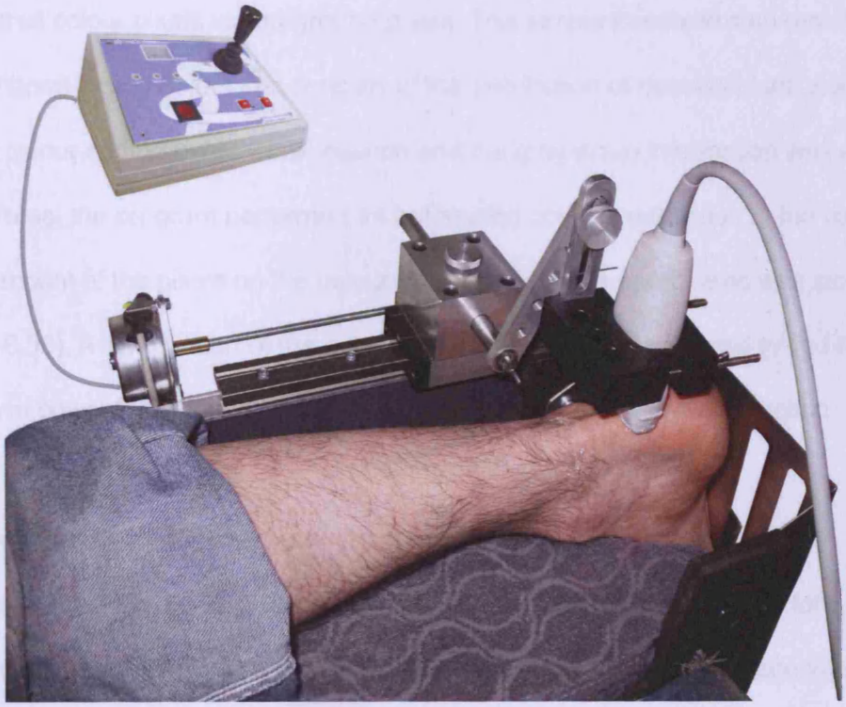

Fig. 6.26 Data acquisition setup

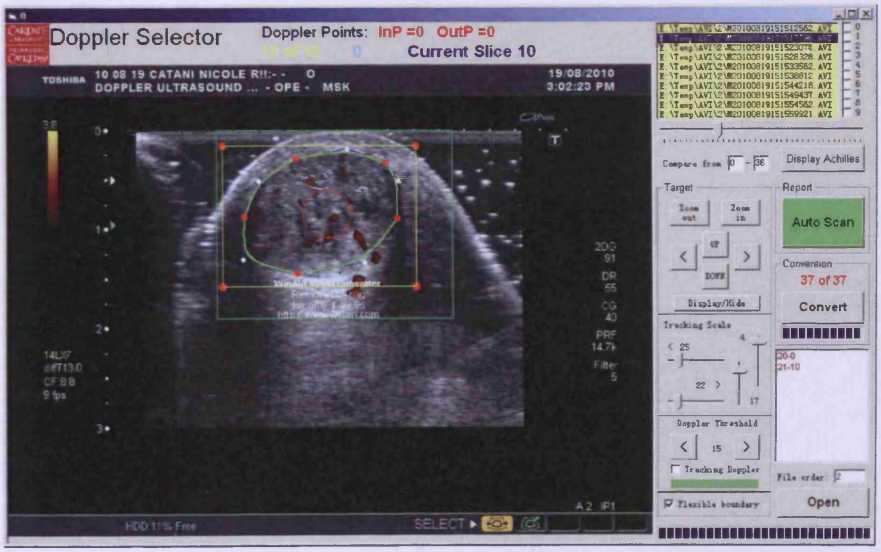

Fig. 6.27 Program interface

Another function of the program was to present a frame with maximal power Doppler signal and another with minimal. For each position, there were 38 frames extracted from each video clip (Fig. 6.29). Our technique treated power Doppler images as binary images by considering all colour pixels as foreground pixels. This simple threshold step resulted in a complex shaped binary object that consists of the distribution of neovascularization. Only the pixels with colour-coding bytes were retained and the grey-scale information was eliminated. For each frame, the program performed an automated contour extraction of the colour data. The total amount of the pixels on the colour-coding objects on each frame was stored in an array (Fig. 6.30). A comparison of the amount of the pixels was performed to find the frame with maximal power Doppler signal, which then be used in the 3D reconstruction.

The program then created 60 representative maximum (systolic) frames and 60 representative minimum (diastolic) frames, which were both reconstructed to form two 3D images of the neovascularization in both phases, using a commercial 3D reconstruction and analysis software. The maximum and minimum volumes of neovascularity (VON) were also computed in the software.

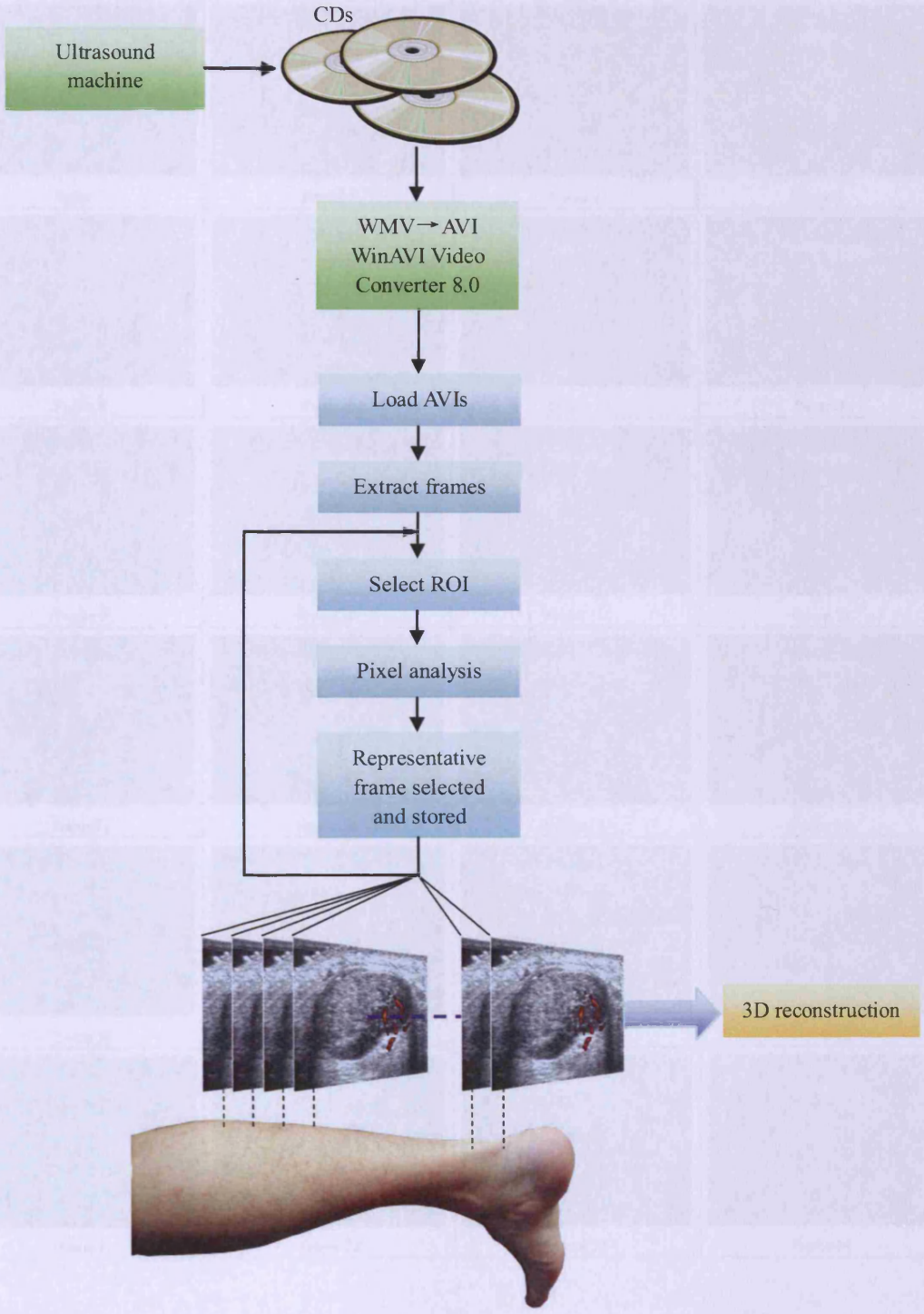

Fig. 6.28 Acquisition flowchart

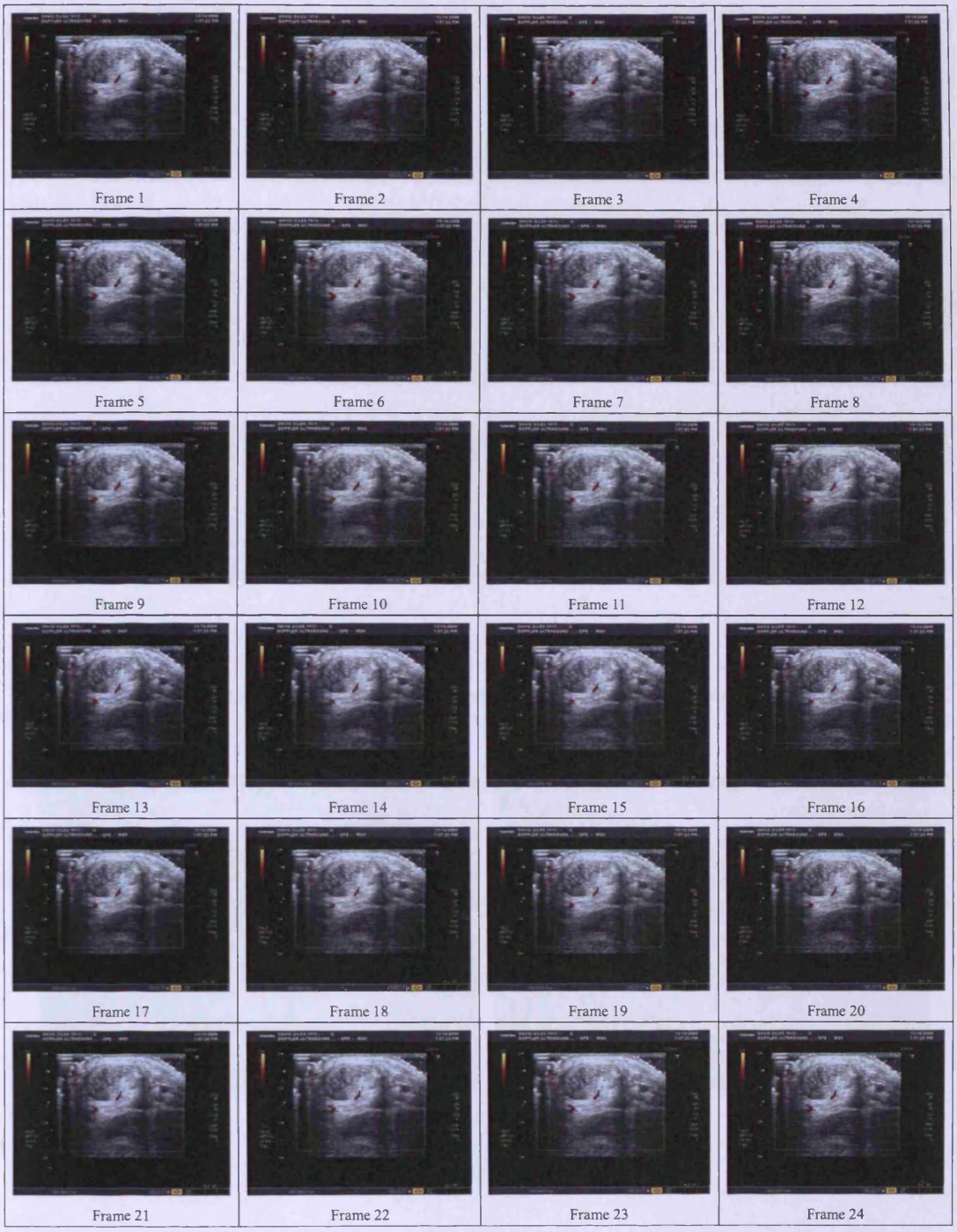

Frame 1 | Frame 2 | Frame 3 | Frame 4

Frame 5 | Frame 6 | Frame 7 | Frame 8

Frame 9 | Frame 10 | Frame 11 | Frame 12

Frame 13 | Frame 14 | Frame 15 | Frame 16

Frame 17 | Frame 18 | Frame 19 | Frame 20

Frame 21 | Frame 22 | Frame 23 | Frame 24

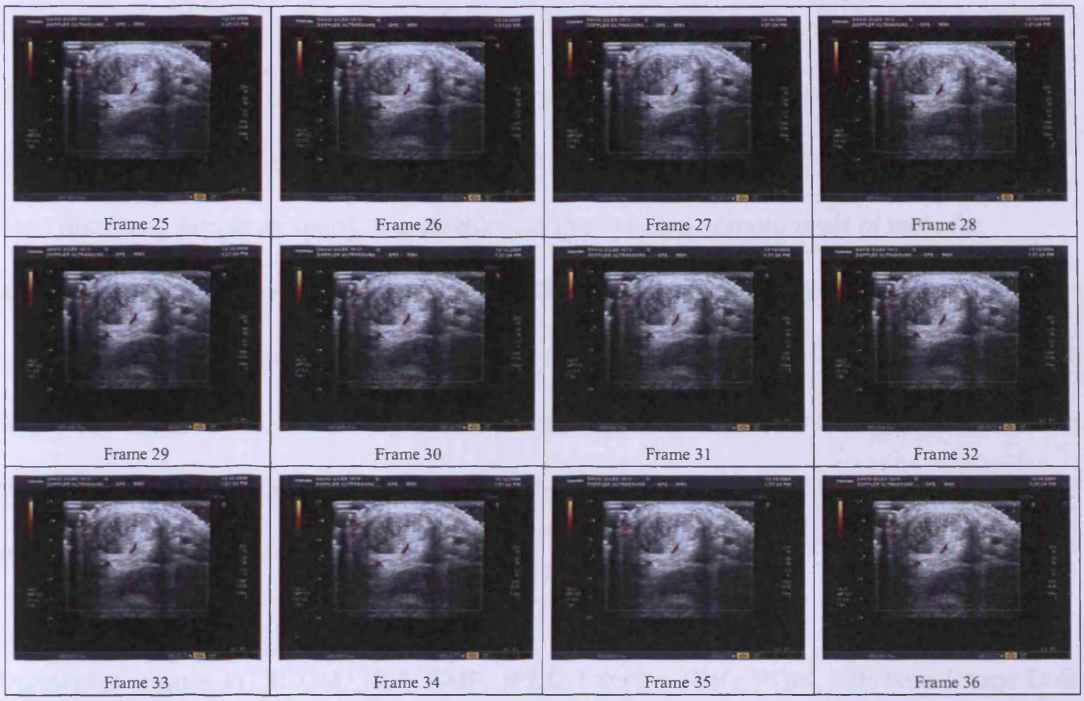

Fig. 6.29 Example of frames extracted from video clip

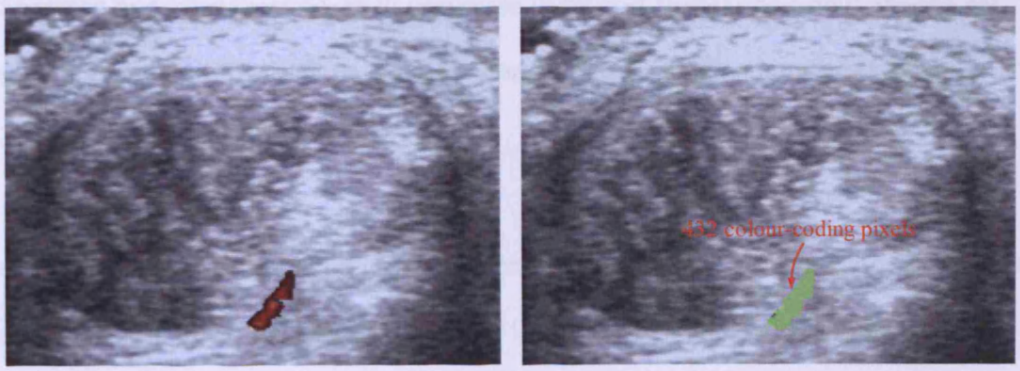

Fig. 6.30 Example of flow extracted

6.4 3D Reconstruction and Volume Measurement

After the representative frames were acquired from the last procedure, a 3D volume reconstruction of the Doppler signal was performed in a commercial 3D imaging analysis software 3D-DOCTOR® (Able Software Corp.)

3D-DOCTOR® is an advanced 3D image rendering, processing, and analysis software, which is approved for medical imaging and 3D visualization applications by US FDA (US Food and Drug Administration). It is developed to provide a complete set of tools for visualizing 3D volume image data, including CT, MRI, Microscopy, ultrasound, and other types of imaging. The software works by extracting object boundaries using 3D image segmentation functions, and creating both 3D surface and volume rendering for visualization, object measurement, and quantitative analysis. It includes all these functions in a single integrated easy-to-use package.

Transverse images in DICOM, TIFF, BMP, JPEG, Interfile, PNG, PGM, GIF, Raw Image Data, and other uncompressed image formats are accepted in 3D-DOCTOR®. Image files in various vendor specific formats can be easily read using 3D-DOCTOR®'s universal image configuration and input function. Both grayscale (8-bit and 16-bit) and colour images are supported. Scanned CT/MRI films can easily be cropped using the template-based function for 3D imaging applications.

The fully automatic texture-based segmentation for grayscale and colour images works with most images. The threshold-based Interactive Segmentation is perfect for processing different images. The region-based Object Segmentation allows quick segmentation of local areas, such as a tumour. The easy-to-use polygon-based manual tracing method provides the flexibility of segmenting tissues with weak edges.

From segmented boundary data, a 3D surface mesh model is created quickly using one of the vector-based surface rendering commands. 3D models of multiple tissue objects are supported for realistic 3D display and quantitative analysis. The surface area, volume, distance, angle, profile and image region histogram are easily measured in 3D-DOCTOR®.

Detailed reports can be produced for quantitative analysis of tissue areas and volumes.

6.5 Subjects

The ethical approval for the current study was given by two ethical committees, Engineering School Research Committee, Cardiff University and South East Wales Research Ethics Committee panel D. The examinations were divided into two sections, system validation and correlation investigation.

In order to investigate whether the quantitative evaluation system was capable of determining the healthy and symptomatic Achilles tendon, I conducted an initial experiment to scan control and patient groups. With the optimized machine settings and other criteria described in Chapter 5, the evaluation system should be able to identify whether an Achilles tendon was undergoing tendinopathy by the VON. If the system showed the capability to pick up the Achilles tendon with pathology, a following clinical trial would be performed to investigate the correlation between the VON and clinical severity. Therefore, the examinations were divided into two sections, system validation and correlation investigation.

6.5.1 Subjects in system validation

Twelve tendons from 10 subjects (9 men and 1 woman) with a mean age of 45 years (range from 23 to 57) with a chronic painful Achilles tendon, and twenty tendons from 10 controls (8 men and 2 women) with a mean age of 41 years (range from 28 to 49) with no history of an Achilles tendinopathy, were prospectively enrolled in the validation of the scanning and reconstruction system. The patients and controls provided written informed consent. Diagnosis of Achilles tendinopathy was confirmed by a consultant orthopaedic surgeon and a conventional ultrasonographic examination.

6.5.2 Subjects in correlation investigation

Forty tendons from 30 patients (16 men and 14 women) with a mean age of 49.7 years (range from 37 to 79) with a chronic painful Achilles tendon were enrolled in the study. Inclusion and exclusion criteria are reported in Table 5.3. The patients provided written informed consent. Diagnosis of Achilles tendinopathy was confirmed by a consultant orthopaedic surgeon and the conventional ultrasonographic examination. After patients had been selected for inclusion by the Trauma Clinic at the University Hospital of Wales, appointments were made for ultrasound examinations. All patients were examined by a single researcher using a standard protocol.

6.6 Reliability

All ultrasound examinations were performed using the system above, which had been calibrated by scanning a known volume gel cube, in which the ultrasound speed (1610 m/s) is similar to that in the soft tissue (1540 m/s). The variation between the real and reconstructed volume was found to be not statistically significant ($p < 0.05$).

To assess reproducibility, all the control and symptomatic subjects were scanned twice on the same apparatus. Afterwards, two experienced researchers performed independent evaluations of the maximum and minimum VON twice for each subject. Images were processed in the same specially developed pixel analysis program to produce 60 representative maximum vascularity frames and 60 representative minimum vascularity frames. Afterwards, the data in a given subject including two sets of maximum and minimum slices were visualized and reconstructed in the same 3D reconstruction software. Thereby, two maximum VONs, sVON1 and sVON2, and two minimum VONs, dVON1 and dVON2, were calculated. The mean maximum VON, derived from (sVON1+ sVON2)/2, and the mean

minimum VON, derived from (dVON1+ dVON2)/2, were used to denote the amounts of neovascularity at maximum (representing the systolic) and minimum (representing the diastolic) phases for each subject, respectively.

Inter-observer variability was evaluated by comparing the mean of the first and the second measurement of each researcher. The assessment of intra-observer variability was based on comparison between the first and the second set of measurements of each researcher. The intra-class correlation coefficient (ICC) was used to evaluate the inter- and intra-observer variability (Shrout and Fleiss 1979). The reliability is excellent if ICC is greater than 0.75, fair to good if ICC is 0.75 to 0.4, and poor if ICC is less than 0.4 (Fleiss 1986).

6.7 Statistical Evaluation

For the statistical analysis in system validation, the SPSS13.0 software (SPSS Inc., Chicago, IL, USA) was used. Inter- and intra-observer variability were analyzed with a one-way random model. A Q-Q plot for the VONs in the system validation and the following clinical trial were obtained in SPSS13.0, which is a graph that can decide whether the data are Normally distributed or not. The Q-Q plot of the VONs in controls, patients were shown in Fig. 6.31, which show that all the data were not normally distributed since the points did not follow the line well. Therefore, all the statistical analysis was performed with non-parametric tests.

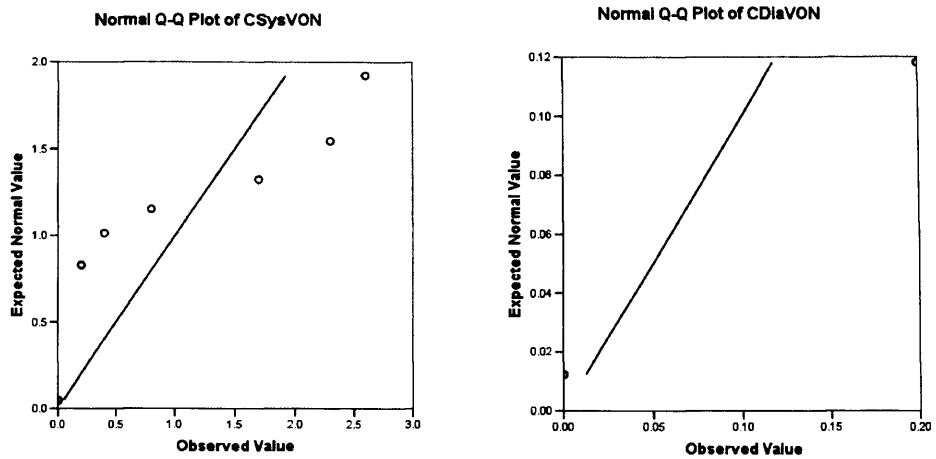

(a)Q-Q plot of the controls in validation (maximum and minimum VON)

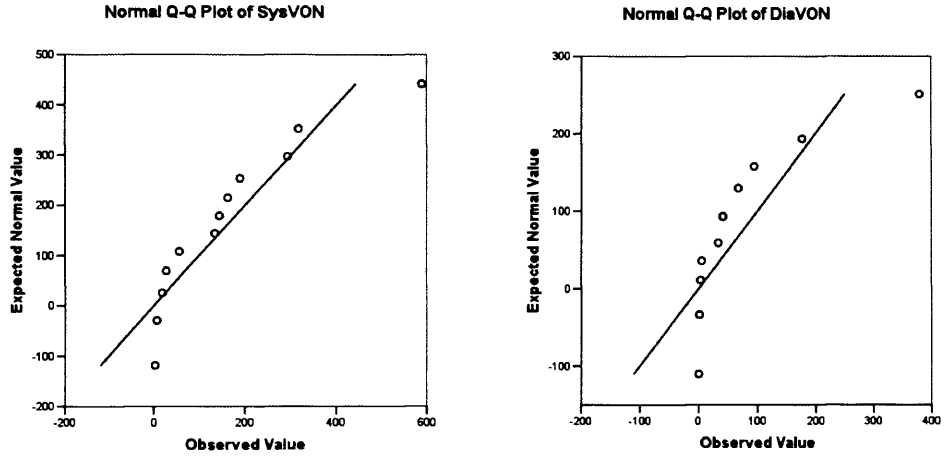

(b)Q-Q plot of the patients in validation (maximum and minimum VON)

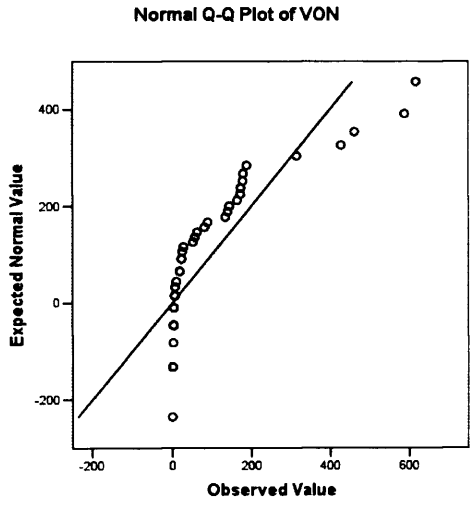

(c)Q-Q plot of the patients in clinical trial (maximum VON)

Fig. 6.31 Q-Q plots of the VONs in controls and patients

The non-parametric Mann-Whitney U and Wilcoxon tests were applied to compare the difference between the volume of vascularity between control and patient group, and the

difference of the volume at maximum and minimum phases within both the control and patient group, respectively. In addition, descriptive statistics were used to characterize the data. In the case of a statistically significant result, the probability value (p value) less than 0.05 was considered to be significant.

For the statistical analysis in correlation investigation, the SPSS 13.0 software (SPSS Inc., Chicago, IL, USA) was used as well. G*Power 3 (Franz Faul, University of Kiel, Germany) was applied for power analysis. Spearman correlation was used to evaluate the degree of association between VON and the scores of VAS and VISA-A. Two tail post-hoc power analysis was performed after the study to find out the significant effects of the VON in predicting the level of pain and the clinical severity.

6.8 Conclusions

This chapter described the designs and structures of the experimental system used in the quantification of the VON in Achilles tendinopathy. A computerized motor-driven track was built to hold the conventional ultrasound probe to scan at a controlled step. A specially developed program was used to retrieve the frame with maximum and minimum Doppler signals. Then the visualization and measurement were performed in a commercial available software 3D-DOCTOR. Subjects were examined both in the system validation, including the investigation of reliability, and in correlation investigation in the novel 3D Doppler ultrasound system. The experimental results will be reported in the next chapter.

7. Results

This thesis focused on the quantification of the VON in Achilles tendinopathy and correlation between VON and the clinical severity of the disease. The VONs in both control and patients with the maximum and minimum values due to the cardiac cycle were first reported. In the following clinical trial, VONs were collected among 40 symptomatic Achilles tendons, as well as the assessment of VAS and VISA-A.

7.1 Intra- and Inter-Observer Variability

The results of the mean VON for both control and patient groups obtained by two researchers are summarized in Table 7.1. The mean maximum VON in control group ranged between 0.3 mm^3 and 0.6 mm^3, The ICC for intra-observer variability was close to 1 for each of the 2 researchers with values of 0.974 and 0.943, respectively. The ICC value derived between the 2 researchers was 0.404 indicating that the inter-observer variability was medium (in the 'fair to good' range).

The mean minimum VON in control group was close to 0 mm^3, The ICC for intra-observer variability was 0.556 and 0.940, respectively, between 2 researchers. The ICC for the inter-observer variability in minimum VON was 0.404.

The mean maximum VON in patient group ranged between 158.2 mm^3 and 165.6 mm^3, The ICC for intra-observer variability was also closed to 1 for each of the 2 researchers with values of 0.986 and 0.964, respectively. The inter-observer variability was small, with an ICC value of 0.964.

The mean minimum VON in patient group ranged between 61.4 mm^3 and 82.1 mm^3. The intra-observer variability was similar to the maximum phase, with the ICC values of 0.986 and 0.964 for the 2 researchers. A small variance was found between 2 researchers, with an ICC value of 0.984.

Table 7.1 Inter- and intra-observer variability for VON in both control and patient groups

	Researcher 1	Researcher 2
Intra-observer variability		
Mean maximum VON in control 1 (mm^3)	0.5(1.1)	0.3(0.8)
Mean maximum VON in control 2 (mm^3)	0.6(1.5)	0.3(0.6)
ICC	0.974	0.943
Inter-observer variability		
Mean maximum VON in control (mm^3)	0.5(1.3)	0.3(0.7)
ICC	0.404	
Intra-observer variability		
Mean minimum VON in control 1 (mm^3)	0(0.1)	0(0.1)
Mean minimum VON in control 2 (mm^3)	0(0)	0(0.1)
ICC	0.556	0.940
Inter-observer variability		
Mean minimum VON in control (mm^3)	0(0.1)	0(0.1)
ICC	0.404	
Intra-observer variability		
Mean maximum VON in patient 1 (mm^3)	163.6(175.0)	165.6(161.5)
Mean maximum VON in patient 2 (mm^3)	158.2(173.2)	159.2(189.8)
ICC	0.986	0.964
Inter-observer variability		
Mean maximum VON in patient (mm^3)	160.9(172.9)	162.4(173.1)
ICC	0.964	
Intra-observer variability		
Mean minimum VON in patient 1 (mm^3)	68.2(106.8)	82.1(145.4)
Mean minimum VON in patient 2 (mm^3)	69.3(104.4)	61.4(89.7)
ICC	0.986	0.964
Inter-observer variability		
Mean minimum VON in patient (mm^3)	68.8(105.3)	71.7(117.2)
ICC	0.984	

7.2 Control Group in Validation

All the healthy subjects were given the identical scanning procedures using the apparatus and off-line analysis described in Chapter 6. Twenty normal Achilles tendons including any vascularity were reconstructed with volume information attached for each case. In control group, the maximum VON ranged from 0 mm^3 to 3 mm^3 with the mean of 0.41 mm^3 (SD=0.8), while the minimum VON ranged from 0 mm^3 to 0.2 mm^3 with the mean of 0.02 mm^3 (SD=0.1), which indicates that, the VON at both the maximum and minimum were very small (Fig. 7.1). Fig. 7.2 shows 10 normal tendons with the volume of vascularity ranged from 0 mm^3 to 3 mm^3, which indicate that, in general terms, the vascularity does not notablely exist in healthy Achilles tendon using ultrasound examinations with optimized machine settings.

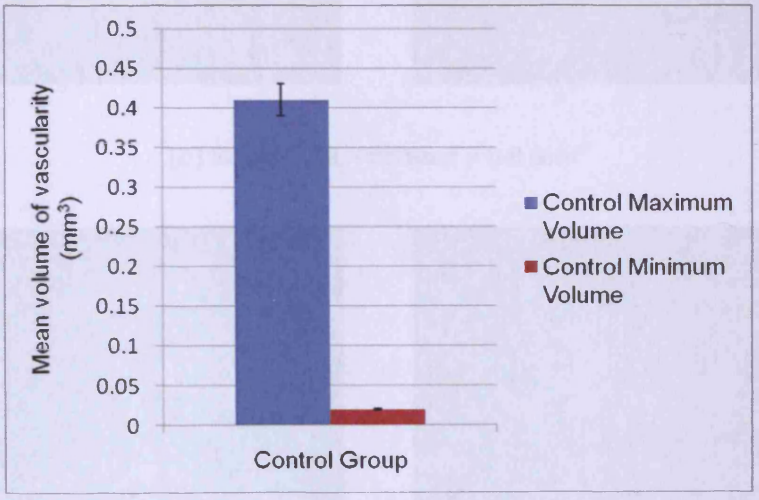

Fig. 7.1 The mean VON at maximum and minimum phases in control group.

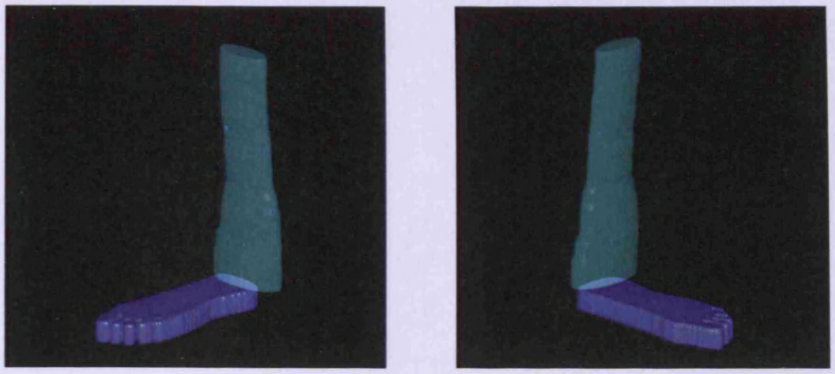

(a) Subject 1L – volume = 0.2 mm³

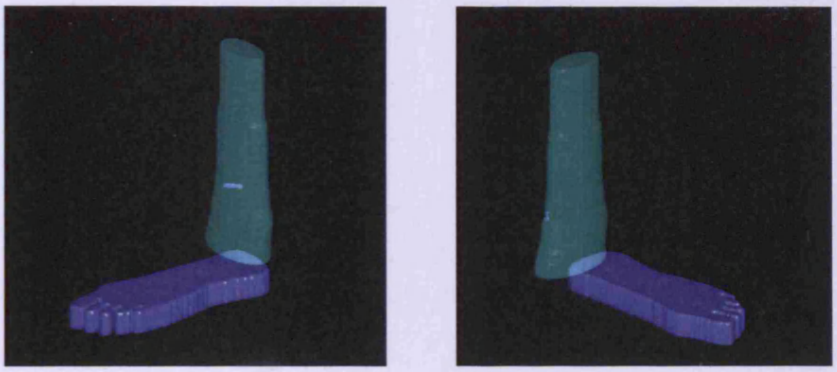

(b) Subject 1R – volume = 0.8 mm³

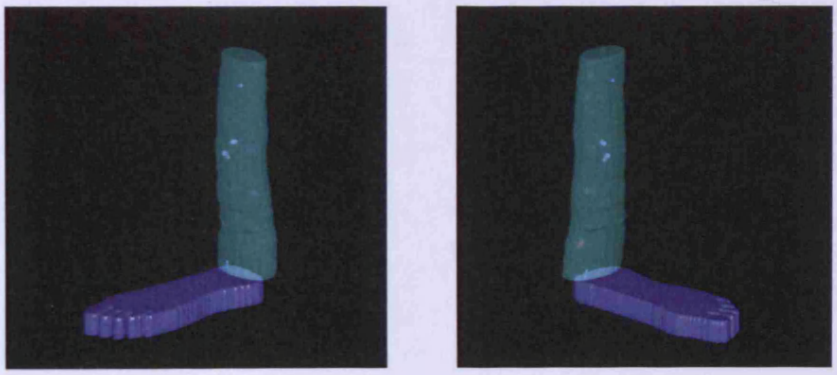

(c) Subject 2L – volume = 1.7 mm³

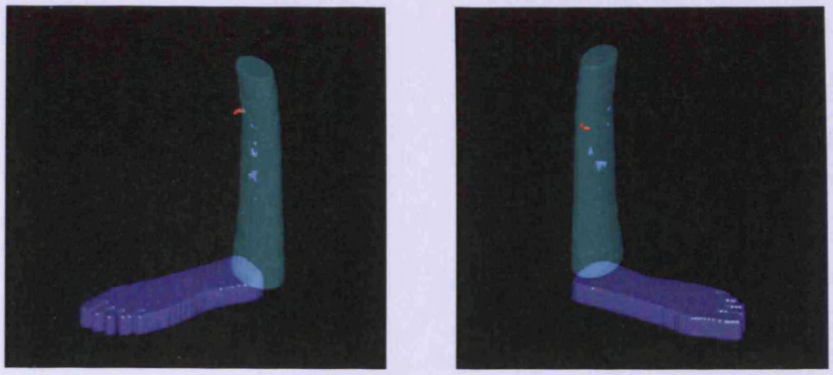

(d) Subject 2R – volume = 2.3 mm³

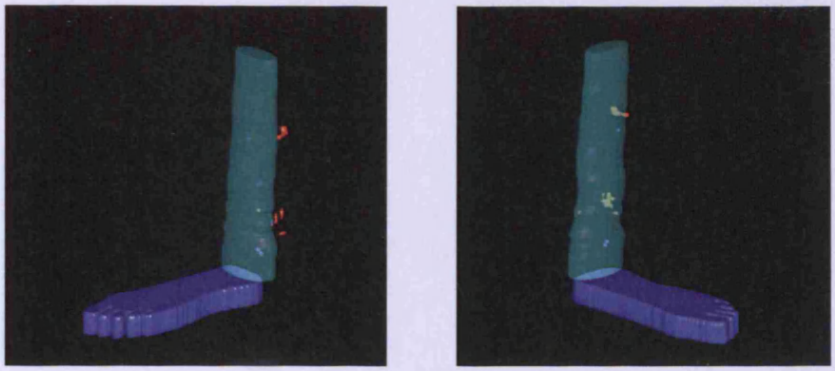

(e) Subject 3L – volume = 0.4 mm³

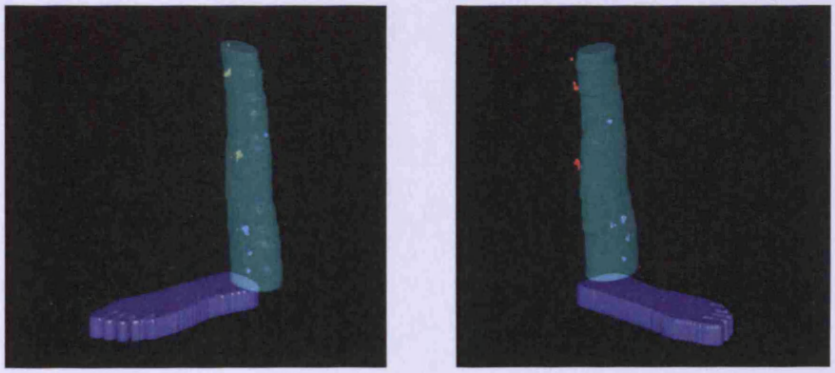

(f) Subject 3R – volume = 2.6 mm³

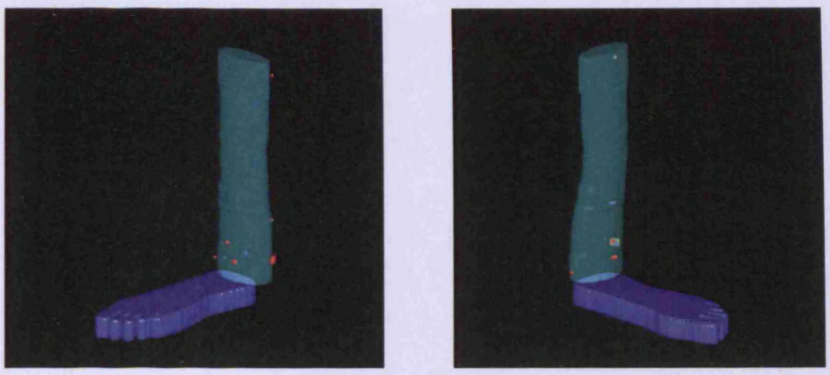

(g) Subject 4L – volume = 0.2 mm³

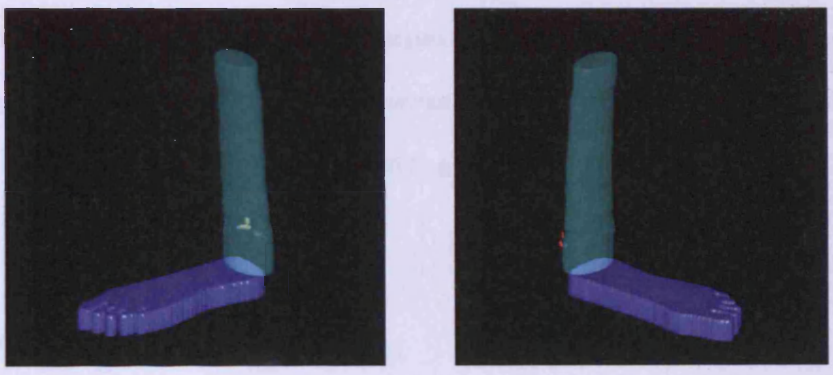

(h) Subject 4R – volume = 0 mm³

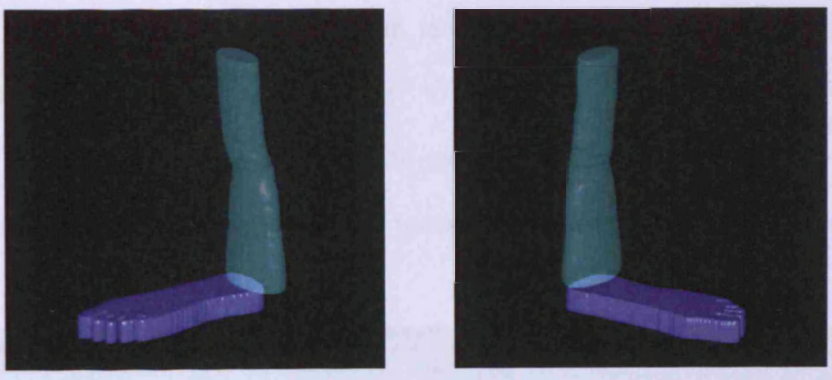

(i) Subject 5L – volume = 0 mm³

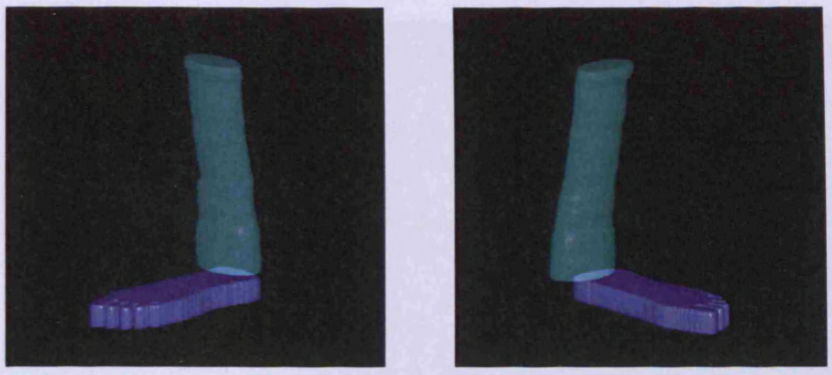

(a) Subject 5R – volume = 0 mm^3

Fig. 7.2 20 normal Achilles tendon reconstruction results with the volume of the vascularity. Green entity in the model is the manually added Achilles tendon, Blue 'foot' is another manual entity used to give the spatial information.

7.3 Patients in Validation

In the patient group, transverse slices were reconstructed (Fig. 7.3), neovascularization was noted in all 12 symptomatic Achilles tendons in 10 patients. The maximum and minimum VON were ranging from 3 mm^3 to 589 mm^3 with the mean of 161.7 mm^3 (SD=171.5) and 0 mm^3 to 380 mm^3 with the mean of 70.3 mm^3 (SD=110.5), respectively (Fig. 7.4), among which two patients were recorded as bilateral Achilles tendinopathy.

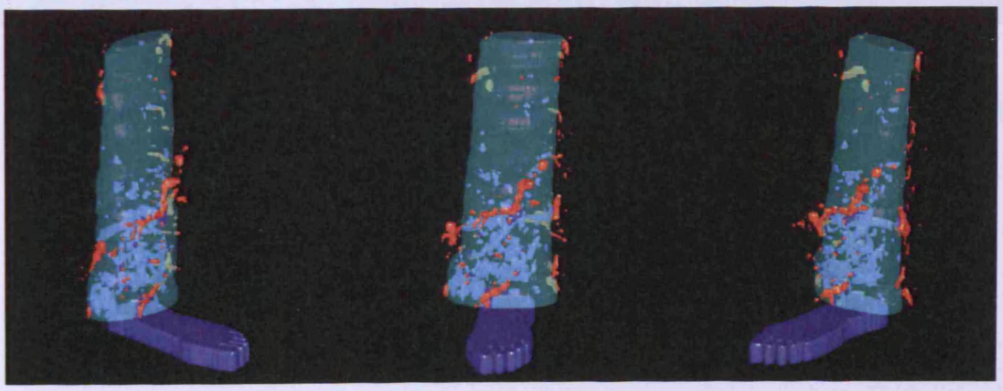

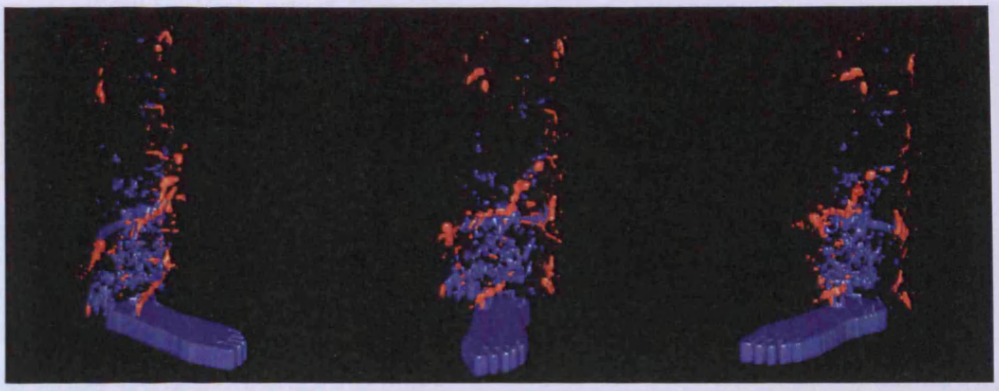

(a) Patient 1 – mean volume = 316 mm³

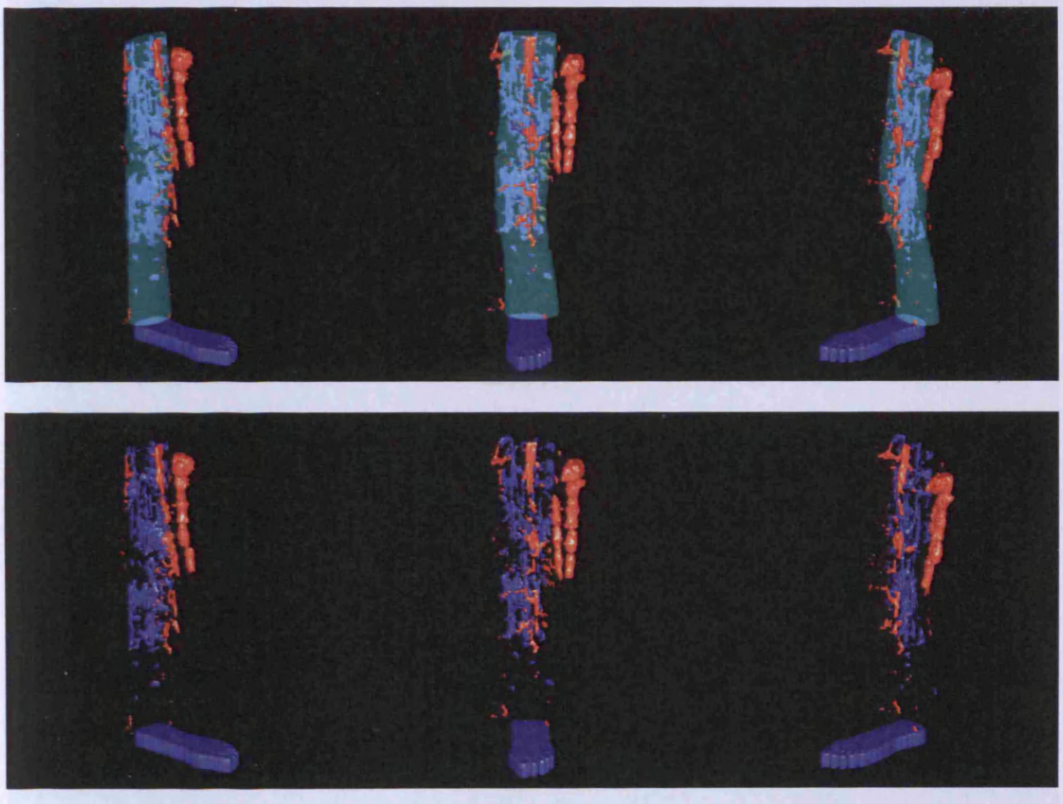

(b) Patient 2 – mean volume = 589 mm³

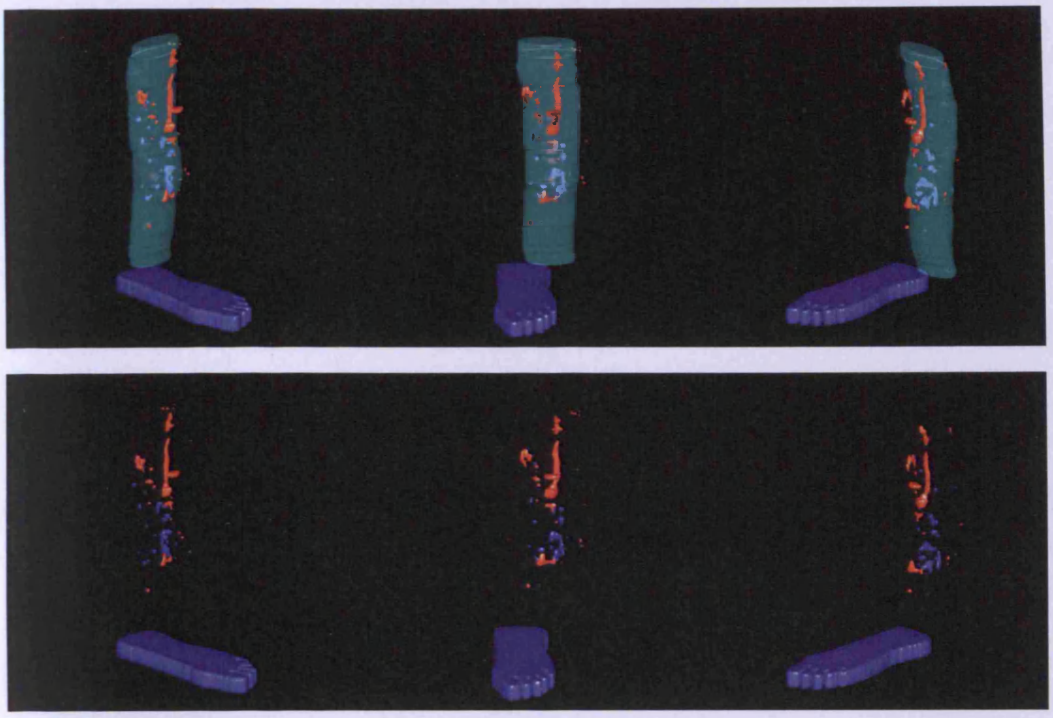

(c) Patient 3 – mean volume = 19 mm^3

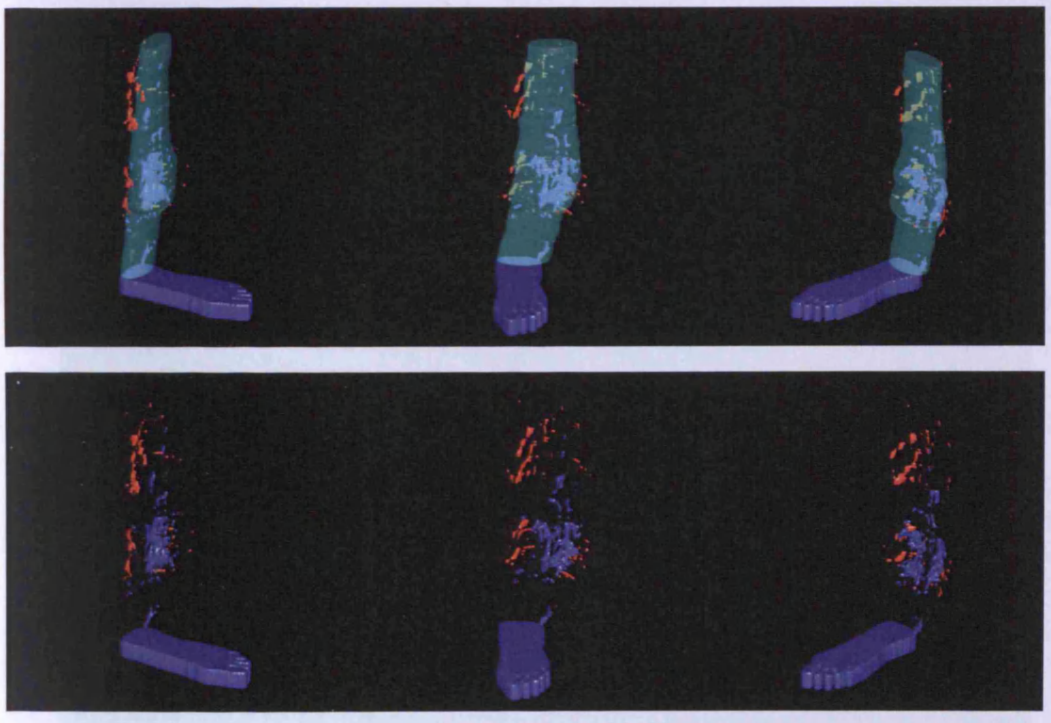

(d) Patient 4 –mean volume = 134 mm^3

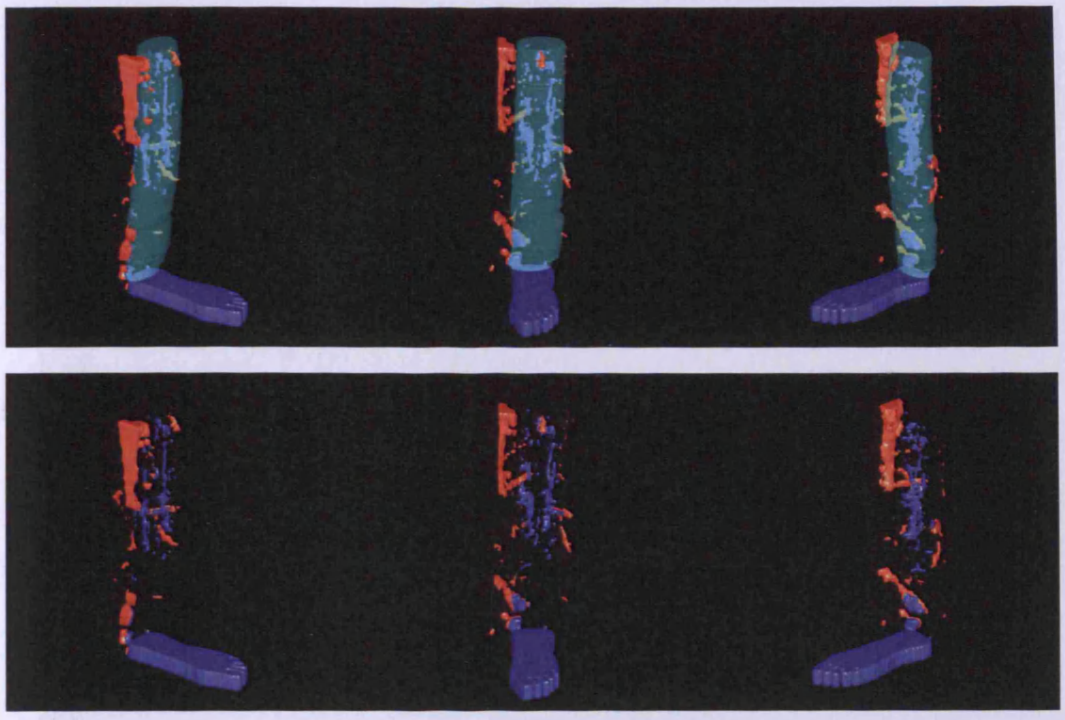

(e) Patient 5 – mean volume = 144 mm³

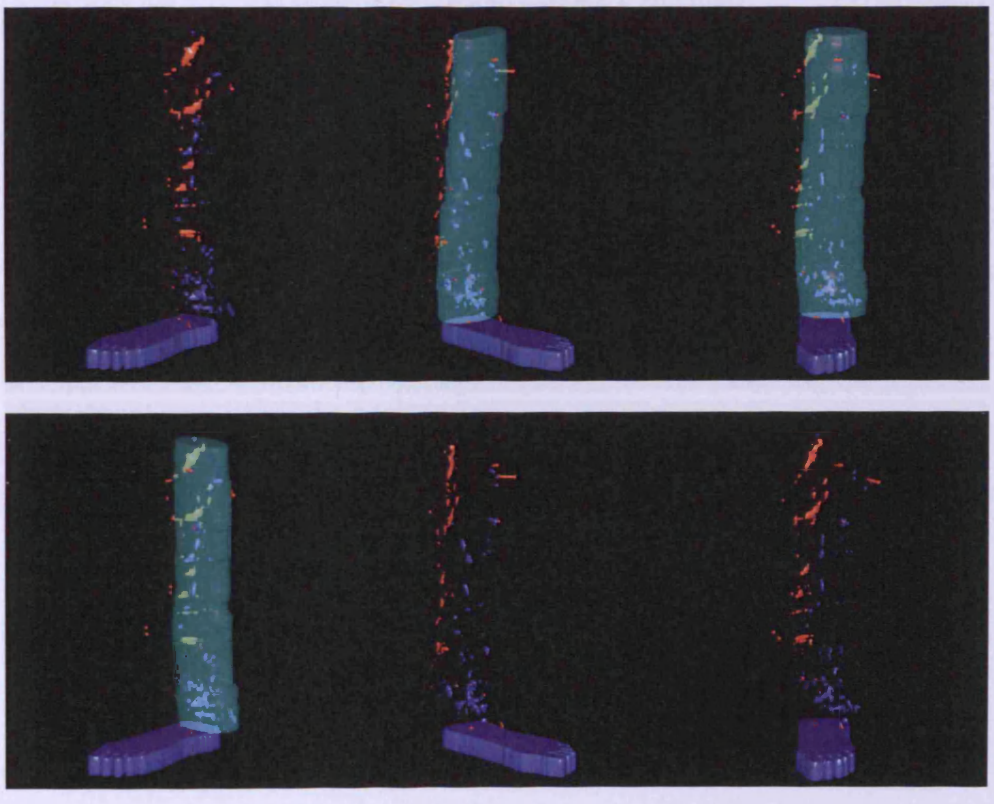

(f) Patient 6L – mean volume = 28 mm³

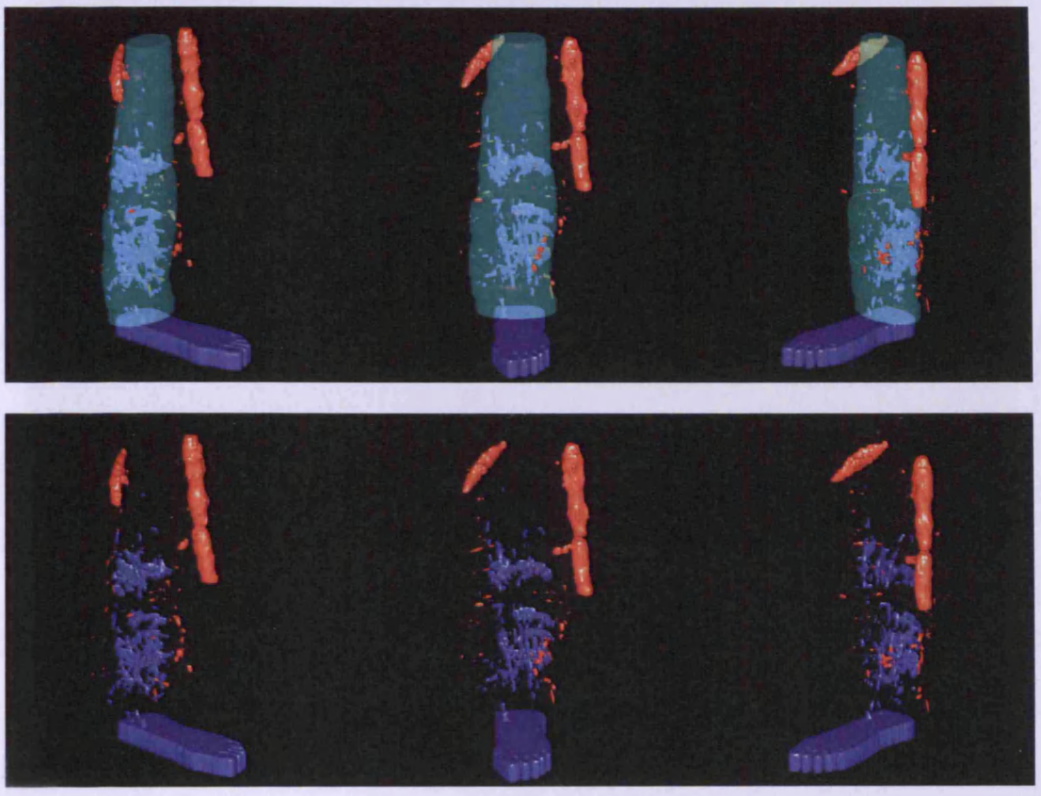

(g) Patient 6R – mean volume = 292 mm³

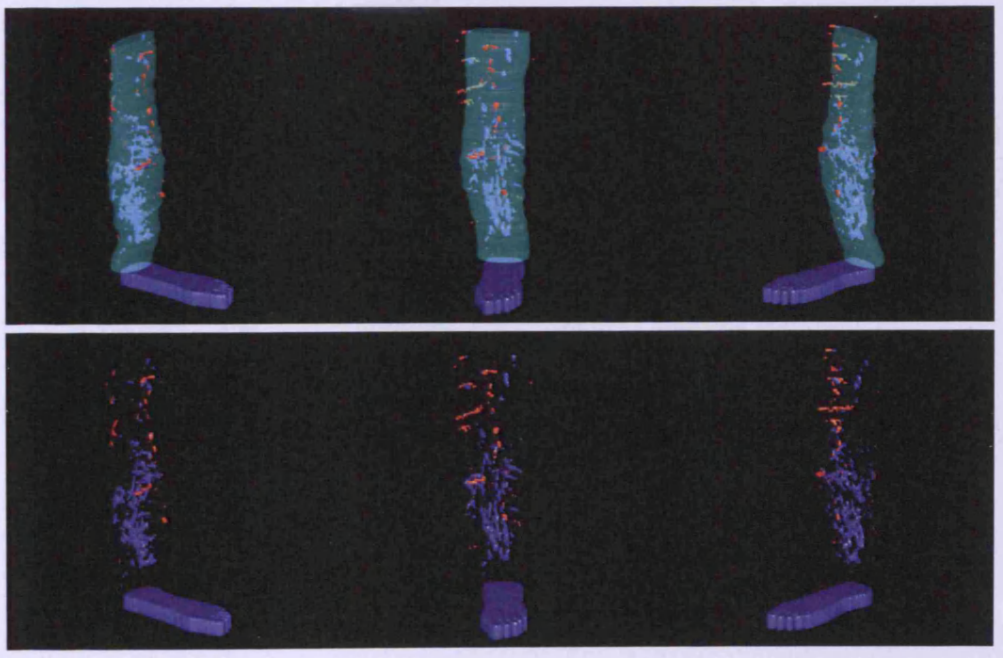

(h) Patient 7L – mean volume = 189 mm³

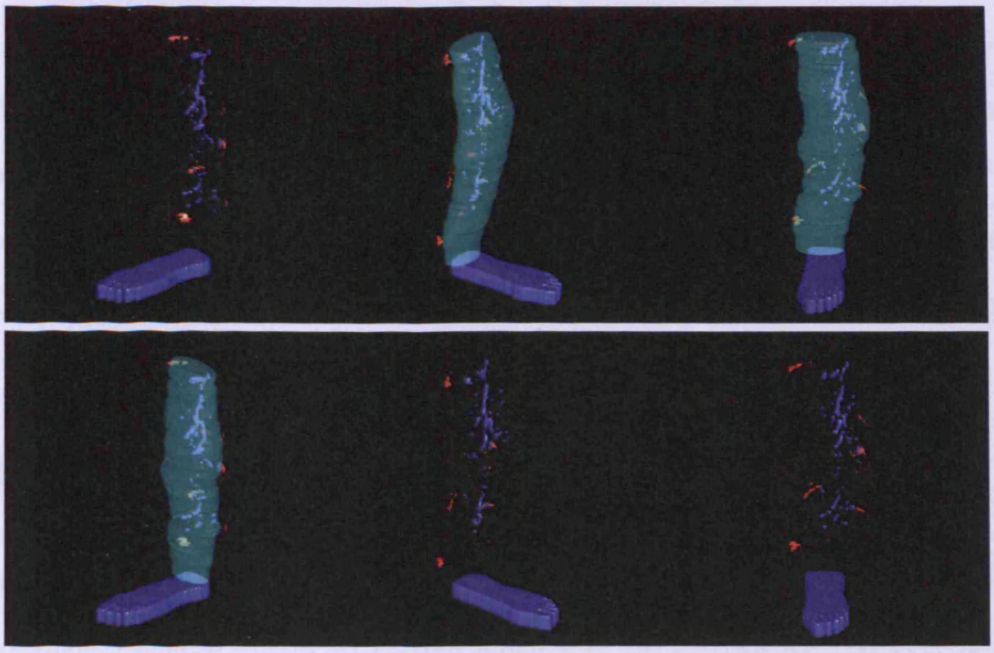

(i) Patient 7R – mean volume = 57 mm^3

Fig. 7.3 3D reconstruction of nine Achilles tendon from seven patients. The blue neo-vessels are the vascularity found in Achilles tendon, the oranges are the blood vessels surrounding the Achilles tendon.

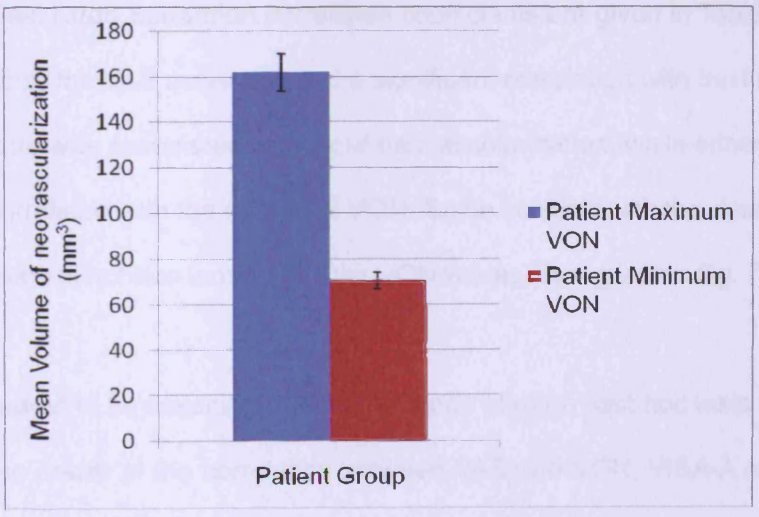

Fig. 7.4 The mean VON at maximum and minimum phases in patient group.

For both control and patient groups in system validation, the mean VON at maximum phase ($p<0.01$) was greater than that in the minimum phase ($p<0.01$).

For both maximum and minimum phases, the mean VON of the patient group was notably greater than the mean volume of vascularity of the control group in Wilcoxon test, reporting a p value of 0.002, and 0.018, respectively. The difference of the VON between maximum and minimum was greater in the patient group than that in the control group.

7.4 Patients in Correlation Investigation

In the following clinical trial, neovascularization was noted in 97.5% (n = 39) of symptomatic subjects among 40 Achilles tendons in the 30 patients. The VON ranged from 0 mm^3 to 618 mm^3 (mean 111 mm^3, SD=161). VAS score ranged from 0 to 100 (mean 41, SD=20), VISA-A score ranged from 2 to 87 (mean 44, SD=17).

A positive Spearman correlation was detected between VAS and VON, while a negative correlation was noted between VISA-A and VON, as shown in Fig. 7.5 and Fig. 7.6, respectively. Calculated Spearman correlation coefficients are given in Table 7.2, which indicates that only the VAS score denoted a significant correlation with the level of VON. A higher VAS score was associated with more neovascularization, while either VISA-A and age was not correlated with the degree of VON. Some subjects with the visualization of neovascularization in Achilles tendon with the VON values were given in Fig. 7.7.

The VON appeared to be associated with the degree of pain, post-hoc tests (Cohen 1988) showed that the power of the correlation between VAS and VON, VISA-A and VON were 0.89 (effect size $|\rho|=0.46$, total sample size=40) and 0.75 (effect size $|\rho|=0.39$, total sample size=40), respectively. The statistical power value, also known as Type II error rate, should be greater than 0.80, to detect a reasonable departure from the null hypothesis (Cohen 1988). Therefore, the probability of correctly rejecting the null

hypothesis of the correlation between VAS and VON is greater than that of the correlation between VISA-A and VON. In addition, the small, medium, and large effect size is defined to be $|\rho|= 0.1$, $|\rho|= 0.3$, and $|\rho|= 0.5$, respectively, this could therefore be more safely to conclude from this thesis that with an effect size between medium and large, the volume of neovascularity (VON) has a potential effect on pain (VAS) in a symptomatic Achilles tendon.

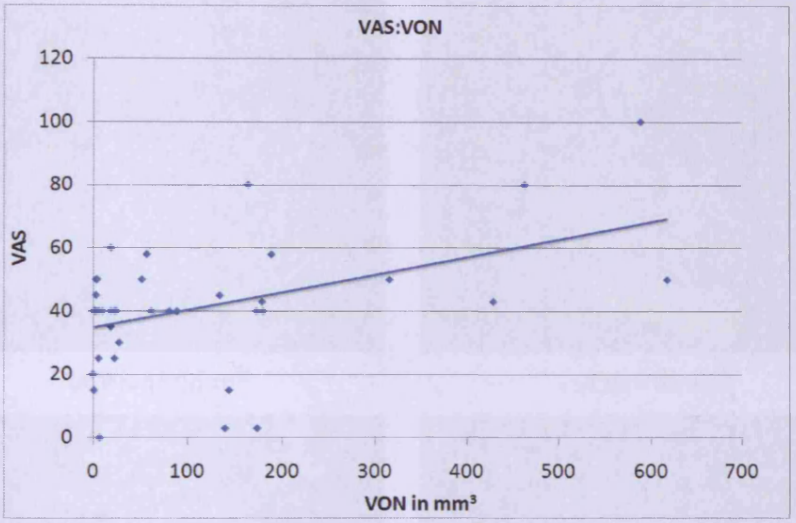

Fig. 7.5 Scatter plot of VAS and VON ($r = 0.326, p = 0.04$)

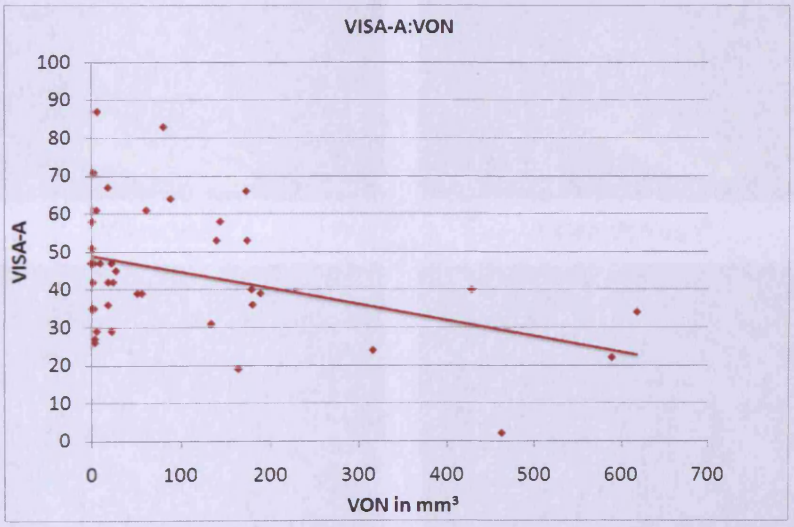

Fig. 7.6 Scatter plot of VISA-A and VON ($r = -0.246, p = 0.127$)

Table 7.2 The Spearman Correlation between different variables and VON

Variable	Spearmen Correlation	*p*-value
VAS	0.326	0.04
VISA-A	-0.246	0.127
Age	-0.058	0.723

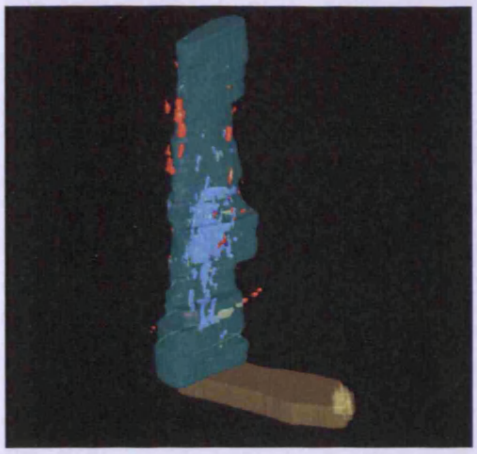

VON=158mm^3

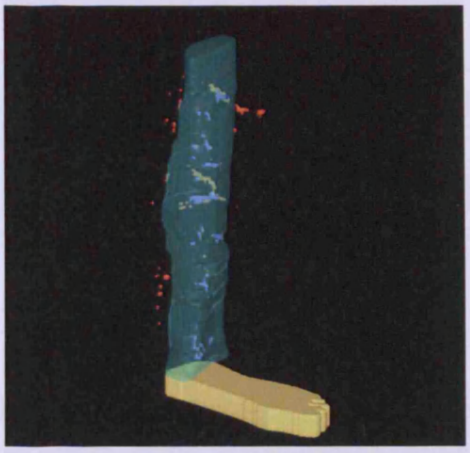

VON=10mm^3

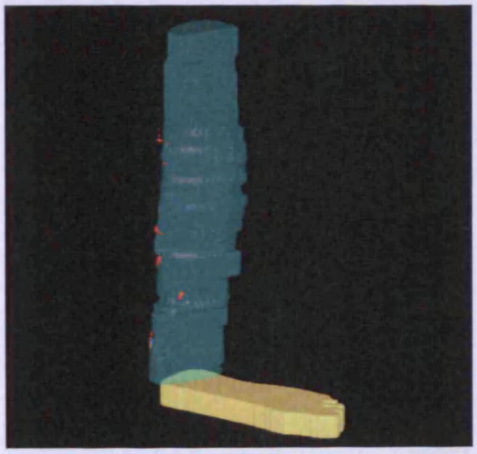

VON=0mm^3

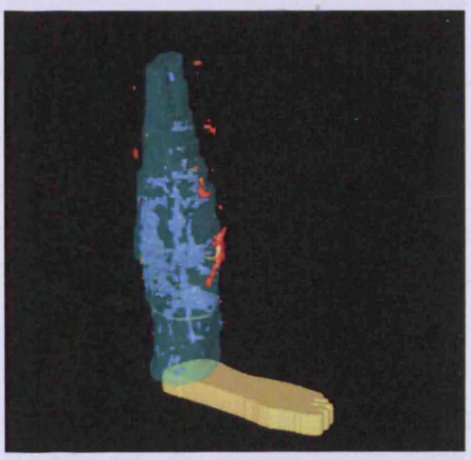

VON=309mm^3

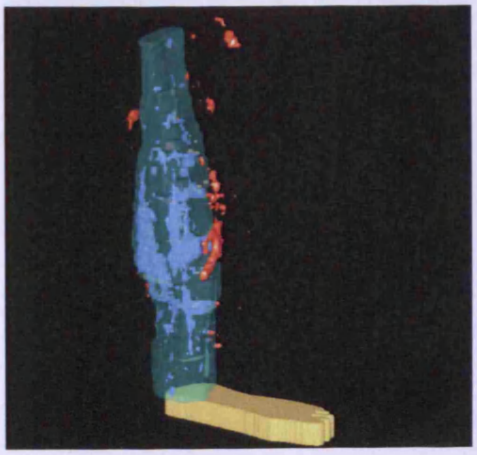

VON=257mm^3

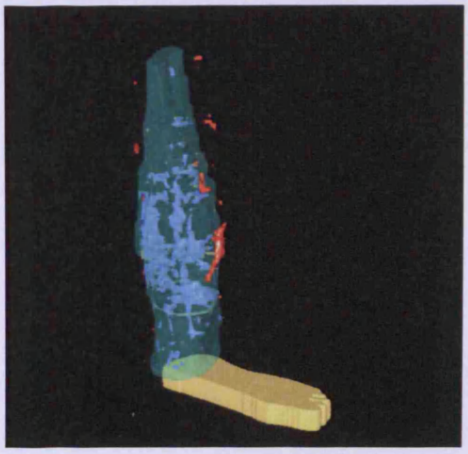

VON=283mm^3

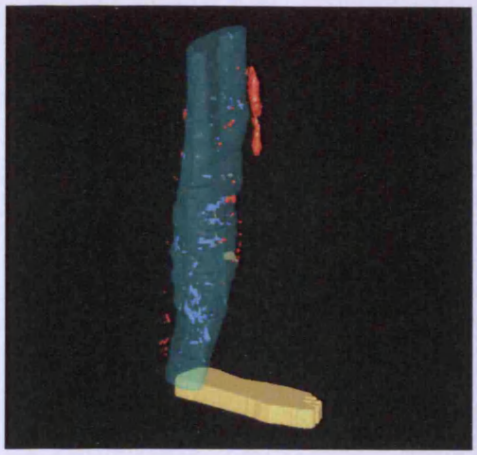

VON=24mm^3

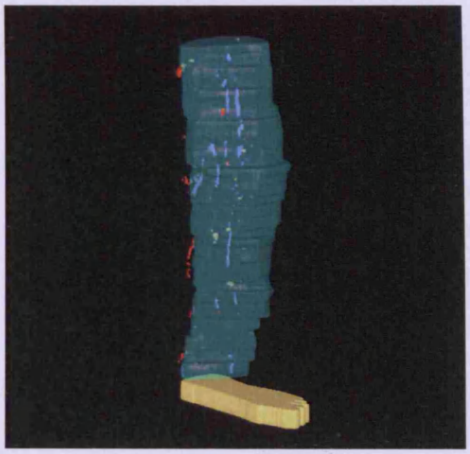

VON=22mm^3

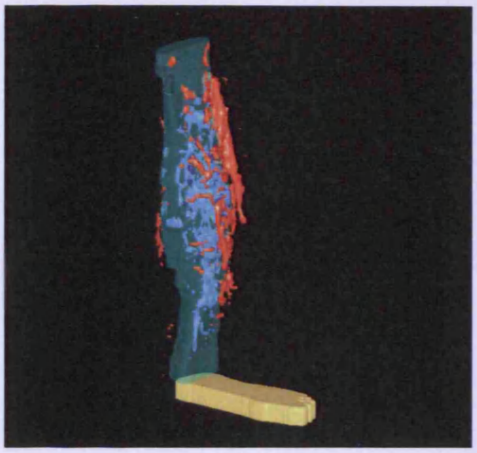

VON=429mm^3

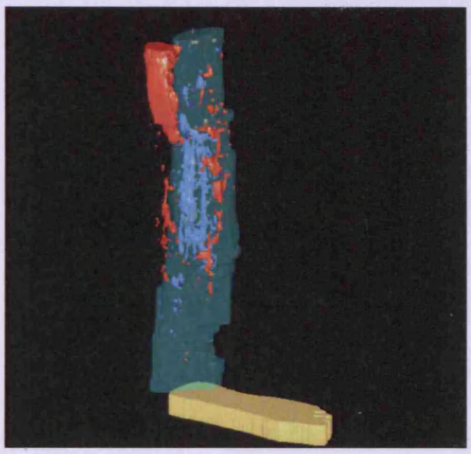

VON=179mm^3

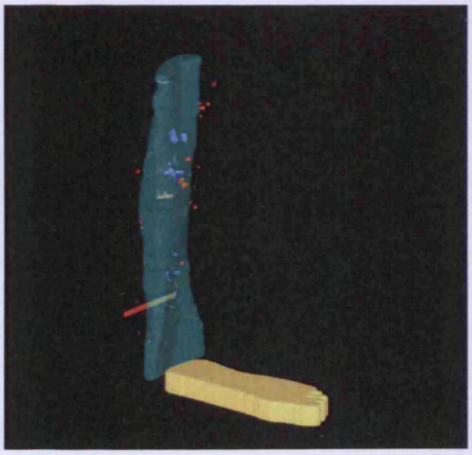

VON=6mm^3

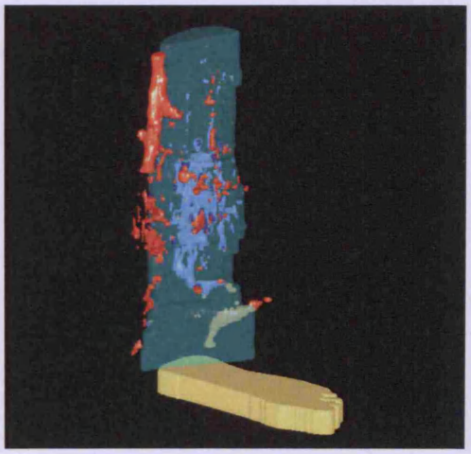

VON=238mm^3

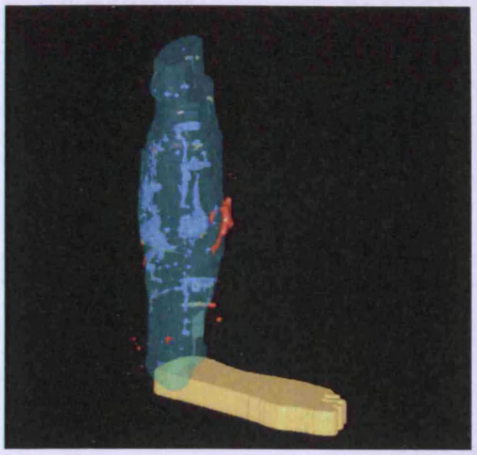

VON=188mm^3

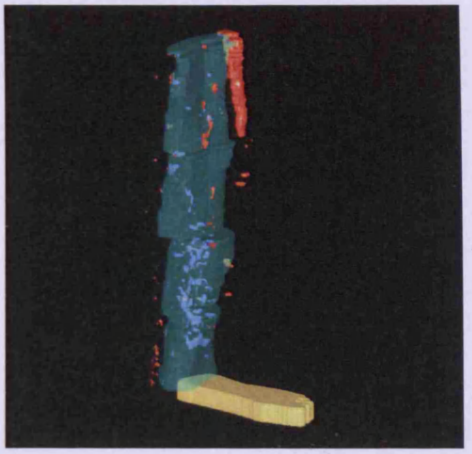

VON=48mm^3

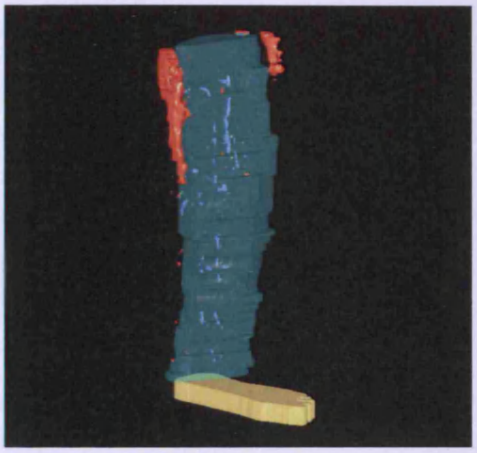

VON=28mm^3

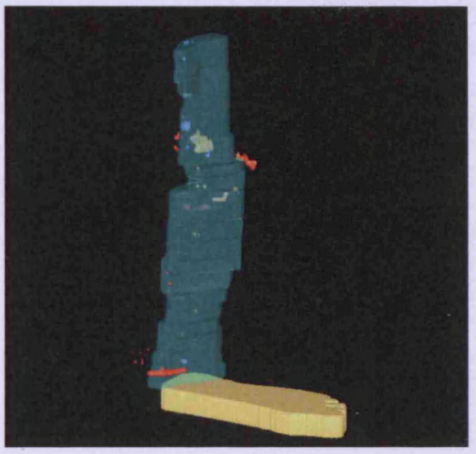

VON=4mm^3

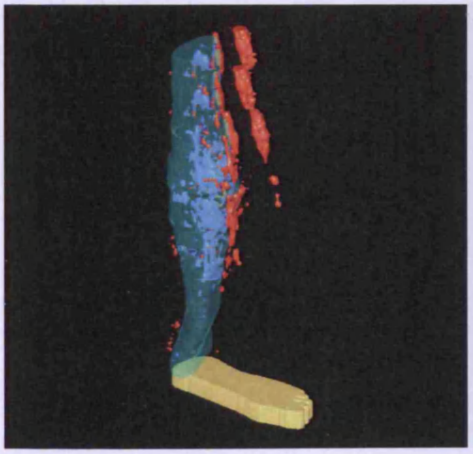

VON=323mm^3

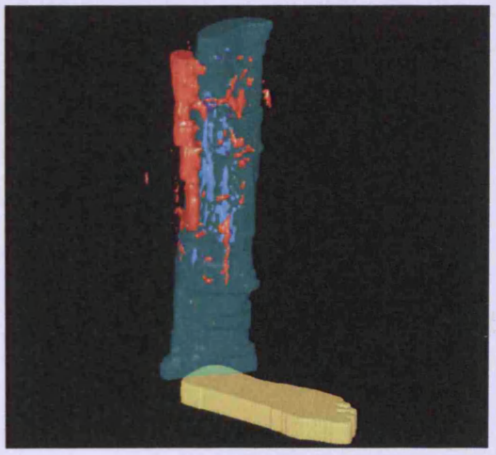

VON=86mm^3

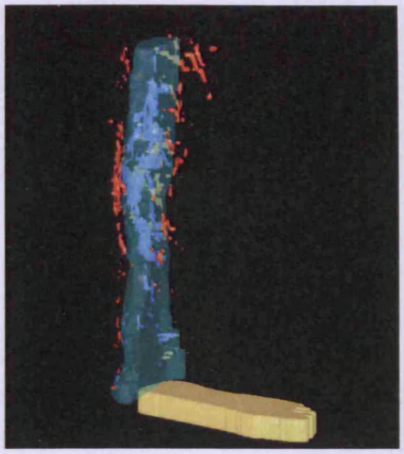

VON=102mm^3

VON=46mm^3

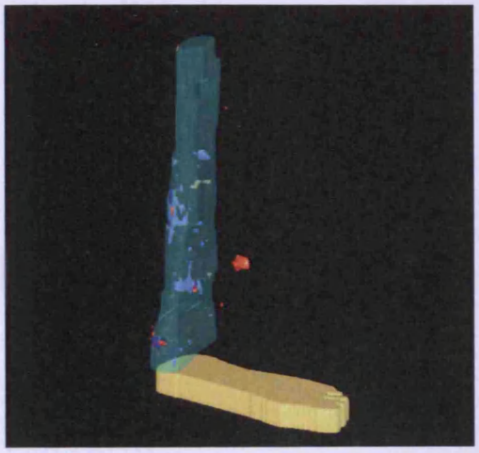

VON=25mm^3

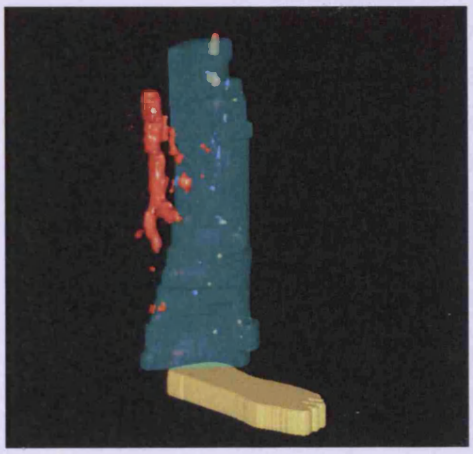

VON=2mm^3

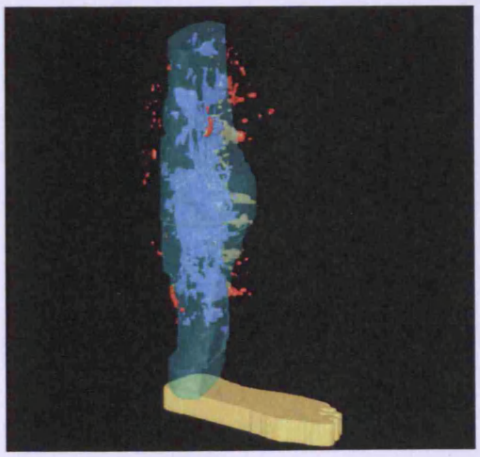

VON=618mm^3

VON=4mm^3

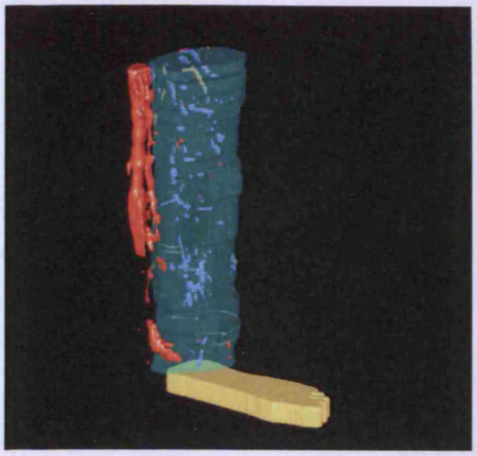

VON=51mm^3

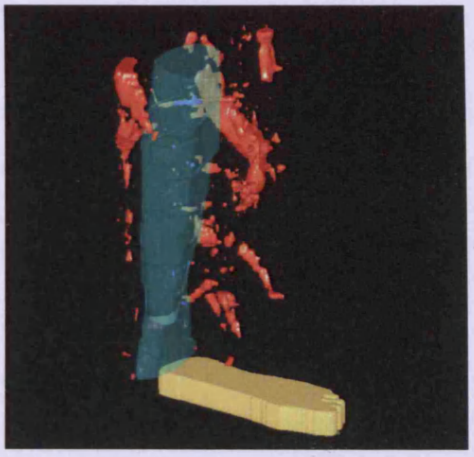

VON=3mm^3

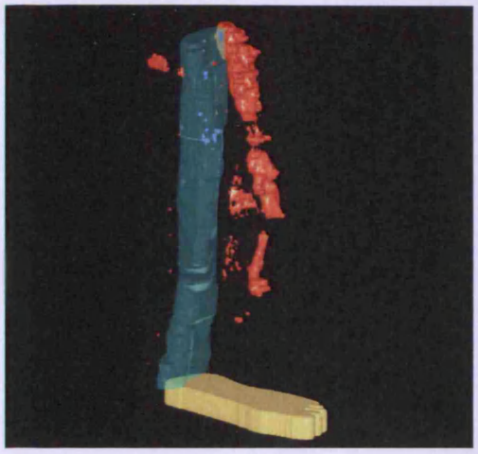

VON=4mm^3

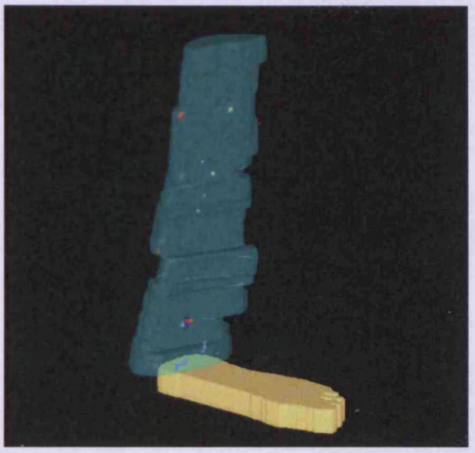

VON=3mm^3

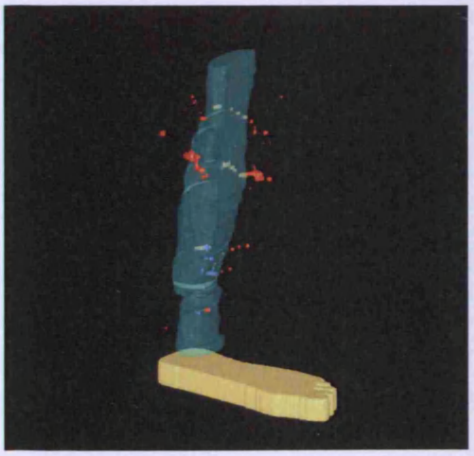

VON=1mm^3

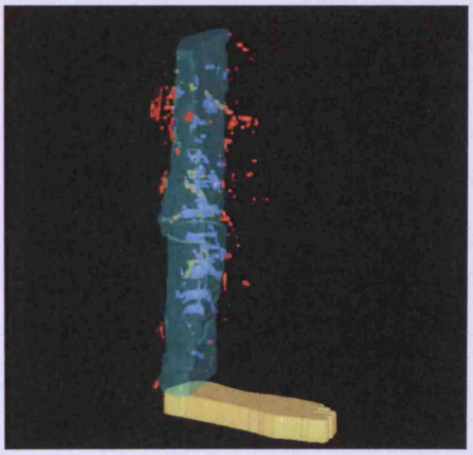

VON=63mm^3

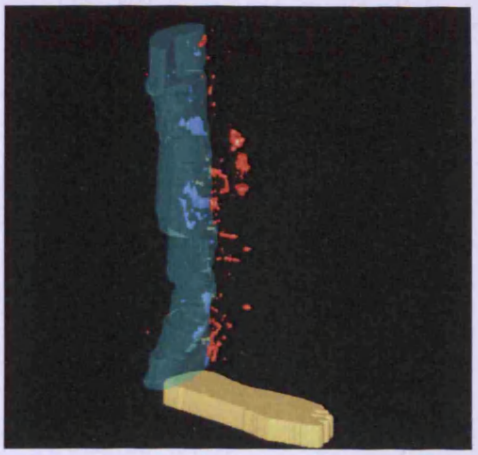

VON=19mm^3

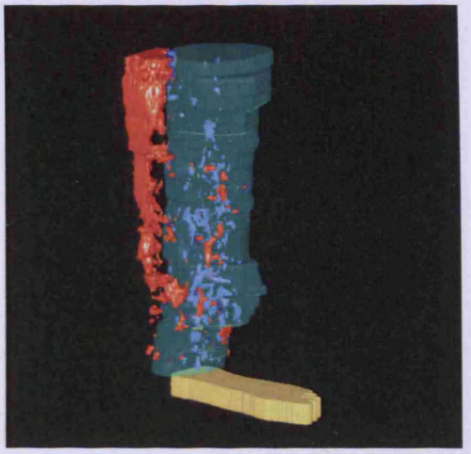

VON=180mm^3

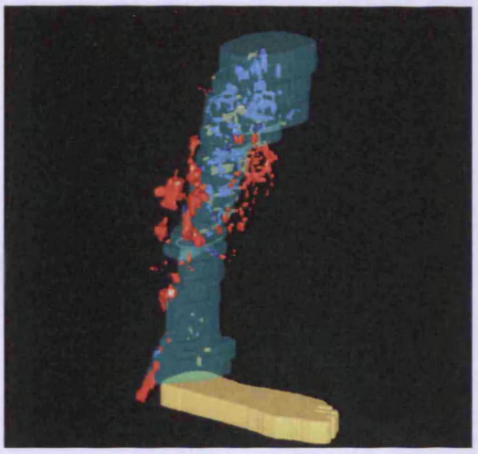

VON=89mm^3

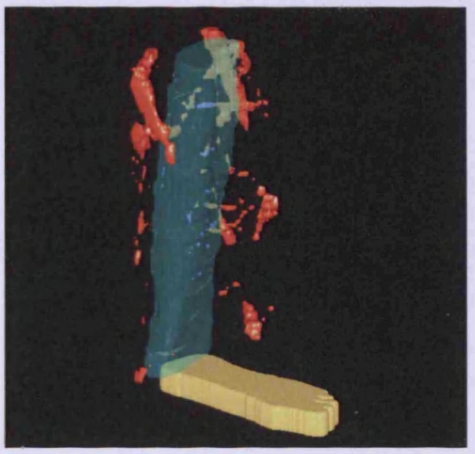

VON=3mm^3

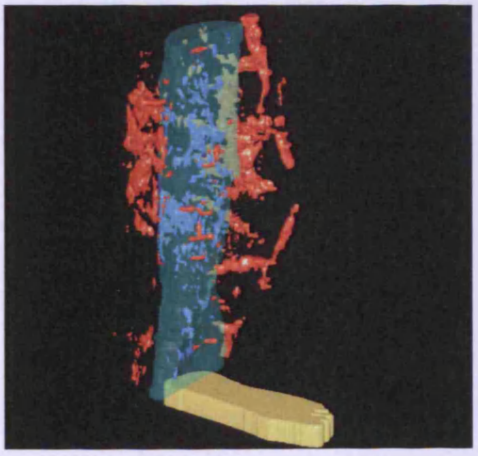

VON=174mm^3

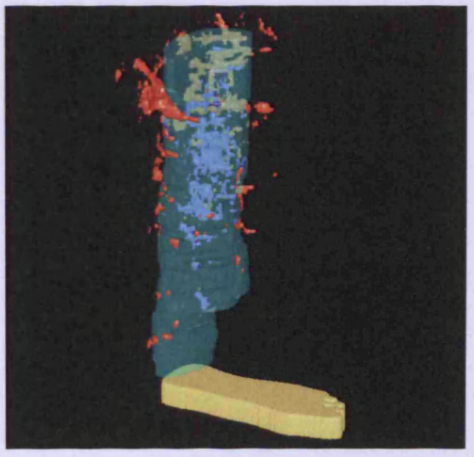

VON=140mm^3

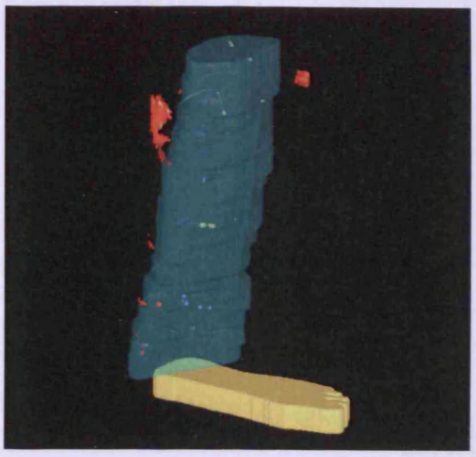

VON=1mm^3

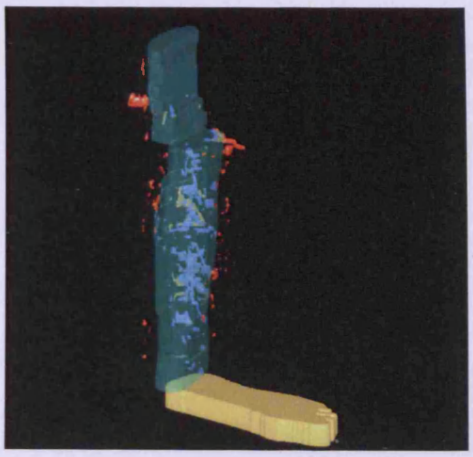

VON=48mm^3

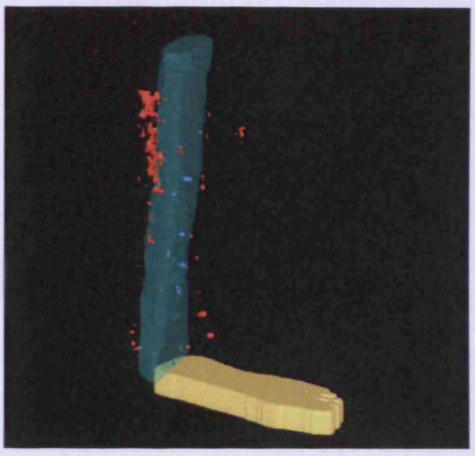

VON=1mm^3

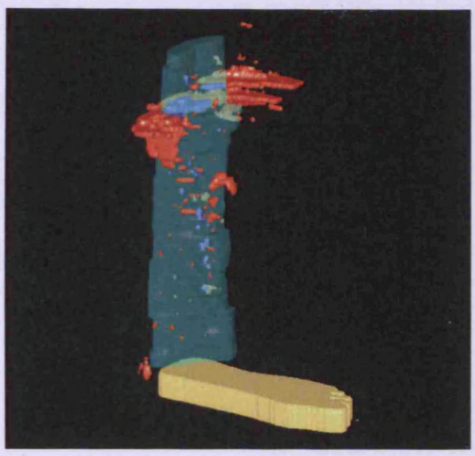

VON=105mm^3

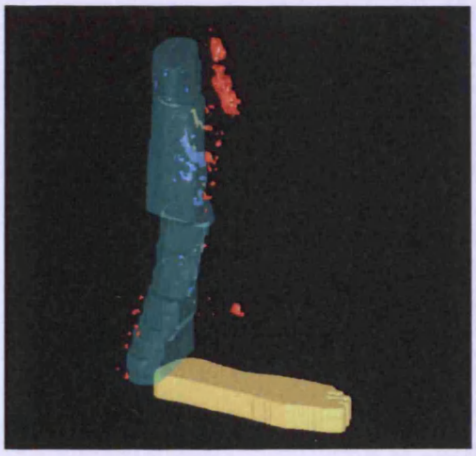

VON=1mm^3

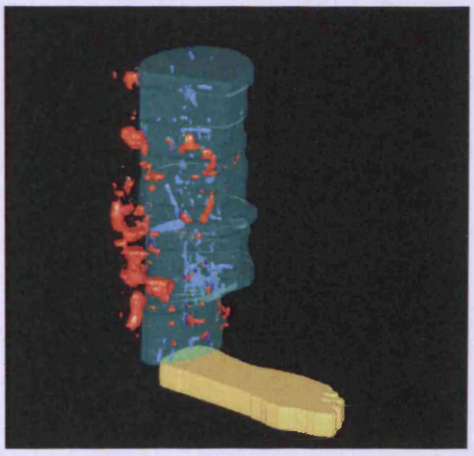

VON=77mm^3

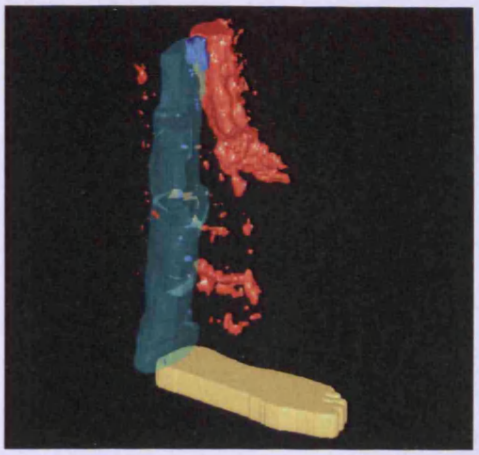

VON=27mm^3

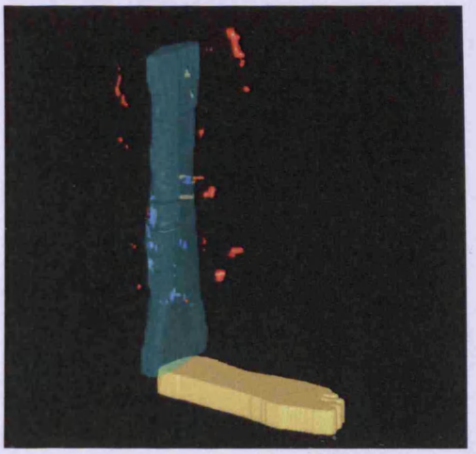

VON=5mm^3

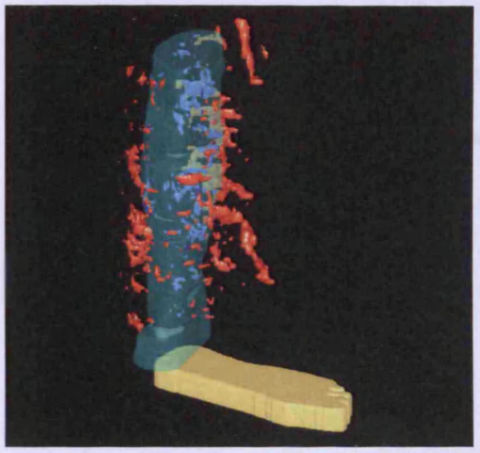

VON=61mm^3

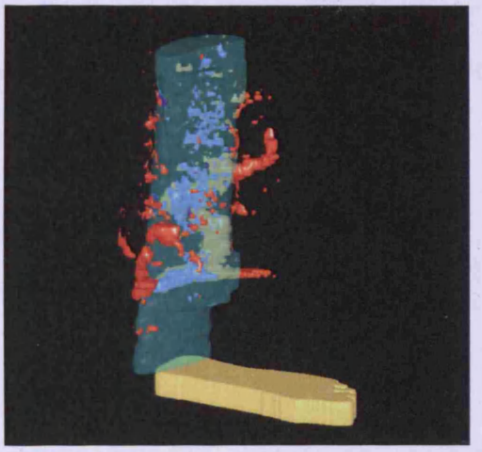

VON=116mm^3

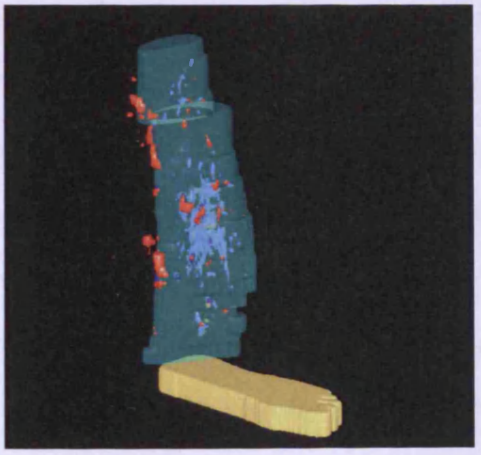

VON=92mm^3

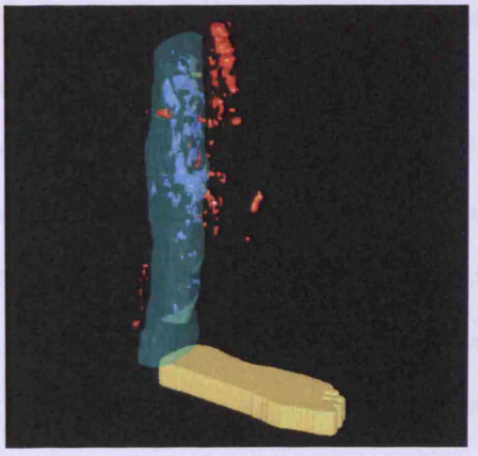

VON=65mm^3

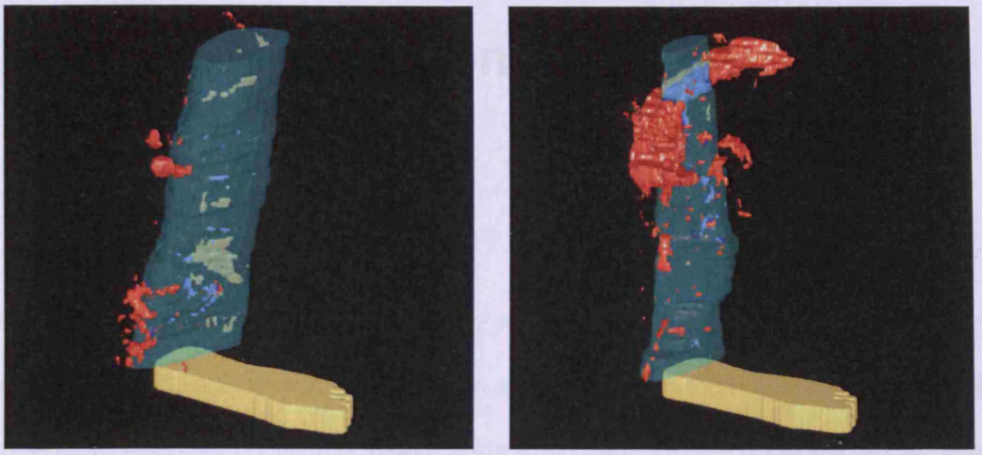

VON=11mm^3 VON=145mm^3

Fig. 7.7 Subjects with the visualization of neovascularization in Achilles tendon with the VON values

7.5 Conclusions

Initial data including the intra- and inter- observer variability, control and symptomatic subjects in system validation, and patients in correlation investigation were reported in this chapter. The ICC values indicated that the system works efficiently in the definition of symptomatic and asymptomatic subjects. The VONs found in controls were not higher than 3 mm^3 (mean = 0.41 mm^3) in this study, while patients showed distinct greater VONs with a mean value of 161.7 mm^3. To correlate the VON and clinical severity, another 40 Achilles tendons were scanned. The results show that the VON was associated with the degree of pain (VAS) but not the severity (VISA-A). The next chapter will discuss and conclude this study further.

8. Discussion and Conclusion

In this thesis, a novel system for quantitatively analyzing neovascularization in Achilles tendon from 3D PDU scans was described. In addition, the analysis system has been also developed as the first step towards *in-vivo* correlation between the neovascularization and clinical severity in Achilles tendinopathy.

8.1 Discussion

8.1.1 Power or colour Doppler ultrasound?

To establish information of the low-speed flows and tiny vessels in the Achilles tendon, PDU was used. PDU is more able to display small vessel flow than CDU because PDU displays the integrated power of the Doppler signal, while CDU displays the mean Doppler frequency shift. Therefore, because noise has a low power, the gain in a PDU can be increased to a point at which low-speed flows in small vessels are visible.

8.1.2 Why was a commercial 3D probe not used?

Currently, the most common type of commercial 3D US scanner is that based on a mechanically swept probe. A 1D transducer array, similar to that in a conventional probe, is mounted inside an enclosure and moved mechanically through a known trajectory. This enables the acquisition of a regular pattern of 2D scans covering a fixed 3D volume. Figure 8.1 shows the internal structure of a classic 3D probe (the RSP6-12, Kretztechnik) working from 6 MHz to 12 MHz with 192 transducer elements. A stepper motor drives a gearbox. The yoke with the array of transducer elements is mounted on the output of the gearbox. The

black bag joins onto the scanning window that forms the probe face. The space between the bag and the probe face contains the transducer array, mounted on the end of the yoke, and is filled with an oily substance (Prager et al. 2009).

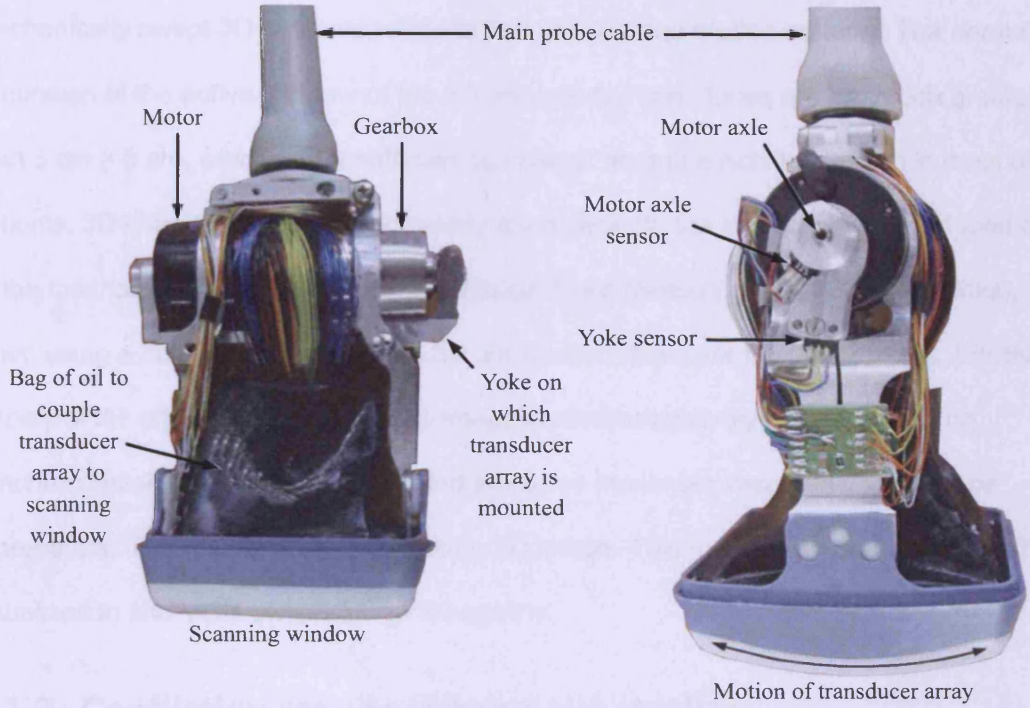

Fig. 8.1 The inter-structure of a 3D mechanically swept probe (Prager et al. 2009)

The structure of a common commercial 3D ultrasound probe (Fig. 8.1) will cause artifacts include those related to acquisition, rendering or editing.

The ultrasound system used in this study was a commercially available scanner with the probe mounted onto a specially constructed scanning apparatus, so that the translation axis was perpendicular to the imaging plane. The probe slider was driven by a stepper motor under a control box in a step- and interval-programmable movement. The probe was held stationary during the image acquisition period, which lasted for 2 seconds, and then moved automatically to the next recording location. Less than 1 second was necessary to translate the probe between two image positions on the apparatus. The time consumed in storing the AVI file on ultrasound machine was less than 1 second. The

specially constructed scanning apparatus was designed to overcome some potential artifacts in the commercial available, mechanically swept 3D ultrasonographic scanners, which have been widely used to date. The main problems encountered when using the mechanically swept 3D systems relate to field of view and motion artifacts. The normal dimension of the active window of the 3D linear array transducer, are not much greater than 5 cm × 5 cm, which is not sufficient to scan of an entire Achilles tendon in most of patients. 3D ultrasound is also particularly susceptible to the motion artifacts induced due to the mechanical movement of the transducer head (Nelson et al. 2000). In addition, when using a commercially available 3D ultrasound, there are timing problems with the display of the ultrasound images. The images are consecutively acquired, with no synchronization to the cardiac cycle and therefore maximum vascularity will only be represented in some parts of the resulting 3D image. This may cause an ambiguous 3D visualization and VON of Achilles tendinopathy.

8.1.3 Conflicting results in previous studies

Previous studies have suggested that the presence of neovascularization, as obtained by both CDU and PDU, gives an important indication to the degree of pain suffered during a bout of Achilles tendinopathy (Ohberg L 2001; Ohberg and Alfredson 2002; Alfredson et al. 2003; Ohberg and Alfredson 2004; Boesen et al. 2006b). Other studies have reported some conflicting results (Koenig et al. 2007; van Snellenberg et al. 2007). One of the possible reasons for this may be due to the blood flow of neovascularization in the Achilles tendon being too slow to be detected; any flow slower than 4-6 mm/sec is unable to be detected by Doppler ultrasound (Peers et al. 2003). Another reason that might cause these contradictory conclusions may be due to the difference of performing Doppler ultrasound examination, in terms of the transducer frequency, settings of ultrasound machine (Yang et al. 2010). The standard settings are essential to distinguish between physiological (slight) Doppler signals and possible pathological signal (Boesen et al.

2006a). Cutoff values of PRF and CG must be defined. Despite uniform optimized machine settings, too few studies have been performed the test of reliability and reproducibility. In addition, the small changes in direction and positioning of the hand-held probe, may make a quantitative calculation of Doppler changes (based on Ohberg's and similar grading systems) difficult in the oblique Achilles tendon (Boesen et al. 2006a). It is also of importance to optimize the degree of plantar flexion and pressure of the ultrasound probe (Alfredson and Ohberg 2005), which may influence of the presence of small vessels on Doppler ultrasound examination (Boesen et al. 2006b). Prior physical activity to the Doppler ultrasound examination could influence the level of neovascularization. A study (de Vos et al. 2007a) recommended 24 hours' abstinence from heavy-load eccentric training, sporting activity, or physical exertion.

8.1.4 Manually added boundary in reconstructions

To clarify the boundary between the intra-neovascularization and the feeder vessels, the border of the Achilles tendon was outlined for each transverse slice before 3D reconstruction. An outlined example is demonstrated in Fig. 8.2. 3D models with outlined Achilles tendon were created for the patient in order to find out the potential existence of the feeder vessels. With the appearance of the outlined Achilles tendon in the 3D view of four scans (Fig. 8.3), it was able to distinguish the vascularity within and surrounding the Achilles tendon.

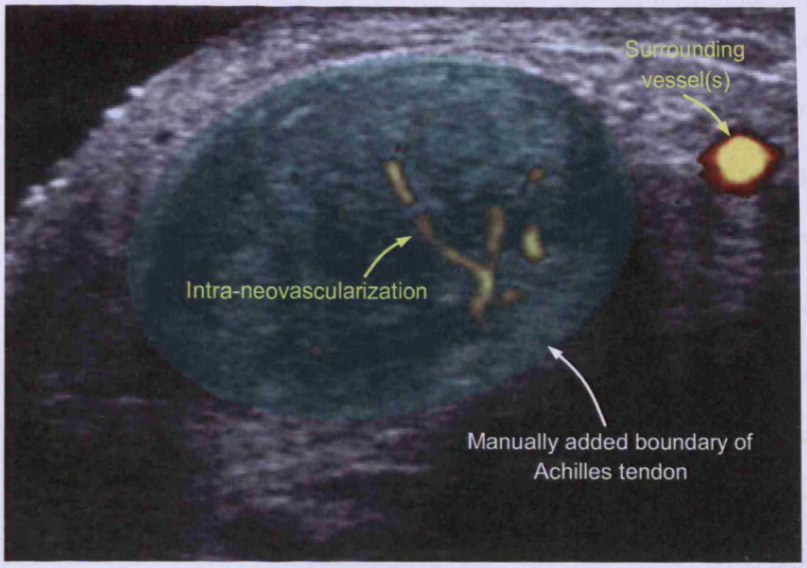

Fig. 8.2 Manually added boundary of Achilles tendon

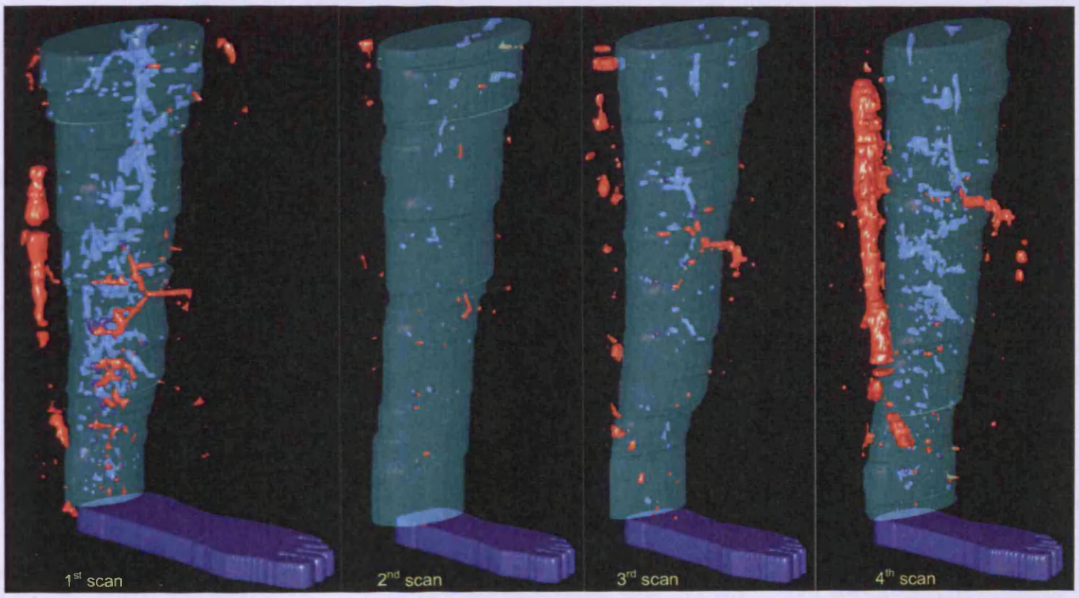

Fig. 8.3 3D reconstruction with manual Achilles tendon

8.1.5 The influence of cardiac cycle

The influence of systolic and diastolic phases on the appearance of vascularity during the Doppler ultrasound examination is an unattended issue. To our knowledge, the difference in the presence of neovascularization during the corresponding phases of the cardiac

cycle on Doppler ultrasound appearance has not been investigated in the previous studies of Achilles tendinopathy. The present study has shown a significant difference in the VON measured during maximum vascularity, compared to that measured during minimum vascularity, in both the control and symptomatic groups. In the present study, we did not cardiac gate the signals and therefore it cannot be sure it was measuring the absolute systolic and diastolic values corresponding to the maximum and minimum vascularity recorded. However, at each position during the scan, a 2 second AVI file consisting of 38 frames was saved by the ultrasound machine. In patients with normal sinus rhythm, more than one entire cardiac cycle is recorded during the 2 second period. This allows the 38 frames to contain sufficient information of the patient's systolic and diastolic flow components. The lumen of neovascularization in transverse images was found to change with the cardiac cycle.

To study the variance of the VON at systole and diastole, the slices with both the minimal and maximal Doppler signals were reconstructed for control and patient group. In the control group (Fig. 8.4), the mean maximum and minimum VON was 0.41 mm^3 (range from 0 mm^3 to 3 mm^3), and 0.02 mm^3 (range from 0 mm^3 to 0.2 mm^3), respectively. In the patient group (Fig. 8.5), the mean maximum and minimum VON were 161.7 mm^3 (range from 3 mm^3 to 589 mm^3) and 70.3 mm^3 (range from 0 mm^3 to 380 mm^3), respectively. For both control and patient groups, the VON at maximum phase was notably greater than that in the minimum phase ($p<0.05$).

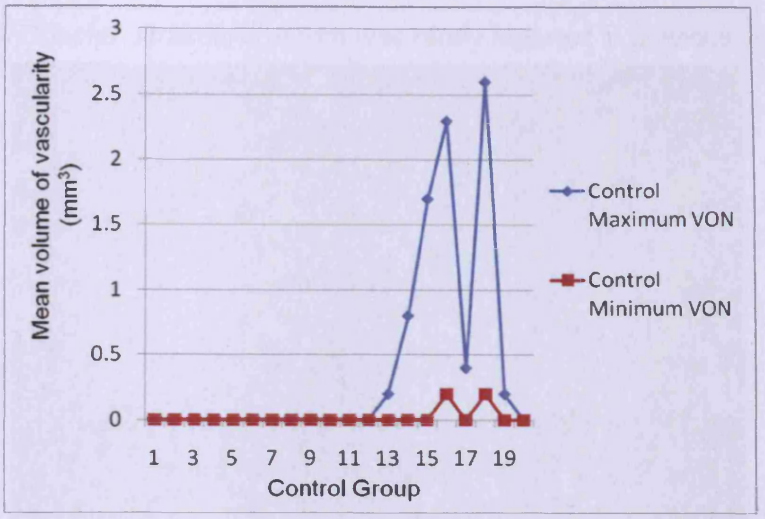

Fig. 8.4 The maximum and minimum VON in control group

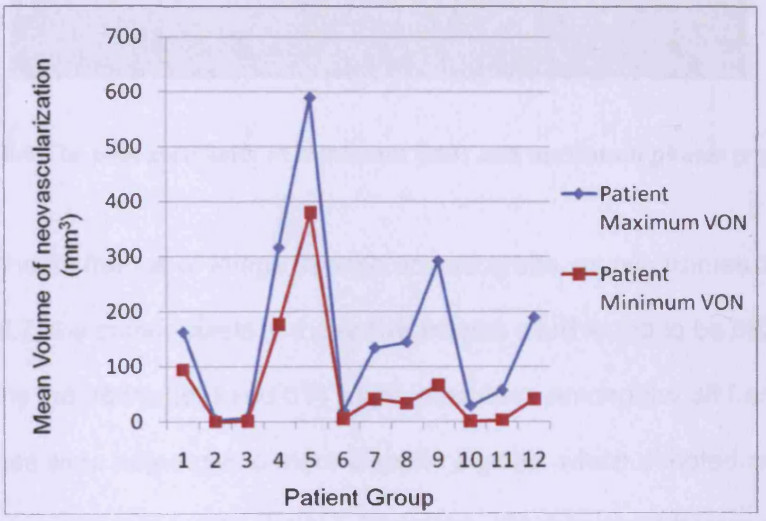

Fig. 8.5 The maximum and minimum VON in patient group

One example of 12 symptomatic Achilles tendons indicating the variance between maximum and minimum VON is given in Fig. 8.6. Both the intra-tendinous vascularity and surrounding blood vessels are notably change between the maximum and minimum phases. The connections of the neovascularization were apparently weakened or disappeared in minimum phase. In all 12 symptomatic Achilles tendons, the average volume variation at minimum phase was 43.4% (70.3/161.7) of maximum, which denotes the cardiac cycle a key factor when quantifying the amount of neovascularization using

either 2D or 3D Doppler ultrasound, which was rarely reported in previous studies.

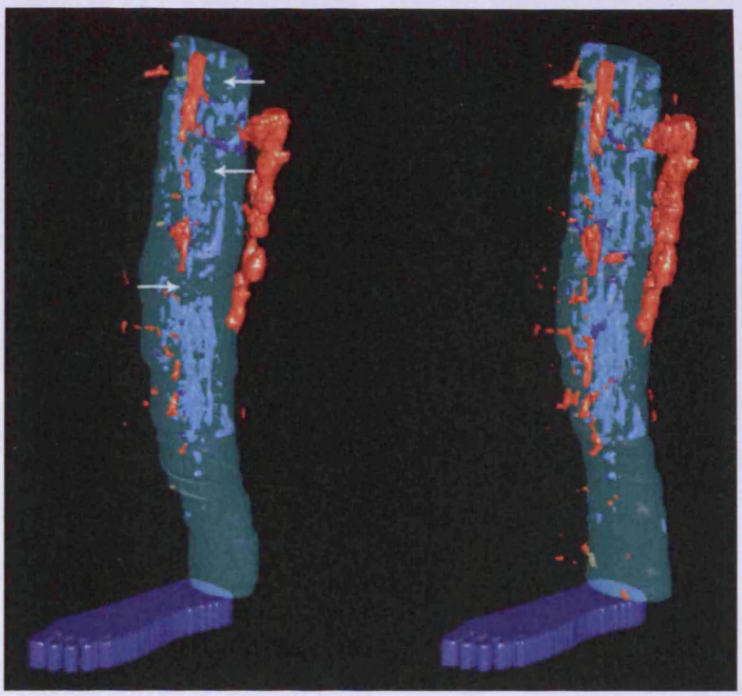

Fig. 8.6 The neovascularity at minimum (left) and maximum phases (right)

By examining the 38 frames of image in each scanning site, as two frames in an example shown in Fig. 8.7, the colour pixels in these two frames were found to be 583 (left, minimum among the 38 frames) and 614 (right, maximum among the 38 frames). The maximum frames were noted giving more Doppler signals, which denoted its capability to visualize more neo-vessels (white circles). Therefore, the maximum frames were always used as the representative image for a specific slice, in the 3D reconstruction. The reconstructed volumes of the neovascularity were considered as maximum VONs.

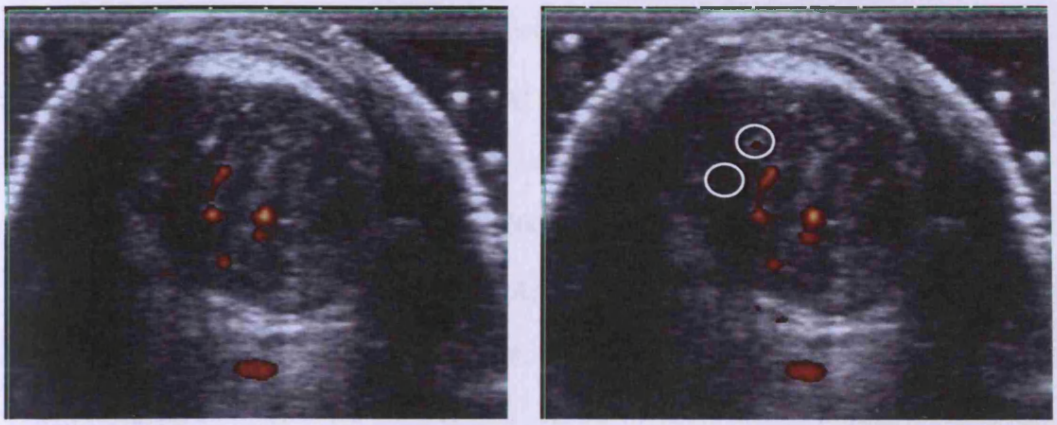

Fig. 8.7 Two of 38 frames from an AVI file with the Doppler signal

8.1.6 Correlations

The positive correlation between VAS and VON found in 40 symptomatic tendons was in accordance with a previous study where the neovascularization seemed to be associated with pain (Zanetti et al. 2003), with a correlation coefficient of 0.326 (p = 0.04). This indicated a medium correlation was found between VAS and VON, the level of VON may be able to predict the score of pain. On the other hand, the Spearman correlation between VISA-A and VON was -0.246 (p = 0.127) in the current study, which indicated a weak correlation between the level of VON and clinical severity, supporting the hypothesis that the clinical outcome was not correlated with neovascularization, which is consistent with some recent studies (de Vos et al. 2007a; Sengkerij et al. 2009). Taken together, these results may indicate that via quantitative PDU measured neovascularity is an expression of the degree of pain but not necessarily a general indication of clinical symptoms.

Because the level of VAS reflects the degree of pain in symptomatic Achilles tendon, while the VON shows the degree of lesions (neovascularity), the positive correlation between them could hypothesize that the in-growth of neovascularity cause the pain. This supports that some studies (Ohberg and Alfredson 2002; Alfredson et al. 2003) by sclerosing the neovascularity in patients with painful chronic mid-portion Achilles tendinosis, the tendon

pain was significantly diminished during activity. Studies using sclerosing agents demonstrated that patients with no remaining neovascularization in the Achilles tendon had no pain during activity, but patients with unchanged neovascularization still demonstrated pain (Ohberg and Alfredson 2002). Combining the results in these studies, It is supposed that the blood flow within the Achilles tendon was significantly correlated with severity of pain, which is associated with the accompanying nerves in neovascularity (Ohberg L 2001).

The continuous numerical result of the VISA-A questionnaire is ideal for comparing symptom progress in the clinical setting (Robinson et al. 2001). The VISA-A questionnaire is a valid, reliable and easy-to-administer measure of the severity of Achilles tendinopathy and appears suitable for both clinical rating and quantitative research. However, the score of VISA-A doesn't seem to correlate with the VON in our samples. This may due to that the VISA-A questionnaire is an index of the severity of a clinically diagnosed condition but not a diagnostic tool (Robinson et al. 2001). Furthermore, limitation of function limits the subject's ability to score well in some questions, especially question 8, even though the Achilles tendon may be uninjured (Robinson et al. 2001). Therefore, the weak Spearman correlation between VISA-A and VON, with the coefficient of -0.246 (p = 0.127), indicated the level of VON couldn't be confidently used to predict the clinical severity.

8.1.7 Future work

A grading system based on the ratio of Doppler signal in the ROI has been used in many previous studies including studies on the role of neovascularization, the effectiveness of extracorporeal shockwave therapy, eccentric training, and sclerosing in Achilles tendinopathy (Ohberg and Alfredson 2002; Boesen et al. 2006a). The grading system is a feasible and easy way to measure the amount or change of neovascularization. Comparing the grading systems, the current study could involve sketching a quantitative

neovascularization map in painful Achilles tendon.

More work is needed to establish the role of neovascularization in Achilles tendinopathy, either by the evaluation of VON or conventional PDU scans. Whether neovascularization is related to symptoms is still uncertain. The current study firstly investigated the VON in both control and symptomatic Achilles tendons to quantify the neovascularity. Large prospective studies on the value of VON are needed to confirm the results here. Our study hopefully will provide an additional tool towards understanding the role of neovascularization in Achilles tendinopathy and help in clinical practice.

8.2 Conclusion

In this thesis, the 3D vascularity map of the neovascularization in Achilles tendinopathy was first created from continuous PDU image transverse slices. The intra- and inter-observer reliability of the system was tested. The high ICCs indicated that the present system was capable to eliminate the artifact yielded from the patient movement during the scan, as well as its capability minimizing the error when determining the amount of neovascularity within the border of Achilles tendon, by manually ROI marking on each slice.

We also optimized protocols for the study of neovascularization in Achilles tendinopathy as the suggestion in Table 8.1.

Table 8.1 Suggested protocol for studying neovascularization in Achilles tendinopathy

Protocol	Description	
Ultrasound machine settings	**Parameter**	**Settings**
	PRF	Lowest possible where 'flash' artefacts are eliminated
	CG	On the threshold to noise
	Doppler frequency	Highest possible to maximize spatial resolution and have good blood flow
Patient selection criteria	**Inclusion criteria**	**Exclusion criteria**
	Aged 18 to 70 years	Previous eccentric loading exercise program just prior to scanning
	Have symptoms in the Achilles tendon more than 6 weeks	Previous Achilles tendon surgery or rupture in the symptomatic lower limb
	Be able to complete the VISA-A and VAS questionnaire	Previous lower limb trauma which may have structural changes on the Achilles tendon
	Score less than 80 on VISA and VAS not equal to 0 on VAS	Pathology at insertional location, bilateral tendinopathy and bursitis
	Pain and swelling positioned at 2 to 6 cm proximal to the calcaneal insertion	Injection of local sclerosis or other anaesthetic effect agents into the Achilles tendon or surrounding area
	B-mode ultrasound detects a local thickening and/or irregular fibre orientation and/or irregular tendon structure with hypoechoic areas	Other systemic disorders
Pre-physical activity	24 hours' abstinence from heavy-load eccentric training, sporting activity, or physical exertion.	
Severity assessment	Using VISA-A and VAS questionnaire	
Degree of ankle plantar flexion	90 degree	

In the validation of the novel system, the volumetric information of neovascularization and pattern were established both in control group and patients. The mean maximum and minimum volumes of the vascularity in control group were 0.41 mm^3 and 0.02 mm^3, respectively. The mean maximum and minimum VONs in patients with painful Achilles tendon were 380 mm^3 and 70.3 mm^3, respectively, which were distinctly greater than that in controls. In patients, the maximum VONs were notably greater than the minimum VONs. Therefore, it is proposed using the maximum VON as the indicator of choice in evaluating neovascularity of Achilles tendon.

In the investigation of the correlation between VON and clinical severity, the mean VON was definitely greater than that in healthy Achilles tendon. Neovascularization was noted in 97.5% (n = 39) symptomatic Achilles tendons in 30 patients. The VAS showed a positive correlation with VON with a Spearman correlation coefficient of 0.326 (p = 0.04, power = 0.89), while no significant correlation was found between VISA-A score and VON. Further studies examining the correlations are needed.

References

Ackermann PW, Li J, Finn A, Ahmed M, Kreicbergs A. Autonomic innervation of tendons, ligaments and joint capsules. A morphologic and quantitative study in the rat. J Orthop Res 2001;19:372-8.

Ahmed IM, Lagopoulos M, McConnell P, Soames RW, Sefton GK. Blood supply of the Achilles tendon. J Orthop Res 1998;16:591-6.

Alfredson H. Chronic midportion Achilles tendinopathy: an update on research and treatment. Clinics in Sports Medicine 2003;22:727-41.

Alfredson H, Bjur D, Thorsen K, Lorentzon R, Sandstrom P. High intratendinous lactate levels in painful chronic Achilles tendinosis. An investigation using microdialysis technique. J Orthop Res 2002;20:934-8.

Alfredson H, Lorentzon R. Sclerosing polidocanol injections of small vessels to treat the chronic painful tendon. Cardiovasc Hematol Agents Med Chem 2007;5:97-100.

Alfredson H, Ohberg L. Sclerosing injections to areas of neo-vascularisation reduce pain in chronic Achilles tendinopathy: a double-blind randomised controlled trial. Knee Surg Sports Traumatol Arthrosc 2005;13:338-44.

Alfredson H, Ohberg L. Increased intratendinous vascularity in the early period after sclerosing injection treatment in Achilles tendinosis : a healing response? Knee Surg Sports Traumatol Arthrosc 2006;14:399-401.

Alfredson H, Ohberg L, Forsgren S. Is vasculo-neural ingrowth the cause of pain in chronic Achilles tendinosis? An investigation using ultrasonography and colour Doppler, immunohistochemistry, and diagnostic injections. Knee Surg Sports Traumatol Arthrosc 2003;11:334-8.

Alfredson H, Pietila T, Jonsson P, Lorentzon R. Heavy-load eccentric calf muscle training for the treatment of chronic Achilles tendinosis. Am J Sports Med 1998;26:360-6.

Almekinders LC, Banes AJ, Ballenger CA. Effects of repetitive motion on human fibroblasts. Med Sci Sports Exerc 1993;25:603-7.

Andres KH, von During M, Schmidt RF. Sensory innervation of the Achilles tendon by group III and IV afferent fibers. Anat Embryol (Berl) 1985;172:145-56.

Archambault JM, Wiley JP, Bray RC. Exercise loading of tendons and the development of overuse injuries. A review of current literature. Sports Med 1995;20:77-89.

Arndt KH. [Achilles tendon rupture]. Zentralbl Chir 1976;101:360-4.

Arnoczky SL-YWPAFHRSP. Tendinopathy in Athletes. Blackwell, 2007.

Aroen A, Helgo D, Granlund OG, Bahr R. Contralateral tendon rupture risk is increased in individuals with a previous Achilles tendon rupture. Scand J Med Sci Sports 2004;14:30-3.

Astrom M, Gentz CF, Nilsson P, Rausing A, Sjoberg S, Westlin N. Imaging in chronic achilles tendinopathy: a comparison of ultrasonography, magnetic resonance imaging and surgical findings in 27 histologically verified cases. Skeletal Radiol 1996;25:615-20.

Astrom M, Westlin N. Blood flow in the human Achilles tendon assessed by laser Doppler flowmetry. J Orthop Res 1994;12:246-52.

Ballas MT, Tytko J, Mannarino F. Commonly missed orthopedic problems. Am Fam Physician 1998;57:267-74.

Barfred T. Experimental rupture of the Achilles tendon. Comparison of various types of experimental rupture in rats. Acta Orthop Scand 1971;42:528-43.

Becker W. Die Ultrastruktur normaler und pathologisch veranderter Insertionen von Sehnen am Knochen. Arch Orthop Unfallchir 1971;69:315-29.

Becker W. Die Tendopathien. Stuttgart: G Thieme 1978;9-19.

Benjamin M, Kaiser E, Milz S. Structure-function relationships in tendons: a review. J Anat 2008;212:211-28.

Benjamin M, McGonagle D. The anatomical basis for disease localisation in seronegative spondyloarthropathy at entheses and related sites. J Anat 2001;199:503-26.

Benjamin M, Toumi H, Suzuki D, Redman S, Emery P, McGonagle D. Microdamage and altered vascularity at the enthesis-bone interface provides an anatomic explanation for bone involvement in the HLA-B27-associated spondylarthritides and allied disorders. Arthritis Rheum 2007;56:224-33.

Boesen MI, Boesen A, Koenig MJ, Bliddal H, Torp-Pedersen S. Ultrasonographic investigation of the Achilles tendon in elite badminton players using color Doppler. Am J Sports Med 2006a;34:2013-21.

Boesen MI, Koenig MJ, Torp-Pedersen S, Bliddal H, Langberg H. Tendinopathy and Doppler activity: the vascular response of the Achilles tendon to exercise. Scand J Med Sci Sports 2006b;16:463-9.

Boesen MI, Torp-Pedersen S, Koenig MJ, Christensen R, Langberg H, Holmich P, Nielsen MB, Bliddal H. Ultrasound guided electrocoagulation in patients with chronic non-insertional Achilles tendinopathy: a pilot study. Br J Sports Med 2006c;40:761-6.

Boushel R, Langberg H, Green S, Skovgaard D, Bulow J, Kjaer M. Blood flow and oxygenation in peritendinous tissue and calf muscle during dynamic exercise in humans. J Physiol 2000;524 Pt 1:305-13.

Breidahl WH, Stafford Johnson DB, Newman JS, Adler RS. Power Doppler sonography in tenosynovitis: significance of the peritendinous hypoechoic rim. J Ultrasound Med 1998;17:103-7.

Buchanan CI, Marsh RL. Effects of exercise on the biomechanical, biochemical and structural properties of tendons. Comp Biochem Physiol A Mol Integr Physiol 2002;133:1101-7.

Butler DL, Grood ES, Noyes FR, Zernicke RF. Biomechanics of ligaments and tendons. Exerc Sport Sci Rev 1978;6:125-81.

C. Niek van Dijk JK, Nicola Maffulli, Hajo Thermann. Achilles Tendon Rupture. DJO Publications, 2008.

Campbell P, Lawton JO. Spontaneous rupture of the Achilles tendon: pathology and management. Br J Hosp Med 1993;50:321-5.

Campbell SC, Cullinan JA, Rubens DJ. Slow flow or no flow? Color and power Doppler US pitfalls in the abdomen and pelvis. Radiographics 2004;24:497-506.

Canty EG, Kadler KE. Collagen fibril biosynthesis in tendon: a review and recent insights. Comp Biochem Physiol A Mol Integr Physiol 2002;133:979-85.

Carr AJ, Norris SH. The blood supply of the calcaneal tendon. Journal of Bone and Joint Surgery 1989;71:100-1.

Chansky HA, Iannotti JP. The vascularity of the rotator cuff. Clin Sports Med 1991;10:807-22.

Chen TM, Rozen WM, Pan WR, Ashton MW, Richardson MD, Taylor GI. The arterial anatomy of the Achilles tendon: anatomical study and clinical implications. Clin Anat 2009;22:377-85.

Christiaens L, Coisne D, Allal J, Blouin P, Dubreuil F, Donal E, Barraine R. Three-dimensional power Doppler imaging: volume reconstruction of pulmonary artery flow with an in vitro pulsatile flow system. European Journal of Ultrasound 1997;6:135-9.

Clain MR, Baxter DE. Achilles tendinitis. Foot Ankle 1992;13:482-7.

Cohen J. Statistical power analysis for the behavioral sciences. Routledge Academic, 1988.

Cook JL, Khan KM, Kiss ZS, Coleman BD, Griffiths L. Asymptomatic hypoechoic regions on patellar tendon ultrasound: A 4-year clinical and ultrasound followup of 46 tendons. Scand J Med Sci Sports 2001;11:321-7.

Coutts A, MacGregor A, Gibson J, Maffulli N. Clinical and functional results of open operative repair for Achilles tendon rupture in a non-specialist surgical unit. J R Coll Surg Edinb 2002;47:753-62.

Cummins E.J. ABJ, Carr B.W., et al. The structure of the calcaneal tendon in relation to orthopedic surgery. Surg Gynecol Obstet 1946;83:

Daftary A, Adler RS. Sonographic evaluation and ultrasound-guided therapy of the Achilles tendon. Ultrasound Q 2009;25:103-10.

de Vos RJ, Weir A, Cobben LP, Tol JL. The value of power Doppler ultrasonography in Achilles tendinopathy: a prospective study. Am J Sports Med 2007a;35:1696-701.

de Vos RJ, Weir A, Visser RJ, de Winter T, Tol JL. The additional value of a night splint to eccentric exercises in chronic midportion Achilles tendinopathy: a randomised controlled trial. Br J Sports Med 2007b;41:e5.

Deangelis JP, Wilson KM, Cox CL, Diamond AB, Thomson AB. Achilles tendon rupture in athletes. J Surg Orthop Adv 2009;18:115-21.

Diffrient, Tilley, Bardagjy. Humanscale 1/2/3 Manual Cambridge. MIT Press, 1974.

Edwards DA. The blood supply and lymphatic drainage of tendons. J Anat 1946;80:147-52 2.

el Hawary R, Stanish WD, Curwin SL. Rehabilitation of tendon injuries in sport. Sports Med 1997;24:347-58.

Elliott DH. STRUCTURE AND FUNCTION OF MAMMALIAN TENDON. Biol Rev Camb Philos Soc 1965;40:392-421.

Fenster A, Downey DB. 3-D ultrasound imaging: a review. Engineering in Medicine and Biology Magazine, IEEE 1996;15:41-51.

Fenwick SA, Hazleman BL, Riley GP. The vasculature and its role in the damaged and healing tendon. Arthritis Res 2002;4:252-60.

Ferrara N. Molecular and biological properties of vascular endothelial growth factor. J Mol Med 1999;77:527-43.

Fish P. Physics and instrumentation of diagnostic medical ultrasound Chichester : Wiley, 1990.

Fisher P. Role of steroids in tendon rupture or disintegration known for decades. Arch Intern Med 2004;164:678.

Fleiss J. The Design and Analysis of Clinical Experiments. New York: John Wiley, 1986.

Fornage BD. Achilles tendon: US examination. Radiology 1986;159:759-64.

Forslund C, Aspenberg P. CDMP-2 induces bone or tendon-like tissue depending on mechanical stimulation. J Orthop Res 2002;20:1170-4.

Franchi M, Trire A, Quaranta M, Orsini E, Ottani V. Collagen structure of tendon relates to function. ScientificWorldJournal 2007;7:404-20.

Fredberg U, Bolvig L. Significance of ultrasonographically detected asymptomatic tendinosis in the patellar and achilles tendons of elite soccer players: a longitudinal study. Am J Sports Med 2002;30:488-91.

Fukuta S, Oyama M, Kavalkovich K, Fu FH, Niyibizi C. Identification of types II, IX and X collagens at the insertion site of the bovine achilles tendon. Matrix Biol 1998;17:65-73.

Furia JP. High-energy extracorporeal shock wave therapy as a treatment for chronic noninsertional Achilles tendinopathy. Am J Sports Med 2008;36:502-8.

Furia JP, Rompe JD. Extracorporeal shock wave therapy in the treatment of chronic plantar fasciitis and achilles tendinopathy. Curr Opin Orthop 2007;18:102-11.

Gardin A, Bruno J, Movin T, Kristoffersen-Wiberg M, Shalabi A. Magnetic resonance signal, rather than tendon volume, correlates to pain and functional impairment in chronic Achilles tendinopathy. Acta Radiol 2006;47:718-24.

Griewing B, Morgenstern C, Driesner F, Kallwellis G, Walker ML, Kessler C. Cerebrovascular disease assessed by color-flow and power Doppler ultrasonography. Comparison with digital subtraction angiography in internal carotid artery stenosis. Stroke 1996;27:95-100.

Guo Z, Moreau M, Rickey DW, Picot PA, Fenster A. Quantitative investigation of in vitro flow using three-dimensional colour Doppler ultrasound. Ultrasound in Medicine & Biology 1995;21:807-16.

Halasi T, Tallay A, Berkes I. Percutaneous Achilles tendon repair with and without endoscopic control. Knee Surg Sports Traumatol Arthrosc 2003;11:409-14.

Hamilton B, Purdam C. Patellar tendinosis as an adaptive process: a new hypothesis. Br J Sports Med 2004;38:758-61.

Hannafin JA, Arnoczky SP, Hoonjan A, Torzilli PA. Effect of stress deprivation and cyclic tensile loading on the material and morphologic properties of canine flexor digitorum profundus tendon: an in vitro study. J Orthop Res 1995;13:907-14.

Hansen P, Aagaard P, Kjaer M, Larsson B, Magnusson SP. Effect of habitual running on human Achilles tendon load-deformation properties and cross-sectional area. J Appl Physiol 2003;95:2375-80.

Harris CA, Peduto AJ. Achilles tendon imaging. Australas Radiol 2006;50:513-25.

Hennerici MG, Neuerburg-Heusler D. Vascular Diagnosis with Ultrasound. New York: Thieme, 2006.

Hess GP, Cappiello WL, Poole RM, Hunter SC. Prevention and treatment of overuse tendon injuries. Sports Med 1989;8:371-84.

Hoksrud A, Ohberg L, Alfredson H, Bahr R. Ultrasound-guided sclerosis of neovessels in painful chronic patellar tendinopathy: a randomized controlled trial. Am J Sports Med 2006;34:1738-46.

Howry D, Posakony G, Cuschman R, Holmes J. Three dimensional and stereoscopic observation of body structures by ultrasound. J Appl Physiol 1956;9:304-6.

Hulmes DJ. Building collagen molecules, fibrils, and suprafibrillar structures. J Struct Biol 2002;137:2-10.

Ippolito E, Natali PG, Postacchini F, Accinni L, De Martino C. Morphological, immunochemical, and biochemical study of rabbit achilles tendon at various ages. J Bone Joint Surg Am 1980;62:583-98.

Jarvinen TAH, Kannus P, Maffulli N, Khan KM. Achilles Tendon Disorders: Etiology and Epidemiology. Foot and Ankle Clinics of North America 2005;10:255-66.

Jensen JA. Medical ultrasound imaging. Prog Biophys Mol Biol 2007;93:153-65.

Joshua F, Edmonds J, Lassere M. Power Doppler ultrasound in musculoskeletal disease: a systematic review. Semin Arthritis Rheum 2006;36:99-108.

Jozsa L, Balint J, Demel Z, Reffy A. [The role of non-progressive myopathies in the spontaneous rupture of tendons (author's transl)]. Magy Traumatol Orthop Helyreallito Seb 1980;23:172-8.

Jozsa L, Balint JB, Kannus P, Reffy A, Barzo M. Distribution of blood groups in patients with tendon rupture. An analysis of 832 cases. J Bone Joint Surg Br 1989;71:272-4.

Jozsa L, Kannus P, Balint JB, Reffy A. Three-dimensional ultrastructure of human tendons. Acta Anat (Basel) 1991;142:306-12.

Jozsa L, Reffy A, Kannus P, Demel S, Elek E. Pathological alterations in human tendons. Arch Orthop Trauma Surg 1990;110:15-21.

Kannus P. Structure of the tendon connective tissue. Scand J Med Sci Sports 2000;10:312-20.

Kannus P, Jozsa L. Histopathological changes preceding spontaneous rupture of a tendon. A controlled study of 891 patients. J Bone Joint Surg Am 1991;73:1507-25.

Kannus P, Natri A. Etiology and pathophysiology of tendon ruptures in sports. Scand J Med Sci Sports 1997;7:107-12.

Kannus P, Niittymaki S, Jarvinen M, Lehto M. Sports injuries in elderly athletes: a three-year prospective, controlled study. Age Ageing 1989;18:263-70.

Katamay R, Fleischlin C, Gugleta K, Flammer J, Orgul S. Volumetric blood flow measurement in the ophthalmic artery using colour Doppler. Klin Monatsbl Augenheilkd 2009;226:249-53.

Ker RF. The implications of the adaptable fatigue quality of tendons for their construction, repair and function. Comp Biochem Physiol A Mol Integr Physiol 2002;133:987-1000.

Khan KM, Cook JL, Kiss ZS, Visentini PJ, Fehrmann MW, Harcourt PR, Tress BW, Wark JD. Patellar tendon ultrasonography and jumper's knee in female basketball players: a longitudinal study. Clin J Sport Med 1997;7:199-206.

Khan KM, Cook JL, Maffulli N, Kannus P. Where is the pain coming from in tendinopathy? It may be biochemical, not only structural, in origin. Br J Sports Med 2000;34:81-3.

Knobloch K. The use of a neovascularization score to predict clinical severity in Achilles tendinopathy. Am J Sports Med 2008;36:395; author reply -7.

Knobloch K, Schreibmueller L, Longo UG, Vogt PM. Eccentric exercises for the management of

tendinopathy of the main body of the Achilles tendon with or without an AirHeel Brace. A randomized controlled trial. B: Effects of compliance. Disabil Rehabil 2008;30:1692-6.

Koenig MJ, Torp-Pedersen S, Holmich P, Terslev L, Nielsen MB, Boesen M, Bliddal H. Ultrasound Doppler of the Achilles tendon before and after injection of an ultrasound contrast agent--findings in asymptomatic subjects. Ultraschall Med 2007;28:52-6.

Komi PV, Bosco C. Utilization of stored elastic energy in leg extensor muscles by men and women. Med Sci Sports 1978;10:261-5.

Krahe MA, Berlet GC. Achilles tendon ruptures, re rupture with revision surgery, tendinosis, and insertional disease. Foot Ankle Clin 2009;14:247-75.

Kraushaar BS, Nirschl RP. Tendinosis of the elbow (tennis elbow). Clinical features and findings of histological, immunohistochemical, and electron microscopy studies. J Bone Joint Surg Am 1999;81:259-78.

Krishna Sayana M, Maffulli N. Insertional Achilles Tendinopathy. Foot and Ankle Clinics of North America 2005;10:309-20.

Krueger-Franke M, Siebert CH, Scherzer S. Surgical treatment of ruptures of the Achilles tendon: a review of long-term results. Br J Sports Med 1995;29:121-5.

Kvist M. Achilles tendon injuries in athletes. Sports Med 1994;18:173-201.

Kvist M, Jozsa L, Jarvinen M, Kvist H. Fine structural alterations in chronic Achilles paratenonitis in athletes. Pathol Res Pract 1985;180:416-23.

Laine HR, Harjula AL, Peltokallio P. Ultrasonography as a differential diagnostic aid in achillodynia. J Ultrasound Med 1987;6:351-62.

Laine VA, Vainio KJ. Spontaneous ruptures of tendons in rheumatoid arthritis. Acta Orthop Scand 1955;24:250-7.

Laszlo G. Jozsa PK. Human tendons : anatomy, physiology, and pathology 1997;69.

Leung JL, Griffith JF. Sonography of chronic Achilles tendinopathy: a case-control study. J Clin Ultrasound 2008;36:27-32.

Lieber RL, Brown CG, Trestik CL. Model of muscle-tendon interaction during frog semitendinosis fixed-end contractions. J Biomech 1992;25:421-8.

Lin TW, Cardenas L, Soslowsky LJ. Biomechanics of tendon injury and repair. J Biomech 2004;37:865-77.

Lind B, Ohberg L, Alfredson H. Sclerosing polidocanol injections in mid-portion Achilles tendinosis: remaining good clinical results and decreased tendon thickness at 2-year follow-up. Knee Surg Sports Traumatol Arthrosc 2006;14:1327-32.

Ljung BO, Forsgren S, Friden J. Substance P and calcitonin gene-related peptide expression at the extensor carpi radialis brevis muscle origin: implications for the etiology of tennis elbow. J Orthop Res 1999;17:554-9.

Longo UG, Ronga M, Maffulli N. Achilles tendinopathy. Sports Med Arthrosc 2009;17:112-26.

Lysholm J, Wiklander J. Injuries in runners. Am J Sports Med 1987;15:168-71.

Maffulli N. The clinical diagnosis of subcutaneous tear of the Achilles tendon. A prospective study in 174 patients. Am J Sports Med 1998;26:266-70.

Maffulli N. Rupture of the Achilles tendon. J Bone Joint Surg Am 1999;81:1019-36.

Maffulli N, Kader D. Tendinopathy of tendo achillis. J Bone Joint Surg Br 2002;84:1-8.

Maffulli N, Kenward MG, Testa V, Capasso G, Regine R, King JB. Clinical diagnosis of Achilles tendinopathy with tendinosis. Clin J Sport Med 2003;13:11-5.

Maffulli N, Regine R, Angelillo M, Capasso G, Filice S. Ultrasound diagnosis of Achilles tendon pathology in runners. Br J Sports Med 1987;21:158-62.

Maganaris CN, Narici MV, Maffulli N. Biomechanics of the Achilles tendon. Disabil Rehabil 2008;30:1542-7.

Magnusson SP, Hansen P, Kjaer M. Tendon properties in relation to muscular activity and physical training. Scand J Med Sci Sports 2003;13:211-23.

Magnusson SP, Narici MV, Maganaris CN, Kjaer M. Human tendon behaviour and adaptation, in vivo. J Physiol 2008;586:71-81.

Magnusson SP, Qvortrup K, Larsen JO, Rosager S, Hanson P, Aagaard P, Krogsgaard M, Kjaer M. Collagen fibril size and crimp morphology in ruptured and intact Achilles tendons. Matrix Biology 2002;21:369-77.

Maier M, Milz S, Tischer T, Munzing W, Manthey N, Stabler A, Holzknecht N, Weiler C, Nerlich A, Refior HJ, Schmitz C. Influence of extracorporeal shock-wave application on normal bone in an animal model in vivo. Scintigraphy, MRI and histopathology. J Bone Joint Surg Br 2002;84:592-9.

Martinoli C, Bianchi S, M. D, al. e. Ultrasound of tendons and nerves. Eur J Radiol 2002;12:44-55.

Martinoli C, Derchi LE. Gain setting in power Doppler US. Radiology 1997;202:284-5.

Martinoli C, Derchi LE, Pastorino C, Bertolotto M, Silvestri E. Analysis of echotexture of tendons with US. Radiology 1993;186:839-43.

McComis GP, Nawoczenski DA, DeHaven KE. Functional bracing for rupture of the Achilles tendon. Clinical results and analysis of ground-reaction forces and temporal data. J Bone Joint Surg Am 1997;79:1799-808.

Mercé LT, Alcázar JL, Engels V, Troyano J, Bau S, Bajo JM. Endometrial volume and vascularity measurements by transvaginal three-dimensional ultrasonography and power Doppler angiography in stimulated and tumoral endometria: Intraobserver reproducibility. Gynecologic Oncology 2006;100:544-50.

Miquel A, Molina V, Phan C, Lesavre A, Menu Y. [Ultrasound of the Achilles tendon after percutaneous repair]. J Radiol 2009;90:305-9.

Moller A, Astron M, Westlin N. Increasing incidence of Achilles tendon rupture. Acta Orthop Scand 1996;67:479-81.

Moller M, Movin T, Granhed H, Lind K, Faxen E, Karlsson J. Acute rupture of tendon Achillis. A prospective randomised study of comparison between surgical and non-surgical treatment. J Bone Joint Surg Br 2001;83:843-8.

Morag G, Maman E, Arbel R. Endoscopic treatment of hindfoot pathology. Arthroscopy: The Journal of Arthroscopic & Related Surgery 2003;19:13-.

Movin T, Ryberg, McBride DJ, Maffulli N. Acute Rupture of the Achilles Tendon. Foot and Ankle Clinics of North America 2005;10:331-56.

Munteanu SE, Landorf KB, Menz HB, Cook JL, Pizzari T, Scott LA. Efficacy of customised foot orthoses in the treatment of Achilles tendinopathy: study protocol for a randomised trial. J Foot Ankle Res 2009;2:27.

Murtaza Ali DMaUD. Signal Processing Overview of Ultrasound Systems for Medical Imaging. Texas Instruments White Paper 2008;

Nelson TR, Pretorius DH. Three-dimensional ultrasound imaging. Ultrasound Med Biol 1998;24:1243-70.

Nelson TR, Pretorius DH, Hull A, Riccabona M, Sklansky MS, James G. Sources and impact of artifacts on clinical three-dimensional ultrasound imaging. Ultrasound Obstet Gynecol 2000;16:374-83.

Nicol AM, McCurdie I, Etherington J. Use of ultrasound to identify chronic Achilles tendinosis in an active asymptomatic population. J R Army Med Corps 2006;152:212-6.

Nikolaou PK, Macdonald BL, Glisson RR, Seaber AV, Garrett WE, Jr. Biomechanical and histological evaluation of muscle after controlled strain injury. Am J Sports Med 1987;15:9-14.

O'Brien M. functional anatomy and physiology of tendons. Clin Sports Med 1992;11:

O'Brien M. Structure and metabolism of tendons. Scand J Med Sci Sports 1997;7:55-61.

Ohberg L, Alfredson H. Ultrasound guided sclerosis of neovessels in painful chronic Achilles tendinosis: pilot study of a new treatment. Br J Sports Med 2002;36:173-5; discussion 6-7.

Ohberg L, Alfredson H. Sclerosing therapy in chronic Achilles tendon insertional pain-results of a pilot

study. Knee Surg Sports Traumatol Arthrosc 2003;11:339-43.

Ohberg L, Alfredson H. Effects on neovascularisation behind the good results with eccentric training in chronic mid-portion Achilles tendinosis? Knee Surg Sports Traumatol Arthrosc 2004;12:465-70.

Ohberg L, Lorentzon R, Alfredson H. Eccentric training in patients with chronic Achilles tendinosis: normalised tendon structure and decreased thickness at follow up. Br J Sports Med 2004;38:8-11; discussion

Ohberg L LR, Alfredson H. Neovascularisation in Achilles tendon with painful tendinosis but not in normal tendons: an ultrasonographic investigation. Knee Surg Sports Traumatol Arthrosc 2001;9:233-8.

Ohtori S, Inoue G, Mannoji C, Saisu T, Takahashi K, Mitsuhashi S, Wada Y, Takahashi K, Yamagata M, Moriya H. Shock wave application to rat skin induces degeneration and reinnervation of sensory nerve fibres. Neuroscience Letters 2001;315:57-60.

Paavola M, Jarvinen TA. Paratendinopathy. Foot Ankle Clin 2005;10:279-92.

Paavola M, Kannus P, Jarvinen TA, Khan K, Jozsa L, Jarvinen M. Achilles tendinopathy. J Bone Joint Surg Am 2002;84-A:2062-76.

Paavola M, Kannus P, Paakkala T, Pasanen M, Jarvinen M. Long-term prognosis of patients with achilles tendinopathy. An observational 8-year follow-up study. Am J Sports Med 2000;28:634-42.

Pauletzki J, Sackmann M, Holl J, Paumgartner G. Evaluation of gallbladder volume and emptying with a novel three-dimensional ultrasound system: Compare with the sum-of-cylinders and the ellipsoid methods. J Clin Ultrasound 1996;24:277-85.

Peacock EE, Jr. A study of the circulation in normal tendons and healing grafts. Ann Surg 1959;149:415-28.

Peers KH, Brys PP, Lysens RJ. Correlation between power Doppler ultrasonography and clinical severity in Achilles tendinopathy. Int Orthop 2003;27:180-3.

Pope CF. Radiologic evaluation of tendon injuries. Clin Sports Med 1992;11:579-99.

Porter BC, Rubens DJ, Strang JG, Smith J, Totterman S, Parker KJ. Three-dimensional registration and fusion of ultrasound and MRI using major vessels as fiducial markers. Medical Imaging, IEEE Transactions on 2001;20:354-9.

Prager R, Ijaz U, Gee A, Treece G. Three-dimensional ultrasound imaging. JEIM 2009;223:

Premkumar A, Perry MB, Dwyer AJ, Gerber LH, Johnson D, Venzon D, Shawker TH. Sonography and MR imaging of posterior tibial tendinopathy. AJR Am J Roentgenol 2002;178:223-32.

Pufe T, Petersen W, Tillmann B, Mentlein R. The angiogenic peptide vascular endothelial growth factor is expressed in foetal and ruptured tendons. Virchows Arch 2001;439:579-85.

Rees JD, Wilson AM, Wolman RL. Current concepts in the management of tendon disorders. Rheumatology (Oxford) 2006;45:508-21.

Reinherz RP, Granoff SR, Westerfield M. Pathologic afflictions of the Achilles tendon. J Foot Surg 1991;30:117-21.

Reiter M, Ulreich N, Dirisamer A, Tscholakoff D, Bucek RA. Colour and power Doppler sonography in symptomatic Achilles tendon disease. Int J Sports Med 2004;25:301-5.

Richards PJ, Braid JC, Carmont MR, Maffulli N. Achilles tendon ossification: pathology, imaging and aetiology. Disabil Rehabil 2008;30:1651-65.

Richards PJ, Dheer AK, McCall IM. Achilles tendon (TA) size and power Doppler ultrasound (PD) changes compared to MRI: a preliminary observational study. Clin Radiol 2001;56:843-50.

Richards PJ, McCall IW, Day C, Belcher J, Maffulli N. Longitudinal microvascularity in Achilles tendinopathy (power Doppler ultrasound, magnetic resonance imaging time-intensity curves and the Victorian Institute of Sport Assessment-Achilles questionnaire): a pilot study. Skeletal Radiol 2009;

Richards PJ, Win T, Jones PW. The distribution of microvascular response in Achilles tendonopathy assessed by colour and power Doppler. Skeletal Radiol 2005;34:336-42.

Ritchie CJ, Edwards WS, Mack LA, Cyr DR, Kim Y. Three-dimensional ultrasonic angiography using power-mode Doppler. Ultrasound Med Biol 1996;22:277-86.

Robinson JM, Cook JL, Purdam C, Visentini PJ, Ross J, Maffulli N, Taunton JE, Khan KM, Victorian Institute Of Sport Tendon Study G. The VISA-A questionnaire: a valid and reliable index of the clinical severity of Achilles tendinopathy. Br J Sports Med 2001;35:335-41.

Romaneehsen B, Kreitner KF. [MR imaging of tendon diseases. Exemplified using the examples of rotator cuff, epicondylitis and achillodynia]. Orthopade 2005;34:543-9.

Rompe JD, Furia J, Weil L, Maffulli N. Shock wave therapy for chronic plantar fasciopathy. Br Med Bull 2007;81-82:183-208.

Rowe RW. The structure of rat tail tendon fascicles. Connect Tissue Res 1985;14:21-30.

Rubin JM, Bude RO, Carson PL, Bree RL, Adler RS. Power Doppler US: a potentially useful alternative to mean frequency-based color Doppler US. Radiology 1994;190:853-6.

Rufai A, Ralphs JR, Benjamin M. Structure and histopathology of the insertional region of the human Achilles tendon. J Orthop Res 1995;13:585-93.

Saltzman CL, Tearse DS. Achilles tendon injuries. J Am Acad Orthop Surg 1998;6:316-25.

Sandmeier R, Renstrom PA. Diagnosis and treatment of chronic tendon disorders in sports. Scand J Med Sci Sports 1997;7:96-106.

Schepsis AA, Jones H, Haas AL. Achilles tendon disorders in athletes. Am J Sports Med 2002;30:287-305.

Schulten-Wijman MJ, Struijk PC, Brezinka C, De Jong N, Steegers EA. Evaluation of volume vascularization index and flow index: a phantom study. Ultrasound Obstet Gynecol 2008;32:560-4.

Schweitzer ME, Karasick D. MR imaging of disorders of the Achilles tendon. AJR Am J Roentgenol 2000;175:613-25.

Seil R, Wilmes P, Nuhrenborger C. Extracorporeal shock wave therapy for tendinopathies. Expert Rev Med Devices 2006;3:463-70.

Sems A, Dimeff R, Iannotti JP. Extracorporeal shock wave therapy in the treatment of chronic tendinopathies. J Am Acad Orthop Surg 2006;14:195-204.

Sengkerij PM, de Vos RJ, Weir A, van Weelde BJ, Tol JL. Interobserver reliability of neovascularization score using power Doppler ultrasonography in midportion achilles tendinopathy. Am J Sports Med 2009;37:1627-31.

Shin D, Finni T, Ahn S, Hodgson JA, Lee HD, Edgerton VR, Sinha S. In vivo estimation and repeatability of force-length relationship and stiffness of the human achilles tendon using phase contrast MRI. J Magn Reson Imaging 2008;28:1039-45.

Shrout P, Fleiss J. Intraclass correlations: Uses in assessing rater reliability. . Psychological Bulletin 1979;86:420-8.

Shutilov VA. Fundamental physics of ultrasound New York : Gordon and Breach Science Publishers, 1988.

Silver FH, Freeman JW, Seehra GP. Collagen self-assembly and the development of tendon mechanical properties. J Biomech 2003;36:1529-53.

Silver FH, Kato YP, Ohno M, Wasserman AJ. Analysis of mammalian connective tissue: relationship between hierarchical structures and mechanical properties. J Long Term Eff Med Implants 1992;2:165-98.

Silvestri E, Biggi E, Molfetta L, Avanzino C, La Paglia E, Garlaschi G. Power Doppler analysis of tendon vascularization. Int J Tissue React 2003;25:149-58.

Snow SW, Bohne WH, DiCarlo E, Chang VK. Anatomy of the Achilles tendon and plantar fascia in relation to the calcaneus in various age groups. Foot Ankle Int 1995;16:418-21.

Soma CA, Mandelbaum BR. Achilles tendon disorders. Clin Sports Med 1994;13:811-23.

Stanish WD, Rubinovich RM, Curwin S. Eccentric exercise in chronic tendinitis. Clin Orthop Relat Res 1986;65-8.

Stein V, Laprell H, Tinnemeyer S, Petersen W. Quantitative assessment of intravascular volume of the

human Achilles tendon. Acta Orthop Scand 2000;71:60-3.

Stilwell DL, Jr. The innervation of tendons and aponeuroses. Am J Anat 1957;100:289-317.

Tan SC, Chan O. Achilles and patellar tendinopathy: current understanding of pathophysiology and management. Disabil Rehabil 2008;30:1608-15.

Terslev L, Qvistgaard E, Torp-Pedersen S, Laetgaard J, Danneskiold-Sams B, Bliddal H. Ultrasound and Power Doppler findings in jumper's knee -- preliminary observations. European Journal of Ultrasound 2001;13:183-9.

Tidball JG. Myotendinous junction injury in relation to junction structure and molecular composition. Exerc Sport Sci Rev 1991;19:419-45.

TM Best WG. Basic science of soft tissue muscle and tendon. Orthopaedic Sports Med 1994;1-45.

Torp-Pedersen ST, Terslev L. Settings and artefacts relevant in colour/power Doppler ultrasound in rheumatology. Ann Rheum Dis 2008;67:143-9.

Trotter JA, Baca JM. The muscle-tendon junctions of fast and slow fibres in the garter snake: ultrastructural and stereological analysis and comparison with other species. J Muscle Res Cell Motil 1987;8:517-26.

Trotter JA, Eberhard S, Samora A. Structural connections of the muscle-tendon junction. Cell Motility and the Cytoskeleton 1983;3:431-8.

van Snellenberg W, Wiley JP, Brunet G. Achilles tendon pain intensity and level of neovascularization in athletes as determined by color Doppler ultrasound. Scand J Med Sci Sports 2007;17:530-4.

Vlaisavljevic V, Reljic M, Gavric Lovrec V, Zazula D, Sergent N. Measurement of perifollicular blood flow of the dominant preovulatory follicle using three-dimensional power Doppler. Ultrasound Obstet Gynecol 2003;22:520-6.

Vora AM, Myerson MS, Oliva F, Maffulli N. Tendinopathy of the Main Body of the Achilles Tendon. Foot and Ankle Clinics of North America 2005;10:293-308.

Wang CJ, Huang HY, Pai CH. Shock wave-enhanced neovascularization at the tendon-bone junction: an experiment in dogs. J Foot Ankle Surg 2002a;41:16-22.

Wang CJ, Wang FS, Yang KD, Weng LH, Hsu CC, Huang CS, Yang LC. Shock wave therapy induces neovascularization at the tendon-bone junction. A study in rabbits. J Orthop Res 2003;21:984-9.

Wang FS, Wang CJ, Sheen-Chen SM, Kuo YR, Chen RF, Yang KD. Superoxide mediates shock wave induction of ERK-dependent osteogenic transcription factor (CBFA1) and mesenchymal cell differentiation toward osteoprogenitors. J Biol Chem 2002b;277:10931-7.

Weinberg EP, Adams MJ, Hollenberg GM. Color Doppler sonography of patellar tendinosis. AJR Am J Roentgenol 1998;171:743-4.

Welsh AW, Humphries K, Cosgrove DO, Taylor MJO, Fisk NM. Development of three-dimensional power Doppler ultrasound imaging of fetoplacental vasculature. Ultrasound in Medicine & Biology 2001;27:1161-70.

Weskott HP. Amplitude Doppler US: slow blood flow detection tested with a flow phantom. Radiology 1997;202:125-30.

Wilson AM, Goodship AE. Exercise-induced hyperthermia as a possible mechanism for tendon degeneration. J Biomech 1994;27:899-905.

Worth N, Ghosh S, Maffulli N. Management of acute Achilles tendon ruptures in the United Kingdom. J Orthop Surg (Hong Kong) 2007;15:311-4.

Yang X, Pugh ND, Coleman DP, Nokes LD. Are Doppler studies a useful method of assessing neovascularization in human Achilles tendinopathy? A systematic review and suggestions for optimizing machine settings. J Med Eng Technol 2010;35:365-72.

Zanetti M, Metzdorf A, Kundert HP, Zollinger H, Vienne P, Seifert B, Hodler J. Achilles tendons: clinical relevance of neovascularization diagnosed with power Doppler US. Radiology 2003;227:556-60.

Zantop T, Tillmann B, Petersen W. Quantitative assessment of blood vessels of the human Achilles tendon: an immunohistochemical cadaver study. Arch Orthop Trauma Surg 2003;123:501-4.

Appendix A-Stepping Motor

7.5° Stepping Motors
Stock Nos. 332-947 and 332-953

7.5° stepper motor
size 1 (RS stock no. 332-947)
and size 2 (RS stock no. 332-953)

Two 7.5° stepper motors each with four 12V⎓ windings (coils) and permanent magnet rotor construction. Designed for unipolar drive, these motors are easily interfaced to simple and relatively low power electronics thus providing economical means of motion and speed control. Due to their permanent magnet rotors these motors have a braking torque even when not energised. This is the detent (residual) torque which is a useful feature for positional integrity.

The size 1 motor is ideal for applications requiring low torque drive but it can also be used with the **RS** range of synchronous gearboxes (**RS** stock nos. 336-400 etc.) to provide finer step angle and increased torque at lower speeds.

The size 2 motor is more powerful general purpose motor ideally suited for direct drive applications.

Figure 1. 7.5° Stepper motors

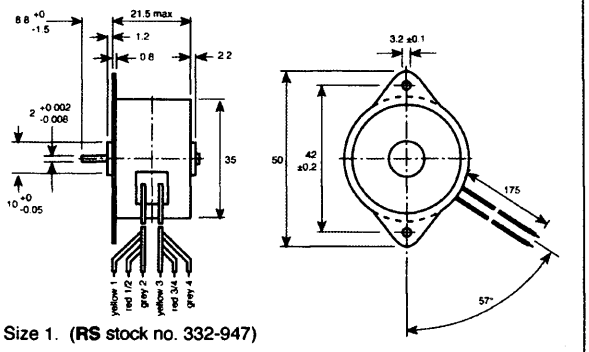

Size 1. (**RS** stock no. 332-947)

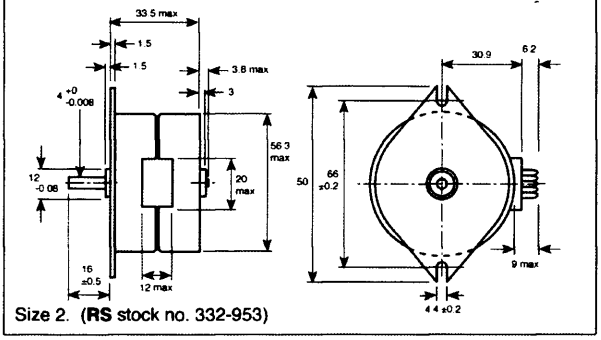

Size 2. (**RS** stock no. 332-953)

Technical specification

	Size 1	Size 2	Units
Power consumption of motor only	2	5.3	W
Maximum working torque	6	57	mNm
Holding torque	10	85	mNm
Torque derating	-0.4	-0.4	%/°C
Maximum pull-in rate	350	130	steps/s
Resistance per phase at +20°C	120	47	Ω
Inductance per phase	160	400	mH
Current per phase	100	240	mA
Permissible ambient temperature range	-20 to +70	-20 to +70	°C
Permissible storage temperature range	-40 to +100	-40 to +100	°C
Permissible motor temperature	120	120	°C
Insulation resistance at 500V (CEE 10)	>2	>2	MΩ
Step angle	7° 30'	7° 30'	
Step angle tolerance, not cumulative	±40'	±20'	
Number of steps per revolution	48	48	
Direction of rotation	reversible	reversible	
Rotor inertia	2.6	45	gmc²
Mass	80	300	g
Maximum radial force	2.5	10	N
Maximum axle force	0.75	1.5	N
Bearings	Slide (bronze)	Slide (sintered bronze)	

Appendix B-Stepping Motor Driver

GB RS Stock No.

217-3611

Max. power dissipated through R = (rated motor current) 2 x R. If the power dissipation is high it is advisable to arrive at the required value of 'R' by using a network of series or parallel resistors. (The use of higher wattage resistors and heat sinks may be required).
Max. current consumption (motor & board) = 2 x (current per phase) + 60mA. Thus ensure power supply cables used are sufficiently rated.
External control signals e.g. full/half step, direction etc. as well as the oscillator (if fitted) stop/run signal can be applied to the circuit in any of the methods of Figure B1.

Connection to RS stepper motors

When the winding of the RS stepper motors are assigned (Ø1 - Ø4) as shown in Fig. B2 , they can be connected to the board according to Figure 42.
If the supply voltage is set to 24Vdc then 'R' values for use with the RS motors are given in table 1 below.

Table 1

Motor	Rated Current (A)	Rated Winding Voltage (V)	R (Ω)	Power Dissipation through R (W)
332-947	0.1	12	120	1.2
332-953	0.24	12	47	3
440-464	2	3	10.5	5

For other details and motors performance refer to RS data sheet on stepper motors.

On-board oscillator assembly

If external clock source is not available, on-board oscillator can be assembled simply by soldering into place the required RS Components listed below.

Note : the oscillator clock output must be externally wired to the clock, input-pin 24a.

If oscillator remote controls are required (e.g. front panel controls) then plug PL1 (5-way inter p.c.b. **RS** stock no.467-576) can be added together with mating cable shell (**RS** stock no. 467-627) and crimp terminals (**RS** stock no.467-598)

Starting (base) and running speed control

The on-board oscillator can be arranged to start at a fixed frequency (thus a fixed motor speed) and then ramp up to a final value (the running motor speed). This facility is available to start the motor within its pull-in performance region and then accelerate the motor through so that it can operate within the pull-out mode. On switch-off the motor decelerates automatically.

Three parameters need to be determined for any application :

a) The starting speed: this should be below the pull-in speed for the motor (with any additional load).
b) The running (final) speed: this should be within the pull-out capability of the motor (with any additional load).
c) The acceleration and deceleration rate between starting and running speeds: this is limited by motor capability to accelerate through its own (plus any load) inertia

Oscillator controls (external)

Note : Oscillator frequency corresponds directly to motor speed in step/s or half step/s depending on motor drive mode.

For a 1.8° stepper motor :

$$\text{speed in revs / min} = \frac{60}{200} \times \text{speed in step/s}$$

or

$$\text{speed in revs / min} = \frac{60}{400} \times \text{speed in 'half' step/s}$$

For a 7.5° stepper motor :

$$\text{speed in revs / min} = \frac{60}{48} \times \text{speed in step/s}$$

or

$$\text{speed in revs / min} = \frac{60}{96} \times \text{speed in 'half' step/s}$$

Technical specification

Size _____ standard Euro card (168 x 100 x 15)
Mating edge connector _____ standard 32-way DIN 41612socket e.g. _____ (RS stock no. 471-503 or 467-453)
Supply (board and motor) _____ 15-30Vdc + 10% max. unregulated smoothed
Current consumption:
Board only _____ 60mA
Motor winding _____ dependent on the motor _____ used-up to 2A per phase max.
On-board auxiliary output _____ 12Vdc 50mA max. regulated
Switching logic control (CMOS and open collector T.T.L. compatible):
Level '0' _____ 0V
Level '1' _____ 12V
Inputs pins:
25. Full / half step _____ Level '1' full step / Level '0' half step
23. Direction. _____ Connecting this pin to Zero volts will change the direction of the motor.
24. Clock _____ 1Hz-25kHz, 10µs min. pulse width negative edge triggered.
22. Preset ____ Active Level '0' set motor drive states to Q1, & Q3 'OFF', Q2 & Q4 'ON' (full step mode) Q1, Q2 & Q3 'OFF', Q4 'ON'(Half step mode)-see Figure42. Automatic preset at switch-on

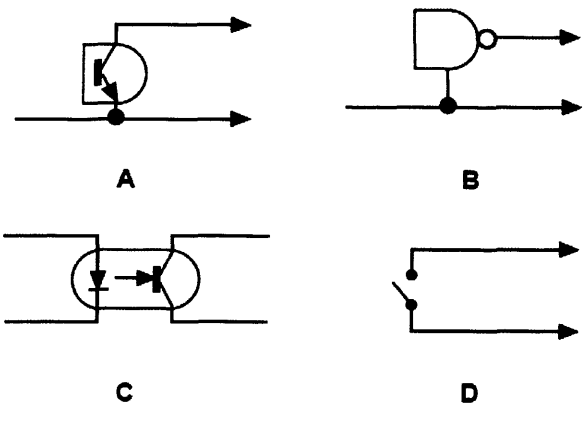

A. Open collector T.T.L.
B. C.M.O.S. (operating @ +12V)
C. Opto-coupler
D. Simple switch

Fig. B1

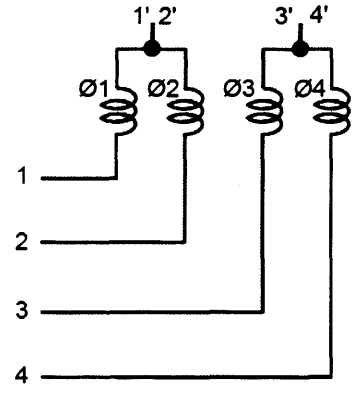

A. Black
B. Orange
C. Red
D. Yellow
E. White / Black
F. White / Orange
G. Red / White
H. Yellow / White

Fig. B2

Appendix C-Controller Box Dimensions

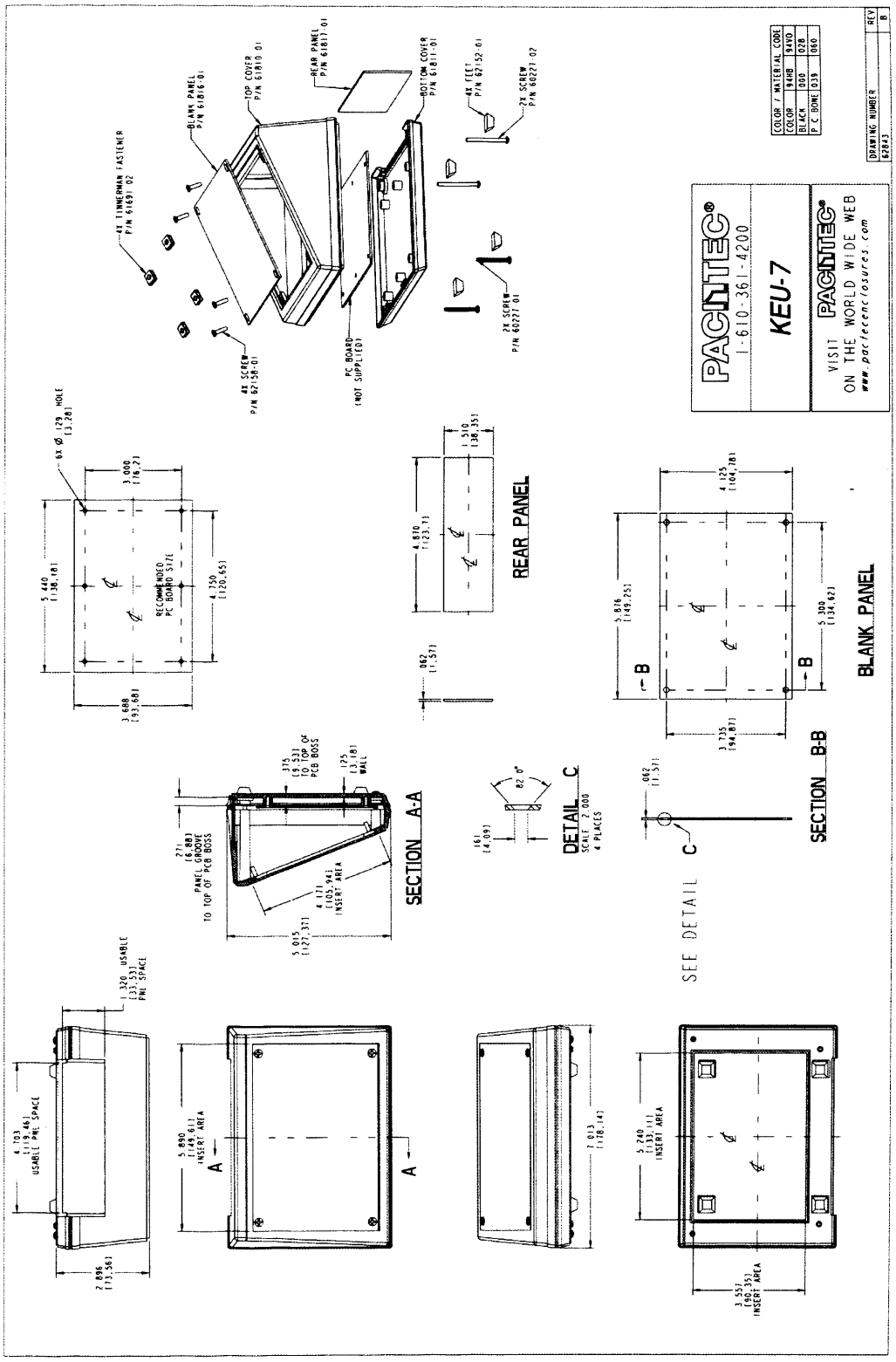

Fig. C1

Appendix D-Program Codes

D.1 Main body

```
'*************************************Function declarations*************************************
Private Declare Function GetPixel Lib "gdi32" (ByVal hdc As Long, ByVal x As Long, _
ByVal y As Long) As Long

Private Declare Function SetPixel Lib "gdi32" (ByVal hdc As Long, ByVal x As Long, _
ByVal y As Long, ByVal crColour As Long) As Long
'*************************************End*************************************

'*************************************Variables definitions*************************************
Dim pColour As Long
Dim R As Long, G As Long, B As Long

Dim x1 As Integer                'initial x position
Dim y1 As Integer                'initial y position
Dim x2 As Integer                'end x position
Dim y2 As Integer                'end y position

Dim flag As Boolean              'drawing flag
Dim dopplerpoints As Long        'count the doppler points
Dim numOpenAVIs As Integer
Dim DateFolder As String
Dim numFrames As Long     'number of frames in video stream
Dim ColourDis As Integer         'threshold
Dim mouseBoxx1, mouseBoxx2, mouseBoxy1, mouseBoxy2 As Integer

Dim lineAch, radCha As Boolean
Dim circenX, circenY As Integer
Dim cirX, cirY As Integer
Dim cirRad, cirR As Integer
Dim cirHei, cirH As Single
Dim dragSen, dragS As Integer
'*************************************End*************************************

'*********************************Form load and unload functions*********************************
Private Sub Form_Load()
Call AVIFileInit                 '// opens AVIFile library
Picture1.ScaleMode = 3
```

```
Slider1.Min = 0
Slider1.Max = 37
Slider2.Value = 20

lineAch = False
radCha = False

circenX = 417
circenY = 128
cirRad = 60
cirHei = 1 / 3

cirX = circenX
cirY = circenY
cirR = cirRad
cirH = cirHei

List1.Enabled = False

End Sub

Private Sub Form_Unload(Cancel As Integer)
Call AVIFileExit                    '// releases AVIFile library
End Sub
'*************************************End*************************************

'*****************************************************************************
Private Sub Command1_Click()

    Dim res As Long             'result code
    Dim ofd As cFileDlg         'OpenFileDialog class
    Dim szFile As String        'filename
    Dim pAVIFile As Long        'pointer to AVI file interface (PAVIFILE handle)
    Dim pAVIStream As Long      'pointer to AVI stream interface (PAVISTREAM handle)

    Dim firstFrame As Long      'position of the first video frame
    Dim fileInfo As AVI_FILE_INFO          'file info struct
    Dim streamInfo As AVI_STREAM_INFO      'stream info struct
    Dim dib As cDIB
    Dim pGetFrameObj As Long                    'pointer to GetFrame interface
    Dim pDIB As Long                            'pointer to packed DIB in memory
    Dim bih As BITMAPINFOHEADER         'infoheader to pass to GetFrame functions
    Dim i As Long
    Dim j As Long
```

```
DateFolder = "E:\temp\~$$ Doppler " + Format(Time, "h-m-s ") + Format(Date, _
"mmm d yyyy")

    MkDir (DateFolder)
    MkDir (DateFolder & "\maxAll")          'save objects including in out and boundary
    MkDir (DateFolder & "\maxIn")           'svae in only
    MkDir (DateFolder & "\maxInBo")         'save in and boundary

    Label1.Caption = "Processing File "
    Label2.Caption = "Creating Slice"

    If List1.List(0) <> "" Then

    Do While List1.List(j) <> ""

    Label3.Caption = (j + 1) & " of " & numOpenAVIs
    Label3.Refresh

    MkDir (DateFolder & "\" & j)
    szFile = List1.List(j)                  'filename pass to res

    'Open the AVI File and get a file interface pointer (PAVIFILE)
    res = AVIFileOpen(pAVIFile, szFile, OF_SHARE_DENY_WRITE, 0&)
    If res <> AVIERR_OK Then GoTo ErrorOut
    'Get the first available video stream (PAVISTREAM)
    res = AVIFileGetStream(pAVIFile, pAVIStream, streamtypeVIDEO, 0)
    If res <> AVIERR_OK Then GoTo ErrorOut
    'get the starting position of the stream (some streams may not start simultaneously)
    firstFrame = AVIStreamStart(pAVIStream)
    If firstFrame = -1 Then GoTo ErrorOut 'this function returns -1 on error
    'get the length of video stream in frames
    numFrames = AVIStreamLength(pAVIStream)
    If numFrames = -1 Then GoTo ErrorOut ' this function returns -1 on error
    'get file info struct (UDT)
    res = AVIFileInfo(pAVIFile, fileInfo, Len(fileInfo))
    If res <> AVIERR_OK Then GoTo ErrorOut
     'print file info to Debug Window
    Call DebugPrintAVIFileInfo(fileInfo)
     'get stream info struct (UDT)
    res = AVIStreamInfo(pAVIStream, streamInfo, Len(streamInfo))
    If res <> AVIERR_OK Then GoTo ErrorOut
     'print stream info to Debug Window
    Call DebugPrintAVIStreamInfo(streamInfo)
```

```
    'set bih attributes which we want GetFrame functions to return
    With bih
        .biBitCount = 24
        .biClrImportant = 0
        .biClrUsed = 0
        .biCompression = BI_RGB
        .biHeight = streamInfo.rcFrame.bottom - streamInfo.rcFrame.top
        .biPlanes = 1
        .biSize = 40
        .biWidth = streamInfo.rcFrame.right - streamInfo.rcFrame.left
        .biXPelsPerMeter = 0
        .biYPelsPerMeter = 0
        .biSizeImage = (((.biWidth * 3) + 3) And &HFFFC) * .biHeight 'calculate total size of RGBQUAD scanlines
(DWORD aligned)
    End With

pGetFrameObj = AVIStreamGetFrameOpen(pAVIStream, bih)
'force function to return 24bit DIBS

    If pGetFrameObj = 0 Then
        MsgBox "No suitable decompressor found for this video stream!", vbInformation, App.title
        GoTo ErrorOut
    End If

    ProgressBar2.Min = 0
    ProgressBar2.Max = numFrames - 1

    'create a DIB class to load the frames into
    Set dib = New cDIB
    For i = firstFrame To (numFrames - 1) + firstFrame
        pDIB = AVIStreamGetFrame(pGetFrameObj, i)   'returns "packed DIB"
        If dib.CreateFromPackedDIBPointer(pDIB) Then
            Call dib.WriteToFile(DateFolder & "\" & j & "\" & i & ".bmp")
            Label4.Caption = i + 1 & " of " & numFrames & " to folder " & j + 1
            Label4.Refresh
            ProgressBar2.Value = i
        Else
        End If
    Next

    Text3.Text = numFrames

    Set dib = Nothing
```

```
    List1.Enabled = True

ErrorOut:
    If pGetFrameObj <> 0 Then
        Call AVIStreamGetFrameClose(pGetFrameObj) '//deallocates the GetFrame resources and interface
    End If
    If pAVIStream <> 0 Then
        Call AVIStreamRelease(pAVIStream) '//closes video stream
    End If
    If pAVIFile <> 0 Then
        Call AVIFileRelease(pAVIFile) '// closes the file
    End If

    If (res <> AVIERR_OK) Then 'if there was an error then show feedback to user
        MsgBox "There was an error working with the file:" & vbCrLf & szFile, vbInformation, App.title
    End If
        j = j + 1
        Loop
    End If

End Sub
'*************************************************************************

'*************************************************************************
Private Sub Command2_Click()
    ProgressBar2.Max = Picture1.Width
    Picture1.AutoRedraw = True
    Const PI = 3.14159265

    SavePicture Picture1.Image, DateFolder & "\maxIn\" & Text2.Text & List1.ListIndex & _"-" & Label8.Caption &
".bmp"

        For i = 0 To Picture1.Width
            ProgressBar2.Value = i
            For j = 0 To Picture1.Height
                If i > mouseBoxx1 And i < mouseBoxx2 And j > mouseBoxy1 And _
j < mouseBoxy2 Then
                    pColour = GetPixel(Picture1.hdc, i, j)
                    R = pColour And &HFF
                    G = (pColour And 65280) / 256
                    B = (pColour And &HFF0000) / 65536

                    If (R > G) And ((Abs(R - G)) > ColourDis Or (Abs(G - B)) > ColourDis _
```

```
Or (Abs(R - B)) > ColourDis) Then
                    pColour = SetPixel(Picture1.hdc, i, j, vbRed)
                    dopplerpoints = dopplerpoints + 1
                Else
                    pColour = SetPixel(Picture1.hdc, i, j, vbBlack)
                End If
            Else
                pColour = SetPixel(Picture1.hdc, i, j, vbBlack)
            End If
        Next j
    Next i

    SavePicture Picture1.Image, DateFolder & "\maxInBo\" & Text2.Text & _
List1.ListIndex & "-" & Label8.Caption & ".bmp"

    If Check1.Value = 1 Then
        Picture1.Circle (cirX, cirY), cirR, vbBlue, , , cirH
'outline Achilles bound
    End If

    If Check1.Value = 1 Then

        a2 = cirR
        b2 = cirH * cirR
        xc = cirX
        yc = cirY

        ProgressBar2.Max = Picture1.Width
        For x = 0 To Picture1.Width
            ProgressBar2.Value = x
            For y = 0 To Picture1.Height
                pColour = GetPixel(Picture1.hdc, x, y)
                R = pColour And &HFF
                G = (pColour And 65280) / 256
                B = (pColour And &HFF0000) / 65536

                'utilize x(t)=Xc+acost    y(t) = Yc+bsint

                If (((x - xc) / a2) ^ 2 + ((y - yc) / b2) ^ 2) > 1 Then
                    If R > 250 And G < 5 And B < 5 Then
                        pColour = SetPixel(Picture1.hdc, x, y, vbWhite)
                    End If
                ElseIf (((x - xc) / a2) ^ 2 + ((y - yc) / b2) ^ 2) < 1 Then
                    If R < 250 Then
```

```
                    pColour = SetPixel(Picture1.hdc, x, y, vbBlue)
                End If
            End If
            Next y
        Next x

    For i = 0 To Picture1.Width
        ProgressBar2.Value = i
        For j = 0 To Picture1.Height
            If i > (mouseBoxx1 - 2) And i < (mouseBoxx2 + 2) And j > _
(mouseBoxy1 - 2) And j < (mouseBoxy2 + 2) Then
            pColour = GetPixel(Picture1.hdc, i, j)
            R = pColour And &HFF
            G = (pColour And 65280) / 256
            B = (pColour And &HFF0000) / 65536

            'pColour = SetPixel(Picture1.hdc, i, j, vbCyan)

            If (R = 255 And G = 0) Or (R = 255 And G = 255 And B = 255) Then
' if found red point, then pset yellow around it
                ProgressBar1.Max = 3
                For ax = (i - 1) To (i + 1)
                    ProgressBar1.Value = ax - i + 1
                    For ay = (j - 1) To (j + 1)
                        pColour = GetPixel(Picture1.hdc, ax, ay)
                        B = (pColour And &HFF0000) / 65536
                        G = (pColour And 65280) / 256
                        R = pColour And &HFF

                        If (B = 255 And G = 0) Then
' if around area is black or blue
                        pColour = SetPixel(Picture1.hdc, ax, ay, vbYellow)
                        End If

                    Next ay
                Next ax
            End If

            End If
        Next j
    Next i

        SavePicture Picture1.Image, DateFolder & "\maxAll\" & Text2.Text & _
List1.ListIndex & "-" & Label8.Caption & ".bmp"
```

```
        End If

        Picture1.AutoRedraw = False
End Sub
'*************************************************************************

'*************************************************************************
Private Sub Command3_Click()

Dim dopplerpoints As Integer
dopplerpoints = 0

ProgressBar2.Max = mouseBoxx2 - mouseBoxx1
        For i = mouseBoxx1 To mouseBoxx2
            ProgressBar2.Value = i - mouseBoxx1
            For j = mouseBoxy1 To mouseBoxy2
                    pColour = GetPixel(Picture1.hdc, i, j)
                    R = pColour And &HFF
                    G = (pColour And 65280) / 256
                    B = (pColour And &HFF0000) / 65536

                    If (R > G) And ((Abs(R - G)) > ColourDis Or (Abs(G - B)) > ColourDis Or _ (Abs(R - B)) >
ColourDis) Then
                            pColour = SetPixel(Picture1.hdc, i, j, vbGreen)
                            dopplerpoints = dopplerpoints + 1
                    End If
            Next j
        Next i

        Label6.Caption = dopplerpoints
End Sub
'*************************************************************************

'*************************************************************************
Private Sub Command4_Click()

SavePicture Picture1.Image, DateFolder & "\max\" & Text2.Text & List1.ListIndex & _
"-" & Label8.Caption & ".bmp"

End Sub
'*************************************************************************

'*************************************************************************
```

```
Private Sub Command5_Click()
    Const PI = 3.14159265
    Picture1.DrawWidth = 2
    Picture1.Cls

    'Picture1.FillStyle = 0
    Picture1.FillColour = vbGreen
    Picture1.Circle (cirX, cirY), cirR, vbGreen, , , cirH

    lineAch = True
End Sub
'*************************************************************************

'*************************************************************************
Private Sub List1_MouseDown(Button As Integer, Shift As Integer, x As Single, y As Single)
    If List1.ListIndex < 0 Then Exit Sub
    If Button = vbLeftButton Then
        Label5.Caption = "File " & List1.ListIndex + 1 & " of " & numOpenAVIs
        Picture1.Picture = LoadPicture(DateFolder & "\" & List1.ListIndex & "\0.bmp")
          'Label6.Caption = DateFolder & "\" & List1.ListIndex & "\0.bmp"
    End If
    Label12.Caption = "Current frame " & List1.ListIndex
    Text1.Text = 0
End Sub
'*************************************************************************

'*************************************************************************
Private Sub open_Click()
    On Error Resume Next
    CommonDialog1.InitDir = "D:\My Documents\My music"
    CommonDialog1.Flags = cdlOFNAllowMultiselect Or cdlOFNExplorer 'multiple selection
    CommonDialog1.Filter = "All Support Files(*.AVI)|*.AVI| All Files(*.*)|*.*|"
    CommonDialog1.filename = ""
    CommonDialog1.DialogTitle = "AVI files"
    CommonDialog1.ShowOpen

    If Len(CommonDialog1.filename) = 0 Then
    Exit Sub
    End If

    filemanyaddress = CommonDialog1.filename

    Files = Split(filemanyaddress, Chr(0))                    'load multi-files
    numOpenAVIs = UBound(Files)
```

```
        For i = 1 To UBound(Files) Step 1
            Files(i) = Files(0) & "\" & Files(i)
        Next i

        For i = 1 To UBound(Files) Step 1
            strfilename = Files(i)
            List1.AddItem strfilename
        Next i

    Dim Message, title, Default, MyValue
    Message = "Enter a pre-number"
    title = "Slice order"
    Default = ""。
    MyValue = InputBox(Message, title, Default, 4500, 4500)

    Text2.Text = MyValue

    If Err.Number = cdlCancel Then Exit Sub
        VarMore = 0
        VarM3u = 19
        VarVCD = 19
End Sub
'*************************************************************************

'*************************************************************************
Private Sub Picture1_MouseDown(Button As Integer, Shift As Integer, x As Single, y As Single)
    'Picture1.AutoRedraw = True
    'Picture1.Cls
    'Picture1.SetFocus
    flag = True
    x1 = x
    y1 = y
    Picture1.DrawWidth = 3
    Picture1.ForeColour = vbYellow
End Sub
'*************************************************************************

'*************************************************************************
Private Sub Picture1_MouseMove(Button As Integer, Shift As Integer, x As Single, y As Single)
    If flag = True Then
        Picture1.Refresh
        x2 = x
        y2 = y
```

```
        Picture1.Line (x1, y1)-Step(x2 - x1, y2 - y1), , B
    End If
End Sub
'*************************************************************************

'*************************************************************************
Private Sub Picture1_MouseUp(Button As Integer, Shift As Integer, x As Single, y As Single)
    flag = False
    Dim i, j As Long
    Dim lastPoints As Long
    Dim maxNum As Integer
    Dim fromFrame As Integer
'   Dim ToFrame As Integer

    ColourDis = Slider2.Value

    dopplerpoints = 0
    lastPoints = 0
    maxNum = 0

    If x1 > x2 Then
        a = x1
        x1 = x2
        x2 = a
    End If

    If y1 > y2 Then
        a = y1
        y1 = y2
        y2 = a
    End If

    ProgressBar2.Min = 0
    ProgressBar2.Max = x2 - x1

    Picture1.DrawWidth = 2
    Picture1.ForeColour = vbRed

    fromFrame = CInt(Text1.Text)

    mouseBoxx1 = x1
    mouseBoxx2 = x2
    mouseBoxy1 = y1
    mouseBoxy2 = y2
```

```
    For p = fromFrame To CInt(Text3.Text) - 1

        Picture1.Picture = LoadPicture(DateFolder & "\" & List1.ListIndex & "\" & p & ".bmp")
        For i = x1 To x2
            ProgressBar2.Value = i - x1
            For j = y1 To y2
                pColour = GetPixel(Picture1.hdc, i, j)
                R = pColour And &HFF
                G = (pColour And 65280) / 256
                B = (pColour And &HFF0000) / 65536

                If (R > G) Then
                    If (Abs(R - G)) > ColourDis Or (Abs(G - B)) > ColourDis Or _
(Abs(R - B)) > ColourDis Then
                        pColour = SetPixel(Picture1.hdc, i, j, vbYellow)
                        dopplerpoints = dopplerpoints + 1
                    End If
                    'pColour = SetPixel(Picture1.hdc, i, j, vbWhite)
                End If
            Next j
        Next i

        Label6.Caption = dopplerpoints
        Label6.Refresh

        Label7.Caption = "Comparing Slice " & p
        Label7.Refresh

        If dopplerpoints > lastPoints Then
        maxNum = p
        lastPoints = dopplerpoints
        End If

        Label8.Caption = maxNum
        Label8.Refresh

        dopplerpoints = 0

    Next p
    Label6.Caption = maxNum

    Picture1.Picture = LoadPicture(DateFolder & "\" & List1.ListIndex & "\" & maxNum &_ ".bmp")
```

```
    Call Command5_Click

End Sub
'*************************************************************************

'*************************************************************************
Private Sub Slider1_MouseMove(Button As Integer, Shift As Integer, x As Single, y As _ Single)
    On Error Resume Next
    Label7.Caption = "Current Slice " & Slider1.Value
    Picture1.Picture = LoadPicture(DateFolder & "\" & List1.ListIndex & "\" & Slider1.Value _ & ".bmp")
End Sub
'*************************************************************************

'*************************************************************************
Private Sub Slider2_MouseMove(Button As Integer, Shift As Integer, x As Single, y As _ Single)
    Label10.Caption = Slider2.Value
End Sub
'*************************************************************************

'*************************************************************************
Private Sub Slider3_MouseDown(Button As Integer, Shift As Integer, x As Single, y As _ Single)
    radCha = True
End Sub
'*************************************************************************

'*************************************************************************
Private Sub Slider3_MouseMove(Button As Integer, Shift As Integer, x As Single, y As _ Single)
    If radCha And lineAch Then
        Picture1.Cls
        Picture1.Circle (cirX, cirY), Slider3.Value, vbGreen, , , cirH
        cirR = Slider3.Value
    End If
End Sub
'*************************************************************************

'*************************************************************************
Private Sub Slider3_MouseUp(Button As Integer, Shift As Integer, x As Single, y As Single)
    radCha = False
End Sub
'*************************************************************************

'*************************************************************************
Private Sub Slider4_MouseDown(Button As Integer, Shift As Integer, x As Single, y As _ Single)
    radCha = True
```

```
End Sub
'*************************************************************************

'*************************************************************************
Private Sub Slider4_MouseMove(Button As Integer, Shift As Integer, x As Single, y As _ Single)
    If radCha And lineAch Then
        Picture1.Cls
        Picture1.Circle (Slider4.Value, cirY), cirR, vbGreen, , , cirH
        cirX = Slider4.Value
    End If
End Sub
'*************************************************************************

'*************************************************************************
Private Sub Slider4_MouseUp(Button As Integer, Shift As Integer, x As Single, y As Single)
    radCha = False
End Sub
'*************************************************************************

'*************************************************************************
Private Sub Slider5_MouseDown(Button As Integer, Shift As Integer, x As Single, y As _ Single)
    radCha = True
End Sub
'*************************************************************************

'*************************************************************************
Private Sub Slider5_MouseMove(Button As Integer, Shift As Integer, x As Single, y As _ Single)
    If radCha And lineAch Then
        Picture1.Cls
        Picture1.Circle (cirX, Slider5.Value), cirR, vbGreen, , , cirH
        cirY = Slider5.Value
    End If
End Sub
'*************************************************************************

'*************************************************************************
Private Sub Slider5_MouseUp(Button As Integer, Shift As Integer, x As Single, y As Single)
    radCha = False
End Sub
'*************************************************************************

'*************************************************************************
Private Sub Slider6_MouseDown(Button As Integer, Shift As Integer, x As Single, y As _ Single)
    radCha = True
```

```
End Sub
'*************************************************************************

'*************************************************************************
Private Sub Slider6_MouseMove(Button As Integer, Shift As Integer, x As Single, y As _ Single)
    If radCha And lineAch Then
        Picture1.Cls
        Picture1.Circle (cirX, cirY), cirR, vbGreen, , , Slider6.Value / 120
        cirH = Slider6.Value / 120
    End If
End Sub
'*************************************************************************

'*************************************************************************
Private Sub Slider6_MouseUp(Button As Integer, Shift As Integer, x As Single, y As Single)
    radCha = False
End Sub
'*************************************************************************
```

D.2 Module-mAVIDecs.bas

```
Option Explicit
' *************************************************************************

Public Declare Function mmioStringToFOURCC Lib "winmm.dll" Alias "mmioStringToFOURCCA" (ByVal sz As String,
ByVal uFlags As Long) As Long 'returns fourcc
Public Declare Function VideoForWindowsVersion Lib "msvfw32.dll" () As Long
Public Declare Sub AVIFileInit Lib "avifil32.dll" ()
Public Declare Function AVIFileOpen Lib "avifil32.dll" (ByRef ppfile As Long, ByVal szFile As String, ByVal uMode
As Long, ByVal pclsidHandler As Long) As Long   'HRESULT
Public Declare Function AVIFileInfo Lib "avifil32.dll" (ByVal pfile As Long, pfi As AVI_FILE_INFO, ByVal lSize As Long)
As Long 'HRESULT
Public Declare Function AVIFileCreateStream Lib "avifil32.dll" Alias "AVIFileCreateStreamA" _
                                        (ByVal pfile As Long, ByRef ppavi As Long, ByRef psi As
AVI_STREAM_INFO) As Long

Public Declare Function AVISaveOptions Lib "avifil32.dll" (ByVal hWnd As Long, _
                                                    ByVal uiFlags As Long, _
                                                    ByVal nStreams As Long, _
                                                    ByRef ppavi As Long, _
                                                    ByRef ppOptions As Long) As Long 'TRUE if
user pressed OK, False if cancel, or error if error
```

```
Public Declare Function AVISave Lib "avifil32.dll" Alias "AVISaveVA" (ByVal szFile As String, _
                                                                      ByVal pclsidHandler As
Long, _
                                                                      ByVal lpfnCallback As
Long, _
                                                                      ByVal nStreams As Long,
_
                                                                      ByRef ppaviStream As
Long, _
                                                                      ByRef ppCompOptions
As Long) As Long

Public Declare Function AVISaveOptionsFree Lib "avifil32.dll" (ByVal nStreams As Long, _
                                                               ByRef ppOptions As Long) As Long

Public Declare Function AVIMakeCompressedStream Lib "avifil32.dll" (ByRef ppsCompressed As Long, _
                                                                    ByVal psSource As Long, _
                                                                    ByRef lpOptions As
AVI_COMPRESS_OPTIONS, _
                                                                    ByVal pclsidHandler As Long) As
Long '

Public Declare Function AVIStreamSetFormat Lib "avifil32.dll" (ByVal pavi As Long, _
                                                               ByVal lPos As Long, _
                                                               ByRef lpFormat As Any, _
                                                               ByVal cbFormat As Long) As Long

Public Declare Function AVIStreamWrite Lib "avifil32.dll" (ByVal pavi As Long, _
                                                           ByVal lStart As Long, _
                                                           ByVal lSamples As Long, _
                                                           ByVal lpBuffer As Long, _
                                                           ByVal cbBuffer As Long, _
                                                           ByVal dwFlags As Long, _
                                                           ByRef plSampWritten As Long, _
                                                           ByRef plBytesWritten As Long) As Long
Public Declare Function AVIStreamReadFormat Lib "avifil32.dll" (ByVal pAVIStream As Long, _
                                                                ByVal lPos As Long, _
                                                                ByVal lpFormatBuf As Long, _
                                                                ByRef sizeBuf As Long) As Long

Public Declare Function AVIStreamRead Lib "avifil32.dll" (ByVal pAVIStream As Long, _
                                                          ByVal lStart As Long, _
                                                          ByVal lSamples As Long, _
                                                          ByVal lpBuffer As Long, _
```

```
                                                    ByVal cbBuffer As Long, _
                                                    ByRef pBytesWritten As Long, _
                                                    ByRef pSamplesWritten As Long) As
Long
Public Declare Function AVIStreamGetFrameOpen Lib "avifil32.dll" (ByVal pAVIStream As Long, _
                                                    ByRef bih As Any) As Long 'returns
pointer to GETFRAME object on success (or NULL on error)
Public Declare Function AVIStreamGetFrame Lib "avifil32.dll" (ByVal pGetFrameObj As Long, _
                                                    ByVal lPos As Long) As Long
'returns pointer to packed DIB on success (or NULL on error)
Public Declare Function AVIStreamGetFrameClose Lib "avifil32.dll" (ByVal pGetFrameObj As Long) As Long '
returns zero on success (error number) after calling this function the GETFRAME object pointer is invalid


Public Declare Function AVIFileGetStream Lib "avifil32.dll" (ByVal pfile As Long, ByRef ppaviStream As Long, ByVal
fccType As Long, ByVal lParam As Long) As Long
Public Declare Function AVIMakeFileFromStreams Lib "avifil32.dll" (ByRef ppfile As Long, ByVal nStreams As Long,
ByVal pAVIStreamArray As Long) As Long

Public Declare Function AVIStreamInfo Lib "avifil32.dll" (ByVal pAVIStream As Long, ByRef psi As
AVI_STREAM_INFO, ByVal lSize As Long) As Long
Public Declare Function AVIStreamStart Lib "avifil32.dll" (ByVal pavi As Long) As Long
Public Declare Function AVIStreamLength Lib "avifil32.dll" (ByVal pavi As Long) As Long
Public Declare Function AVIStreamRelease Lib "avifil32.dll" (ByVal pavi As Long) As Long 'ULONG
Public Declare Function AVIStreamClose Lib "avifil32.dll" Alias "AVIStreamRelease" (ByVal pavi As Long) As Long
'ULONG
Public Declare Function AVIFileRelease Lib "avifil32.dll" (ByVal pfile As Long) As Long
Public Declare Function AVIFileClose Lib "avifil32.dll" Alias "AVIFileRelease" (ByVal pfile As Long) As Long
Public Declare Sub AVIFileExit Lib "avifil32.dll" ()

'*****************************************************************************/
Public Declare Function AVIMakeStreamFromClipboard Lib "avifil32.dll" (ByVal cfFormat As Long, ByVal hGlobal
As Long, ByRef ppstream As Long) As Long
Public Declare Function AVIPutFileOnClipboard Lib "avifil32.dll" (ByVal pAVIFile As Long) As Long
Public Declare Function AVIGetFromClipboard Lib "avifil32.dll" (ByRef ppAVIFile As Long) As Long
Public Declare Function AVIClearClipboard Lib "avifil32.dll" () As Long

Private Const BMP_MAGIC_COOKIE As Integer = 19778 'this is equivalent to ascii string "BM"
Public Type BITMAPFILEHEADER '14 bytes
        bfType As Integer '"magic cookie" - must be "BM" (19778)
        bfSize As Long
        bfReserved1 As Integer
        bfReserved2 As Integer
        bfOffBits As Long
```

```
End Type
'//BITMAP DEFINES (from mmsystem.h)
Public Type BITMAPINFOHEADER '40 bytes
    biSize As Long
    biWidth As Long
    biHeight As Long
    biPlanes As Integer
    biBitCount As Integer
    biCompression As Long
    biSizeImage As Long
    biXPelsPerMeter As Long
    biYPelsPerMeter As Long
    biClrUsed As Long
    biClrImportant As Long
End Type

Public Type BITMAPINFOHEADER_MJPEG '68 bytes
    biSize As Long
    biWidth As Long
    biHeight As Long
    biPlanes As Integer
    biBitCount As Integer
    biCompression As Long
    biSizeImage As Long
    biXPelsPerMeter As Long
    biYPelsPerMeter As Long
    biClrUsed As Long
    biClrImportant As Long
    '/* extended BITMAPINFOHEADER fields */
    biExtDataOffset As Long
    '/* compression-specific fields */
    '/* these fields are defined for 'JPEG' and 'MJPG' */
    JPEGSize As Long
    JPEGProcess As Long
    '/* Process specific fields */
    JPEGColourSpaceID As Long
    JPEGBitsPerSample As Long
    JPEGHSubSampling As Long
    JPEGVSubSampling As Long
End Type

Public Type AVI_RECT
    left As Long
    top As Long
```

```
    right As Long
    bottom As Long
End Type

Public Type AVI_STREAM_INFO
    fccType As Long
    fccHandler As Long
    dwFlags As Long
    dwCaps As Long
    wPriority As Integer
    wLanguage As Integer
    dwScale As Long
    dwRate As Long
    dwStart As Long
    dwLength As Long
    dwInitialFrames As Long
    dwSuggestedBufferSize As Long
    dwQuality As Long
    dwSampleSize As Long
    rcFrame As AVI_RECT
    dwEditCount    As Long
    dwFormatChangeCount As Long
    szName As String * 64
End Type

'for use with AVIFIleInfo
Public Type AVI_FILE_INFO    '108 bytes?
    dwMaxBytesPerSecond As Long
    dwFlags As Long
    dwCaps As Long
    dwStreams As Long
    dwSuggestedBufferSize As Long
    dwWidth As Long
    dwHeight As Long
    dwScale As Long
    dwRate As Long
    dwLength As Long
    dwEditCount As Long
    szFileType As String * 64
End Type

Public Type AVI_COMPRESS_OPTIONS
    fccType As Long                '/* stream type, for consistency */
    fccHandler As Long             '/* compressor */
```

```
    dwKeyFrameEvery As Long      '/* keyframe rate */
    dwQuality As Long            '/* compress quality 0-10,000 */
    dwBytesPerSecond As Long     '/* bytes per second */
    dwFlags As Long              '/* flags... see below */
    lpFormat As Long             '/* save format */
    cbFormat As Long
    lpParms As Long              '/* compressor options */
    cbParms As Long
    dwInterleaveEvery As Long    '/* for non-video streams only */
End Type

Global Const AVIERR_OK As Long = 0&

Private Const SEVERITY_ERROR      As Long = &H80000000
Private Const FACILITY_ITF        As Long = &H40000
Private Const AVIERR_BASE         As Long = &H4000

Global Const AVIERR_BADFLAGS      As Long = SEVERITY_ERROR Or FACILITY_ITF Or (AVIERR_BASE + 105)
'-2147205015
Global Const AVIERR_BADPARAM      As Long = SEVERITY_ERROR Or FACILITY_ITF Or (AVIERR_BASE + 106)
'-2147205014
Global Const AVIERR_BADSIZE       As Long = SEVERITY_ERROR Or FACILITY_ITF Or (AVIERR_BASE + 107)
'-2147205013

Global Const AVIERR_USERABORT     As Long = SEVERITY_ERROR Or FACILITY_ITF Or (AVIERR_BASE + 198)
'-2147204922

'// Flags for dwFlags
Global Const AVIFILEINFO_HASINDEX           As Long = &H10
Global Const AVIFILEINFO_MUSTUSEINDEX       As Long = &H20
Global Const AVIFILEINFO_ISINTERLEAVED      As Long = &H100
Global Const AVIFILEINFO_WASCAPTUREFILE     As Long = &H10000
Global Const AVIFILEINFO_COPYRIGHTED        As Long = &H20000

'// Flags for dwCaps
Global Const AVIFILECAPS_CANREAD            As Long = &H1
Global Const AVIFILECAPS_CANWRITE           As Long = &H2
Global Const AVIFILECAPS_ALLKEYFRAMES       As Long = &H10
Global Const AVIFILECAPS_NOCOMPRESSION      As Long = &H20

Global Const AVICOMPRESSF_INTERLEAVE        As Long = &H1       '// interleave
Global Const AVICOMPRESSF_DATARATE          As Long = &H2       '// use a data rate
Global Const AVICOMPRESSF_KEYFRAMES         As Long = &H4       '// use keyframes
Global Const AVICOMPRESSF_VALID             As Long = &H8       '// has valid data?
```

```
Global Const OF_READ    As Long = &H0
Global Const OF_WRITE As Long = &H1

Global Const OF_SHARE_DENY_WRITE As Long = &H20
Global Const OF_CREATE As Long = &H1000

Global Const AVIIF_KEYFRAME    As Long = &H10

'/* DIB colour table identifiers */
Global Const DIB_RGB_COLOURS    As Long = 0       '/* colour table in RGBs */
Global Const DIB_PAL_COLOURS    As Long = 1       '/* colour table in palette indices */

'/* constants for the biCompression field */
Global Const BI_RGB              As Long = 0
Global Const BI_RLE8             As Long = 1
Global Const BI_RLE4             As Long = 2
Global Const BI_BITFIELDS        As Long = 3

'Stream types for use in VB (translated from C macros)
Global Const streamtypeVIDEO          As Long = 1935960438 'equivalent to: mmioStringToFOURCC("vids", 0&)
Global Const streamtypeAUDIO          As Long = 1935963489 'equivalent to: mmioStringToFOURCC("auds", 0&)
Global Const streamtypeMIDI           As Long = 1935960429 'equivalent to: mmioStringToFOURCC("mids", 0&)
Global Const streamtypeTEXT           As Long = 1937012852 'equivalent to: mmioStringToFOURCC("txts", 0&)

'// For GetFrame::SetFormat - use the best format for the display
Global Const AVIGETFRAMEF_BESTDISPLAYFMT    As Long = 1

'// defines for uiFlags (AVISaveOptions)
Global Const ICMF_CHOOSE_KEYFRAME             As Long = &H1      '// show KeyFrame Every box
Global Const ICMF_CHOOSE_DATARATE             As Long = &H2      '// show DataRate box
Global Const ICMF_CHOOSE_PREVIEW              As Long = &H4      '// allow expanded preview dialog
Global Const ICMF_CHOOSE_ALLCOMPRESSORS       As Long = &H8      '// don't only show those that
                                                                 '// can handle the input format
                                                                 '// or input data

' /****************************************************************************
' *
' *   'STANDARD WIN32 API DECLARES, UDTs and Constants
' *
' ****************************************************************************/
Private Declare Function SetRect Lib "user32.dll" _
    (ByRef lprc As AVI_RECT, ByVal xLeft As Long, ByVal yTop As Long, ByVal xRight As Long, ByVal yBottom As
Long) As Long 'BOOL
```

```
Private Declare Function GetProcessHeap Lib "kernel32.dll" () As Long 'handle
Private Declare Function HeapAlloc Lib "kernel32.dll" (ByVal hHeap As Long, ByVal dwFlags As Long, ByVal dwBytes As Long) As Long 'Pointer to mem
Private Declare Function HeapFree Lib "kernel32.dll" (ByVal hHeap As Long, ByVal dwFlags As Long, ByVal lpMem As Long) As Long 'BOOL
Private Declare Sub CopyMemory Lib "kernel32.dll" Alias "RtlMoveMemory" (ByRef dest As Any, ByRef src As Any, ByVal dwLen As Long)

Private Const HEAP_ZERO_MEMORY As Long = &H8

Global gfAbort As Boolean 'allows user to abort an AVI Save operation (see Callback function below)

Public Function AVISaveCallback(ByVal nPercent As Long) As Long 'should return C BOOL

End Function

' /**************************************************************************
' *
' *   'UTILITY FUNCTIONS FOR WORKING WITH AVI FILES
' *
' **************************************************************************/
Public Sub DebugPrintAVIStreamInfo(asi As AVI_STREAM_INFO)
Debug.Print ""
Debug.Print "**** AVI_STREAM_INFO (START) ****"
  With asi
      Debug.Print "fccType = " & .fccType
      Debug.Print "fccHandler = " & .fccHandler
      Debug.Print "dwFlags = " & .dwFlags
      Debug.Print "dwCaps = " & .dwCaps
      Debug.Print "wPriority = " & .wPriority
      Debug.Print "wLanguage = " & .wLanguage
      Debug.Print "dwScale = " & .dwScale
      Debug.Print "dwRate = " & .dwRate
      Debug.Print "dwStart = " & .dwStart
      Debug.Print "dwLength = " & .dwLength
      Debug.Print "dwInitialFrames = " & .dwInitialFrames
      Debug.Print "dwSuggestedBufferSize = " & .dwSuggestedBufferSize
      Debug.Print "dwQuality = " & .dwQuality
      Debug.Print "dwSampleSize = " & .dwSampleSize
      Debug.Print "rcFrame.left = " & .rcFrame.left
      Debug.Print "rcFrame.top = " & .rcFrame.top
      Debug.Print "rcFrame.right = " & .rcFrame.right
      Debug.Print "rcFrame.bottom = " & .rcFrame.bottom
      Debug.Print "dwEditCount = " & .dwEditCount
```

```
    Debug.Print "dwFormatChangeCount = " & .dwFormatChangeCount
    Debug.Print "szName = " & .szName
  End With
  Debug.Print "**** AVI_STREAM_INFO (END) ****"
  Debug.Print ""
End Sub

Public Sub DebugPrintAVIFileInfo(afi As AVI_FILE_INFO)
Debug.Print "**** AVI_FILE_INFO (START) ****"
  With afi
    Debug.Print "dwMaxBytesPerSecond = " & .dwMaxBytesPerSecond
    Debug.Print "dwFlags = " & .dwFlags
    Debug.Print "dwCaps = " & .dwCaps
    Debug.Print "dwStreams = " & .dwStreams
    Debug.Print "dwSuggestedBufferSize = " & .dwSuggestedBufferSize
    Debug.Print "dwWidth = " & .dwWidth
    Debug.Print "dwHeight = " & .dwHeight
    Debug.Print "dwScale = " & .dwScale
    Debug.Print "dwRate = " & .dwRate
    Debug.Print "dwLength = " & .dwLength
    Debug.Print "dwEditCount = " & .dwEditCount
    Debug.Print "szFileType = " & .szFileType
  End With
  Debug.Print "**** AVI_FILE_INFO (END) ****"
  Debug.Print ""
End Sub
```

D.3 Class Module-cDIB.cls

```
Option Explicit

Private Const BMP_MAGIC_COOKIE As Integer = 19778 'this is equivalent to ascii string "BM"
'//BITMAP DEFINES (from mmsystem.h)
Private Type BITMAPFILEHEADER '14 bytes
        bfType As Integer '"magic cookie" - must be "BM"
        bfSize As Long
        bfReserved1 As Integer
        bfReserved2 As Integer
        bfOffBits As Long
End Type

Private Type BITMAPINFOHEADER '40 bytes
    biSize As Long
```

```
    biWidth As Long
    biHeight As Long
    biPlanes As Integer
    biBitCount As Integer
    biCompression As Long
    biSizeImage As Long
    biXPelsPerMeter As Long
    biYPelsPerMeter As Long
    biClrUsed As Long
    biClrImportant As Long
End Type

Private Type RGBQUAD
    Red As Byte
    Green As Byte
    Blue As Byte
    Reserved As Byte
End Type

Private Type BITMAP
    bmType As Long
    bmWidth As Long
    bmHeight As Long
    bmWidthBytes As Long
    bmPlanes As Integer
    bmBitsPixel As Integer
    bmBits As Long
End Type

'/* constants for the biCompression field */
Private Const BI_RGB    As Long = 0&

Private Declare Function GetProcessHeap Lib "kernel32.dll" () As Long 'handle
Private Declare Function HeapAlloc Lib "kernel32.dll" (ByVal hHeap As Long, ByVal dwFlags As Long, ByVal
dwBytes As Long) As Long 'Pointer to mem
Private Declare Function HeapFree Lib "kernel32.dll" (ByVal hHeap As Long, ByVal dwFlags As Long, ByVal lpMem
As Long) As Long 'BOOL
Private Declare Sub CopyMemory Lib "kernel32.dll" Alias "RtlMoveMemory" (ByRef dest As Any, ByRef src As Any,
ByVal dwLen As Long)

Private Const HEAP_ZERO_MEMORY As Long = &H8

Private m_memBits() As Byte
Private m_memBitmapInfo() As Byte
```

```
Private m_bih As BITMAPINFOHEADER
Private m_bfh As BITMAPFILEHEADER


Public Function CreateFromFile(ByVal filename As String) As Boolean
    Dim hFile As Long

    If Not ExistFile(filename) Then
        MsgBox "File does not exist:" & vbCrLf & filename, vbCritical, App.title
        Exit Function
    End If

    hFile = FreeFile()

    '<====ERROR TRAP ON
    On Error Resume Next
    Open filename For Binary Access Read As #hFile
    If Err Then
        If Err.Number = 70 Then
            MsgBox "File is locked - cannot access:" & vbCrLf & filename, vbCritical, App.title
        Else
            MsgBox Err.Description, vbInformation, App.title
        End If
        Exit Function 'assume file was not opened
    End If
    On Error GoTo 0
    '====>ERROR TRAP OFF

    'OK, file is opened - now for the real algorithm...
    Get #hFile, , m_bfh 'get the BITMAPFILEHEADER this identifies the bitmap

    If m_bfh.bfType <> BMP_MAGIC_COOKIE Then 'this is not a BMP file
        MsgBox "File is not a supported bitmap format:" & vbCrLf & filename, vbInformation, App.title
        Close #hFile
        Exit Function
    Else
        'now get the info header
        Get #hFile, Len(m_bfh) + 1, m_bih 'start at the 15th byte

        'now get the bitmap bits
        ReDim m_memBits(0 To m_bih.biSizeImage - 1)
        Get #hFile, m_bfh.bfOffBits + 1, m_memBits

        'and BitmapInfo variable-length UDT
```

```
        ReDim m_memBitmapInfo(0 To m_bfh.bfOffBits - 14) 'don't need first 14 bytes (fileinfo)
        Get #hFile, Len(m_bfh) + 1, m_memBitmapInfo

        Close #hFile    'Close file
    End If

    CreateFromFile = True 'indicate success

End Function

Public Function CreateFromPackedDIBPointer(ByRef pDIB As Long) As Boolean
Debug.Assert pDIB <> 0
'Creates a full-colour (no palette) DIB from a pointer to a full-colour memory DIB

'get the BitmapInfoHeader
Call CopyMemory(ByVal VarPtr(m_bih.biSize), ByVal pDIB, Len(m_bih))
If m_bih.biBitCount < 16 Then
    Debug.Print "Error! DIB was less than 16 colours."
    Exit Function 'only supports high-colour or full-colour dibs
End If

'now get the bitmap bits
If m_bih.biSizeImage < 1 Then Exit Function 'return False
ReDim m_memBits(0 To m_bih.biSizeImage - 1)
Call CopyMemory(m_memBits(0), ByVal pDIB + 40, m_bih.biSizeImage)

'and BitmapInfo variable-length UDT
ReDim m_memBitmapInfo(0 To 39) 'don't need first 14 bytes (fileinfo)
Call CopyMemory(m_memBitmapInfo(0), m_bih, Len(m_bih))

'create a file header
With m_bfh
    .bfType = BMP_MAGIC_COOKIE
    .bfSize = 55 + m_bih.biSizeImage 'size of file as written to disk
    .bfReserved1 = 0&
    .bfReserved2 = 0&
    .bfOffBits = 54 'BitmapInfoHeader + BitmapFileHeader
End With

'and return True
CreateFromPackedDIBPointer = True

End Function
```

```
Public Function WriteToFile(ByVal filename As String) As Boolean
Dim hFile As Integer
On Error Resume Next
hFile = FreeFile()
Open filename For Binary As hFile
    Put hFile, 1, m_bfh
    Put hFile, Len(m_bfh) + 1, m_memBitmapInfo
    Put hFile, , m_memBits
Close hFile
WriteToFile = True
End Function

Private Function ExistFile(ByVal sSpec As String) As Boolean
    On Error Resume Next
    Call FileLen(sSpec)
    ExistFile = (Err = 0)
End Function

Public Property Get BitCount() As Long
    BitCount = m_bih.biBitCount

End Property

Public Property Get Height() As Long
    Height = m_bih.biHeight
End Property

Public Property Get Width() As Long
    Width = m_bih.biWidth
End Property

Public Property Get Compression() As Long
    Compression = m_bih.biCompression
End Property

Public Property Get SizeInfoHeader() As Long
    SizeInfoHeader = m_bih.biSize
End Property

Public Property Get SizeImage() As Long
    SizeImage = m_bih.biSizeImage
End Property

Public Property Get Planes() As Long
```

```
    Planes = m_bih.biPlanes
End Property

Public Property Get ClrImportant() As Long
    ClrImportant = m_bih.biClrImportant
End Property

Public Property Get ClrUsed() As Long
    ClrUsed = m_bih.biClrUsed
End Property

Public Property Get XPPM() As Long
    XPPM = m_bih.biXPelsPerMeter
End Property

Public Property Get YPPM() As Long
    YPPM = m_bih.biYPelsPerMeter
End Property

Public Property Get FileType() As Long
    FileType = m_bfh.bfType
End Property

Public Property Get SizeFileHeader() As Long
    SizeFileHeader = m_bfh.bfSize
End Property

Public Property Get BitOffset() As Long
    BitOffset = m_bfh.bfOffBits
End Property

Public Property Get PointerToBits() As Long
    PointerToBits = VarPtr(m_memBits(0))
End Property

Public Property Get PointerToBitmapInfo() As Long
    PointerToBitmapInfo = VarPtr(m_memBitmapInfo(0))
End Property

Public Property Get SizeBitmapInfo() As Long
    SizeBitmapInfo = UBound(m_memBitmapInfo()) + 1
End Property
```

D.4 Class Module-cFileDlg.cls

```
Option Explicit

Private Const MAX_PATH = 1024
Private Const MAX_FILE = 512

    'Windows desktop virtual folder at the root of the name space
    vbCSIDL_DESKTOP = &H0&      'File system directory that contains the
'user's program groups (which are also file      'system directories)
    vbCSIDL_PROGRAMS = &H2&
'Control Panel - virtual folder containing
'icons for the control panel applications
    vbCSIDL_CONTROLS = &H3&
'Printers folder - virtual folder containing        'installed printers.
    vbCSIDL_PRINTERS = &H4&      'File system directory that serves as a
'common repository for documents (My Documents folder)
    vbCSIDL_PERSONAL = &H5&
'File system directory that contains the
'user's favorite Internet Explorer URLs
    vbCSIDL_FAVORITES = &H6&
'File system directory that corresponds to the
'user's Startup program group
    vbCSIDL_STARTUP = &H7&
'File system directory that contains the
'user's most recently used documents (Recent folder)
    vbCSIDL_RECENT = &H8&      'File system directory that contains
'Send To menu items        Public Const
    vbCSIDL_SENDTO = &H9&
'Recycle bin file system directory containing file
'objects in the user's recycle bin. The location of
'this directory is not in the registry; it is marked
'with the hidden and system attributes to prevent the
'user from moving or deleting it.
    vbCSIDL_BITBUCKET = &HA&
'File system directory containing Start menu items
    vbCSIDL_STARTMENU = &HB&
'File system directory used to physically store
'file objects on the desktop (not to be confused
'with the desktop folder itself).
    vbCSIDL_DESKTOPDIRECTORY = &H10&
'My Computer - virtual folder containing everything
'on the local computer: storage devices, printers,
'and Control Panel. The folder may also contain      'mapped network drives.
```

```
    vbCSIDL_DRIVES = &H11&
   'Network Neighborhood - virtual folder representing
   'the top level of the network hierarchy
    vbCSIDL_NETWORK = &H12&
   'File system directory containing objects that
   'appear in the network neighborhood
    vbCSIDL_NETHOOD = &H13&
   'Virtual folder containing fonts
    vbCSIDL_FONTS = &H14&
   'File system directory that serves as a
   'common repository for document templates      '(ShellNew folder.)
    vbCSIDL_TEMPLATES = &H15&
End Enum
Private Declare Function SHGetSpecialFolderLocation Lib "shell32.dll" _
                                                    (ByVal hWndOwner As Long, _
                                                    ByVal nFolder As SPECIAL_FOLDERS, _
                                                    pidl As Long) As Long 'returns NOERROR on success

'Converts an item identifier list to a file system path.
Private Declare Function SHGetPathFromIDList Lib "shell32.dll" _
   Alias "SHGetPathFromIDListA" _
  (ByVal pidl As Long, _
   ByVal pszPath As String) As Long

Private Declare Sub CoTaskMemFree Lib "ole32.dll" (ByVal pv As Long)

Private Const NOERROR As Long = &H0

Private Type OPENFILENAME
    lStructSize As Long          ' Filled with UDT size
    hWndOwner As Long            ' Tied to Owner
    hInstance As Long            ' Ignored (used only by templates)
    lpstrFilter As String        ' Tied to Filter
    lpstrCustomFilter As String  ' Ignored (exercise for reader)
    nMaxCustFilter As Long       ' Ignored (exercise for reader)
    nFilterIndex As Long         ' Tied to FilterIndex
    lpstrFile As String          ' Tied to FileName
    nMaxFile As Long             ' Handled internally
    lpstrFileTitle As String     ' Tied to FileTitle
    nMaxFileTitle As Long        ' Handled internally
    lpstrInitialDir As String    ' Tied to InitDir
    lpstrTitle As String         ' Tied to DlgTitle
    Flags As Long                ' Tied to Flags
    nFileOffset As Integer       ' Ignored (exercise for reader)
```

```
    nFileExtension As Integer      ' Ignored (exercise for reader)
    lpstrDefExt As String          ' Tied to DefaultExt
    lCustData As Long                ' Ignored (needed for hooks)
    lpfnHook As Long                 ' Ignored (good luck with hooks)
    lpTemplateName As Long           ' Ignored (good luck with templates)
End Type

Private Declare Function GetOpenFileName Lib "COMDLG32" _
    Alias "GetOpenFileNameA" (filestruct As OPENFILENAME) As Long
Private Declare Function GetSaveFileName Lib "COMDLG32" _
    Alias "GetSaveFileNameA" (filestruct As OPENFILENAME) As Long
Private Declare Function GetFileTitle Lib "COMDLG32" _
    Alias "GetFileTitleA" (ByVal szFile As String, _
    ByVal szTitle As String, ByVal cbBuf As Integer) As Integer
'VFW "customized" File Dialogs
Private Declare Function GetOpenFileNamePreview Lib "MSVFW32" _
    Alias "GetOpenFileNamePreviewA" (filestruct As OPENFILENAME) As Long
Private Declare Function GetSaveFileNamePreview Lib "MSVFW32" _
    Alias "GetSaveFileNamePreviewA" (filestruct As OPENFILENAME) As Long

Public Enum EOpenFile
    OFN_READONLY = &H1&
    OFN_OVERWRITEPROMPT = &H2&
    OFN_HIDEREADONLY = &H4&
    OFN_NOCHANGEDIR = &H8&
    OFN_SHOWHELP = &H10&
    OFN_ENABLEHOOK = &H20&
    OFN_ENABLETEMPLATE = &H40&
    OFN_ENABLETEMPLATEHANDLE = &H80&
    OFN_NOVALIDATE = &H100&
    OFN_ALLOWMULTISELECT = &H200&
    OFN_EXTENSIONDIFFERENT = &H400&
    OFN_PATHMUSTEXIST = &H800&
    OFN_FILEMUSTEXIST = &H1000&
    OFN_CREATEPROMPT = &H2000&
    OFN_SHAREAWARE = &H4000&
    OFN_NOREADONLYRETURN = &H8000&
    OFN_NOTESTFILECREATE = &H10000
    OFN_NONETWORKBUTTON = &H20000
    OFN_NOLONGNAMES = &H40000
    OFN_EXPLORER = &H80000
    OFN_NODEREFERENCELINKS = &H100000
    OFN_LONGNAMES = &H200000
End Enum
```

```
Private Declare Function CommDlgExtendedError Lib "COMDLG32" () As Long

Public Enum EDialogError
    CDERR_DIALOGFAILURE = &HFFFF&

    CDERR_GENERALCODES = &H0&
    CDERR_STRUCTSIZE = &H1&
    CDERR_INITIALIZATION = &H2&
    CDERR_NOTEMPLATE = &H3&
    CDERR_NOHINSTANCE = &H4&
    CDERR_LOADSTRFAILURE = &H5&
    CDERR_FINDRESFAILURE = &H6&
    CDERR_LOADRESFAILURE = &H7&
    CDERR_LOCKRESFAILURE = &H8&
    CDERR_MEMALLOCFAILURE = &H9&
    CDERR_MEMLOCKFAILURE = &HA&
    CDERR_NOHOOK = &HB&
    CDERR_REGISTERMSGFAIL = &HC&

    PDERR_PRINTERCODES = &H1000&
    PDERR_SETUPFAILURE = &H1001&
    PDERR_PARSEFAILURE = &H1002&
    PDERR_RETDEFFAILURE = &H1003&
    PDERR_LOADDRVFAILURE = &H1004&
    PDERR_GETDEVMODEFAIL = &H1005&
    PDERR_INITFAILURE = &H1006&
    PDERR_NODEVICES = &H1007&
    PDERR_NODEFAULTPRN = &H1008&
    PDERR_DNDMMISMATCH = &H1009&
    PDERR_CREATEICFAILURE = &H100A&
    PDERR_PRINTERNOTFOUND = &H100B&
    PDERR_DEFAULTDIFFERENT = &H100C&

    CFERR_CHOOSEFONTCODES = &H2000&
    CFERR_NOFONTS = &H2001&
    CFERR_MAXLESSTHANMIN = &H2002&

    FNERR_FILENAMECODES = &H3000&
    FNERR_SUBCLASSFAILURE = &H3001&
    FNERR_INVALIDFILENAME = &H3002&
    FNERR_BUFFERTOOSMALL = &H3003&

    CCERR_CHOOSECOLOURCODES = &H5000&
```

```
End Enum



Private Const sEmpty As String = ""

'Class member variables
Private m_FileMustExist As Boolean
Private m_MultiSelect As Boolean
Private m_ReadOnly As Boolean 'read only
Private m_HideReadOnly As Boolean
Private m_Filter As String
Private m_FilterIndex As Long
Private m_InitDir As String
Private m_DlgTitle As String
Private m_DefaultExt As String
Private m_Flags As Long
Private m_OverwritePrompt As Boolean
Private m_hWnd As Long

Private Sub Class_Initialize()
'Initialize default values
m_hWnd = -1&
m_FileMustExist = True
m_MultiSelect = False
m_HideReadOnly = True
m_DlgTitle = App.title
m_OverwritePrompt = True
m_InitDir = GetSpecialFolderLocation(vbCSIDL_PERSONAL) 'default to My Documents folder

End Sub

Property Get OwnerHwnd() As Long
    OwnerHwnd = m_hWnd
End Property
Property Let OwnerHwnd(ByVal vHwnd As Long)
    m_hWnd = vHwnd
End Property

Property Get FileMustExist() As Boolean
    FileMustExist = m_FileMustExist
End Property
Property Let FileMustExist(ByVal vNewValue As Boolean)
    m_FileMustExist = vNewValue
```

```
End Property

Property Get MultiSelect() As Boolean
    MultiSelect = m_MultiSelect
End Property
Property Let MultiSelect(ByVal vNewValue As Boolean)
    m_MultiSelect = vNewValue
End Property

Property Get ReadOnly() As Boolean
    ReadOnly = m_ReadOnly
End Property

Property Get HideReadOnly() As Boolean
    HideReadOnly = m_HideReadOnly
End Property
Property Let HideReadOnly(ByVal vNewValue As Boolean)
    m_HideReadOnly = vNewValue
End Property

Property Get Filter() As String
    Filter = m_Filter
End Property
Property Let Filter(ByVal vFilterString As String)
    m_Filter = vFilterString
End Property

Property Get FilterIndex() As Long
    FilterIndex = m_FilterIndex
End Property
Property Let FilterIndex(ByVal vIndex As Long)
    m_FilterIndex = vIndex
End Property

Property Get InitDirectory() As String
    InitDirectory = m_InitDir
End Property
Property Let InitDirectory(ByVal DirPath As String)
    m_InitDir = DirPath
End Property

Property Let InitDirectorySpecial(ByVal SpecialDirectory As SPECIAL_FOLDERS)
    m_InitDir = GetSpecialFolderLocation(SpecialDirectory)
End Property
```

```
Property Get DlgTitle() As String
    DlgTitle = m_DlgTitle
End Property
Property Let DlgTitle(ByVal title As String)
    m_DlgTitle = title
End Property

Property Get DefaultExt() As String
    DefaultExt = m_DefaultExt
End Property
Property Let DefaultExt(ByVal fileExt As String)
    m_DefaultExt = fileExt
End Property

Property Get Flags() As EOpenFile
    Flags = m_Flags
End Property
Property Let Flags(ByVal vFlags As EOpenFile)
    m_Flags = vFlags
End Property

Property Get OverwritePrompt() As Boolean
    OverwritePrompt = m_OverwritePrompt
End Property
Property Let OverwritePrompt(ByVal vShowPrompt As Boolean)
    m_OverwritePrompt = vShowPrompt
End Property

Public Function VBGetOpenFileName(filename As String, _
                                  Optional FileTitle As String) As Boolean

    Dim opfile As OPENFILENAME
    Dim s As String
    Dim afFlags As Long
    Dim ch As String
    Dim i As Integer

With opfile
    .lStructSize = Len(opfile)

    ' Add in specific flags and strip out non-VB flags
    .Flags = (-m_FileMustExist * OFN_FILEMUSTEXIST) Or _
             (-m_MultiSelect * OFN_ALLOWMULTISELECT) Or _
```

```
            (-m_ReadOnly * OFN_READONLY) Or _
            (-m_HideReadOnly * OFN_HIDEREADONLY) Or _
            (m_Flags And CLng(Not (OFN_ENABLEHOOK Or _
                                   OFN_ENABLETEMPLATE)))
' Owner can take handle of owning window
If m_hWnd <> -1 Then .hWndOwner = m_hWnd
' InitDir can take initial directory string
.lpstrInitialDir = m_InitDir
' DefaultExt can take default extension
.lpstrDefExt = m_DefaultExt
' DlgTitle can take dialog box title
.lpstrTitle = m_DlgTitle

' To make Windows-style filter, replace | and : with nulls
For i = 1 To Len(Filter)
    ch = Mid$(Filter, i, 1)
    If ch = "|" Or ch = ":" Then
        s = s & vbNullChar
    Else
        s = s & ch
    End If
Next
' Put double null at end
s = s & vbNullChar & vbNullChar
.lpstrFilter = s
.nFilterIndex = m_FilterIndex

' Pad file and file title buffers to maximum path
s = filename & String$(MAX_PATH - Len(filename), 0)
.lpstrFile = s
.nMaxFile = MAX_PATH
s = FileTitle & String$(MAX_FILE - Len(FileTitle), 0)
.lpstrFileTitle = s
.nMaxFileTitle = MAX_FILE
' All other fields set to zero

If GetOpenFileName(opfile) Then
    VBGetOpenFileName = True
    filename = left$(.lpstrFile, InStr(.lpstrFile, vbNullChar) - 1)
    FileTitle = left$(.lpstrFileTitle, InStr(.lpstrFileTitle, vbNullChar) - 1)
    m_Flags = .Flags
    ' Return the filter index
    m_FilterIndex = .nFilterIndex
    ' Look up the filter the user selected and return that
```

```
        m_Filter = FilterLookup(.lpstrFilter, m_FilterIndex)
        If (.Flags And OFN_READONLY) Then m_ReadOnly = True
        'save directory as init directory for user
        m_InitDir = .lpstrFile
    Else
        VBGetOpenFileName = False
        filename = vbNullChar
        FileTitle = vbNullChar
        Flags = 0
        FilterIndex = -1
        Filter = vbNullChar
    End If
End With
End Function


Public Function VBGetOpenFileNamePreview(filename As String, _
                                Optional FileTitle As String) As Boolean

    Dim opfile As OPENFILENAME
    Dim s As String
    Dim afFlags As Long
    Dim ch As String
    Dim i As Integer

With opfile
    .lStructSize = Len(opfile)

    ' Add in specific flags and strip out non-VB flags
    .Flags = (-m_FileMustExist * OFN_FILEMUSTEXIST) Or _
             (-m_MultiSelect * OFN_ALLOWMULTISELECT) Or _
             (-m_ReadOnly * OFN_READONLY) Or _
             (-m_HideReadOnly * OFN_HIDEREADONLY) Or _
             (m_Flags And CLng(Not (OFN_ENABLEHOOK Or _
                                    OFN_ENABLETEMPLATE)))
    ' Owner can take handle of owning window
    If m_hWnd <> -1 Then .hWndOwner = m_hWnd
    ' InitDir can take initial directory string
    .lpstrInitialDir = m_InitDir
    ' DefaultExt can take default extension
    .lpstrDefExt = m_DefaultExt
    ' DlgTitle can take dialog box title
    .lpstrTitle = m_DlgTitle
```

```
    ' To make Windows-style filter, replace | and : with nulls
    For i = 1 To Len(Filter)
        ch = Mid$(Filter, i, 1)
        If ch = "|" Or ch = ":" Then
            s = s & vbNullChar
        Else
            s = s & ch
        End If
    Next
    ' Put double null at end
    s = s & vbNullChar & vbNullChar
    .lpstrFilter = s
    .nFilterIndex = m_FilterIndex

    ' Pad file and file title buffers to maximum path
    s = filename & String$(MAX_PATH - Len(filename), 0)
    .lpstrFile = s
    .nMaxFile = MAX_PATH
    s = FileTitle & String$(MAX_FILE - Len(FileTitle), 0)
    .lpstrFileTitle = s
    .nMaxFileTitle = MAX_FILE
    ' All other fields set to zero

    If GetOpenFileNamePreview(opfile) Then
        VBGetOpenFileNamePreview = True
        filename = left$(.lpstrFile, InStr(.lpstrFile, vbNullChar) - 1)
        FileTitle = left$(.lpstrFileTitle, InStr(.lpstrFileTitle, vbNullChar) - 1)
        m_Flags = .Flags
        ' Return the filter index
        m_FilterIndex = .nFilterIndex
        ' Look up the filter the user selected and return that
        m_Filter = FilterLookup(.lpstrFilter, m_FilterIndex)
        If (.Flags And OFN_READONLY) Then m_ReadOnly = True
        'save directory as init directory for user
        m_InitDir = .lpstrFile
    Else
        VBGetOpenFileNamePreview = False
        filename = vbNullChar
        FileTitle = vbNullChar
        Flags = 0
        FilterIndex = -1
        Filter = vbNullChar
    End If
End With
```

```
End Function

Public Function VBGetSaveFileName(filename As String, _
                                  Optional FileTitle As String) As Boolean

    Dim opfile As OPENFILENAME, s As String
With opfile
    .lStructSize = Len(opfile)

    ' Add in specific flags and strip out non-VB flags
    .Flags = (-m_OverwritePrompt * OFN_OVERWRITEPROMPT) Or _
             OFN_HIDEREADONLY Or _
             (m_Flags And CLng(Not (OFN_ENABLEHOOK Or _
                                    OFN_ENABLETEMPLATE)))
    ' Owner can take handle of owning window
    If m_hWnd <> -1 Then .hWndOwner = m_hWnd
    ' InitDir can take initial directory string
    .lpstrInitialDir = m_InitDir
    ' DefaultExt can take default extension
    .lpstrDefExt = m_DefaultExt
    ' DlgTitle can take dialog box title
    .lpstrTitle = m_DlgTitle

    ' Make new filter with bars (|) replacing nulls and double null at end
    Dim ch As String, i As Integer
    For i = 1 To Len(Filter)
        ch = Mid$(Filter, i, 1)
        If ch = "|" Or ch = ":" Then
            s = s & vbNullChar
        Else
            s = s & ch
        End If
    Next
    ' Put double null at end
    s = s & vbNullChar & vbNullChar
    .lpstrFilter = s
    .nFilterIndex = m_FilterIndex

    ' Pad file and file title buffers to maximum path
    s = filename & String$(MAX_PATH - Len(filename), 0)
    .lpstrFile = s
    .nMaxFile = MAX_PATH
    s = FileTitle & String$(MAX_FILE - Len(FileTitle), 0)
    .lpstrFileTitle = s
```

```
    .nMaxFileTitle = MAX_FILE
    ' All other fields zero

    If GetSaveFileName(opfile) Then
        VBGetSaveFileName = True
        filename = left$(.lpstrFile, InStr(.lpstrFile, vbNullChar) - 1)
        FileTitle = left$(.lpstrFileTitle, InStr(.lpstrFileTitle, vbNullChar) - 1)
        m_Flags = .Flags
        ' Return the filter index
        m_FilterIndex = .nFilterIndex
        ' Look up the filter the user selected and return that
        m_Filter = FilterLookup(.lpstrFilter, FilterIndex)
        'save directory as init directory for user
        m_InitDir = .lpstrFile
    Else
        VBGetSaveFileName = False
        filename = vbNullChar
        FileTitle = vbNullChar
        m_Flags = 0
        m_FilterIndex = 0
        m_Filter = vbNullChar
    End If
End With
End Function

Private Function FilterLookup(ByVal sFilters As String, ByVal iCur As Long) As String
    Dim iStart As Long
    Dim iEnd As Long
    Dim s As String

    iStart = 1
    If sFilters = vbNullChar Then Exit Function
    Do
        ' Cut out both parts marked by null character
        iEnd = InStr(iStart, sFilters, vbNullChar)
        If iEnd = 0 Then Exit Function
        iEnd = InStr(iEnd + 1, sFilters, vbNullChar)
        If iEnd Then
            s = Mid$(sFilters, iStart, iEnd - iStart)
        Else
            s = Mid$(sFilters, iStart)
        End If
        iStart = iEnd + 1
        If iCur = 1 Then
```

```
                FilterLookup = s
                Exit Function
            End If
            iCur = iCur - 1
        Loop While iCur
End Function

Private Function StrZToStr(s As String) As String
    Dim TempString As String

    TempString = left$(s, InStr(s, vbNullChar) - 1)
    If TempString = "" Then
        'if VB string is accidently passed in there will be no NULL
        'so just pass back the original string in that case
        StrZToStr = s
    Else
        StrZToStr = TempString
    End If
End Function

'This fuction is courtesy of Randy Birch and VBNet <www.mvps.org/vbnet>
'however I changed it a bit to fit my class
Private Function GetSpecialFolderLocation(CSIDL As SPECIAL_FOLDERS) As String

    Dim sPath As String
    Dim pidl As Long

  'fill the idl structure with the specified folder item
    If SHGetSpecialFolderLocation(m_hWnd, CSIDL, pidl) = NOERROR Then

      'if the pidl is returned, initialize
      'and get the path from the id list
       sPath = Space$(MAX_PATH)

       If SHGetPathFromIDList(ByVal pidl, ByVal sPath) Then

          'free the pidl and return the path
           Call CoTaskMemFree(ByVal VarPtr(pidl))
           GetSpecialFolderLocation = left(sPath, InStr(sPath, Chr$(0)) - 1)

       End If

    End If
```

```
End Function

' Test file existence with error trapping
Public Function ExistFile(ByVal sSpec As String) As Boolean
    On Error Resume Next
    Call FileLen(sSpec)
    ExistFile = (Err = 0)
End Function

'Get FileTitle (filename without path) from any full path
Public Function VBGetFileTitle(sFile As String) As String
    Dim sFileTitle As String, cFileTitle As Integer

    cFileTitle = MAX_PATH
    sFileTitle = String$(MAX_PATH, 0)
    cFileTitle = GetFileTitle(sFile, sFileTitle, MAX_PATH)
    If cFileTitle Then
        VBGetFileTitle = ""
    Else
        VBGetFileTitle = left$(sFileTitle, InStr(sFileTitle, vbNullChar) - 1)
    End If

End Function
```

Appendix E-Slices in Cases

E.1 Radial blood vessels in an application case

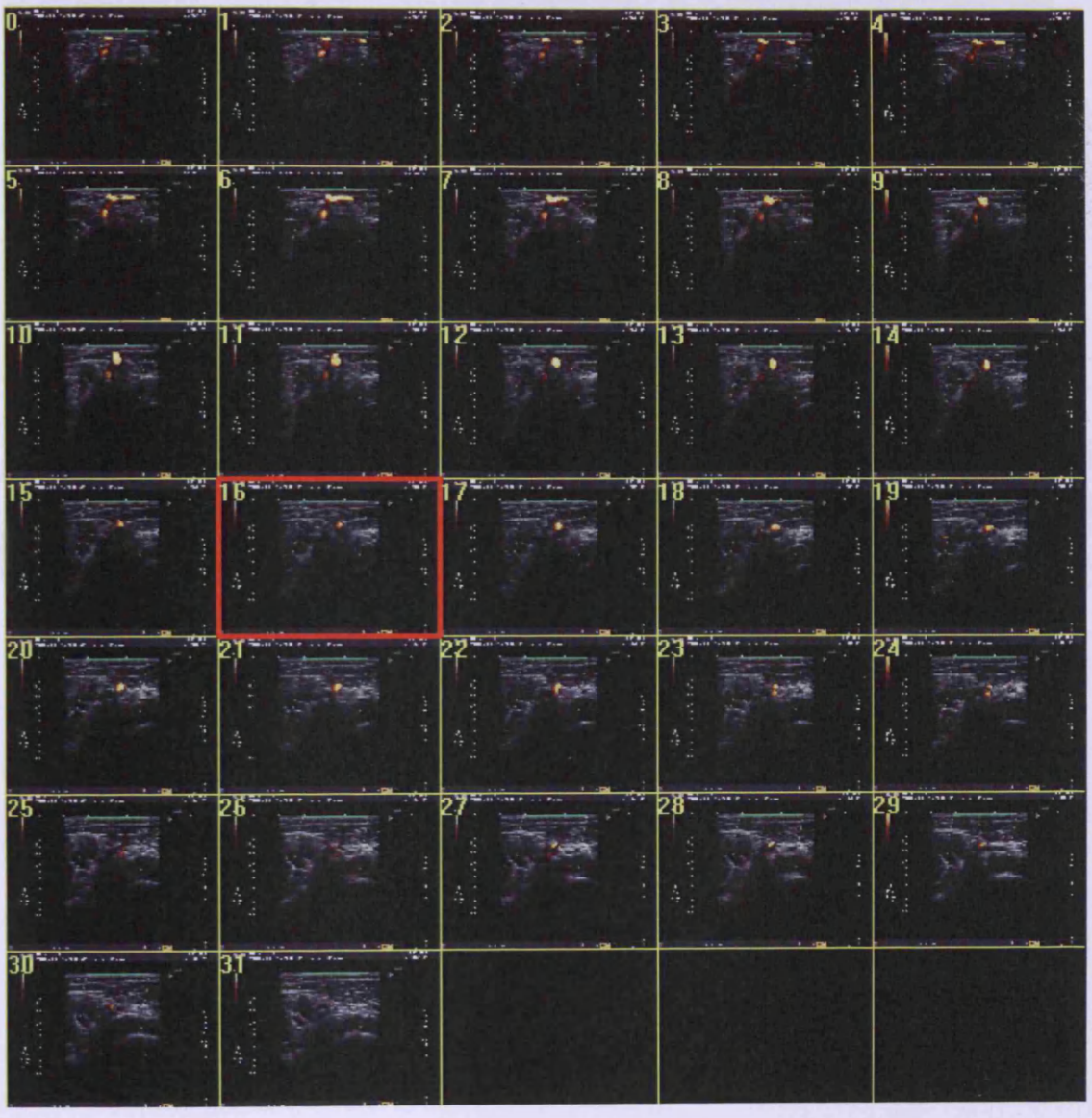

E.2 Achilles tendon of a professional athlete

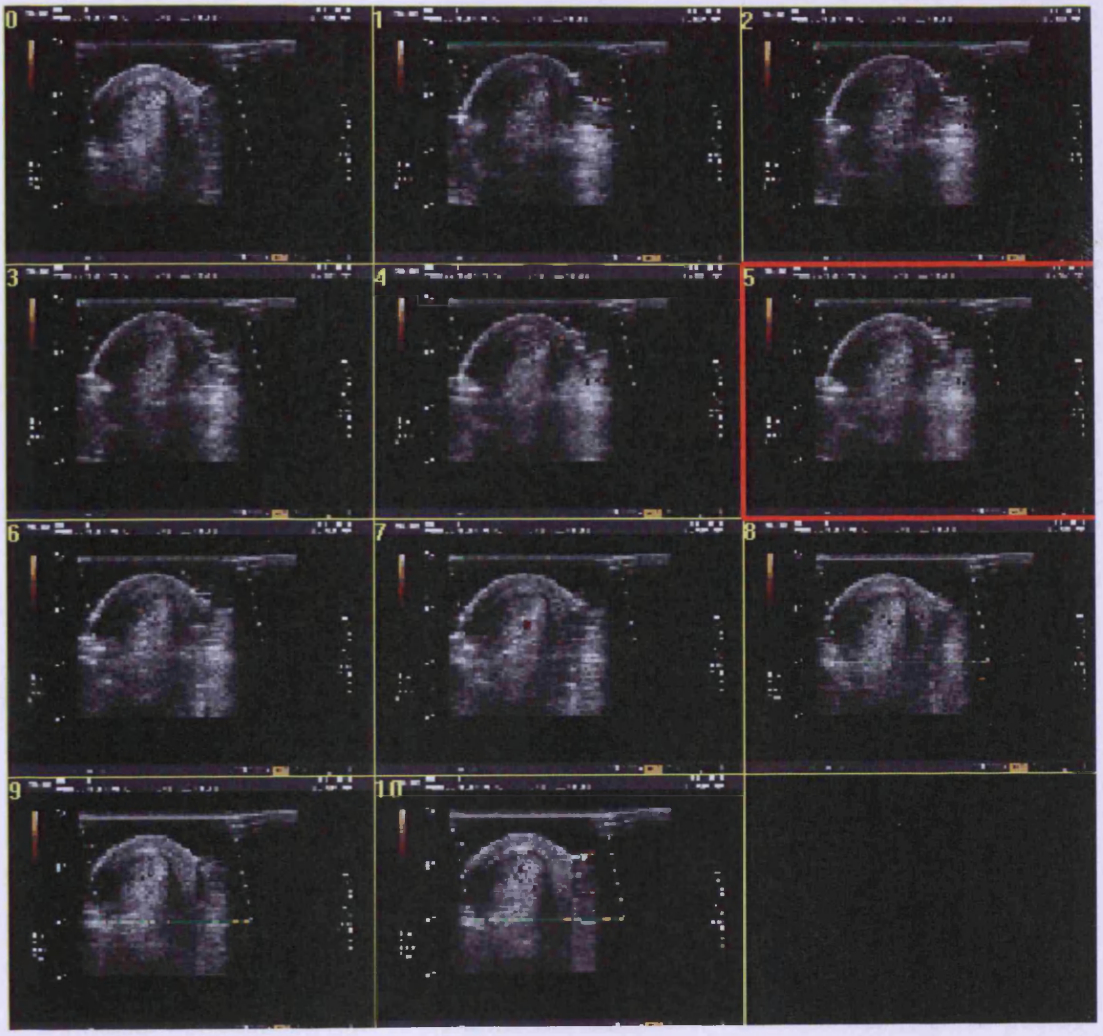

Appendix F- More Details in Patient A

F.1 Scanning 1

Volume of the neovascularization = 463 mm^3

(Blue – vascularization in the Achilles tendon, Orange – vascularization outside the Achilles tendon):

Anterior without suppliers

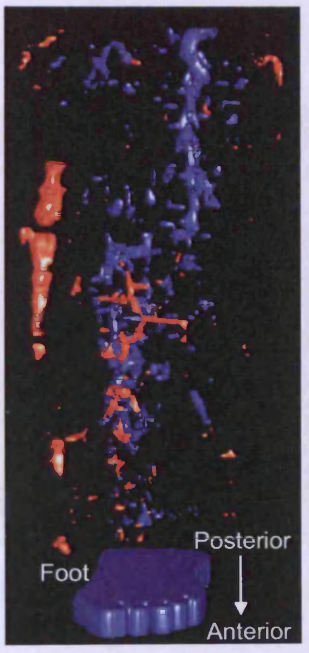

Anterior with supplier

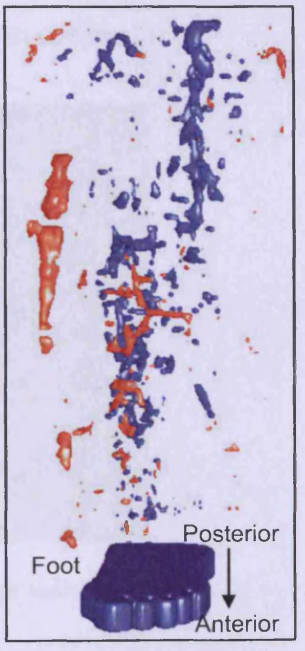

Anterior background reverse

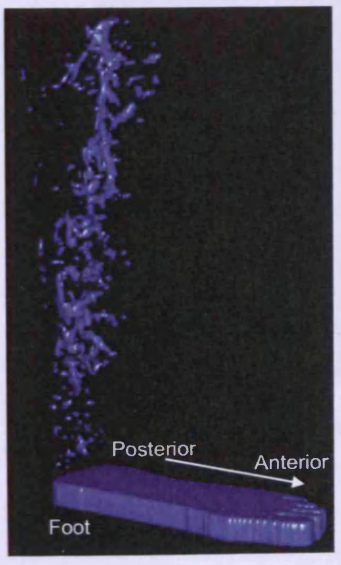

Lateral (left) without suppliers

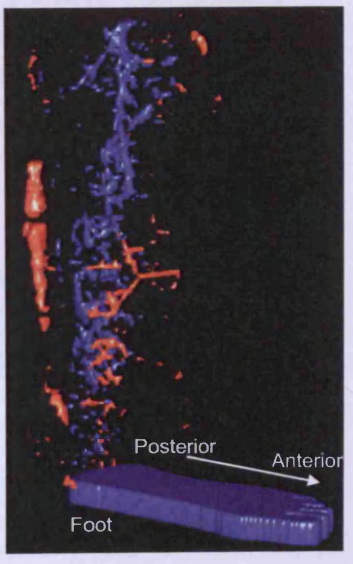

Lateral (left) with suppliers

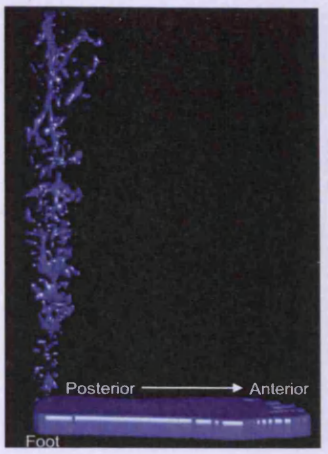

Lateral without suppliers

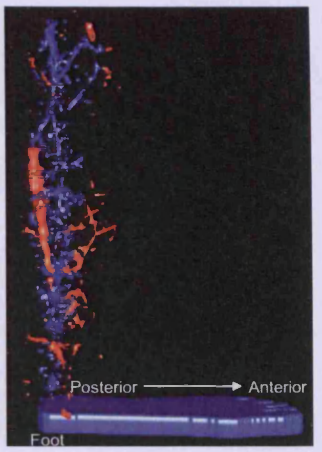

Later with suppliers

Posterior without suppliers

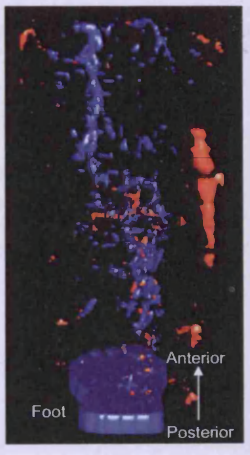

Posterior with suppliers

Lateral (right) without suppliers

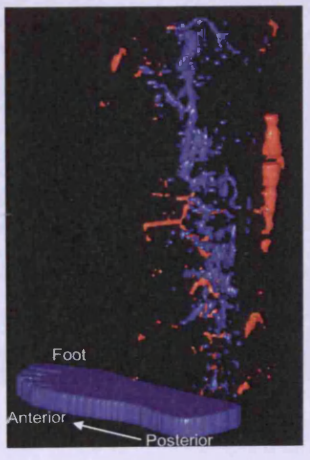

Later (right) with suppliers

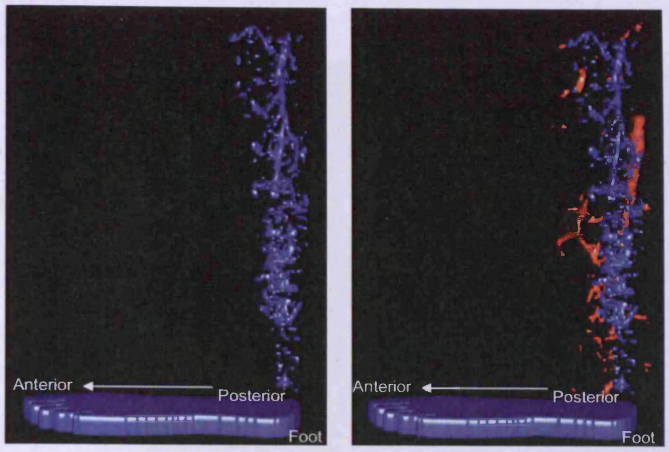

Lateral (right) without suppliers Later (right) with suppliers

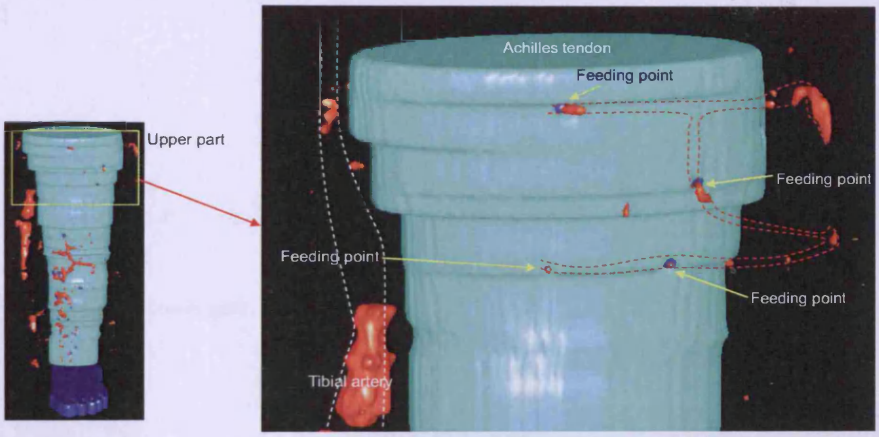

Achilles tendon is shown

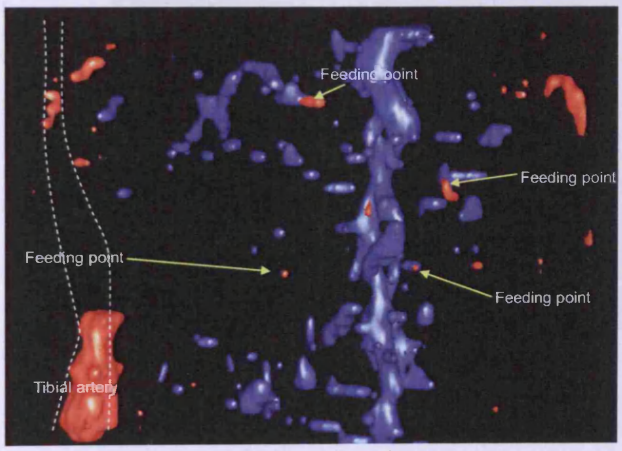

Achilles tendon is not shown

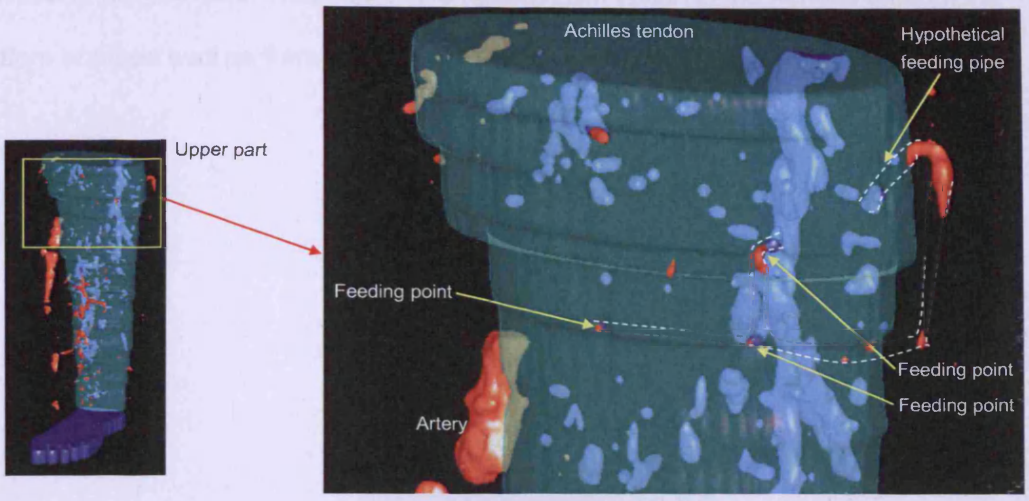
Upper part
Achilles tendon
Hypothetical
feeding pipe
Feeding point
Feeding point
Feeding point
Artery

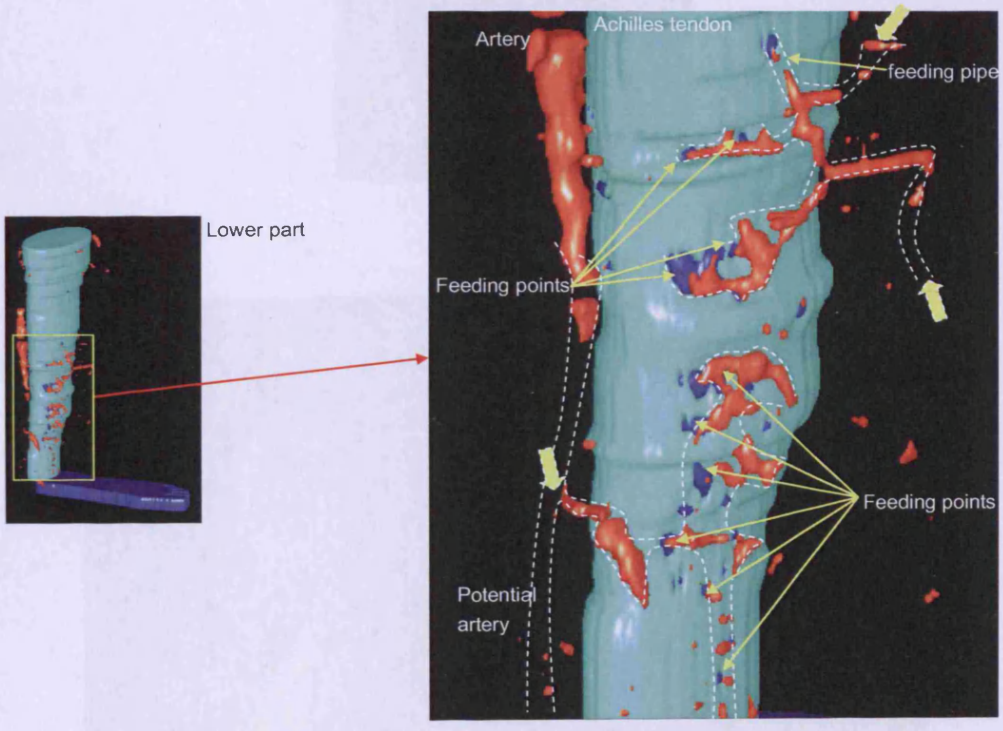
Lower part
Artery
Achilles tendon
feeding pipe
Feeding points
Feeding points
Potential
artery

According to the different aspects of the neovascularization in the Achilles tendon, the pattern analysis was performed in two sections - upper and lower.

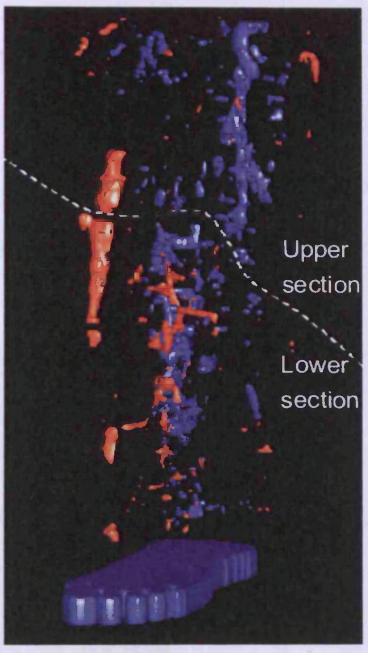

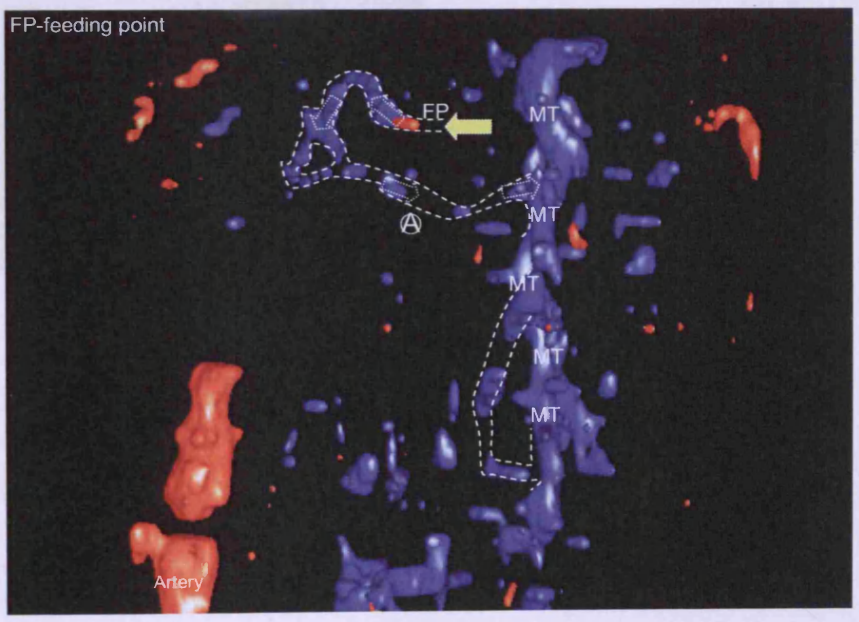

Upper

The upper section of the neovascularization shows a special branch type in the 3D model. According to the feeding analysis above, the point marked by FP near a yellow arrow is

thought to be one of the feeders in upper section. Due to the resolution of the Doppler ultrasound, the hypothetical connection (marked by Ⓐ) intermittently links the FP and main trunk (marked by MT). If we look into the neovascularization only, a rough tree-like sketch can be demonstrated in the graph below. The sketch is created by manually outlining the vascularization in the 3D model. Due to some Doppler signals are missing in slices, artificial connection is applied to predict an entire tree-like model and to observe the circulation in the neovessels. At the bottom of the upper section, a corridor to the lower section can be seen.

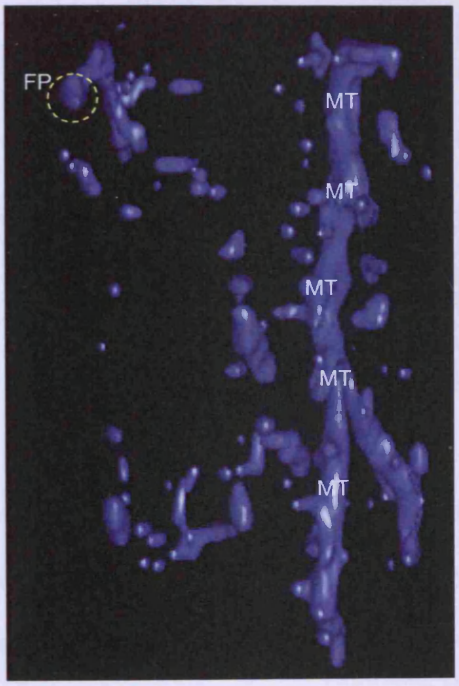

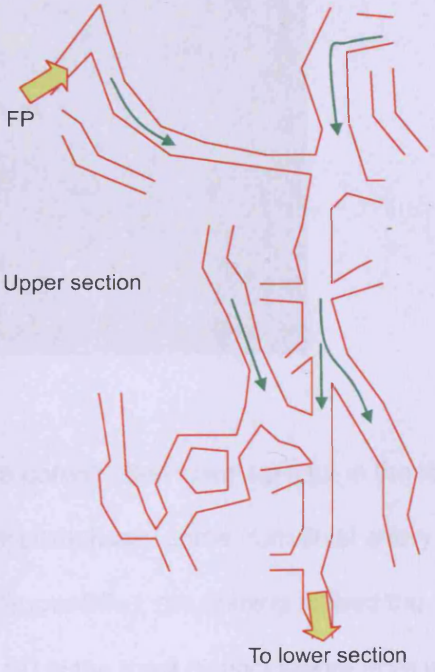

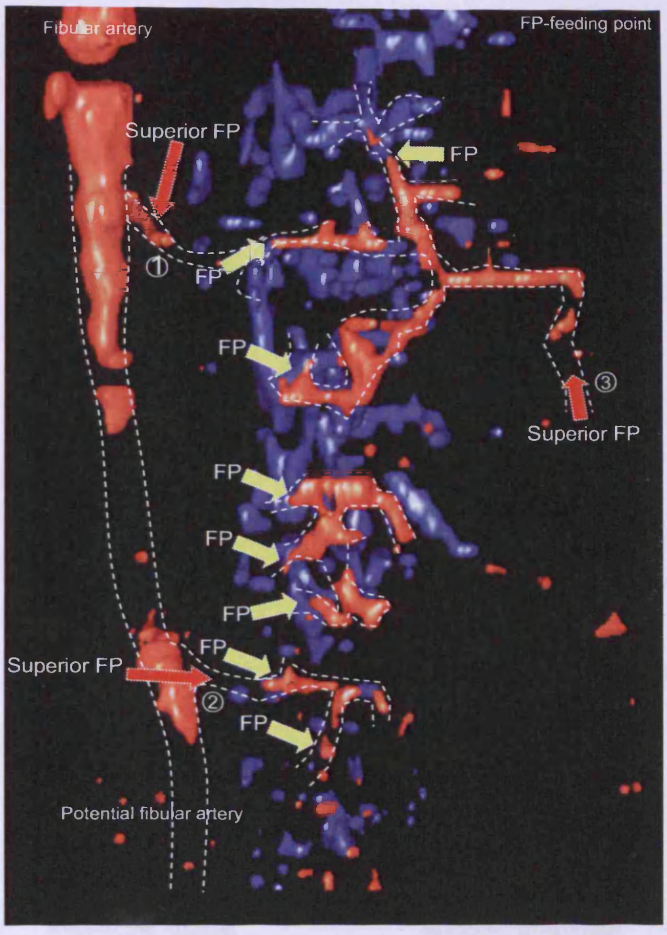

However, the pattern changes significantly into a complicated spiral up type in the lower section as shown above. More feeders, which hypothetically come from tibial artery at two locations (marked with ① and ② and nearby Super FPs), are coming to feed the neovessels. Another superior FP (marked with ③) is the most distinct feeder from anterior potential blood vessels.

F.2 Scanning 2

Volume of the neovascularization = 9 mm^3

Anterior without suppliers

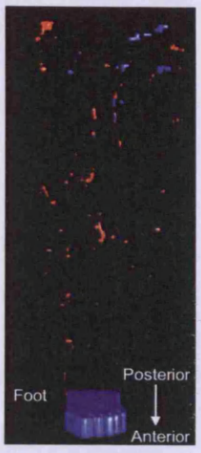

Anterior with suppliers

Lateral (left) without suppliers

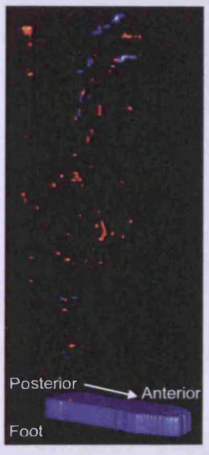

Lateral (left) with suppliers

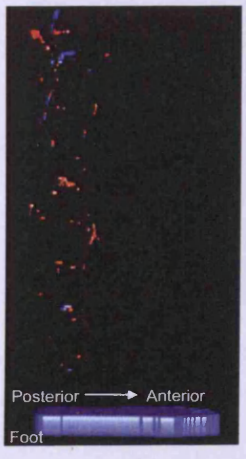

Lateral without suppliers

Lateral with suppliers

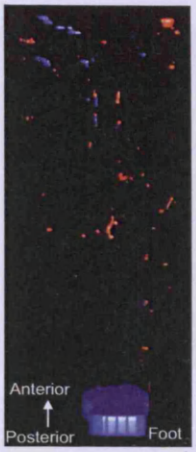

Posterior without suppliers

Posterior with suppliers

Lateral (right) without suppliers

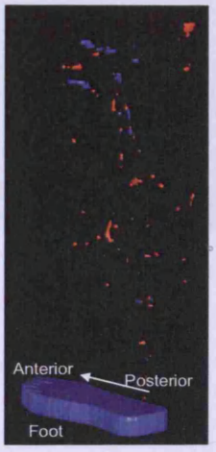

Later (right) with suppliers

Lateral (right) without suppliers

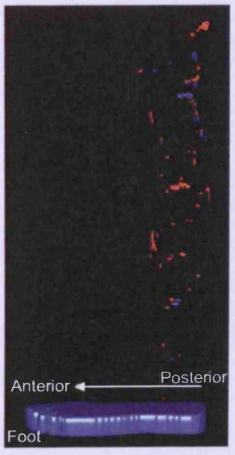

Later (right) with suppliers

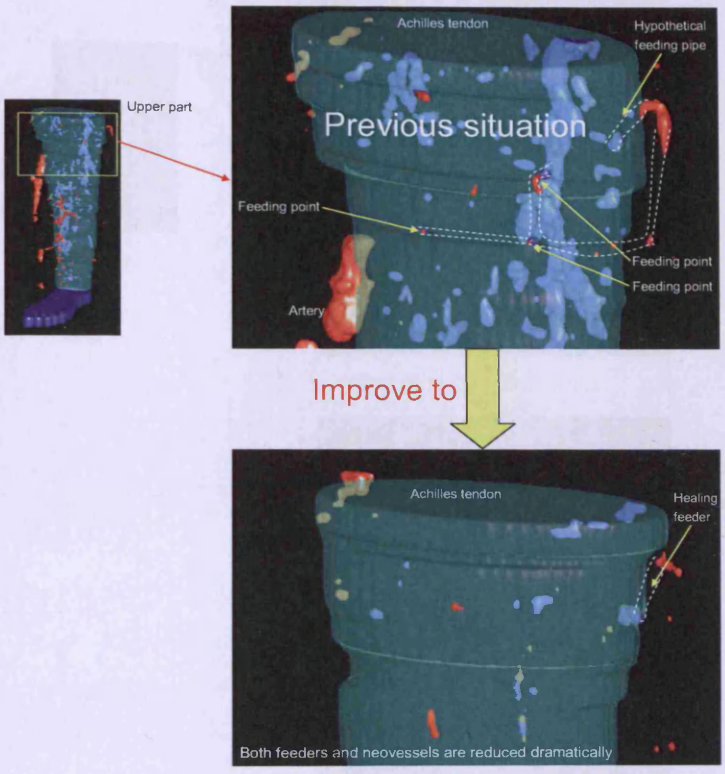
Upper part
Achilles tendon
Hypothetical feeding pipe
Previous situation
Feeding point
Feeding point
Feeding point
Artery
Improve to
Achilles tendon
Healing feeder
Both feeders and neovessels are reduced dramatically

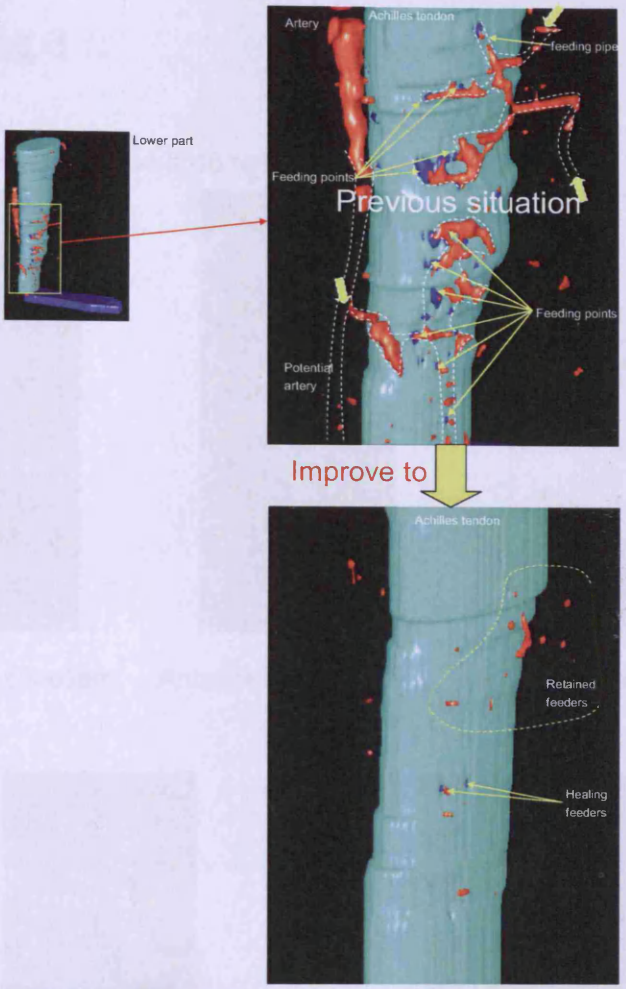
Lower part
Artery
Achilles tendon
Feeding pipe
Feeding points
Previous situation
Feeding points
Potential artery
Improve to
Achilles tendon
Retained feeders
Healing feeders

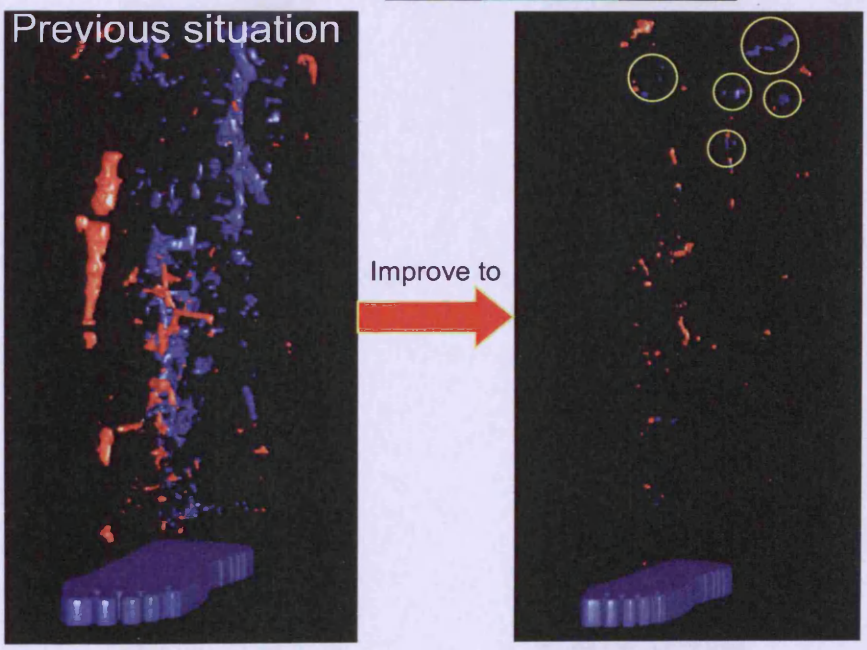
Previous situation
Improve to

F.3 Scanning 3

Volume of the neovascularization = 48 mm^3

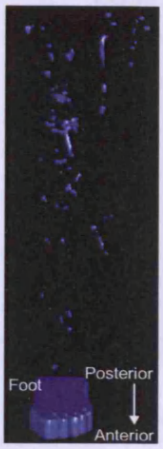

Anterior without suppliers

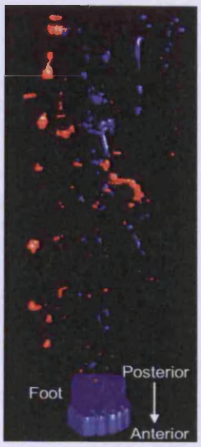

Anterior with suppliers

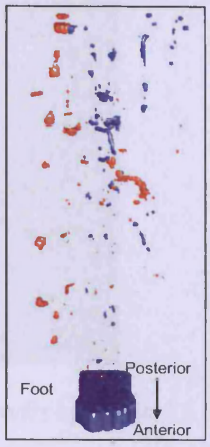

Anterior background reverse

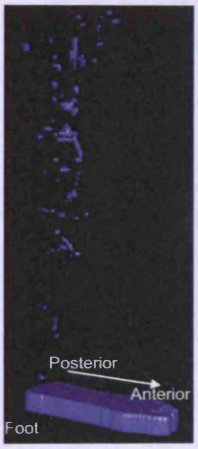

Lateral (left) without suppliers

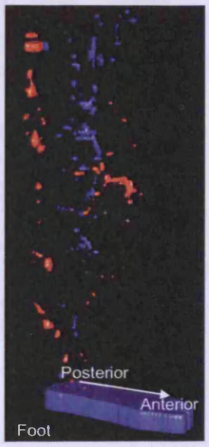

Lateral (left) with suppliers

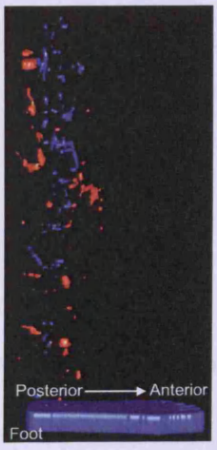

Lateral without suppliers

Posterior without suppliers

Later with suppliers

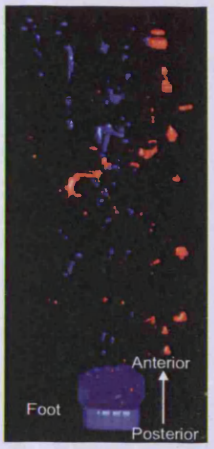

Posterior with suppliers

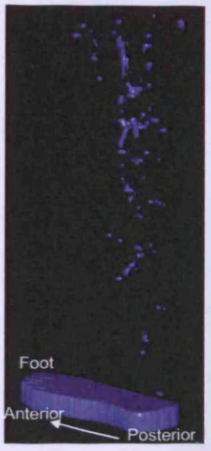

Lateral (right) without suppliers

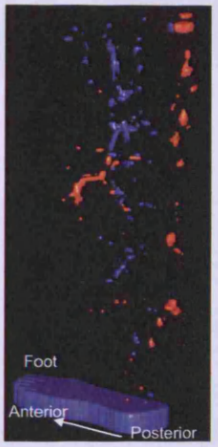

Later (right) with suppliers

Lateral (right) without suppliers

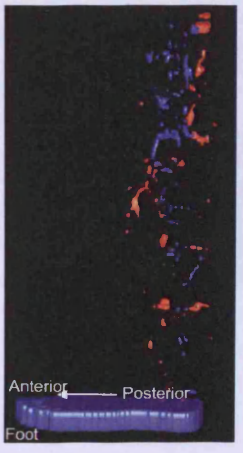

Later (right) with suppliers

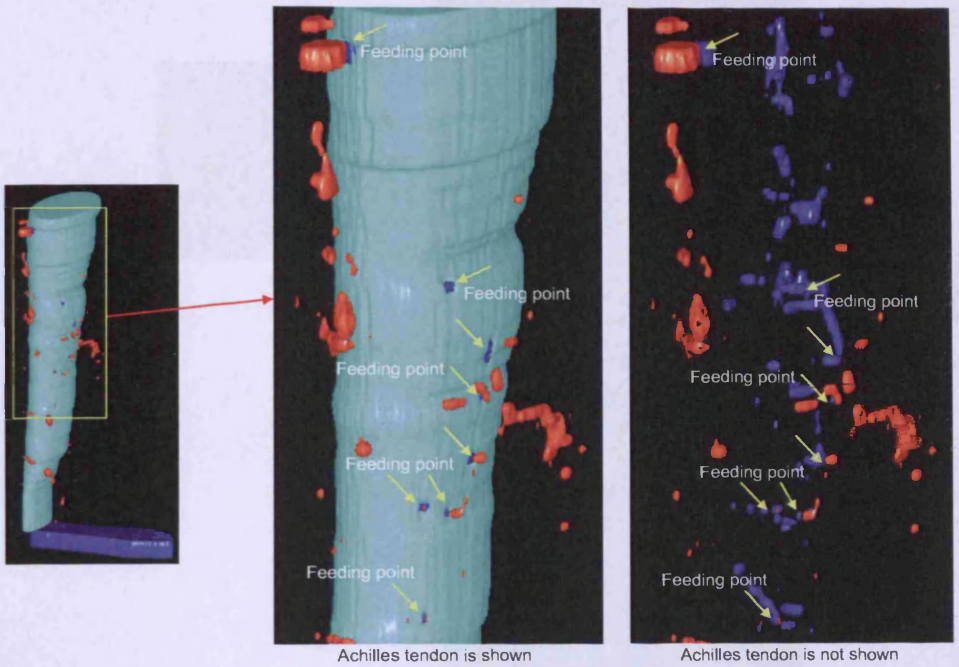

Achilles tendon is shown

Achilles tendon is not shown

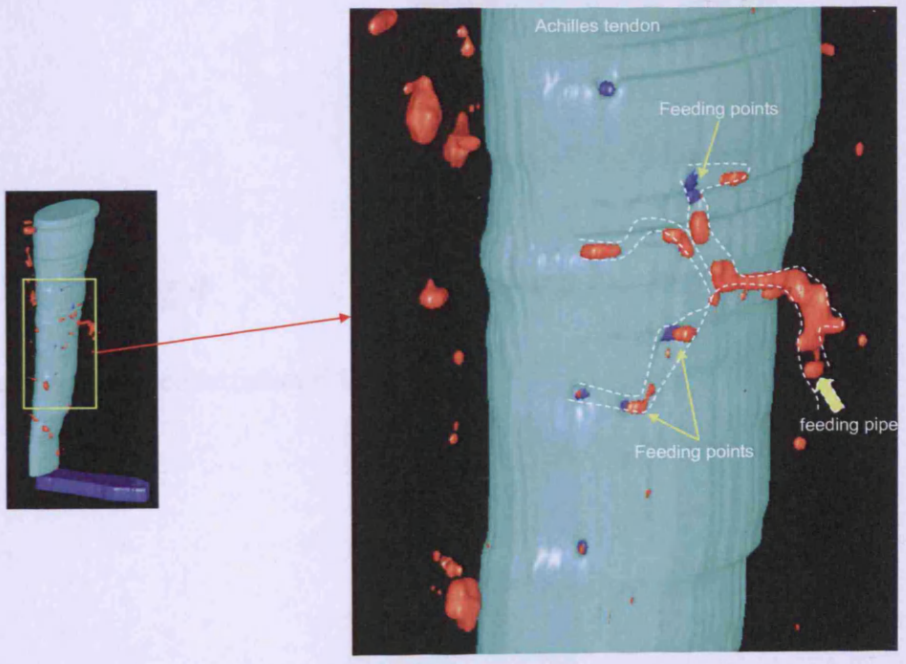

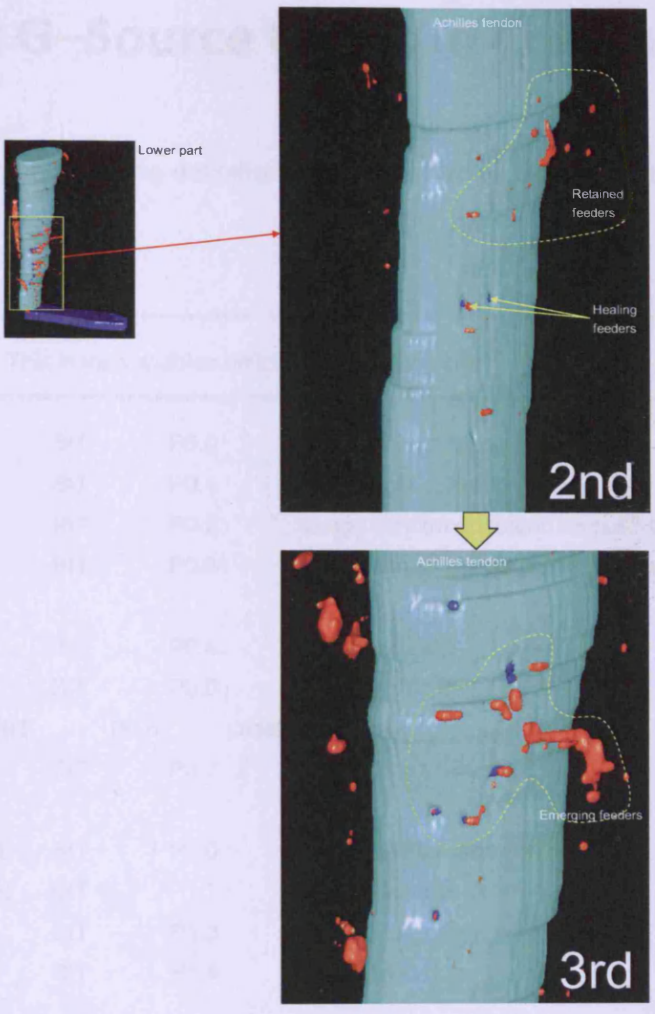

F.4 Scanning 4

Volume of the neovascularization = 117 mm^3

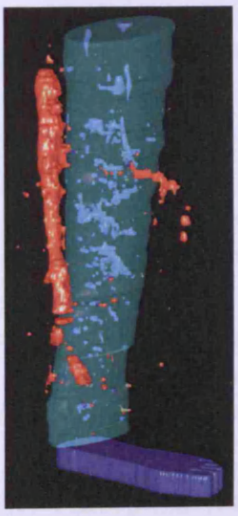

Appendix G–Source Codes in Controller

The first part shown below is the definition of some variables involved in the following software.

```
;*****************************************************************************************************
;**********          This is the variables definition in the software          **********
; *****************************************************************************************************
        S_L             BIT     P0.0    ; assign left operation on joystick
        S_R             BIT     P0.1    ; assign right operation on joystick
        S_O             BIT     P0.2    ; assign confirm operation on push button
        S_C             BIT     P0.3    ; assign cancel operation on push button

        LED_L           BIT     P0.4    ; assign left LED
        LED_R           BIT     P0.5    ; assign right LED
        LED_RUNBIT      P0.6    ; assign run LED
        LED_S           BIT     P0.7    ; assign stop LED

        HALF_FULL       BIT     P1.0    ; assign half/full step control bit
        DIRECTION       BIT     P1.1    ; assign direction control bit
        DOT_H           BIT     P1.3    ; assign LED dots
        DOT_L           BIT     P1.4    ; assign LED dots

        MOTORCLK        BIT     P3.0    ; assign motor clock output bit

        LED_ONOFF       EQU 30H     ; assign LED status variable
        LED_FLASH       EQU 31H     ; assign LED flash status
        SEVEN_DIS       EQU 32H     ; assign 7-seg display status

        JOYFUNC     EQU 33H     ; assign joystick function variable
        JOYSTEP     EQU 34H     ; assign joystick step variable
        JOYFILT         EQU 40H     ; assign joystick filter variable

        OKFUNC      EQU 35H     ; assign OK function variable
        CALFUNC     EQU 35H     ; assign Cancel function variable

        MOVE_STEP       EQU 37H     ; assign step variable
        MOTORC1         EQU 38H     ; assign motor variable
        MOTORC2         EQU 39H     ; assign motor variable

        FILTER1         EQU 41H     ; assign filter1 variable
        FILTER2         EQU 42H     ; assign filter2 variable
```

```
STAGE           EQU 43H     ; assign stage variable
INCREASE        EQU 44H     ; assign increase variable
DECREASE        EQU 45H     ; assign decrease variable

INTERNAL        EQU 46H     ; assign internal variable
STEPS           EQU 47H     ; assign steps variable
SCAN_STEP       EQU 48H     ; assign scan_step variable
INTERNA_COUNT   EQU 49H ; assign internal counter
STEP_COUNT EQU 50H      ; assign step counter

;**********                End of the assignments                **********
```

The main function in the software as shown below is to set a proper stack before execute the rest of the codes. There are three CALL functions to call for the subfunctions to test the seven-segment display, LED indicators, and initialize the scanning procedure, respectively. A JMP instruction will loop the main function in order to do another scan.

```
;*************************************************************************************************
;**********                This is the main function                **********
; *************************************************************************************************
MAIN:
        MOV     SP, #55H            ; set stack pointer SP=55H
        CALL    TEST_SEVEN          ; call the test_seven subfunction
        CALL    TEST_LED                ; call the test_led subfunction

        MOV     JOYFILT, #00            ; set joyfilter=0
        MOV     STAGE, #00              ; set stage=0
        CALL        INT_POS             ; call the ini_pos subfunction

        JMP         START                   ; loop

;**********                End of the function                **********
```

When the controller is energized, all the display devices including LED indicators and seven-segment display should be tested automatically to make sure the status display in the scanning are correct. The below is the test functions for the display devices.

```
;*************************************************************************************************
;**********                This is the test function                **********
```

```
;*************************************************************************************************
TEST_SEVEN:
        MOV     LED_ONOFF, #0FFH; set the led initial status
        MOV     LED_FLASH, #0FFH ; set the flash variable
        CALL        LEDS                    ; call leds subfunction
        MOV     R7, #10                 ; counter r7=10
        MOV     SEVEN_DIS, #00H   ; set 7-segment display status to 00
LOOP_7:
        CALL        SEVEN                   ; 7-segment display on
        MOV     R3, #20                 ; delay counter r3=20
        CALL        DELAY_F             ; call delay function
        DJNZ        R7, COUNTUP         ; delay
        RET
COUNTUP:
        MOV     A, SEVEN_DIS        ; accumulator a=seven_dis
        ADD     A, #11H                 ; a adds up with 11h
        DA          A                       ; display conditioning
        MOV     SEVEN_DIS, A        ; put back the value to seven_dis
        JMP         LOOP_7                  ; loop
TEST_LED:
        MOV     SEVEN_DIS, #0FFH ; set seven_dis=ffh
        CALL        SEVEN                   ; 7-segment display on
        MOV     LED_ONOFF, #0EFH; led_onoff=efh
        MOV     LED_FLASH, #0EFH ; led_flash=efh
        CALL        LEDS                    ; LEDs on
        MOV     LED_ONOFF, #0DFH      ; led_onoff=dfh
        MOV     LED_FLASH, #0DFH; led_flash=dfh
        CALL        LEDS                    ; LEDs on
        MOV     LED_ONOFF, #0BFH; led_onoff=bfh
        MOV     LED_FLASH, #0BFH ; led_flash=bfh
        CALL        LEDS                    ; LEDs on
        MOV     LED_ONOFF, #07FH; led_onoff=7fh
        MOV     LED_FLASH, #07FH ; led_flash=7fh
        CALL        LEDS                    ; LEDs on
        RET
SEVEN:
        MOV     A, SEVEN_DIS        ; a=seven_dis
        MOV     P2, A                   ; output from p2
        RET
LEDS:
        MOV     A, LED_ONOFF            ; a=led_onoff
        MOV     P0, A                   ; output from p0
        CALL        D_D                     ; delay with switches detection
        MOV     A, LED_FLASH        ; a=led_flash
```

```
        MOV     P0, A               ; output from p0
        CALL        D_D                     ; delay with switches detection
        RET

;**********                          End of the function                          **********
```

When the display devices tests are finished, the system will be waited for scanning settings. Meanwhile, the joystick can freely activate the stepper motor to drive the ultrasound probe travel either left or right along the rail. The functions involved are shown below.

```
;*************************************************************************************************
;**********                  This is the initial position function                  **********
; *************************************************************************************************
INT_POS:
        MOV     SEVEN_DIS, #00          ; seven_dis=0
        CALL        SEVEN                   ; 7-segment display on
INT_LOOP:
        MOV     LED_ONOFF, #4FH  ; led_onoff=4fh
        MOV     LED_FLASH, #7FH  ; led_flash=7fh
        MOV     JOYFUNC, #00        ; joyfunc=00, joystick used to move the probe
PROBE:
        MOV     OKFUNC, #00         ; okfunc=0, ok used to enter the next state
        MOV     CALFUNC, #00        ; calfunc=0, cancel used to clear the display
DIS:
        MOV     MOVE_STEP, #95   ; step set to 2mm as default
        CALL        LEDS                    ; LEDs on
        JMP         INT_LOOP                ; loop

;**********                          End of the function                          **********
```

During the delay necessary in the seven-segment display or LEDs operations, joystick and push buttons should be also taken care to determine whether they have been activated. The functions below are to detect the status of different buttons during the delay process, following a normal delay subfunction called by many places.

```
;*************************************************************************************************
;**********                      This is the delay function                         **********
; *************************************************************************************************
; ***************************DELAY WITH SWITCHES DETECTION
D_D:
```

```
        MOV     R0, #20                 ; r0=20
DD1:
        MOV     R1, #20                 ; r1=20
DD2:
        JNB         S_L, SW_L               ; detect joystick (left)
        JNB         S_R, SW_R               ; detect joystick (right)
        JNB         S_O, SW_O               ; detect ok button
        JNB         S_C, SW_C               ; detect cancel button
        MOV     R2, #248                ; r2=248
        DJNZ        R2, $               ; delay
        DJNZ        R1, DD2                 ; delay
        DJNZ        R0, DD1                 ; delay
        RET

; ***************************DELAY WITH TIME SET
DELAY_F:
DF1:
        MOV     R4, #20                 ; r4=20
DEF2:
        MOV     R5, #248                ; r5=248
        DJNZ        R5, $               ; delay
        DJNZ        R4, DF2                 ; delay
        DJNZ        R3, DF1                 ; delay
        RET

;**********                          End of the function                          **********
```

There are four buttons can be used to set the system running parameters, left and right on joystick, ok and cancel on push buttons. The following functions are to detect and save the status of these buttons.

```
;*************************************************************************************************
;**********                  This is the switches detection function             **********
; ************************************************************************************************
; ***************************SWITCHES PROCESSING
SW_L:
        SETB        DIRECTION               ; direction=1 as default
PRE_FILTER:
        PUSH        ACC                 ; push acc to stack
        MOV     A, JOYFILT              ; a=joyfilt
        CJNE        A, #01, NOFILT      ; condition jump
FILTERING:
        CALL        FILTER                  ; call filter function
```

```
        JNB     DIRECTION, CH_R  ; direction determination
        JB      S_L, PRE_JOY_PRO      ; joystick preprocessing
        JMP     FILTERING             ; filter
CH_R:
        JB      S_R, PRE_JOY_PRO      ; joystick preprocessing
        JMP     FILTERING             ; filter
SW_R:
        CLR     DIRECTION             ; clear direction variable
        JMP     FILTERING             ; filter
NOFILT:
        POP     ACC             ; pop acc from stack
        JMP     JOYPRO          ; jump to joystick processing

;**************************JOYSTICK PROCESSING
PRE_JOY_PRO:
        POP     ACC             ; pop acc from stack
JOY_PRO:
        PUSH    ACC             ; push acc to stack
        MOV     A, JOYFUNC      ; a=joyfunc
        CJNE    A, #0, JOYFUNC1       ; determine the joystick status
        POP     ACC             ; pop acc from stack
        CALL    MOVING          ; call driving function
        RET

JOYFUNC1:
        CJNE    A, #1, JOYFUNC2       ; joystick status check
        POP     ACC             ; pop acc from stack
        CALL    SET_VAL         ; call set value function
        RET

JOYFUNC2:
        CJNE    A, #2, JOYFUNC3       ; joystick status check
        POP     ACC             ; pop acc from stack
        CALL    READY           ; call ready function

JOYFUNC3:
        POP     ACC             ; pop acc from stack
        RET

;**************************SWITCHES PROCESSING OK
SW_O:
        CALL    FILTER          ; filter
        JB      S_O, OK_PRO     ; check ok button
        JMP     SW_O            ; call operation
```

```
OK_PRO:
        PUSH        ACC             ; push acc to stack
        MOV     A, OKFUNC           ; a=okfunc
        CJNE        A, #01, OK          ; check and jump

;**********                End of the function                **********
```

After the joystick and push buttons are set by user, all the parameters will be saved in the variables to guide the controller driving the ultrasound probe. The settings including interval, step, direction are performed by the joystick, where the codes to scan the joystick are shown below.

```
;*************************************************************************************************
;**********                This is the scan and move function                **********
; ************************************************************************************************
; *************************START_SCAN
START_SCAN:
        POP     ACC             ; pop acc from stack
OK:
        POP     ACC             ; pop acc from stack
        PUSH        ACC             ; push acc to stack
        MOV     A, STAGE        ; a=stage
        CJNE        A, #0, CHECK_1      ; determine the distance setting
        CALL        DISTANCE_SET        ; call distance_set function
CHECK_1:
        CJNE        A, #1, CHECK_2      ; determine the step setting
        CALL        STEPS_SET           ; call step_set function
CHECK_2:
        CJNE        A, #2, CHECK_3      ; determine the direction setting
CHECK_3:
        JMP         START_SCAN      ; loop
SW_C:
        JMP         $

;**********                End of the function                **********
```

The instructions used to control the stepper motor consist of the pulse generator and counter used to determine whether the target steps have been finished. The running status including the counter down on seven-segment display and indicators are also provided to tell the

performance of the system.

```
;*****************************************************************************************************
;**********          This is the moving and status display function                    **********
; ****************************************************************************************************
; ***************************MOVING THE PROBE
MOVING:
        JB          DIRECTION, SIMPLE_L      ; determine the moving direction
        CALL        SIMPLE_R                 ; call simple_r funciton
MOVING_LOOP:
        SETB        MOTORCLK                 ; set the bit
        CALL        DELAY_MOTOR              ; call delay
        CLR         MOTORCLK                 ; clear the bit
        CALL        DELAY_MOTOR              ; call delay
        DJNZ        MOVE_STEP, MOVING_LOOP   ; generate pulse wave
        RET

; ***************************SIMPLE LED ON WHEN MOVING THE PROBE
SIMPLE_L:
        SETB        LED_R                    ; led_r dim
        SETB        LED_S                    ; led_s dim
        CLR         LED_L                    ; led_r light
        CLR         LED_RUN                  ; led_run light
        JMP         MOVING_LOOP              ; loop
SIMPLE_R:
        SETB        LED_L                    ; led_l dim
        SETB        LED_S                    ; led_s dim
        CLR         LED_R                    ; led_r light
        CLR         LED_RUN                  ; led_run light
        RET

; ***************************SWITCH FILTER
FILTER:
        MOV     FILTER1, #4BH       ; filter1=4bh
F1:
        MOV     FILTER2, #0F8H          ; filter2=0f8h
        DJNZ        FILTER2, $              ; loop
        DJNZ        FILTER1, F1             ; delay
        RET

;**********                          End of the function                          **********
```

The interval, step, and direction are three main parameters during the ultrasound probe

driven. Three subfunctions below record the user's input to variables and feedback the settings through seven-segment display and indicators.

```
;*************************************************************************************************
;**********              This is the parameters record function              **********
; ************************************************************************************************
; ***************************INTERVAL SET
DISTANCE_SET:
        POP     ACC             ; pop acc from stack
        MOV     STAGE, #1               ; stage=1
        MOV     JOYFILT, #1             ; need filter
        MOV     INCREASE, #5    ; increase by 0.5mm
        MOV     DECREASE, #95H  ; decrease=95h
        MOV     SEVEN_DIS, #20H ; initial interval is 2.0mm
        CLR         DOT_H                   ; change point
        SETB        DOT_L                   ; change point
        CALL        SEVEN                   ; 7-seg display on
DISTANCE_LOOP:
        MOV     LED_ONOFF, #4FH ; led status
        MOV     LED_FLASH, #7FH ; led flash
        MOV     JOYFUNC, #1     ; joystick used to set value
        MOV     OKFUNC, #0              ; ok to enter the next state
        MOV     CALFUNC, #0     ; cancel used to clear the display
        CALL        LEDS                    ; leds on
        JMP         DISTANCE_LOOP   ; loop

; ***************************STEP SET
STEPS_SET:
        POP     ACC             ; pop acc from stack
        MOV     STAGE, #2               ; stage=2
        MOV     JOYFILT, #1             ; need filter
        MOV     INCREASE, #2    ; increase by 2 step
        MOV     DECREASE, #98H  ; decrease=98h
        MOV     SEVEN_DIS, #50H ; initial step 50
        CLR         DOT_L                   ; change point
        SETB        DOT_H                   ; change point
        CALL        SEVEN                   ; 7-seg display on
SETP_LOOP:
        MOV     LED_ONOFF, #4FH ; led status
        MOV     LED_FLASH, #7FH ; led flash
        MOV     JOYFUNC, #1     ; joystick used to set value
        MOV     OKFUNC, #0              ; ok used to enter the next state
        MOV     CALFUNC, #0     ; cancel used to clear the display
```

```
        CALL    LEDS                    ; leds on
        JMP     STEP_LOOP               ; loop

;**************************DIRECTION SET
RL_SET:
        POP     ACC             ; pop acc from stack
        MOV     STAGE, #3               ; stage=3
        MOV     JOYFILT, #1             ; need filter
        MOV     SEVEN_DIS, #0ABH ; display data
        SETB    DOT_L                   ; change point
        SETB    DOT_H                   ; change point
        CALL    SEVEN                   ; 7-seg display on
RL_LOOP:
        MOV     LED_ONOFF, #4FH ; led status
        MOV     LED_FLASH, #7FH ; led flash
        MOV     JOYFUNC, #2     ; joystick used to set direction
        MOV     OKFUNC, #0              ; ok used to enter the next state
        MOV     CALFUNC, #0     ; cancel used to clear the display
        CALL    LEDS                    ; leds on
        JMP     RL_LOOP         ; loop

;**********                    End of the function                    **********
```

The pulse wave used to drive the stepper motor correspond to the interval distance set by the user is calculated in the last section of the software demonstrated below. The rest step is also altered on the seven-segment display during the ultrasound probe scanning by the calculation in the SET_VAL function below.

```
;*************************************************************************************************
;**********                    This is the pulse wave creation function                **********
;*************************************************************************************************
;**************************FINISHING THE SETTINGS
READY:
        MOV     STAGE, #4               ; stage=4
        MOV     JOYFILT, #0             ; need filter
        MOV     SEVEN_DIS, STEPS; display step
        CALL    SEVEN                   ; 7-seg display on

        MOV     JOYFUNC, #3     ; joystick is useless
        MOV     OKFUNC, #1              ; okfunc=1
        MOV     CALFUNC, #0     ;calfunc=0
```

```
; ***************************CALCULATE EACH STEP
        JB          DIRECTION, SCAN_L    ; determine the direction
SCAN_R:
        MOV     LED_ONOFF, #57H  ; led status
        MOV     LED_FLASH, #57H  ; led flash
        CALL        LEDS                 ; leds on
        JMP         SCAN_R               ; loop
SCAN_L:
        MOV     LED_ONOFF, #67H  ; led status
        MOV     LED_FLASH, #67H  ; led flash
        CALL        LEDS                 ; leds on
        JMP         SCAN_L               ; loop

; ***************************MOTOR CLOCK DELAY
DELAY_MOTOR:
        MOV     MOTORC1, #12         ; motorc1=12
DM1:
        MOV     MOTORC2, #150        ; motorc2=150
        DJNZ        MOTORC2, $           ; delay
        DJNZ        MOTORC1, DM1         ; pulse wave generation
        RET

; ***************************SET_VAL
SET_VAL:
        JNB         DIRECTION, GOUP  ; count up
        JMP         GODOWN           ; count down
GOUP:
        MOV     A, SEVEN_DIS     ; a=seven_dis
        ADD     A, INCREASE      ; sum
        DA          A                    ; conditioning
        MOV     SEVEN_DIS, A     ; save back to seven_dis
        PUSH        ACC              ; push acc into stack
        MOV     A, STAGE         ; a=stage
        CJNE        A, #1, STORE_STEP; store step
        POP     ACC              ; pop acc from stack
        MOV     INTERNAL, A          ; internal=a
        CALL        SEVEN                ; 7-seg display on
        RET
GODOWN:
        MOV     A, SEVEN_DIS     ; a=seven_dis
        ADD     A, DECREASE      ; deduction
        DA          A                    ; conditioning
        MOV     SEVEN_DIS, A     ; save back to seven_dis
        PUSH        ACC              ; push acc into stack
```

```
        MOV     A, STAGE            ; a=stage
        CJNE        A, #1, STORE_STEP; store step
        POP     ACC                 ; pop acc from stack
        MOV     INTERNAL, A             ; internal=a
        CALL        SEVEN                   ; 7-seg display on
        RET
STORE_STEP:
        POP     ACC                 ; pop acc from stack
        MOV     STEPS, A            ; steps=a
        CALL        SEVEN                   ; 7-seg display on
        RET

        END

;**********                  End of the software                  **********
```